Imperial College London

Development of Sustainable Chemical Technologies Using Low-cost Ionic liquids for Waste Decontamination and Valorization

Aida Rafat Said Abouelela

Department of Chemical Engineering and Chemical Technology

Imperial College London

Thesis submitted as partial fulfilment of the requirements for the degree of Doctoral of Philosophy (PhD)

January 2021

Declaration of Originality and Copyright

I declare that this thesis has been composed by myself. I confirm that the work conducted in this thesis is my own work, unless otherwise stated. This work was carried out in Imperial College London between November 2016 and September 2020 and has not be submitted for any other degree or professional qualification.

All the work of the thesis is going to be subjected to embargo for a period of one year from submission.

The following publications are a result of my own PhD work or collaborative projects conducted during my PhD:

1. Abouelela, A.R, Tan, S.; Kelsall, G.H.; Hallett, J. P. (2020), Towards A Circular Economy: Decontamination and Valorization of Post-Consumer Waste Wood Using ionoSolv Process. *ACS Sustainable Chemistry & Engineering*. 8 (38), 14441-14461.
2. Abouelela, A. R., Gschwend, F. V., Malaret, F., & Hallett, J. P. (2020). Commercial Aspects of Biomass Deconstruction with Ionic Liquids. In *Commercial Applications of Ionic Liquids* (pp. 87-127). Springer, Cham.
3. Bukowski, A., Esau, D., Rafat Said, A. A., Brandt-Talbot, A., & Albert, J. (2020). Combining Cost-Efficient Cellulose and Short-Chain Carboxylic Acid Production: The Polyoxometalate (POM)-Ionosolv Concept. *ChemPlusChem*, *85*(2), 373-386.
4. Chen, M., Malaret, F., Firth, A. E., Verdía, P., Abouelela, A. R., Chen, Y., & Hallett, J. P. (2020). Design of a combined ionosolv-organosolv biomass fractionation process for biofuel production and high value-added lignin valorisation. *Green Chemistry*, *22*(15), 5161-5178.

Abstract

This work proposed and investigated key strategies that contribute to the advancements of low-cost protic ILs (PILs) for use in the future sustainable chemical industry, particularly in the areas of waste valorization and decontamination.

In large, this PhD research contributed to the ongoing development of a lignocellulose fractionation process using PILs. First, the use of contaminated waste wood was investigated as a low-cost alternative feedstock to expensive virgin biomass. Fractionation of post-consumer waste wood collected from construction activities was shown to be highly effective using 1-methylimidazolium chloride [H_1Cim]Cl, producing a highly digestible metal-free cellulose pulp, with >70% glucose yield during enzymatic hyrolysis. Evaluation of key process parameters such as solid loading, waste wood composition variation, metal chelation with lignin and IL-clean up were also investigated. The study was expanded to include the valorization of hazardous creosote waste wood using the low-cost PIL *N,N,N*-dimethylbutylammonium hydrogen sulfate [DMBA][HSO_4]. The fractionation produced a highly digestible, PAH-free cellulose pulp stream with 70% glucose release, and a PAH-lignin stream.

Second, to develop a better understanding of the process boundary conditions, water use as co-solvent and anti-solvent was investigated using a variety of promising lignocellulosic biomass. It was shown that the impact of water as a co-solvent on the fractionation ability of [DMBA][HSO_4] is feedstock-dependent. A reduced water input for lignin precipitation was found not to compromise the cellulose digestibility, while significantly reducing the process energy. In addition, the impact of ionoSolv pretreatment severity on fractionation performance was evaluated using a modified pretreatment severity factor, incorporating the Hammett acidity of the aqueous IL solution. The modified severity factor can better predict the fractionation outcome compared to the classical pretreatment severity factor, particularly regarding delignification and hemicellulose removal. Attention was then turned to utilization of the cellulose pulp derived from the ionoSolv process to produce functionalized nanocellulose crystals (CNCs). Alkaline-H_2O_2 oxidation was used as a simple and more environmentally friendly method for facile extraction of carboxylated CNCs. The impact of pretreatment severity and cellulose composition on the properties of extracted CNCs was evaluated. The produced CNCs had the ability to form self-standing nanofilms and exhibited similar thermal and colloidal stability to CNCs produced by TEMPO-mediated oxidation.

Lastly, a novel approach for textile waste decontamination and synthetic dye reuse using PILs was developed. The PIL [DMBA][HSO_4] was used to selectively extract dyes from polyester-based synthetic textiles, leaving the dye-free polyester fiber behind for upcycling. Subsequent dyeing using the dye-rich [DMBA][HSO_4] solutions was shown to be possible, achieving a similar color strength to commercially dyed products. The process provides key and novel advantages that can provide a new circular dimension to the textile recycling sector by eliminating virgin dye use, applying a closed-loop solvent-based dyeing process, and creating dye-free polyester fibers.

Glossary

[C_2C_1im]	1-ethyl-3-methylimidazolium
[C_4C_1im]	1-butyl-3-methylimidazolium
[DMBA]	*N*,*N*,*N*-dimethylbutylammonium
[MBHA]	Methylbutylammonium
[HC_4im]	*N*-butylimidazolium
[HC_1im]	*N*-methylimidazolium
[TEA]	triethylammonium
[2-HEA]	2-hydroxyethylammonium
[HSO_4]	Hydrogen sulfate
[OAc]	Acetate
AFEX	ammonia fiber expansion
AIL	acid insoluble lignin
AIR	acid insoluble residue
APIL	aprotic ionic liquid
ASL	acid soluble lignin
CCA	chromated copper arsenate
G	guaiacyl
GHG	greenhouse gases
H	*p*-hydroxyphenyl
HMF	5-hydroxymethylfurfural
IL	ionic liquid
PIL	protic IL
PAH	polycyclic aromatic hydrocarbons
APIL	aprotic IL
M_w	Weight average molecular weight
NREL	National Renewable Energy Laboratory
ppm	parts per million
S	syringyl

Acknowledgement

Writing an acknowledgment means that I am almost done. I have mixed feelings of happiness, sadness, and nostalgia (already). This PhD was a wild ride that came with unforgettable moments of laughter and sacrifices. The very first person that I would like to thank deeply is Adam. Thank you for unlimited support, love and encouragement despite my long inexcusable hours in the lab, all the nights you made sure I'm back safe in the house, and more importantly, for listening to me, comforting me and advising me all the time. I would also like to thank my family, my parents (Rafat and Ragaa), my brother Mohamed, and my sisters, Lina, Deema and Hala. You all have nothing but incredible, providing me unlimited support and love.

I would like to thank Prof. Jason Hallett. Not because it is a formality to have to acknowledge your PhD supervisor, but because he did provide me the great opportunity to be part of his group and the freedom to be carry research independently. In addition, I would also like to thank people who contributed to the research work conducted in this thesis, namely Jesus Lemus, Sze Tan, Subhashree Balaji, Eero Kontturi, Ecaterina Ware.

There are few key people in the Hallett's who I would like to thank. Without them, this PhD would not be the same. These are: Amir Alghatta, Louis Hennequin, Anton Firth, Coby Clark, Francisco Malarat and Meng Cheng (Angela). Thank you to all my London friends who made my days much happier and brighter; Waleed, Hassan, Maya, Mudassir and Rahim, Valentini, Anna and Carlos. Finally, I would like to thank Freddie Mercury for the genius singer he was, without "Don't Stop Me Now" and "Radio Ga Ga" tracks, I could not have possibly worked as hard as I did. Greatest motivation of all time.

Table of Contents

List of Figures

List of Tables

Chapter 1 : Literature review

1.1 Introduction

There is growing demand to transform our current fossil fuel-based economy to a sustainable renewable-based economy. This will require cumulative global efforts to design pioneering technologies to make these new processes as efficient and reliable as the conventional fossil fuels-based technologies. While all renewable energy resources (e.g. solar, wind, nuclear) are inherently designed and/or implemented for power generation, production of biofuels, chemical molecules and polymers can only by accomplished via valorizing one natural source: biomass.[1] Lignocellulose biomass is the world's most abundant organic matter and largest possible reservoir to produce essential chemical building blocks for our economy and society.[2] However, the use of lignocellulose instead of the readily or easily fermentable matter (e.g. corn s, sugarcane) comes with price of introducing an additional processing step called "pretreatment" or "fractionation".[2,3] The main objective of this process is to deconstruct the complex structure of the lignocellulose to achieve effective separation of its three biopolymers: cellulose, lignin and hemicellulose.[4] With ongoing interest to use Ionic Liquids (ILs) and the quest to leverage their unique properties to the chemical industry, ILs found their way to the sphere of lignocellulose fractionation technologies.

One of the advancements in this area is a technology known as "ionoSolv" developed in Imperial College London by Dr. Agnieszka Brandt in Prof. Tom Welton's group, and then further developed by Prof. Jason Hallett's group in Imperial College London.[5,6] The technology is based on the use of low-cost protic ionic liquids (price range of $0.78 to $1.2 per kg) to fractionate the recalcitrant lignocellulose biopolymer into: i) a high quality cellulose pulp that can be further processed to produce bioethanol or upgraded to value-added products such as paper, textiles, composites and nanocellulose and, ii) high quality lignin that can be used for power generation and heat recovery, or upgraded to platform of aromatic compounds such as carbon fibers , phenols and bioplastics. Resolving the high-cost barrier that has been always associated with ILs was one of the key milestones that enabled the process development both from research & development perspectives as well as from commercialization perspective. However, to fully realize this vision, several key process developments needed to be investigated to improve the technoeconomic profile of the process. This is essentially important as cost has been

almost always the key barrier to market entry for any new process, in addition to technology readiness and the state of the economy. The factor of cost for new technologies is signified when considering chemical processes with mega infrastructure with multi-million capital investment and long return of investment. Therefore, looking at every opportunity where cost can be reduced is crucial for rapid process development and translation to large-scale operation. This can be accomplished by careful process design and intensification and finding the right niche for market entry.[7]

From a process intensification and design perspective, it is important to develop the technology using industrially relevant conditions to expedite process translation to industry. Process intensification and design are often overlooked by many researchers with many papers focusing on high product yield and selective product composition as the two sole parameters for the process success. Such enthusiastic conclusions are often made without analyzing and reflecting whether the conditions used to produce the product are translatable to large-scale operations. However, it is also reasonable in process development to first obtain the desired product yield and composition, and then consider improving and intensifying the process conditions to improve the process economics. The same route of development was followed when developing the ionoSolv process over the past few years, with the main process optimization focusing on space-time parameters. One of the key cost elements in the process is related to the amount of IL used and the water circulating in the process. The cost and energy use associated with water use is not obvious in a lab-scale protocol, however, soon after the first process simulation and high-level technoeconomic assessment were conducted, the energy related to water use in the process was highlighted as potential barrier to further technology development. Therefore, it is essential to re-visit the evaluation of process performance using more industrially adaptable conditions to highlight any potential energy saving.

Since ILs are quite unknown to industry, the use of ILs for biomass fractionation in general can be perceived as a high technological risk. Both the technology (the use of ILs) and intended application (biomass fractionation) have an embedded deployment risk. Although many process-related advantages have been claimed, none is yet proven at scale. It is therefore essential to find a currently under-served niche application where there is a clear unmet customer need that can be addressed. Turning to biomass waste

as feedstock can be a good strategy to speed process development as a) the feedstock has low to negative cost and, b) there is growing pressure to utilize waste materials for circular processes. This also solves many of the concerns associated with feedstock source, cost, supply, availability and sustainability in biorefinery.[8,9] One of the largest waste wood streams is generated from construction and demolition waste (CDW). The CDW waste wood has high proportion of heavy metals contamination that was added early on the wood to prolong its lifetime and protect it from biodegradation. Valorization of the CDW waste wood has been highlighted to be a key challenge with current and near-future applications restricted to energy recovery applications for relatively "clean" waste wood. Therefore, it is of great interest to explore new pathways to valorize the currently landfilled hazardous waste wood streams for applications beyond energy recovery.

Finding the right niche is not only restricted to exploring new feedstocks, but it can also be applied to exploring new products of nascent growing markets. The biopolymers produced from the ionoSolv technology can be transformed by mechanical, chemical or biological pathways to variety of valuable products. Due to the high complexity of lignin and the need to use lignin as heating source in the process, cellulose remains to be the main product of the process. Valorization of hemicellulose and its dehydration products is an interesting route; however, it is more challenging compared to cellulose as these molecules remain soluble in the IL with methods for their effective separation remain under investigation. Cellulose has wide range of established applications and markets including paper, packaging, textiles and composites. One of the recently most explored end-products of cellulose is nanocellulose in its many forms and shapes. The growing interest on nanocellulose provides a new product development opportunity for the cellulose-pulp substrates produced in ionoSolv process. It is therefore important to investigate how the new cellulose substrates generated in ionoSolv process can be used to produce nanocellulosic materials.

The use of low-cost protic ionic liquids in circular-economy process concepts can inspire the development of circular processes in other fields. Textile waste is another highly challenging and rapidly growing waste stream in our society with valorization and recycling methods at early stage of development. The waste stream is particularly challenging as it contains wide variety of natural and synthetic fibers that has been

mixed, chemically treated and dyed. Sorting and separating these fibers and further processing them to yarns with specifications that match the initial feedstock is highly challenging with few pilot-scale technologies currently under development. A key challenge that renders innovation in the textile industry stems from the highly fragmented and decentralized supply chain which makes transparency and traceability highly challenging. Such industry does not only require circular-based processes, but they also require more centralized processes with multiple functionalities. During this PhD work, a process called "Dye Recycle" was developed. The process aims to recycle synthetic dyes from textile waste using ILs and re-use these dyes to colour new fibers. The process contributes solving two grand challenges in the textile supply chain: water-intensive fiber dyeing (upstream challenge) and overwhelming non-recycled textile waste (downstream challenge).

The research conducted throughout this thesis discusses all the highlighted knowledge gaps of i) investigating the use of highly challenging and contaminated waste wood streams as alternative feedstocks, ii) evaluating water role in ionoSolv biomass fractionation process, ii) investigating the impact of pretreatment severity conditions on the fractionation efficiency and outputs, iii), iv) exploring new method to extract nanocellulose from cellulose substrates, and v) exploring new circular processes where low-cost protic ionic liquids can be used to tackle key challenges in the textile industry supply chain.

1.2 Ionic Liquids

Ionic substances (*i.e.* salts) often exist in solid state due to the very strong electrostatic bond between the anion and the cation counterparts. The strong bond results in a very systematic structure and high melting points for these salts such as 801 and 851 ºC for NaCl and $NaCO_3$ salts, respectively. On the other hand, Ionic liquids (ILs) are group of salts that are liquids at low temperature of <100 ºC due to the much less symmetrical structure and bulkiness of the anions and cations which reduce the ability to form ordered structures.[10] The first discovered IL was ethnolammonium nitrate by Gabriel in 1881 with a melting point of 52-55 ºC.[11] This was followed by Paul Walden who reported the properties of ethylammonium nitrate with a melting point of 12.5 ºC.[12] The main reason behind ILs having low melting point is the bulkiness and low symmetry. A second factor is the delocalization of the ion charge over more than one atom in both the cation

and anions (except for halides). The delocalization of charge causes the reduction in lattice energy. Cations with more than one alkyl chain have a lower symmetry thus lowering the melting point of the ionic liquid.[13] Figure 1.1 shows common cations and anions used in the synthesis of most commonly used ILs. The cation in IL is usually comprised of a alkylated organic ion such as amines imidazole or pyridines while the anions are usually polyatomic (except for halides) and can be either organic or inorganic such as tetrafluoroborate $[BF_4]^-$, hexafluorophosphate $[PF_6]^-$, trifluoromethanosulfate $[Otf]^-$, methyl sulfate $[MeSO_3]^-$, acetate [OAc], or halides.[12,14]

ILs are known to be "designer solvents" as each anion-cation pair has its own unique properties which makes them suitable to be tailored to fit task-specific applications. Compared to the 600 molecular organic solvents in use today, it was estimated that one million binary ionic liquids can be potentially synthesized.[15] In addition, the hybrid ionic-organic nature of ILs make them capable to participate in wide variety of interactions from the weak and isotropic forces (e.g., van der Waals, solvophobic) to strong (Coulombic), specific, and anisotropic forces (e.g., hydrogen bonding, , electron pair donor/acceptor interactions).[16] The designer characteristics of ILs made them experience huge fame among scientists and engineers since they can be tailored to fit wide variety of applications as solvents and catalysts. Applications include chemical synthesis[17,18], electrochemistry[19], carbon capture[20] as well as lignocellulose pretreatment.[21–23]

In a common petrochemical plant, the use of an organic solvent requires the addition of flares and catalytic burners to ensure that emissions are below the threshold established by legislation. On the other hand, ILs have very low flammability (scare quantitative data) as well as negligible vapor pressure and therefore requires no extra units to dispose of vapors.[24] However, the high cost associated with ILs and their toxicity to aquatic life and low biodegradability requires that quantitative recovery be achieved.[25] In this matter, an efficient separation of the products is needed to guarantee high recovery and minimize the washing steps and IL traces in wastewater. Historically, ILs have been often hailed as "green solvents" since many of the investigated ILs in research have very low vapor pressure, which is an important property to reduce atmospheric pollution from the classic volatile organic solvents.[15] The low vapor pressure property also reduces the risk of volatile emissions encountered with conventional organic

solvents during transportation and storage as well as increase the solvent recyclability rate. However, it is important to note that the single property of low vapor pressure does not qualify all ILs to be classified "green solvents". Such an exaggerated and non-assessed claim was toned down in recent IL studies for two main reasons. First is the increase awareness of the relativity concept as there is no solvent can be "green" in absolute sense. A new solvent performance will always have to be assessed for the specific intended application and then compared to other solvent options. The application of this relativity concept is imbedded in the life cycle assessment (LCA) approach, the standard method to evaluate the environmental impact and performance of technologies.[26–28] Currently, the lack of LCA studies to critically assess IL performance in many potential technologies was addressed as one of the main challenges for ILs use at larger scale.[29] Second, there has been evidence that certain ILs have greater ecotoxicity than molecular solvents[30] and there is therefore concern about the environmental benefits of using ILs over traditional solvents. The protic ILs used in ionoSolv pretreatment for example have not been studied for their health and ecological impacts.

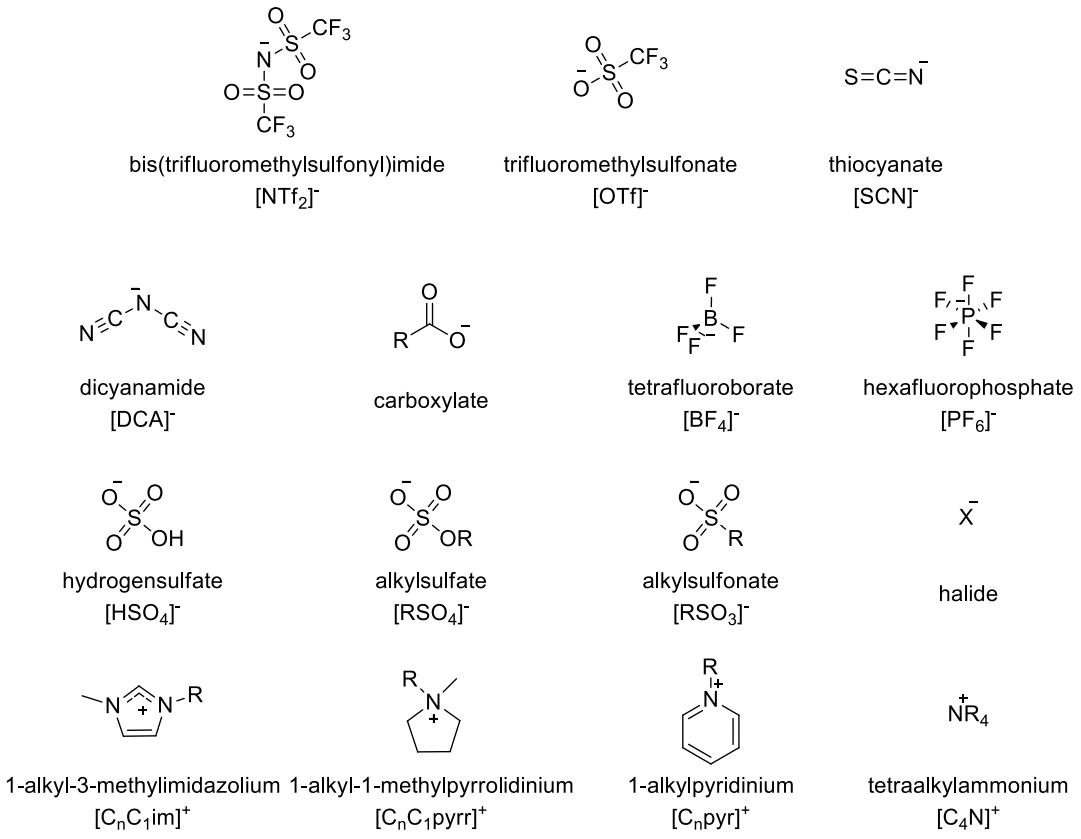

Figure 1.1: Examples for most reported ILs anions and cations

1.2.1 Protic Ionic Liquids

1.2.1.1 General

Protic Ionic Liquids (PILs) are a class of ILs that are synthesized by a single step acid-base neutralization reaction. In fact, the first discovered IL in 1881 was ethanolammonium nitrate, which is a protic IL.[16] PIL is formed when the proton from Brønsted acid acid is transferred to Brønsted acid base as per the following reaction:

$$HA + B \leftrightarrow BH^+ + A^- \qquad (1.1)$$

This leads to a key characteristic that distinguishes PILs from other ILs, which is the availability of proton to form an inter and intra hydrogen bonding network between the anion and the cation as well as dissolved solutes.[11]

Once the proton transfer is complete during the formation reaction of PIL, the only species that should be present ideally are the anion and cation. However, this is not the case in reality as the proton transfer is not always complete which results in the presence of neutral acid and base species. Tso date, there is no established technique to quantify the ionicity of PILs, and questions such as how complete the proton transfer has to be for the product to be called PIL still does not have a robust answer.[31] It is generally accepted for any compound to be referred to as pure, the level of impurities has to < 1%, and this guideline applies to PIL. This means that the degree of proton transfer in the acid-base reaction has to be >99% for the product to be referred to as pure PIL.[31]

The simple acid-base neutralization reaction gives PILs a great economic advantage compared conventional ILs, which are by referred to as aprotic ILs (APILs). The key barrier towards industrial large-scale use of commonly used APILs is their high production cost which is usually 5 to 20 times more expensive compared to organic solvents.[12] The high production cost of APILs mainly stems from: i) high cost of the starting materials, ii) low atom efficiency during their synthesis via alkylation and salt metathesis and, iii) lengthy extensive purification steps which leads to generation of salty wastewater that needs further treatment steps.[32] The significant reduction in processing steps as well as the use of inexpensive starting materials (e.g. mineral acids and amines) make PILs more attractive for industrial application. For example, triethylammonium hydrogen sulfate [TEA][HSO_4] requires 7 steps for its synthesis from raw (oil, N_2,H_2, O_2,S_8,H_2O) compared to 29 steps for 1-ethyl-3-methylimidazolium acetate [C_2C_1im][OAc]. [33] Simplifying the manufacturing steps is of high importance as historically many common industrial solvents were adapted for multi-ton industrial scale because they are generated as inexpensive byproducts in the production line of other higher value products (e.g. acetone is a byproduct of phenol production, toluene is a byproduct of gasoline production). Chen *et al.* was the first to develop a methodology to estimate the production cost of protic ionic liquids at large-scale, where the price ranged between \$1.24 kg^{-1} to \$4 kg^{-1}, depending mainly on the selection amine precuser.[33] In 2020 paper, Baaqel *et al.* have estimated the direct cost of production [TEA][HSO_4] to be \$0.78 kg^{-1} whereas 1-methylimidazolium hydrogen sulfate [H_1Cim][HSO_4] had higher cost of \$1.46 kg^{-1}.[34]

The higher cost of [H_1Cim][HSO_4] is due the larger number of steps to synthesize the amine precursors where the cost to produce 1-methylimidazole was double the production cost of triethylamine ($2.8 kg^{-1} vs. $1.4 kg^{-1}). The same study estimated the production cost of acetone to be $1 kg^{-1}, which highlights the competitive edge PILs have with common cheap organic solvents. Others have estimated the price of two tetramethylguanidinium based PILs to be of $1.94 kg^{-1} and $1.84 kg^{-1}.[35] It is interesting to note that more than 60% of the PIL cost is associated with the amine precursor cost as sulfuric acid price costing only $0.05 kg^{-1}.

1.2.1.2 Key physiochemical properties

APILs are usually hailed for their non-volatile nature as they have extremely low vapor pressure. However, this is not always the case for PILs as many PILs have a measurable boiling point and can be distilled.[36,37] This feature is directly related to PILs formation mechanism. PILs exist in equilibrium with their parent acid and amine. This means that heating a PIL leads to its boiling rather than decomposition as the equilibrium reaction is reversed to form the more volatile neutral acid or base species.[11] In fact, the volatility of a PIL is highly dependent on their ionocity and degree of proton transfer. Ideally, the proton transfer from the acid to the base must be complete such that only ionic species exist to form a true PIL that has and ideal Walden behaviour.[38] However, this is not always the case as depending on the parent acid and base, the proton transfer can be only partial.[39] Yoshizawa *et al.* proposed the use of ΔpKa as a practical qualitative indication of the proton transfer completeness of PILs (or degree of ionicity) without conducting any direct measurement.[38] They defined $\Delta pKa = pKa(HB^+) - pKa(HA)$ where $pKa(HB^+)$ and pKa(HA) represent acid dissociation constants of HB^+ and HA in aqueous environment. It was demonstrated that ΔpKa have a direct impact on the boiling point and volatility of the prospective PIL, with greater ΔpKa suggesting more complete proton transfer and less presence of molecular species, and hence a higher product boiling point.[40,41]

A distinct characteristic of PILs is their supposed Brønsted acidity.[42] Since pH measurements and electrodes are limited to aqueous solutions, one cannot use pH to measure the acidity of IL solvents. In addition, typical pH measurements are limited to dilute and ideal solutions are readings between 0-14, beyond these values the ions [H^+]

or [OH^-] are too concentrated and start interacting with each other, rendering the solution from the "ideal" assumption.[43] The acidity of non-aqueous solvents such as ionic liquids can be measured in several ways with Hammett Acidity being the most established. Since the acidity of a solution lies in its ability to protonate a basic species, Hammett acidity method uses UV-vis probes that measures the extent of protonation of uncharged indicator bases (named B) in a solution.[44]

$$B + H^+ \leftrightharpoons BH^+ \qquad (1.2)$$

The chosen indicators are typically dinitroanilines. Assuming the solvent is dissociating with regards to the base, the Hammett acidity function is defined as the following:

$$H_0 = pK_{BH^+} - \log\left(\frac{[BH^+]}{[B]}\right) \qquad (1.3)$$

in which pK_{BH+} is the pK_a of the conjugate acid of the probe base (referred to ideal dilute solution in water), and [BH^+] and [B] are the concentrations of the base in its protonated and unprotonated forms. Nitroanilines are very weak bases, with pK_{BH+} values from 1 to -11 and therefore they are suitable to measure the acidity of very acidic solvents such as protic ILs. When Hammett bases are partially protonated, there are two peaks present in the UV spectrum, one due to B and one due to BH^+. That the process of measuring H0 in 100% neat ionic liquids is extremely arduous is not an overstatement.[43] From choosing the appropriate base that does not interfere with the IL to the high viscosity of the ILs solvents where the dissolution of the base can be an issue. For these reasons, Hammett acidity measurements for neat ILs are scarce and typically the H_0 is measured for ILs mixed with water or organic solvents to overcome these challenges.[45]

ILs thermal stability is an important characteristic that needs to be evaluated as it directly impacts the useability of the IL at large-scale operations. Low thermal stability at process conditions promotes IL degradation and the accumulation of decomposition products. High decomposition and degradation rate correspond to lower recycling rate and larger make-up stream, which impact the process OPEX significantly. Thermogravimetric analysis (TGA) is extensively used characterization technique to investigate the thermal stability of ILs. Usually, the thermal stability of ILs is assessed by T_{onset}, which is the temperature where the initial decomposition of material starts. T_{onset} is obtained from the TGA curve as the intersection of the baseline weight and the tangent of the weight dependence on the temperature curve.

PILs undergo decomposition when heated at temperatures higher than their T_{onset}, and therefore their onset temperature is taken as the upper limit of their use. George *et al.* investigated the thermal stability of the several alkylammonium [HSO_4]-based PILs where T_{onset} ranged between 294 °C (monoethylammonium) to 277 °C (triethylammonium), with an observed trend of decreasing thermal stability with increasing hydroxylethyl chain number. Overall, the study concluded that the decomposition of alkylammonium [HSO_4]-based ILs occurs at temperatures well above than that for [C_2C_1im][OAc] with T_{onset} of 215 °C.[46] Although T_{onset} provides a good estimation regarding the thermal stability of the IL under investigation, it was found that T_{onset} can sometimes overestimate the thermal stability as some ILs tend to degrade at lower temperatures than their T_{onset}. Some studies have proposed the use of a more practical parameter referred to as the operational upper stability temperature, expressed as $T_{x/z}$, where x represents a given decomposition extent (e.g. 1% weight loss) in z length of time (e.g. 10 hours) to estimate the "long" term thermal stability of ILs. MacFarlane and co-workers determined that $T_{0.01/10}$ for several imidazolium pyrrolidinium and phosphonium ILs, and found them to be ~110 °C lower compared to the T_{onset} temperatures.[47] Clough *et al.* conducted an isothermal analysis using [C_2C_1][OAc] at temperature range between 105 and 170 °C.[48] The outcomes showed high degradation can occur after only a few hours at 120 °C and over 50% degradation after 3 hours at 170 °C, corresponding to $T_{0.01/10}$ of 102 °C. This temperature is below the operating temperature of IL-based procedures, which emphasizes that the famously used [C_2C_1im][OAc] is not suitable for economical biomass processing[48] Therefore, the higher thermal stability of alkylammonium [HSO_4]-based PILs is a key advantage, particularly for biomass processing applications where high operating temperatures (120 to 170 °C) are required, and high recycling rate (>99%) are needed for financially stable process.[49]

1.1.2.3 Ecological impacts

Recently, LCA study was published to compare the ecological impacts (toxicity and biodegradability) of PILs compared to common organic solvent such as acetone (from fossil fuels) and glycerol (from renewable sources).[34] The approach was based monetization method where environmental impact factors are turned into currency referred to as "externalities". The total cost is then calculated as a single factor that combines the solvent production cost (economic) and externalities (environmental

including human health, ecosystem quality and resource availability). Among the investigated solvents, the PIL [TEA][HSO_4] showed the lowest total cost, followed by acetone (Figure -a). The PIL 1-methylimidazolium hydrogen sulfate [H_1Cim][HSO_4] had higher total cost than [TEA][HSO_4] and acetone due to its higher externalities due to the higher impact on human health and ecosystem quality. On the other hand, glycerol had the highest total cost due to both its high direct production cost (high cost of rapeseed soybean oils are costly precursors) as well as the high cost of its externalities where producing 1 kg of glycerol requires almost 100 times more land area than [H_1Cim][HSO_4].

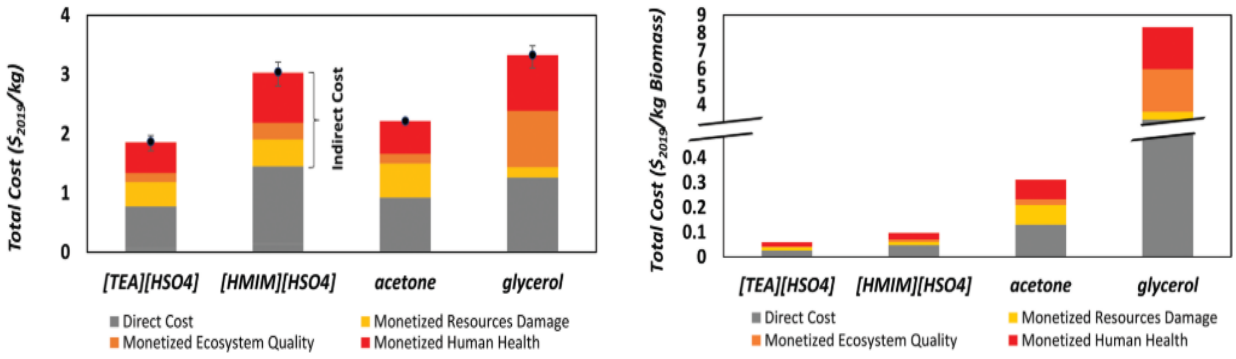

Figure 1.2: a) total cost of solvent production combining direct production cost with externalities b) Total cost of solvent production on a per-weight basis of pre- treated biomass. Taken from reference 34

The authors also highlighted the importance of comparing the total solvent cost considering the solvents' use phase to give more valuable insights about the potential benefit of using one solvent over the other. Therefore, the total cost of the solvents were compared for biomass pretreatment application using the total cost per-weight-of-treated-biomass basis concluded (Figure 1.2-b). In this case, both PILs had much lower cost compared to acetone and glycerol. The reason behind this was attributed to the near 100% recycling rate PILs can achieve in the process compared to the other solvents, which significantly reduces the amount of make-up needed (PIL make up is estimated at 32 kg ton^{-1} vs. glycerol make up 2,500 kg ton^{-1}).[34] This highlighted that solvents produced from renewable resources do not necessarily present lower externalities or lower overall cost compared to solvents derived from fossil resources, including ionic liquids.

1.3 Biomass Valorization

A biorefinery, as defined by National Renewable Energy Laboratory (NREL), is a "facility that integrates biomass conversion processes and equipment to produce fuels, power, and chemicals from biomass".[50] Biorefinery should be an analogous to today's fossil-fuel based refinery that is capable of producing heat, power, chemicals and fuels, yet from renewable biomass feedstock.

Bioethanol is one of the two major targeted liquid fuels from biorefinery since it can be obtained from any plant type, unlike biodiesel for example that can only be obtained from oily plants.[51] The production of bioethanol from biorefinery largely depends on how easy to convert the feedstock to sugar monomers (i.e. glucose) which would in turn be converted by microbial fermentation to produce bioethanol. Biofuels have been accordingly categorized based on their feedstock and subsequent processing as 1st generation biofuels and 2nd generation biofuels (Figure 1.3).[52] 1st generation biofuels include those that are relatively easy to process, for example sugarcane that is available in the form of glucose and thus can be readily fermented to ethanol, or starch (e.g. corn) that needs to be enzymatically hydrolyzed first to glucose followed by fermentation. 2nd generation biofuels on the other hand represents is more challenging to produce as it is based on the use of more recalcitrant feedstock: lignocellulosic biomass.[53]

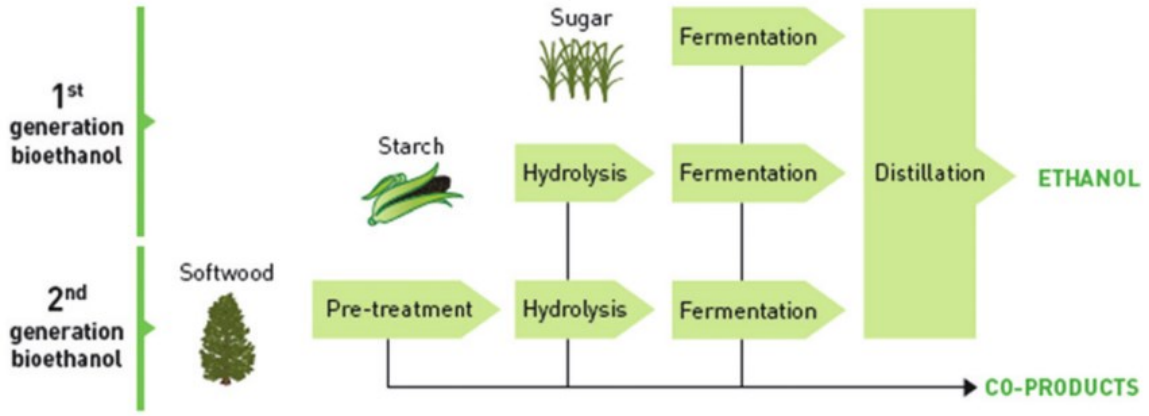

Figure 1.3: 1st generation bioethanol from sugary plants only requires fermentation and in the case of starchy plants a hydrolysis step while 2nd generation bioethanol requires an additional processing step called "pretreatment". Taken from reference 3

1st generation biofuels and their processing steps have been known to humankind since ancient times, way before the reliance on fossil-fuel. Early engines have been engineered with the intension that they will be operated using biofuels such as bioethanol or biodiesel.[54,55] All these attempts have been demolished with the exponential growth of oil industry and the increase reliance on oil as source of energy. It was not until few decades ago when the biofuels re-sparked the interest of the scientific community as potentially more sustainable alternative to fossil fuels. These efforts have eventually slowed down following the long debate whether these biofuels do provide sustainable solution due to the direct competition with food production and what is known as "land-use change" impacts.[56] The land-use change associated with 1st generation biofuel production can be defined as the unintended consequences of increasing CO_2 emissions due to the expansion in using crop agricultural lands for biofuel production in response to the consistent growing demands of fuels.[56] Overall, due to the land-use change associated effects with production of 1st generation biofuels (e.g. farm land losses, overall CO_2 emissions, irrigation water, fertilizer use), it was realized that the downsides of 1st generation biofuels may outweigh their intended benefits.[57,58] It is important to note that reports and studies on environmental benefits and energy efficiency of 1st generation biofuels remain to be highly controversial with high degree of variability and uncertainty due to the inherent complexity and changeability of the system inputs.[59] The dilemma associated with 1st generation biofuels sparked the interest to switch to what is known as 2nd generation biofuels (or advanced biofuels) which is based on the utilization of lignocellulosic biomass; the woody non-edible parts of the plants. The lignocellulose biomass usually comes from waste sources such as agricultural waste (e.g. corn stover, sugarcane bagasse), forest waste (hardwood and softwood) or dedicated energy crops (e.g. *Miscanthus*, switchgrass). This makes lignocellulosic biomass essentially an abundance renewable resource for biofuel production with virtually no direct competition with food production.[60] However, the use of the lignocellulosic biomass comes with the price of introducing an additional processing step called "pretreatment" or "fractionation".[50,61] The objective of a pretreatment process is to deconstruct the structure of the lignocellulose to increase the subsequent yield of glucose in the enzymatic hydrolysis step which would increase the overall ethanol production. The lignocellulose fractionation step is highly likely to account for a significant fraction of the total energy consumption in the process chain.[44] This has indeed motivated

researchers and engineers to investigate several pretreatment/fractionation processes aiming to reduce the process energy intensity which would in turn makes the overall bioethanol production more cost-effective and competitive to fossil-fuel.[51,52] Various pretreatment methods are currently under development, such as steam explosion[64], Ammonia Fiber Expansion (AFEX),[64] dilute acid,[64] hot water,[64] organosolv[65] and ionic liquid pretreatment,[66] including ionoSolv pretreatment.[67,68] It is important to note that pretreatment, enzymatic hydrolysis and fermentation of lignocellulosic biomass is all under the biological conversion of this renewable source to produce biofuel.[69] The thermochemical conversion of lignocellulosic biomass which includes combustion, pyrolysis or gasification[70–72] are alternative promising routes to utilize this renewable resource to produce heat, bio-oils, charcoal and syngas.

1.4 Lignocellulose structure

Lignocellulose is the material that makes up the cell walls of woody plants and it is composed of three biopolymers: cellulose (~35-50%), hemicellulose (~30-40%) and lignin (~10-35%). These three polymers are arranged in a three-dimensional structure that has naturally evolved to resist degradation and deconstruction, which is essential to maintain the plant structural integrity. The remaining fraction of lignocellulose biomass includes proteins, extractives (e.g. waxes and lipids) and ash.[73] The linear cellulose bundles are surrounded by the branched hemicellulose which is in turn cross linked with lignin that fills the space between the cellulose/hemicellulose bundles. The composition of lignocellulose biomass (i.e. wt% of lignin, cellulose and hemicellulose) varies depending on the species, growth conditions and growth stage.[3]

Unfortunately for us, the increased structural complexity of lignocellulose makes it highly recalcitrant to mild chemical or biological modification.[51] Therefore, the use of lignocellulose biomass as a viable feedstock in a biorefinery requires integrating an additional processing step called “pretreatment” or “deconstruction”.[73,74] As mentioned earlier, the objective of this processing step is to effectively deconstruct the rigid lignocellulose structure to facilitate their subsequent processing to fuels, chemicals and materials. For bioethanol production, the deconstruction effect improves the enzymatic hydrolysis of the carbohydrate polymers to their sugar monomers. For biochemicals and materials production, the fractionation process is fundamentally important to effectively isolate each biopolymer from the lignocellulose matrix for subsequent upgrading and

transformation to value-added products.[75] Lignocellulosic biomass is categorized as: i) softwood (seed producing plants, they have needles instead of leaves), ii) hardwood (reproduce by flowers and characterized with big leaves) and, iii) grasses and dedicated energy crops such as switchgrass and *Miscanthus*. Each plant types presents a promising candidate in the establishment of the future biorefinery.[76,77] Each type of these lignocellulose is different in terms of chemical composition of cellulose, hemicellulose and lignin which consequently impact , their deconstruction efficiency.[76]

1.4.1 Cellulose

Cellulose is the most abundant biopolymer on earth with a formula composed solely of glucose units linked together via 1-4-β glycosidic bonds, giving its linear macromolecular formula $(C_6H_{10}O_5)_n$, where n = 10,000 to 15,000, depending on the cellulose source material. Each glucose unit contains primary C6 hydroxyl groups as well as two secondary hydroxyl groups (C2-OH and C3-OH).[79] The hydroxyl groups gives cellulose hydrophilic character for cellulose. On the other hand, the abundant of C-H groups in the axial direction gives the cellulose its hydrophobic nature (Figure 1.4).

Cellulose serves as dominant reinforcing phase in woody plants, cotton, hemp and other plant-based materials. Cellulose forms a large fraction of the plant cells in lignocellulosic biomass, with its composition in the range of 35 to 50 wt%. Each anhydrous glucose molecule in a cellulose polymer chain forms three hydrogen bonds: two hydrogen bonds with adjacent glucose molecules on each side of the same chain and one hydrogen bond with glucose molecule in another polymer chain that lies on the same plane.[80] On the other hand, the polymeric planes of cellulose interact via Van Dar Waals bonds.[81] Based on the monomer glucose, each cellulose chain is referred to as “glucan”. Each glucan chain is highly aligned, ordered and bonded which gives it a crystalline structure needed to resist attacks and biodegradation. The glucan chain in cellulose is referred to as elementary fibril. When multiple glucans come together, they form a “microfibril” which are relatively stiff which gives the cell wall the required rigidity.[80] Due to its high molecular weight and high degree of polymerization, cellulose is insoluble in water and most of the inorganic solvents. The high intermolecular hydrogen bonding as well as Van Dar Waals interactions between cellulose fibers contribute to the insolubility of cellulose in many solvents.

The morphological hierarchy of cellulose is defined by elementary fibrils, which pack into larger units called microfibrils, which are in turn assembled into fiber.[82] Within the cellulose elementary fibrils, there are regions that are highly crystalline and other disordered amorphous regions. This change in morphology within the cellulose fibrils occur during the synthesis phase of the microfibrils in the plant cell, where some of the hemicellulose get physically trapped within the microfibril, thereby making this region more amorphous compared to the rest of the crystalline microfibirl.[83] Overall, the degree of crystallinity of native cellulose varies depending on the feedstock and isolation method with typical range between 40 to 70%.[84]

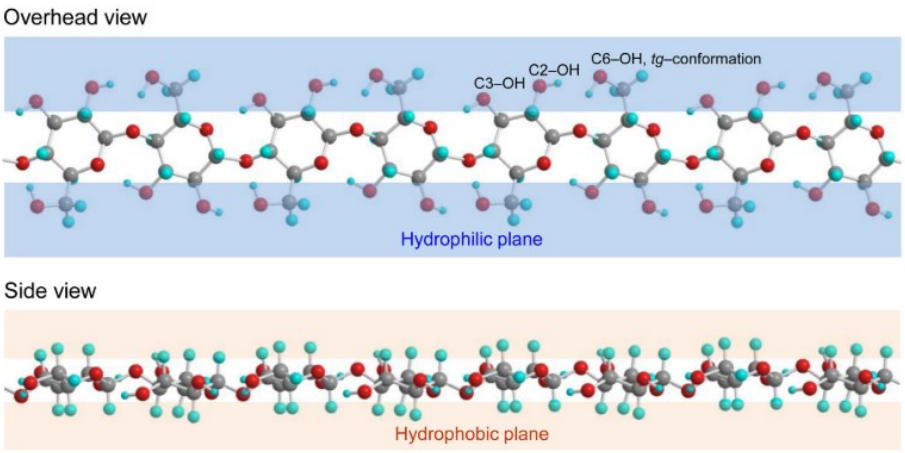

Figure 1.4: Hydrophilic and hydrophobic planes of cellulose molecules, marked with the primary C6–OH, and secondary C2–OH and C3–OH groups in glucosyl unit, corresponding to cellulose I structure taken from reference 79

There are six molecular orientations of crystalline cellulose, with cellulose I, II, III and IV being the most common polymorphs.[80] Cellulose I is the crystalline cellulose that is naturally produced by a variety of organisms (trees, plants, tunicates, algae, and bacteria), it is sometimes referred to as "natural" cellulose. Its structure is thermodynamically metastable and can be converted to either cellulose II or III. Cellulose II is the most thermodynamically stable structure of cellulose and it has high technical relevance as it can be produced by two processes: regeneration (solubilization and recrystallization) and mercerization (aqueous sodium hydroxide treatments). Cellulose II has been used to make cellophane (transparent films), Lyocell, Viscose and Tencel™ (synthetic textile fibers). Cellulose III can be formed from Cellulose I or II through liquid ammonia treatments, and subsequent thermal treatments can then be used to form Cellulose IV.[80]

Cellulose-based materials are heavily used in industry today and it is typically obtained from wood pulping process using Kraft process or Acid Sulphite process, depending on the end-use of cellulose.[51] Kraft process is used mainly used to produce cellulose for paper and packaging applications as the process is capable to retain the mechanical integrity and strength of the cellulose fibers compared to the acidic sulphite process. The letter Sulphite process is used mainly to produce high quality cellulose pulp called "dissolving pulp".[61,85] Dissolving pulp, as the name indicates, is not made for paper based applications, but to be dissolved and further spun to produce cellulosic textile fibers . The dissolution process of dissolving pulp cellulose takes place by derivatization using carbon disulfide (CS_2) as a solvent which is used in the Viscose process, or direct dissolution using N-methylmorpholine N-oxide (NNMO) in a process known as the Lyocell process.[86] Alternatively, dissolving grade pulp can react with variety of chemicals forming wide range of cellulose derivatives (e.g. cellulose ethers, cellulose triacetate, methylcellulose).[87] Dissolving pulp is bleached typically in a multi-stage bleaching process to reach high level of purity and brightness. Dissolving pulp needs to be highly pure with alpha-cellulose content >90%. Obtaining a very low hemicellulose content in dissolving pulp is very important as hemicellulose can interfere with the cellulose reactivity and solubilization in the subsequent processes.[88] Kraft process can also be used to produce the high-grade dissolving cellulose pulp, however, an acid hydrolysis step needs to be added prior to the main process, and the process is called pre-hydrolysis Kraft process (PHK). The prime purpose of the pre-hydrolysis step is to effectively remove the hemicellulose polymer that is typically not effectively removed in the stand-alone Kraft process. The PHK process accounts for 56% of the world's dissolving pulp production as per 2014 data, while Acid Sulphite pulping account for the reminder. The major market of dissolving pulp is Viscose yarn production, with 88% of the dissolving pulp from PHK and 80% of that produced from the AS process are used to produce Viscose yarn.[89] The reminder smaller fraction of the dissolving product is used to produce specialty cellulose products, mainly; Cellulose acetate (including cigarette filters), microcrystalline cellulose (pharmaceutical and food additives), nitrocellulose (printing inks, paints and food casings) and cellulose ethers.[90]

The use of cellulose as a renewable and sustainable building block for production of value-added chemicals has been recognized by the US Department of Energy. These value-added chemicals include levulinic acid[91], lactic acid[91] and 5-hydroxymethyl

furfural (5-HMF)[92]. Figure 1.5 shows the route to obtain 5-HMF and levulinic acid from glucose (cellulose monomer) which involves dehydration reaction followed by hydrolysis.[93] 5-HMF is a versatile molecule to produce chemicals platform and it is listed by the US Department of Energy as one of the most important renewable chemicals that can be obtained from lignocellulose biomass.[94] A key product that can be obtained from 5-HMF is 2,5-furandicarboxylic acid (FDCA), which has been proposed as a replacement for terephthalic acid in the production of polyesters. 5-HMF can also be converted to 2,5-dimethylfuran (DMF), a liquid that is a potential biofuel with a greater energy content than bioethanol. The hydrolysis of HMF produces levulinic acid which is a versatile building block for fuel additives, polymer precursors, and resin precursors.[91]

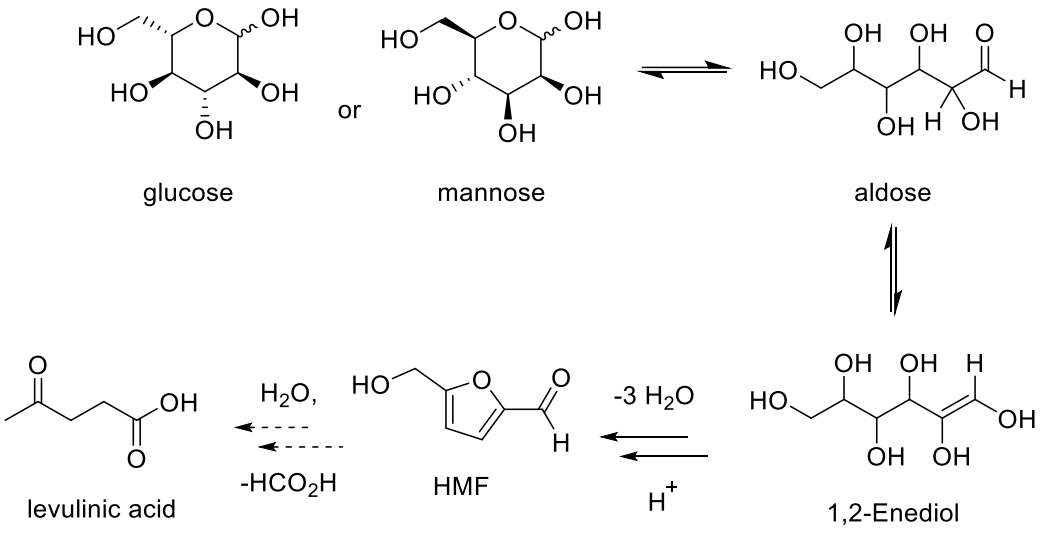

Figure 1.5: Proposed acid catalysed mechanism for the formation of HMF and levulinic acid from glucose or mannose. Taken from reference 93

1.4.2 Hemicellulose

Hemicellulose is name that is given for the group of heterogeneous polysaccharides that are made of hexose sugars (e.g. glucose, mannose, galactose) and pentose sugars (xylose, arabinose).[95] Hemicellulose is the 2nd largest component of lignocellulose biomass after cellulose as it makes up around 20 to 30% of its weight. The amorphous hemicellulose binds non-covalently the cellulose microfibril surface increasing its overall stiffness.[3] In contract to cellulose, hemicellulose polysaccarides are branched and have much less degree of polymerization of around 100 to 200 units. In addition,

polysaccharides in the hemicellulose have some other functional groups such as acetyl, methyl cinnamic, glucuronic and galacturonic acids. It has been proposed that the acetylation of some of the hemicellulose sugars increases its affinity to lignin which increases the overall cohesion of the lignocellulose biopolymer matrix.[96] Due to the lower degree of polymerization and branching, hemicellulose polysaccharides are much easier to hydrolyze under mild conditions compared to cellulose. The characteristics and composition of hemicellulose is different from one species to another. For example, mannan (C_6 sugar) is the main component in softwood's hemicellulose (e.g. galactoglucomannan polysaccaride) while xylan (C_5 sugar) is the highest in hardwood and grasses (e.g. glucuronoxylan polysaccaride).[3]

Similar to what happens in cellulose, hexoses sugars in hemicellulose can also undergo dehydration reactions forming 5-HMF. The pentose sugars on the other hand dehydrate to form furfural under acidic conditions (Figure 1.6) or in the presence of metal chlorides.[97] Similar to 5-HMF, furfural is also a versatile platform chemical and promising candidate for the replacement of the production of many furan-based resins and chemicals.[98,99]

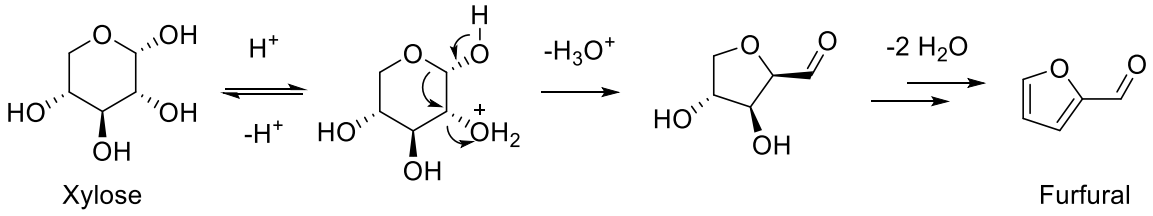

Figure 1.6: Proposed acid catalysed formation of furfural from xylose. Taken from reference 93

1.4.3 Lignin

Lignin is an aromatic heterogeneous polymer that fills the space in the cell wall. Lignin plays a crucial role in providing mechanical reinforcement and structural rigidity to the polysaccharides and further resistance to biological and microbial attacks.[100] Lignin is a hydrophobic and water insoluble polymer which provides water-proofing for the cell wall. The biosynthesis of lignin is a highly complex process that involves random radical polymerization of three monomers: coniferyl, sinapyl and p-coumaryl alcohols.[3] Once polymerized, the monomers (also called monolignols) are identified based on their

aromatic structure as guaiacyl (G), syringyl (S) and p-hydroxyphenyl (H) subunits, respectively (Figure 1.7). These subunits are different in terms of their degree of methoxylation. The S unit has two methoxy groups located at C_3 and C_5 positions; the G unit only has one methoxy group at C_3 position; while the H unit has no methoxy groups directly attaching to the aromatic ring. The free position C_5 position in G unit makes the ring reactive and more likely to C-C crosslinks during lignin biosynthesis as well as during deconstruction/delignification process.[101] In contrast, the C_5 position in the S unit has a methoxyl group which makes it unable to crosslink during deconstruction. The C-C crosslinking in the G unit is not readily hydrolyzed, which makes softwood delignification during biomass deconstruction more challenging compared to hardwood or grasses deconstruction. The proportion of these subunits is different from one lignocellulose source to another.[57] Softwood lignin is made almost exclusively from G unit while hardwood lignin has equal proportions of G and S units. On the other hand, the three subunits are found in grass lignin.[102] S-lignin features higher levels of labile β-*O*-4' ether linkages which are readily cleavable during pretreatment, producing small fragments which could facilitate lignin removal.[103] The influence of H-lignin on biomass recalcitrance has been less investigated, though several studies have revealed that high H-lignin in grasses exhibited reduced biomass recalcitrance.[103] The variation in lignin composition as well as subunit proportion have major impacts of the delignification chemistry which would directly impact the overall deconstruction process.

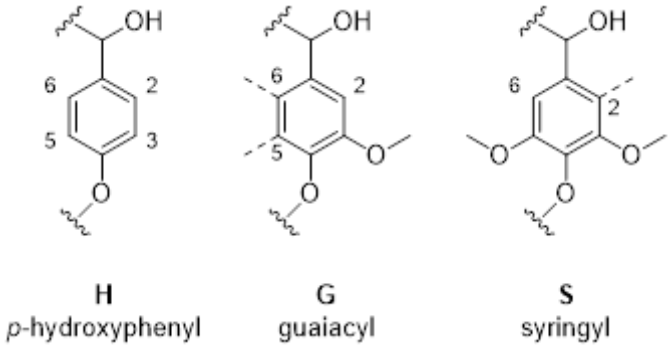

Figure 1.7: Structures of the building block monomeric aromatic precursors of lignin

Lignin is heterogeneous with random branched structure with C-O-C bond being dominant as an ether bond or as part of the furan ring. The β-O-4' ether bond specifically accounts for about 45 to 48% of the bonding pattern in native lignin while ether bonds such as 4-O-5 present in a lesser extent. C-C bonds are also highly present in lignin as β-5, β-1, β- β' and 5-5'.[70,104] Up to date, the complete full picture of native lignin structure can't be drawn and even its natural degree of polymerization remains unknown. This highlights the very complex polymeric structure of native lignin with >20 known bonding pattern, making lignin the strongest and most complex biopolymer known.[101]

With respect to pretreatment and deconstruction of lignocellulose biomass, the presence of lignin is considered one of the prime reasons behind the difficulty in processing lignocellulose biomass and thus the necessity to have a pretreatment step.[105,106] Lignin shields the cellulose which physically prevent the enzymes from hydrolyzing the cellulose to glucose. Lignin also renders the enzymatic hydrolysis of cellulose by binding ineffectively with enzymes, restricting the necessary movement for enzymes to degrade the polysaccharides.[107] Therefore, delignification (*i.e.* lignin extraction from biomass) is one of the major mechanisms adapted in multiple deconstruction technologies to enhance cellulose accessibility to enzymes and improve overall glucose yield – to be discussed in more details in the following section.

It is also worth mentioning that the aromatic structure of lignin macromolecule has sparked the interest to be a renewable source of aromatic-based hydrocarbons.[108] Therefore, based on the great potential lignin holds, developing lignin depolymerization techniques became the gold-rush for many academics worldwide.[108] Lignin chemical depolymerization techniques include homogenous acid/base catalyzed deconstruction, oxidative depolymerization using strong oxidizing agents and ionic liquid catalyzed depolymerization.[101] Currently, applications for lignin are limited and lignin-derived products remain at early stage of development with >80% of lignin produced worldwide from pulping industry being used as a heating source in the process. Lignin is not typically recovered as a solid in a conventional Kraft process. Once extracted in the process liquor (called black liquor after lignin extraction), the black liquor is sent to a multi-effect evaporator to be concentrated before sent to boilers for heat recovery.

The cooking chemicals (*i.e.* NaOH and NaHS) are recovered. There are two current commercial processes where lignin is recovered from the black liquor: LignoBoost and LignoForce. The separation of lignin from the black liquor in these processes allows the use of lignin as a solid fuel and for specialty chemicals.

1.5 Deconstruction of lignocellulose

1.5.1 Paper pulping

The deconstruction process for lignocellulosic biomass did not originate for biofuel production purposes. It was established back in the 19th century for pulping and paper industry. The Kraft pulping is the most dominating pulping or deconstruction process that has been employed for decades in the paper production industry using softwood as a feedstock. In Kraft pulping, an aqueous mixture of sodium hydroxide (NaOH) and sodium hydrogen sulfide (NaHS) (called the cooking liquor or white liquor) is used to deconstruct the lignocelluosic biomass in a continuous or batch pressurized digesters at 130-180 ºC for several hours. [21,50] Lignin dissolves and fragments in the liquor during deconstruction leaving a cellulose rich pulp. The presence of strong nucleophiles in the liquor such as sulfide ions aids in lignin removal and limit lignin re-condensation reactions.[3] The spent liquor (also called black liquor) is sent to an energy intensive multi-step recovery system where lignin is recovered and used in the process for energy production and liquor is recycled back to the process. Sulfite pulping is another widespread pulping process that uses sulfurous acid salts to extract lignin. These conventional deconstruction processes for wood can in theory be used for bioethanol production. However, these processes have been optimized over the years to produce high purity cellulose fibers with high fiber strength to reduce bleaching requirement. [109] This requirement does not necessarily match the biorefinery objectives which targets high quality sugar yields (C_6 and C_5) to be produced in economically viable and environmentally sustainable manner along with other possible value-added product streams. Kraft pulping industry is also known to produce large volumes of pollutants that are discharged to air or water streams, making the environmental impacts of pulp and paper industries a major global concern. [110,111]

1.5.2 Pretreatment for biorefinery

In the context of biorefinery, the deconstruction of lignocellulose biomass has been re-defined to match its technical objectives and it has been given the name “pretreatment”. The main technical objectives of a pretreatment process include[112]: i) reduce the

recalcitrance of the lignocellulose biomass, ii) obtain high glucose yield for subsequent fermentation, iii) avoid the formation of carbohydrate degradation products that inhibit enzymes and reduce sugar yield, and iv) maximize the formation of other valuable high quality products such as lignin.

Several pretreatment processes have been developed over the years aiming to overcome the chemical and structural complexity of the lignocellulose biomass to achieve the outlined technical objectives. [78–84] These pretreatment routs include thermochemical. biological and mechanical processes. Biological processes are based on the use of enzymes and microorganisms such as fungi to attack cellulose or lignin. Although biological processes have the advantage of low energy input and no chemical use, they are the least famous and least used due to their very slow kinetics and large infrastructure, which makes economically and commercially unattractive. Mechanical pretreatment is based on the use of mechanical methods such as ball milling, hammer milling and disk milling to increase the accessible surface area of cellulose. Mechanical methods are known to be highly energy intensive and they can only achieve limited glucose digestibility (<50%). For instance, pretreatment based exclusively on ball-milling has been estimated to require >1500 kWh ton^{-1} of wood, which corresponds to ~30% of the energy content of wood itself.[120] Other mechanical pretreatment methods are based on the use of microwave radiation and are often combined with chemical methods to improve cellulose accessibility and digestibility. However, microwave-based processes do not have a commercial appear due to their high energy input.

The four main thermochemical mechanisms adapted for lignocellulose pretreatment processes are: i) particle size reduction (e.g. ball milling),[121] ii) decrystallizing cellulose (e.g. ionic liquid dissolution process)[122] and, iii) hemicellulose extraction (e.g. dilute acid, liquid hot water processes, steam explosion), [106,64] iv) protein and lignin extraction (e.g. AFEX process) and v) hemicellulose and lignin extraction (e.g. alkaline, Organosolv , IonoSolv processes).[123] While the above technical objectives can be achieved to varying extent by multiple pretreatment technologies in small scale, the real challenge that faces all pretreatment technologies up to date is the techno-economic effectiveness; low capital cost, low operating cost and low energy requirement.[124] In reality, it is difficult to find such an ideal process, however, two of the three points have to be achieved for the process to be attractive for scale-up. Steam explosion and dilute acid pretreatments

are the only two processes that have been reported as “cost-effective” relative to the other pretreatment technologies and two are the nearest to communalization thus far. A demonstration plant by IOGEN Co. in Canada is based on steam explosion process with plant capacity of 40M liters per year.[125]

Steam explosion process applies high temperature and pressure using steam (10 to 50 bar) followed by a sudden pressure reduction which causes the cells to explode and cleave the lignin-hemicellulose bonds.[126] Steam explosion functions as an auto-catalyzed hydrolysis process where acetic acid and other release hydrolyzed acids from the hemicellulose acts as a catalyst for the hydrolysis. The effective removal of hemicellulose from the biomass matrix and improved exposure of the cellulose fibers increases the cellulose enzymatic digestibility to glucose. Dilute acid uses sulfuric acid (0.1 t 1 wt%) as a catalyst at 160 – 220 °C for 5 to 30 minutes. The acid extracts the hemicellulose polymer and depolymerizes it into oligomers, sugar monomers and dehydration products such as furfural and formic acid.[127] Despite the very limited delignification achieved in dilute acid pretreatment, the method is highly effective in increasing the enzymatic digestibility of low-lignin containing biomass (e.g. agricultural waste), with limited success using softwood and hardwood. The release of sugars during acidic pretreatment reduces the enzymes loading needed to hydrolyze the biopolymers. However, very careful optimization of process conditions are needed for both steam explosion and dilute acid pretreatment due to the high tendency of inhibitory products, namely sugar dehydration products such as furfural and 5-HMF as well as weak organic acids such as formic acid, levulinic acid. The formation of these compounds retard the downstream enzymatic digestion and fermentation processes as they alter the pH of the medium.[51]

Alkaline pretreatment uses alkali solutions such as lime, NaOH and ammonia, resembling the Kraft pulping, process to delignify the biomass, thus improving cellulose accessibility. Alkaline-based processes typically use lower operating temperatures and pressures; however the time of the operation extends to several hours (6 to 8 hours). During the pretreatment, the ester and ether linkages in lignin structure are cleaved, allowing for its depolymerization and solubilization in the pretreatment medium. In contrast to acidic pretreatment methods where extracted lignin can easily re-deposit on the surface of the biomass, alkaline mediums have higher lignin solubility. The removal

of lignin (*i.e.* delignification) that shields the cellulose in the biomass matrix allows larger exposure of the cellulose to enzymes during saccharification. AFEX process has particularly gained huge attention in recent years due to its high effectiveness in delignifying herbaceous residues of low lignin content, with quantitative glucose yield.[128] Compared to acidic-aqueous based pretreatment methods, alkaline-based pretreatment methods produce less inhibitors. The nature of the inhibitors derived from alkaline-based pretreatment are mainly phenolic groups compounds derived from lignin such as aromatic acids and vanillin.

Organosolv pretreatment is a biomass fractionation/delignification method where an organic solvent – (e.g. acetone, ethanol, butanol, ethylene glycol, benzene) is used as the main pretreatment medium.[129,130] The process can operate with or without acid catalyst and typically the organic solvent is mixed with water (20 to 80 wt%) and the biomass is exposed to the medium at 150 to 200 °C for 30 to 150 minutes. A key feature of OrganoSolv process as a fractionation method is the pre-removal of lignin as a separate by-product stream, whereas all the previous methods do not recover lignin. The recovery of lignin allows it to be used for heat recovery to satisfy the process energy requirement through heat integration. In addition, removal of lignin reduces the enzymes loading and process equipment size. High delignification for wide variety of biomass were able to be achieved using Organosolv pretreatment (60 to 90% lignin removal).[131] In addition, lignin produced by OrganoSolv pretreatment is typically high pure, which makes it also high valuable to be used for lignin-based applications.[132] The key disadvantage of OrganoSolv process is the use of hazardous organic solvents which require high pressure equipment and very strict handling procedure.

1.6 Ionic liquids and biomass

In 2002, Rogers *et al.* explored the use of ILs to extract cellulose from variety of hardwood and softwood lignocellulosic feedstocks. It was found that 1-butyl-3-methylimidazolium chloride [C_4C_1im]Cl was able to partially dissolve the woody material.[109] Cellulose was recovered by adding an antisolvent (1:1 acetone-water, dichloromethane or acetonitrile) and the properties of the reconstituted cellulose were found to be very similar to the properties of pure microcrystalline cellulose subjected to the same process. In the same year, Kilpeläinen *et al.* published a study to investigate the use of several imidazolium-based ILs with chloride anion in dissolving hardwood and softwood feedstocks.[133] It was found that the solubilization efficiency and dissolution profiles are highly affected by the

wood particle size. The addition of water as an antisolvent recovered an amorphous material that constitute mixture of the wood components. The amorphous nature of the recovered material sparked the interest to investigate its enzymatic digestibility where it found that 60% of the theoretical amount of glucose was released vs. 12% release from the untreated control. Even though the solubility of the lignocellulose materials did not exceed 10 wt%, these early studies established the foundation of a new research field of using ionic liquids as novel platform for lignocellulose biomass processing. In the past decade, two IL-based pretreatment approaches were developed: i) biomass dissolution process (non-selective solubilization of the biomass components) and ii) fractionation process (selective solubilization of lignin and hemicellulose). Each approach uses ionic liquids that interact differently with lignocellulose biomass biopolymers.[3]

1.6.1 Dissolution process

The use of ionic liquid for biomass dissolution has gained great attention in the recent years with the largest data being collected for 1-ethyl-3-methylimidazolium acetate [C_2C_1im][OAc][23] and 1-butyl-3-methylimidazolium chloride [C_4C_1im][Cl].[109] The main highlight in IL dissolution process is the use of a biomass-dissolving IL that is capable to solubilize the entire biomass biopolymers; cellulose, hemicellulose and lignin. This is usually conducted by heating the biomass-IL mixture at temperatures between 90 to 160 ºC for several hours, depending on the feedstock and IL used.[134] Following, two step precipitation is conducted using an anti-solvent (water or organic solvent/water mixture) to first precipitate the cellulose and then precipitate lignin.[109] The mechanism behind the biomass dissolution is related to largely disturbing the hydrogen bond network in cellulose via forming new stronger hydrogen bond between IL anion (e.g. acetate, formate or chloride - Kamlet-Taft β value > 0.8; strong hydrogen bond acceptors) and hydroxyl groups in cellulose.[135] Therefore, the recovered cellulose becomes much less crystalline and more amorphous, which significantly enhances initial enzymatic hydrolysis rate. Although biomass dissolution process using ILs was studied extensively by several research groups and was given a special attention by Joint BioEnergy Institute (JBEI) – US Department of Energy Bioenergy Research Center. During the course of the process development, several disadvantages were identified as potential process limiting-step in a commercial operation. These disadvantages include: i) ILs used in dissolution process up to date suffer from low thermal stability at processing temperature, e.g. T_{onset} of [C_2C_1im][OAc] is 215 °C. The low thermal stability of the IL

translates to lower recycling rate and therefore larger IL-make up stream and ii) IL used has to be completely dry since cellulose is highly insoluble in water; this provides technical and economical challenge due to the extensive drying requirement and the unavoidable build-up of water in the process.[3,135]

1.6.2 Fractionation process

The first patent of using ionic liquids to selectively extract lignin from the biomass matrix was published by D. R. MacFarlane *et al* in 2008.[136] They indicated that using ILs of organic or inorganic cation along with organic acid-based anion (mainly sulfonate) can fractionate lignocellulosic material where lignin is solubilized in the ionic liquid and a cellulose-rich pulp remains highly intact during the process. The selective dissolution of lignin and hemicellulose in the IL medium gives the process the "fractionation" feature, with lignin removal (or delignification) being the main deconstruction mechanism. Lignin was subsequently recovered by adding an antisolvent (e.g. water), changing the solution pH or temperature. Another patent was filed in 2008 by S. Varanasi *et al.* to describe the same biomass fractionation effect using ionic liquids and the subsequent successful enzymatic hydrolysis of cellulose to glucose.[137] Interestingly, the ionic liquids used for the fractionation were $[C_2C_1im][OAc]$ and $[C_4C_1im]Cl$, which are the same ionic liquids reported earlier for their ability to dissolve the whole biomass components, including cellulose. What made the major difference between the two processing strategies was the use of much higher biomass loading (33 wt% vs. <5 wt% for dissolution[109]) which weakens the ability of the ionic liquid to dissolve the entire biomass components. Alternatively, mixing the cellulose dissolving ILs with water reduces the ability of these ILs to form hydrogen bonds with the cellulose.[46]

There are several advantages associated with the use of fractionation processes due to the distinctive process feature of lignin pre-extraction. These advantages include; i) reduced enzymes loading in saccharification step due to lower lignin content, ii) high glucose yield due to reducing non-productive binding with lignin, iii) lower inhibitors derived from lignin-carbohydrate (pseudo lignin) products, iv) smaller enzymatic hydrolysis and fermentation reactors due to pre-extraction and, v) isolated lignin as a solid by-product with specialized functional groups that can be used as a solid fuel or converted to high-value added products. [15,57,102] IonoSolv is another example of IL-based biomass fractionation process.[6,46,140] The name is analogous to Organosolv process due to the distinct similarities between the two methods biomass as fractionation processes.

IonoSolv process is based on the use of low-cost protic ionic liquids (PILs) to achieve effective delignification of biomass. The PILs used in the process are synthesized in one-step acid-base reaction using inexpensive amines and mineral acids (HCl or H_2SO_4). The estimated bulk-scale production cost of these PILs was a major milestone in the process development, solving a key process bottleneck that all other IL-based processes suffer from: the high cost of ILs solvents.

IonoSolv fractionation process has multiple unique features compared to IL dissolution process starting from the fundamental mechanism to the overall process flow. IL dissolution process has been relying on small number of ILs, namely $[C_2C_1im][OAc]$ and $[C_4C_1im]Cl$, which have high-hydrogen bond basicity and low hydrogen bond acidity; an essential requirement for cellulose solubility.[119,120] These ILs suffer from low thermal stability[48], low tolerance of water[143], and high production cost (e.g. $[C_2C_1im][OAc]$ production cost range from $20 to 101 per kg).[144] On the other hand, ionoSolv process uses aqueous mixtures of low cost PILs that are capable to dissolve lignin with estimated price of $0.78 to 1 per kg for alkylammonium $[HSO_4]$-based PIL.[145,146] In addition, there are larger number of ILs capable of dissolving lignin than are capable of dissolving cellulose, which gives fractionation-based processes greater flexibility in terms of IL structural design. In previous IonoSolv studies, several $[HSO_4]$-based PILs were used such as 1-butylimidazolium hydrogen sulfate, $[HC_4im][HSO_4]$[138], triethylammonium hydrogen sulfate $[TEA][HSO_4]$[6], and *N,N,N* di-methylbutylammonium hydrogen sulfate $[DMBA][HSO_4]$[147]. The delignification of the biomass using these ILs is governed by the nucleophilic acidic nature of $[HSO_4]$ anion that acts as a catalyst or reactant during delignification.[148,149] Hemicellulose removal also takes place to near quantitative in these $[HSO_4]$ PIL mediums. IonoSolv studies have considered the delignification of wide variety of promising lignocellulosic biomass feedstocks such as *Miscanthus*[6], pine wood[147], Eucalyptus[150], willow[151], sugarcane bagasse and high-ash agricultural resides[152].

Gschwend *et al.* recently proposed a four-stage mechanism that explains delignification during ionoSolv process.[153] The first stage of the lignin extraction in $[HSO_4]$- based PILs is initiated by the hydrolysis of the glycosidic bonds in the lignin-carbohydrate complexes. Simultaneously, mild cleavage within the lignin macromolecules start taking place, which helps the lignin fragments to escape the lignocellulose matrix. During the

second stage, the extraction of the shorter lignin polymer overlaps with the further hydrolysis and fragmentation of the already extracted lignin. In the third stage, the delignification process slows down and most of the extracted lignin continue to hydrolyze and starts forming more condensed structures. In the final fourth stage, lignin hydrolysis ceases and condensation reactions continue where lignin fragments undergo further re-polymerization reactions or react with hemicellulose degradation products. Controlling the delignification mechanism/stages can be achieved by careful optimization of the pretreatment severity defined by the operating condition (temperature, time, IL concertation, solid loading) or the IL structural design (acid: base ratio, cation/anion selection and Hammet acidity). Ideally, it is desired to achieve the second stage of delignification as the further progression towards the third and fourth stages delignification stages which induce the formation of what is known as "pseudo-lignin" or "humins". The term pseudo-lignin is used to describe lignin-like polymer structures that are formed in the pretreatment medium due to the polymerization of the polysaccharides degradation products (e.g. furfural), and/or the polymerization with extracted lignin fragments.[154] For an economical bioethanol production, it is essential to avoid the formation of pseudo lignin due to its high tendency to re-deposit on the cellulose surface, causing an adverse impact on the enzymatic digestibility of the pulp.[95,139] The formation of pseudo-lignin is typically encountered in other acidic pretreatment method such as dilute acid pretreatment. The common and easy way to identify the formation of pseudo-lignin is through conducting structural compositional analysis for the recovered cellulose pulp. The compositional analysis procedure is unable to distinguish between the native residual lignin on the cellulose or the deposited pseudo-lignin, as they both are insoluble in sulfuric acid.[154,155] Therefore, pseudo lignin can be generally defined as an aromatic material that yields a positive Kalson lignin value. In ionoSolv process, the formation of pseudo-lignin was evidence particularly at high severity conditions (e.g. high temperature, long reaction times, high IL concentration, acidic IL, or combination of these conditions).[142,147]

At optimal severity condition, the extraction of lignin by the acidic [HSO_4] PIL significantly enhances and improves glucose yield via enzymatic saccharification. Characterization of the cellulose-rich pulps obtained from ionoSolv studies confirmed that the cellulose remains highly crystalline.[156] This is oppose to IL-based biomass dissolution process where the low crystallinity of the regenerated cellulose is the reason

behind the high digestibility of the pulps.[156] In ionoSolv, and other fractionation mechanism, the larger surface exposure of cellulose fibrils after effective lignin removal is behind the improved and accelerated cellulose digestibility.[46,156]

The dissolved extracted lignin can be recovered from the PIL medium by the addition of anti-solvent such as water.[157] The fragments of lignin with high molecular weight are the first to precipitate while the lower molecular weight fragments may favor staying in IL liquor due to the stronger π-π interactions between aromatic lignin mono- and oligomers and the ionic liquid cation.[158] To recycle the IL back to the process, the water added for lignin precipitation needs to be removed to restore the initial water concentration.

To improve space-time yield of a reactor, it is important to optimize the reaction kinetics which are usually hugely dependent on temperature. IonoSolv fractionation performance was investigated at different temperatures and residence times for pretreatment using [TEA][HSO_4] IL with 20 wt% H_2O on *Miscanthus giganteus* feedstock.[6,153] The enzymatic hydrolysis of cellulose to glucose changed dramatically as the recovered cellulose pulp composition varied depending on the pretreatment severity. Reaching the optimum glucose yield was significantly accelerated when the pretreatment was conducted at higher temperatures. For example, to achieve 75% glucose yield, the pretreatment should be conducted for 15 mins at 180 °C instead of for 8 hours at 120 °C. The increase in glucose yield was directly correlated to the improved and accelerated delignification achieved at higher temperatures. Approaching or exceeding the glass transition temperature (T_g) of lignin (estimated to be around 130 to 150 °C) was important to improve the kinetics of lignin removal. The ability to achieve high glucose yield while reducing the reactor volume by a factor of 32 offers a substantial economic advantage as it translates to an optimized reactor volume and higher throughput processing times in industrial scale process.[153] This is true even if the process will be operated at higher temperatures as the reactor energy can be supplied through process heat integration, using lignin as a heating source.

The necessity to exceed the glass transition temperature of lignin to achieve effective delignification was also emphasized in several IL biomass processing studies using aprotic ILs. Li *et al.* reported accelerated dissolution of bagasse and pine using the aprotic IL [C_2C_1im][OAc] in 10 minutes when operating at temperatures above 170 °C

compared to 16 hours at 110 °C, highlighting the importance of operating at temperatures that exceeds T_g.[142] Arora *et al.* also observed a remarkable increase in switchgrass delignification using the aprotic IL [C_2C_1im][OAc] at temperatures ≥150 °C which was correlated to the increase in cellulose enzymatic hydrolysis to glucose.[159]

Another important process intensification factor is the biomass loading (*i.e.* the weight percent of biomass in the reactor relative to IL weight percent). As mentioned earlier, biomass loading is a key cost driver in IL-based biomass pretreatment process as it reduces the amount of the IL required and therefore the cost associated with IL use in the process. Higher solid loading (≥ 15 wt%) also brings several other advantages such as more concentrated product stream, lower energy input, lower water consumption, smaller reactor size and lower MESP.[49,160] At the same time, increasing solid loading also brings several processing challenges such as difficulty of mixing and handling, poor heat and mass transfer and increased inhibitors concentration.[160,161] The use of high solids loadings also has implications on the density and viscosity of the reaction product slurry which would require higher power to overcome the high yield stresses at high concentrations.[162] Gschwend *et al.* recently investigated the impact of using higher solid loadings (5 to 50 wt%) using 1-methylimidazolium hydrogen sulfate [H_1Cim][HSO_4] and pine wood as a feedstock. The highest glucose yield of 78% was achieved at the lowest solid loading and it decreased to 40% at 50 wt% loading. The decrease in glucose yield indicates the lower lignin extraction achieved during the process due to the limited particle wetting at higher solid loading. However, increasing the solid loading from 10 to 20 wt% reduced the glucose yields by only 10%. Doubling the solid loading would lower the process CAPEX significantly according to the economics of scale.[147]

1.7 Expanding new feedstock: Waste wood

Rapid urbanization, booming economy and unprecedented development of our societies have all contributed in creating one of the biggest challenges in our present time: waste management. The generally adapted waste management strategy by governments and organizations follows the priority hierarchy of prevent, reduce, reuse, recycle, energy recovery and disposal. The implementation of waste management hierarchy should transform our society foundation from linear economy to circular economy. While linear economy is based on the easy approach of take, use and dispose, the prime principles of circular economy is to be responsive, restorative and regenerative where waste

material is a resource and not a burden.[163] Energy recovery from waste is an important aspect in waste management as it offers a viable solution for waste materials that cannot be recycled due to technical, environmental or economic reasons. This option is well suited when considering waste wood as wood itself was the first fuel known to man. However, waste wood is highly variable in composition and degree of contamination as it originates for wide variety of sources. A guideline developed by the UK government categorizes waste wood based on its relative cleanliness and recyclability is presented in Table 1.1.[164]

Table 1.1: Summary of waste wood categories in the UK based on waste wood sources, contamination and end-use. The content of the table is taken from reference 160

Classification	Sources	Contamination	End-use
Grade A	Packaging and retailing	Nails and minor amount of paints	Animal bedding and panelboard sectors
Grade B	60% Grade A waste wood mixed with demolition material, domestic furniture made from solid wood	Nails/metal fixings. Some paints, plastics, glass, grit	Feedstock for industrial wood processing
Grade C	Grade A, B and construction and demolition waste	Paints coatings and glues, paper, plastics and, rubber, glass, grit. Coated and treated timber	Disposal at special facilities or biomass fuel for use in the generation of electricity and/or heat in WID compliant installations
Grade D	Fencing Transmission Poles Railway sleepers Cooling towers	Copper/ Chrome/ Arsenic preservation treatments Creosote	Requires disposal at special facilities

1.7.1 Contamination and disposal

Mechanical or material contamination of waste wood such as plastics and sand is relatively easy to handle and can be mostly removed by mechanical separation methods such as sieving and magnetic separation.[165] On the other hand, chemical contamination contains several chemical agents and compounds that were added early in the service life of the waste wood, making the wood predominantly contaminated towards its end-

of-life. These preservatives were used mainly to extend the service life of the wood by providing mechanical strength and preventing pest infestation, or in the form of pigments, paint and surface coatings.[166] Due to the non-homogeneity and/or predominantly chemically contaminated nature of grade C and D, it is challenging to recycle these two types of waste wood for energy recovery. The hazardous nature of grade D waste wood limits its use for energy recovery due to technical challenges in containing and handling the carcinogenicity and toxicity of metals that can be released from CCA treated wood while processing. In CCA treated wood, copper plays the major preservation role against fungi and arsenic plays a secondary role as fungicide while chromium is added as a fixation agent and for UV resistance. The use of CCA wood is currently very limited in USA, Europe, Australia and Canada as a response to the Environmental Protection Agency agreement to phase-out CCA wood.[163] Nonetheless, since CCA wood has been extensively used in construction for more than 7 decades, it is expected that the disposal of CCA wood will continue to be a problem when it comes out of service in the next 25 to 50 years.

Metal leaching from CCA wood using an acid is a possible remediation strategy before its disposal.[167] However, the process is not attractive economically and according to a recent study, it costs $115 per ton of CCA wood which is close to the landfill cost.[168] The high cost is due to the high volumes of hazardous sludge generated from leachate treatment via coagulation-precipitation methods. Therefore, the current disposal routes for CCA wood are limited to landfill as in USA or specialist incineration as practiced in Europe. Both options are far from sustainable as landfill accumulates metals in the site and leach them to environment and incineration generates concentrated, highly contaminated and hazardous ashes and particulate matter, which end up in landfill..[169] This was confirmed by a 9-year study conducted in Sweden that looked into waste wood supplied to combustion facilities. The formation of arsenic contaminated slag and ashes, prevented the ash potential use, e.g. for spreading in forests.[170] The same issue of heavy metal accumulation in ash were found when waste wood was used as feedstock for gasification.[171] Waste wood collected from construction demolition activities also contain variety of metals such as Pb, Fe, Zn, Cd and Co which originate from pigments and coatings. Waste wood also contains has high level of inorganic contaminants such as creosote, concrete, sand, brick, adhesives, resins and plastics. Both metallic and inorganic contaminants need to be sorted and/or monitored if the waste wood is

intended to be used in any WtE process as they can cause many technical issues. For example, Zn plays a key role in fouling of boilers and Cl from PVC plastic can stimulate aggressive pitting corrosion.[170]

1.7.2 Decontamination methods

The highly heterogenous and contaminated nature of waste wood also brings a significant technical challenge as the presence of metals contaminants can cease the entire downstream processing (enzymatic hydrolysis and fermentation). Current decontamination methods for waste wood are very similar to the treatment of sludge waste where chemical extraction is applied to remove heavy metal contaminants. Chemical extraction methods are based on the use of inorganic or organic acids (H_2SO_4, HCl, HNO_3, citric and oxalic acid)[172,173], or the use of strong acidic chelating agents (ethylenediaminetetraacetic acid (EDTA) and nitrilotriacetic acid (NTA)).[172] During the acid treatment, the heavy metals are dissolved via an exchange of protons, therefore, strict pH control is key in this process. On the other hand, extraction with strong chelating agents forms an EDTA/NTA-metal complex.[174] Higher extractions can be achieved at exceptionally low acidic conditions (pH <2).[175] This requires the use of expensive acid-resistant materials of construction and strict pH control. Handling the challenging treatment and recovery of the acid is a key disadvantage of acid-based treatment methods as large volumes of alkali solution (CaO, $NaHCO_3$, NaOH) are needed to neutralize the heavy metals-rich acid, followed by a chemical sulfide precipitation method to precipitate the heavy metals.[175–177] In addition, the treated sludge also requires neutralization with large amounts of alkali solutions to neutralize its pH. Chelating agents such as EDTA/NTA were reported to have similar to lower heavy metals removal efficiency while still requiring the same neutralization recovery method.[174,178] Organic acids such as citric acid can also achieve high levels of extraction, however, the extraction kinetics are very slow requiring days before high removals can be achieved with similar chemical neutralization methods are still needed to precipitate the heavy metals.[175,179] The large volumes of waste generated during these conventional decontamination methods makes the methods inherently flawed and non-attractive, particularly for high-volume waste streams.

The use of ILs as alternative solvents to extract heavy metals from waste wood has been explored only recently, using 1-methylimidazolum chloride [H_1Cim]Cl and CCA treated wood as feedstock.[180] Surprisingly, the use of ILs to extract metals from solid substrates

gained limited attention in literature so far with few studies focusing on decontamination of sludge. Metals and heavy metal extraction using IL-aqueous biphasic system have been of huge interest since 1998. In these biphasic systems, the IL can either act as inert diluent or as an active extractant, depending on its structure.[181] Hydrophobic ILs with bulky fluorinated anions and large alkylated cations have been mostly investigated to create these biphasic systems to reduce IL losses in the aqueous phase to minimum levels. In fact, the loss of the IL to the aqueous phase is one of the key challenges rendering the effective use of ILs in metal extraction application. Another key challenge is extreme high viscosity of the bulky hydrophobic ILs, which are tens to hundred times more viscous to traditional organic solvents, leading to slow extraction kinetics.[181] Efforts to eliminate these challenges considered what is called as homogenous liquid-liquid extraction, where the biphasic system is heated up to reduce the IL viscosity and improve the kinetics. Once the temperature is cooled, phase separation takes place with the metal complex formed in the IL phase. The unique structure of the ILs also make them excellent chelating agents for heavy metals and their ionic structure makes them natural electrolytes, facilitating easy and low-energy electrodeposition operation compared to aqueous environments.[181,182]

1.7.3 Economic and ecological advantage

The use of waste wood for heat recovery is currently widely used in many places around the world. The upgrade of waste wood to liquid biofuel is still in its infancy due to the same technological and economic challenges associated with the pretreatment as well as the added complexity to the system due to the waste wood complex nature. As briefly discussed in section 5, the direct and indirect land-use changes associated with the use of biomass for biofuel production has been controversial in terms of their sustainability and GHG emissions. A study published in Science has projected that the land-use change would be the largest contributor on GHG emissions for both corn ethanol and cellulosic ethanol, with GHG emissions increase of 50 and 93%, respectively vs. gasoline GHG emissions.[58] The analysis took into account the use of agricultural waste (i.e. corn stover) to produce cellulosic ethanol, yet still, the potential conversion of corn fields to dedicated energy crops such as switchgrass could trigger GHG emissions that can in turn cause this 50% increase in GHGs over 30 years.[58] The same study projected that the elimination of land-use change can reduce the GHGs of cellulosic ethanol by 70%

vs. gasoline. Waste wood is essentially a post-consumer product that were collected from forest roughly >25 years ago. Therefore, the use of waste wood as feedstock can provide a significant reduction in GHG emissions (including methane emissions from landfill) compared to gasoline petrol. Kang and Tan have also shown that the energy efficiency of bioethanol production from corn can be significantly reduced if the feedstock was switched to waste wood as fossil fuel input for cultivation can be set to zero.[59] On the other side of the Equation, feedstock cost is considered one of the major contributors to the minimum ethanol selling price (MESP), defined as minimum price that ethanol must sell for in order to generate a net present value (NPV) of zero for a 10% internal rate of return (IRR).[183] A study that compared six different pretreatment technologies to produce bio-ethanol from switchgrass has shown that feedstock cost contributes to 45-53 % of MESP for all six pretreatment technologies at a switchgrass cost of \$69 (dry tonne)$^{-1}$.[184] In a recent report from Lux Research Inc., decreasing the cost of the biomass feedstock was stated as "pivotal step" for cellulosic ethanol to achieve cost parity.[185]

The obstacles facing conventional biomass feedstocks should be viewed as an opportunity for waste wood producers to explore the potential of valorizing waste wood beyond energy recovery.

1.8 Evaluating pretreatment: Severity factor

Most of pretreatment technologies that process lignocellulosic biomass are based on hydrothermal methods such as steam explosion, dilute acid, ammonia fiber expansion and wet oxidation. Although water plays a major role as a solvent in all these pretreatment methods, there is a huge variation in these methods in terms of pH, temperature, time and chemical additives.[186] This variation in conditions result in different response and interactions with the biomass components. The combination of different conditions that governs the pretreatment response is referred to as the severity factor R_0. The concept of the pretreatment severity factor was developed by Overend and Chornet in 1987 as part of studying steam-aqueous based pretreatment methods.[187] Overend and Chornet indicated that the cellulose pulp quality or enzymatic accessibility is controlled by temperature and time and that the kinetics seems to follow first-law concentration dependence and the reaction constant has Arrhenius-type dependence temperature. Therefore, the time (t) and temperature (T) can be both combined into a

single factor to express the reaction ordinate. At their study, P-factor derived from Brasch & Free[187] was used as a guide to indicate the pretreatment severity level, which they later renamed it as R_0 – the severity factor using the following Equation:

$$R_0 = \int_a^b \exp(\frac{T-T_0}{\omega})\ \mathrm{dt} = \mathrm{t}\,.\exp(\frac{T-T_0}{\omega}) \qquad (1.4)$$

in which R_0 is the severity factor, t is the time in minutes, T_0 is the reference temperature assigned as 100 °C, T is the temperature during pretreatment in °C. ω is a fitted parameter with a fitted value of 14.75 which is based on the activation energy when pseudo first order kinetics are assumed. The exponential term is consistent with the heuristic that the reaction rate will double for every 10 °C increase in temperature. Furthermore, once a particular combination of time and temperature has been identified to give a target yield. R_0 has the unit of time, however typically the logarithmic value of R_0 (*i.e.* $\log R_0$) to easily compare the numerical values of the severity factor. It is important to note that The Arrhenius behavior in such complex heterogenous systems that comprise of macromolecules is indeed an approximation which is valid only for narrow ranges of experimental conditions where kinetic information can be correlated by means of rate expressions introducing nominal or pseudo-kinetic constants (*i.e.* pre-exponential factors and activation energies). The reason behind this limitation is because the energy probability factor (*i.e.* exp(-E/RT)) is applicable to systems where energy is represented by two square terms, translational and rotational.

Since acid and base catalysts play important role in pretreatment medium, Abatzoglou *et al.* developed Equation 1.5 which takes into account the proton concentration in the pretreatment.[188]

$$R_0' = R_0.[H^+] \qquad (1.5)$$

R_0' is typically referred to as the combined severity factor. The logarithm of Equation 1.5 yields the following:

$$\log R_0' = \log(R_0.[H^+]) = \log R_0 - \mathrm{pH} \qquad (1.6)$$

The logarithm of the severity factor ($\log R_0$) and the logarithm of the combined severity factor $\log R_0'$ have been very useful to compare different pretreatment strategies in terms of cellulose digestibility with respect to xylan solubilization and lignin reduction.[189] Equation 1.3 does not accurately represent the severity of the pretreatment under

alkaline (pH >7) conditions.[189,190] Therefore, Equation 1.6 was derived to describe the impact of both acidic and alkaline of pretreatment on cellulose digestibility.

$$\log R_0'' = \log R_0 + |pH - 7| \quad (1.7)$$

Equation 1.7 provides more accurate and fair comparison across the acidic and alkaline pretreatments. Table 1.2 presents a comparison between different pretreatment methods highlighting the differences in the conditions used (time, temperature and pH). The Table also highlights how the use of log R_0'' is more accurate representation of pretreatment severity compared to log R_0' especially when comparing acidic and alkaline pretreatment as alkaline pretreatment ranks very low when using log R_0'.

Table 1.2: Severity of different scenarios when varying pretreatment temperature, time and pH and comparison between the corresponding severity factors. Adapted from reference 186

#	Method	Temperature (℃)	Time (min)	pH	log R_0	log R_0'	log R_0''
1	Microbial	25	10,080	5	1.8	-3.2	3.8
2	Acid hydrolysis	30	60	1	-0.3	-1.3	5.7
3	Alkali	140	10	13	-10.8	-10.8	8.2
4	Acid steam explosion	180	10	2	1.4	1.4	8.4
5	Acid steam explosion	250	10	1	4.4	4.4	11.4

The use of acidic ILs to deconstruct biomass components became popular in recent years. Acidic ILs were shown to be efficient in delignifying the biomass by cleaving the β-O-4 ether linkages. Relative to other process parameters such as temperature, time and IL concentration, the role that the IL acidity plays to achieve effective delignification was investigated by few researchers. Cox *et al.* evaluated the role of IL acidity on lignin degradation using series of acidic protic ILs.[191] Hammet acidity was used to determine the IL acidity and ILs under investigation included 1-methylimidazolium cation with chloride, bromide, hydrogen sulfate, and tetrafluoroborate counterions along with 1-butyl-3-methylimidazolium hydrogen sulfate. The most acidic IL is $[H_1Cim]Cl$, with an H_0 value of 1.48. The H_0 values of other ILs, $[H_1Cim][BF_4]$, $[H_1Cim][HSO_4]$, $[H_1Cim]Br$, and $[C_4C_1]HSO_4]$, are 1.70, 1.99, 2.04, and 2.08, respectively. The study highlighted that IL acidity alone did not correlate with the ability of the IL to catalyze β-O-4 ether bond

hydrolysis. The use of pretreatment severity factor in ILs-based pretreatment is very limited compared to its use in aqueous-based pretreatment. Only very few IL biomass pretreatment studies incorporated the use of pretreatment severity factor to evaluate and predict the effectiveness of the pretreatment.[150] The role that IL medium's acidity play in the deconstruction of the biomass was given even smaller attention.

1.9 Exploring new product: Nanocellulose

The increasing demand from industry and consumers to use more sustainably produced products sparked the interest on commercial use of nanocellulose derived from renewable cellulose substrates. Since the last century, cellulosic products derived from wood pulp have severed billions of consumers around the world in the form of paper, cellulose composites, textiles etc. These 1st generation cellulose-based products capitalized on the high mechanical strength/weight, functionality and flexibility of the cellulose polymer.[84] It is expected that nanocellulose materials will derive the 2nd generation cellulose-based products in high performance materials in a rapidly developing consumer market.[80] Extraction of cellulose at the nanoscale eliminates the majority of the defects associated with hierarchical structure, and a new cellulose based "building block" is available for the next generation of cellulose based composites.[192] Examples of these defects include high moisture absorption and poor compatibility with the hydrophobic polymer matrix, which have significantly reduced the application of cellulosic materials in polymer composites. The use of nanocellulose, better adhesion between fiber/fiber and fiber/polymer matrix is achieved and therefore, in contrast to conventional cellulose fillers which require high loading, small amount of well-dispersed nanocellulose is able to achieve the mechanical improvement needed in the polymer matrix.[80,192]

Nanocellulose refers to cellulose materials with one dimension in the nanometer range.[193] The variety of dimensions, morphologies, degree of crystallinity depends on the source of cellulosic material and conditions under which preparation is carried out. There are mainly two types of nanocellulose that can be extracted from cellulosic fibers differing in the steps involved in their isolation and in their structure. The two main types of nanocellulose are: i) cellulose nanocrystals (CNCs), also known as cellulose nano-whiskers (CNWs) and, ii) cellulose nanofibrils (CNFs). The rigid rod-like nanocrystals are often obtained by chemical methods such as acid hydrolysis or

oxidation methods whereas the nanofibers are typically produced by mechanical methods.[84] The isolation of CNCs or CNFs from biomass structure is divided into two key stages: i) extraction and purification of cellulose substrates from wood or plants and, ii) separation and disintegration of the purified cellulose fibers into their microfibrillar and/or crystalline components.[80,193] The first stage can be accomplished using wide variety of processes such as the well-established Kraft and Acid Sulphite processes or biomass fractionation processes such as ionoSolv, OrganoSolv, steam explosion and dilute acid hydrolysis. The cellulose purity generated by these processes typically limited and rarely exceed 85%, which is highly preferred to facilitate nanocellulose isolation. Therefore, a second extraction process involves further purification of the cellulose pulp by removing residual hemicellulose and lignin to obtain high purity cellulose (>90% glucan) which is typically accomplished by hot or cold caustic extraction followed by a multi-step bleaching process.[88] Only very few exceptional methods were able to produce high cellulose purity pulp suitable to produce nanocellulose without bleaching. Chen *et al.* have used gamma-valerolactone (GVL) solvent to fractionate wood chips producing a pulp with 95% cellulose content, exceeding the bleached Kraft wood pulp with cellulose content of 78% (lignin = 0.5%, hemicellulose = balance).[194] However, obtaining such very high cellulose purity without bleaching step remains the exception, while using bleached cellulose substrates remain to be the norm in nanocellulose-based studies. The highly pure microcrystalline cellulose (MCC) - a commercially available cellulose material used for applications in pharmaceutical and food industry- has been extensively used as starting material to prepare CNCs in laboratories.[80]

The second stage of nanocellulose isolation is based on effective extraction of nanocellulose from the fibrils. The most common nanocellulose isolation methods to obtain CNFs involve the use of mechanical homogenization methods,[195] whereas CNCs production is typically accomplished by two common methods: i) sulfuric acid hydrolysis, or ii) TEMPO (2,2,6,6-tetramethylpiperidine-1-oxyl)-mediated oxidation. Other less commonly used methods for CNCs isolation include the use of oxidizing agents such as hydrogen peroxide (H_2O_2),[196] ammonium persulfate (APS),[197] and periodate oxidation.[198] Surface functionality of CNC is very important as it directly impacts its performance in end-use applications.[199]

The large number of hydroxyl groups naturally present in CNC structures restricts their applications to hydrophilic or polar media. Many of the intended CNC applications (e.g. composites, electronics, cosmetics, biomedical and environmental applications) depend on their effective dispersion in aprotic organic solvents and polymer matrices.[199,200] More importantly, the lack of any surface functionality promotes the aggregation of CNCs via hydrogen bonding and van der Waals forces.[200] Therefore, chemical functionalization *in-situ* during the CNC extraction process or in a post treatment is an important prerequisite to effectively use of the extracted CNCs. Sulfuric acid catalysed hydrolysis produces CNCs functionalized by sulfate ester groups whereas CNCs produced by oxidation methods using (TEMPO-mediated, APS, H_2O_2) are typically functionalized with carboxyl groups or aldehyde groups (periodate and chlorite).[201] Although the negatively charged sulfate ester groups in CNCs provides effective colloidal stability in dispersion, it was found that the presence of the sulfate ester groups compromised the thermal stability of the CNCs.[202] Other surface groups on CNCs can be obtained via acetylation, etherification or amidation.[199]

1.9.1 Acid hydrolysis

Acid hydrolysis is the most common and oldest method to produce CNCs, with the first CNCs isolation dating back to the 1950s.[203] In this method, the highly pure cellulose substrate is subjected to acid hydrolysis, typically using sulfuric acid. The hydrolysis conditions need to be strictly controlled as it has huge impact on the dimensions, morphology and crystallinity of the isolated CNCs. Typical conditions used in sulfuric acid is 64 wt% acid concentrations at a temperature of 45 °C for 25 to 45 minutes.[204] The amorphous regions in the cellulose fibrils that act as structural defects are easily hydrolyzed by the acid into soluble oligomers and sugars. The hydrolysis of the amorphous regions leaves behind the crystalline regions and induce their transverse cleavage into rod-like CNCs as seen in Figure 1.9.[199] The reaction product in the form of slurry is quenched with excess water to cease the reaction. The slurry then undergoes a series of separation (centrifugation or filtration) and washing/ rinsing steps followed by dialysis against deionized water to remove the remaining acid or neutralized salt. Ultrasonic treatment is then used to facilitate dispersion and disintegration of the crystalline cellulose in the aqueous suspension. The typical diameter of the CNC produced by sulfuric acid hydrolysis ranges between 2–20 nm width and length of 100 to 600 nm.[205] Other acids have also been used to produce CNCs such as hydrochloric,

phosphoric, and hydrobromic acids.[206] However, if the CNCs are prepared by hydrochloric or hydrobromic acid hydrolysis, their dispersion tends to flocculate.[207] When sulfuric and phosphoric acids are used, they react with the surface hydroxyl groups to yield charged surfaces bearing sulfate or phosphate esters that promote a spontaneous dispersion of CNCs in water. Altering the conditions, concentration and type of the mineral acid used during acid hydrolysis can produce other types of nanocellulose, e.g. spherical cellulose II CNCs can be obtained from cellulose hydrolysed by H_2SO_4/HCl mixtures.[208,209] Dispersibility of CNCs is of key importance for their effective use in composite applications to be mixed with polymer matrices.[204] The weight recovery ratio obtained from acid hydrolysis is often low at only 30 to 50%.[207]

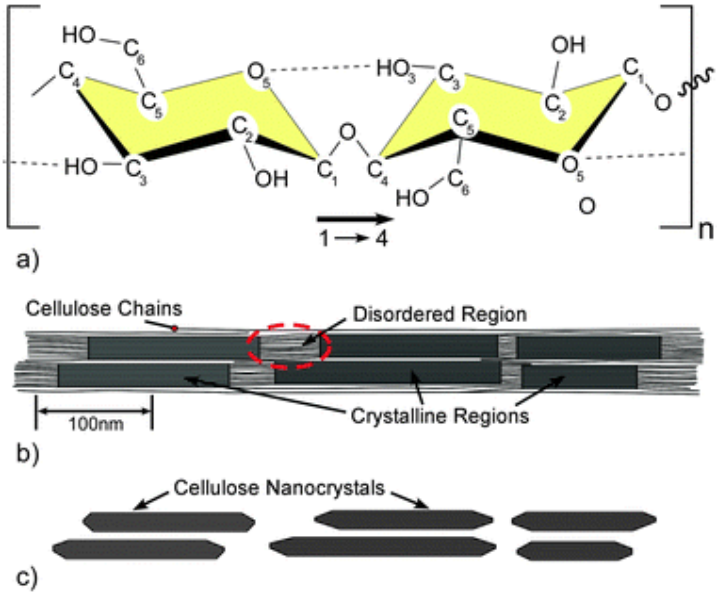

Figure 1.8: Hydrolysis of the amorphous regions in the cellulose fibrils induces the cleavage of the fibers into nanocrystals. Taken from reference 80

1.9.2 TEMPO-mediated oxidation

TEMPO/NaBr/NaClO oxidation is another extensively studied route for CNCs isolation where the hydroxyl group at the cellulose surface is converted into charged carboxyl groups. In this system, catalytic amounts of TEMPO and NaBr were dissolved in cellulose containing solution at pH 10–11 (adjusted by NaOH addition), and the oxidation is initiated by the addition of NaClO solution as a primary oxidant. During the oxidation reaction, NaClO oxidizes TEMPO to $TEMPO^+$ that in turns the C6 primary hydroxyls groups to C6-aldehydes.[210] Part of C6-aldehydes formed are directly oxidized to carboxyl groups with NaClO and/or NaBrO. The reduced TEMPO is oxidized by

NaBrO, which is formed from NaBr oxidation with NaClO.[211] Thus, TEMPO and NaBr act as catalysts with only inexpensive NaClO being consumed during the oxidation. Because acidic carboxyl groups are formed by the oxidation, a small amount of 0.5 M NaOH solution is added during the reaction to maintain the aqueous reaction medium at pH 10.[212] This transforms the water insoluble C6 carboxyl groups to water-soluble sodium C6-carboxylate groups, which is also known as cellouronic acid Na salt.[79] Figure 1.10 presents the catalytic reaction mechanism of C6 oxidation in cellulose in TEMPO/NaBr/NaClO system.

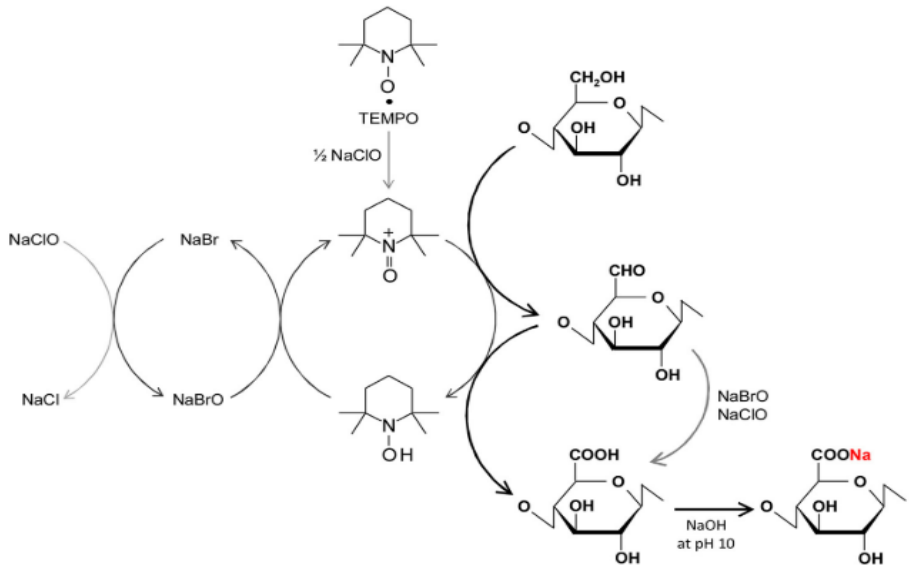

Figure 1.9: Catalytic oxidation mechanism of C6–OH groups of cellulose by TEMPO/NaBr/NaClO in water at pH 10. Taken from reference 194

The catalytic reaction is typically conducted at room temperature for <90 minutes and the recovered insoluble cellulose fraction after TEMPO-mediated oxidation is typically >90%.[79] A bromide free TEMPO/NaClO/NaClO2 oxidation for CNCs production requires much longer reaction times of 48 to 80 hours compared to < 2 hours in TEMPO/NaClO/NaBr system.[213] The crystalline structure of cellulose I is typically maintained during the oxidation, and the carboxylation takes place only in one side of the crystallites surface as the other side of the hydroxyl groups are embedded within the crystalline particle.[79,199] Depending on the post processing methods used on the oxidized cellulose, carboxylated CNFs, CNCs or a both CNFs and CNCs can be obtained. When the oxidized cellulose-water slurry mixture (0.1% w/v) is processed mechanically using ultrasonic homogenizer or high-pressure homogenizer, cellulose nanofibrils of ≈3

nm and lengths >1 μm can be obtained. On the other hand, if the oxidized cellulose-water slurry (0.1% w/v) is subjected to high sonication for extended time (60 to 90 minutes), needle-like CNCs are produced in suspension with average lengths of 150 to 200 nm and width of ≈3 nm.[79] One of the key advantages of TEMPO-mediated oxidation method compared to the more conventional sulfuric acid hydrolysis method is the high selectivity in introducing the functional group to the cellulose surface. The carboxyl group content in oxidized cellulose ranges between 1.2 to 1.7 mmol/g, depending on the NaOCl concentration, whereas the content of sulfate ester groups is typically around 0.3 mmol/g.[195,212] Surface functionality of CNCs or CNFs is one of the key properties that define their usability and interaction within polymer metrices.[192]

Mechanical treatment methods such as high-pressure homogenizers, grinders/refiners, cryocrushing and high intensity ultrasonic treatments are typically used to extract thin CNFs from cellulose substrates with width of ≈10 nm and length of several microns.[214] Depending on the intensity of the mechanical treatment and the applied conditions, microfibrillated cellulose (MFC) which contains bundles of CNFs can be also obtained. MFC has been produced from wood pulp/water slurries at the industrial level by repeated high- pressure homogenization treatment. To facilitate the extraction of the thin CNFs, chemical or enzymatic treatment is often applied as a pre-treatment to the mechanical technique. This also helps to reduce the high energy intensity requirement associated with the mechanical methods.[193]

1.9.3 Other CNCs extraction methods

In general, conventional methods to extract nanocellulose from purified cellulose substrates involves the use of corrosive and toxic chemicals as well as extensive processing steps (centrifugation, filtration, dialysis, sonication, washing).[193] More recent methods aimed to overcome these limitations that can render the commercial development of CNCs/CNFs. Table 1.3 summarizes the work of some of the recent papers reporting novel methods for CNCs/CNFs isolation and their characteristics. Several studies investigated periodate and chlorite mediated oxidations to produce electrostatically stabilized CNCs.[198,215,216] The periodate oxidation cleaves the cellulosic bonds via breaking the C2-C3 linkage and converting the secondary hydroxyls groups to aldehyde groups, which can be subsequently converted to carboxyl groups. Recently, both spherical and rod-like carboxylated CNCs were produced using ammonium persulfate (APS) as oxidizing agent due to the cleavage of the peroxide bond in the APS

and the *in-situ* production of free radicals and hydrogen peroxide (H_2O_2) under acidic conditions (pH =1) for 6 to 8 hours.[217,197] Acid hydrolysis with concentrated dicarboxylic acids (g. oxalic acid and maleic acid) acid were also used to produce carboxylated CNC via a *Fischer–Speier* esterification mechanism.[218,219] Enzymatic hydrolysis is considered an environmentally friendly CNC preparation method starting from cellulosic substrates. Enzymatic treatment is often used as a pre-treatment for mechanical disintegration methods to reduce their high energy. However, as with most enzymatic-based processes, the process is slow and time-consuming and cellulase enzymes are expensive, making the process economically challenging at large-scale.[220,221]

Table 1.3: Summary of recent new methods to isolate nanocellulose from cellulose substrates

Feedstock/product	Isolation method and conditions	Key characteristics	References
Bleached bagasse pulp/carboxylated CNCs and CNFs	Acid hydrolysis using mono caborxylic weak citric acid + ultrasonication 60 to 80 wt%, 80–100 °C, 0.5–4 hours	CNCs, D= 20–30 nm, L= 250–450 nm CNFs, D= 30–60 nm, L= 500–1000 nm Carboxyl group content: 0.65 mmol g^{-1} (CNCs), 0.30 mmol g^{-1} (CNFs) CNCs yield = 30%	[222]
Bleached eucalyptus kraft pulp/carboxylated CNCs and CNFs	Acid hydrolysis using dicarboxylic oxalic acid	CNCs, D= 23 nm, L = 263 nm Carboxyl group content: 0.1 to 0.4 mmol g^{-1}	[218]
Bleached softwood sheet/carboxylated CNCs	Catalytic oxidation using 30 wt% H_2O_2 and copper catalyst for 72 hours at 60 °C	CNCs, D= 23 nm, L = 263 nm Carboxyl group content: 1.0 mmol g^{-1} CNC yield = 54%	[223]
Bleached wood pulp/carboxylated CNCs	Oxidation using ammonium persulfate (APS) in 1 M solution at 60 °C for 16 h with vigorous stirring	CNCs, D =6 nm , L = 124 nm Caborxyl group content: 0.19 mmol g^{-1} CNC yield = 28 to 36%	[217]

1.10 Exploring new process: Dye recycling

98% of textile waste around the world ends-up in landfill, this underutilized waste is estimated to be worth more than $500 billion according to Ellen Macarthur

Foundation.[224] Large contributor to this number is the unprecedented growth of fast fashion retailers and online stores who provide hundreds to thousands of new designs every week, what is known as fast fashion.[224] And the second large contributor to the issue is the lack of efficient recycling and utilization scheme of this valuable waste stream that is rich of material and compounds.

1.10.1 Synthetic dyes

The relationship between man and colour date back to immemorial time; the stone age. Archaeological evidence show that man extracted colours and natural dyes from vegetables, fruits, flowers, minerals and insects.[225] A dye molecule contains a chromophoric group that is capable to interact with lights, giving the impression of colour. The very first synthetic dye was discovered accidently by Sir William Henry Perkin in 1865, while he was attempting to synthesise a compound to cure malaria. His discovery sparked a surge of interest in synthetic dyes and colour science which drove the manufacturing of these compounds at large-scale. The exceptional recent growth and rapid development of the fashion and apparel industry had significantly increased the demand of synthetic dyes. As most of the world's textile mills are operating in developing countries, the surge in use of synthetic dyes has caused significant deterioration of waterways due to the lack of wastewater treatment infrastructure and poor environmental regulations.[226] According to Confederation of Indian Textile Industry, the 3441 textile mills in India are discharging approximately 1.2 billion liters per day of "colored "wastewater into the natural water bodies without proper treatment.[226] The large amount of wastewater effluents in dyeing processes are typically originated from i) cleaning the dye tank following the preparation of the dye bath solution, and ii) cleaning and draining the dye tank at the end of the batch dyeing cycle.[227] The treatment of the wastewater effluents generated in these dyeing processes require a combination of two to three advanced wastewater treatment technologies including; coagulation/flocculation, adsorption, ozonation and membrane filtrations.[228] The most common classification of synthetic dyes today is based on the fibers they intend to colour for and their chemical structure. Natural fibers typically contain a negative or positive surface charge, and therefore the dye used to colour it should exhibit a counter charge to create electrostatic interaction between the dye and the fiber.[228] Cotton and cellulose fibers naturally possess negative charge and therefore cationic vat, direct, reactive and sulfur dyes are used to colour the fibers . On the other hand, protein

and polyamide-based fibers (leather, silk, wool) have a cationic charge on the surface and therefore anionic acidic dyes are used to colour these fibers. On the other hand, synthetic fibers such as polyester, nylon and cellulose acetate do not exhibit any surface charge, and therefore the use of any of the previously mentioned dyes cannot colour these synthetic fibers . Disperse dyes are the only class of dyes that are used to dye synthetic fibers. Disperse dyes are low molecular weight organic molecules that has very low solubility in water and high affinity to hydrophobic fibers.[229] The two major classes of disperse dyes are classified based on their chromophoric group as azo dyes and anthraquinone dyes. Anthraquinone dyes were the early dyes developed to dye cellulose acetate fibers .[229] Their structure, properties and bright shade mimic natural dyes, particularly the red and blue dyes. However, despite many of the unique advantages they have, anthraquinone dyes are highly polluting and expensive to manufacture. Therefore, many of the traditional anthraquinone dyes were replaced by azo dyes due to their ease and cheap manufacture and inherently intense chromophore.[229]

1.10.2 Dyeing technologies

Dyeing processes aim to produce a uniformly coloured textile with an even shade and an appropriate fastness performance to its final use. All dyeing methods are based on the adsorption of the dye molecule from the liquor to the surface of the substrate, followed by the diffusion of the dye molecule into the fibers free space volume.[230] The dyeing process starts with first preparation of the dye solution to obtain the colour required. The substrate fabric is bleached to ensure the removal of any external contamination. After bleaching, the dyeing process takes place in a batch or continuous mode. Following the dyeing process, dye fixation is very important step to ensure maximum adherence between the dye molecule and the fiber. Dye fixation is a measure of the dye that was fixed to the fibers relative to the amount of dye available in the dyeing bath.[229] The dyeing process can be operated in three modes: i) batch mode also called exhaustion method ii) semi- continuous mode and, ii) continuous mode for high production volumes. The choice of the process mode depends on the type of make-up, the chosen class of dye, the equipment available and the cost involved. Batch dyeing is the oldest method of dyeing where a certain amount of the textile is loaded into the dyeing vessel (typically 100 to 1,000 kg) and allowed to reach equilibrium with the

solution containing the dye and the auxiliary chemicals over a period ranging between minutes to hours. Batch dyeing machines come in different configurations and machines (e.g. beam dyeing, jet dyeing, winch dyeing and jigger dyeing) depending on the fabric type and state (knitted or woven).[231] A key parameter in batch dyeing is the solid loading or the liquor ratio, which is the ratio of the fabric substrate in kilograms to the dye containing solution in Liters. The liquor ratio has significant impact on the process economics as it relates directly to the size of the dyeing vessel as well as to the amount of water and energy consumed in the process. Batch dyeing liquor ratio is highly variable, ranging between 1:8 to 1:40 g g^{-1}. When the dyeing shade required is achieved, the spent dye bath is drained, and the textile material is washed to remove unfixed dyes and chemicals. Washing is usually carried out in the same equipment.[229,231]

Continuous and semi-continuous dyeing operates by passing the fabric between rollers that apply the dyestuff. The textiles are fed to the dye containing solution at speed of 50 to 250 metres per minute, and therefore the process is used for high production volume by large dyeing houses where the throughput is 10,000 metres of fabric.[232] The dye fixation step is typically accomplished by application of heat by drying or steam. The only difference between the continuous and the semi-continuous operation is that the fixation and washing steps are performed in a discontinuous manner. Liquor ratio parameter not used in continuous operations, the wet pick up percentage is used instead to measure the grams of liquor picked up by 100 grams of the fabric. In addition, to obtain effective dyeing, the process operates in one of the following modes: i) dyebath circulation systems, ii) textile material moving systems and, iii) both dyebath circulation and textile material moving systems.[232,233]

Polyethylene terephthalate (PET) is the largest synthetic fiber produced in the world by volume. The fiber is manufactured by linear macromolecules that contains at least 85% by mass of an ester of a diol and benzene-1,4-dicarboxylic acid (terephthalic acid).[229] The synthetic fiber is highly hydrophobic retaining 0.4% moisture at 65% relative humidity. It is also known for its high breathability and therefore is extensively used for sportswear. To improve comfortability and durability, polyester is typically blended with other fibers such as cotton to produce what is known as polycotton. Polyester applications and uses are not only limited to the fashion industry, but also in household furniture (e.g. carpets, curtains, duvets, sofas, computer mouse pads).[233] Polyester

dyeing is typically conducted in a batch operation using pressurized jet-dyeing machines. Before the use of jet-dyeing machines, several fiber phenol-based swelling agents and carriers were required to swell the polyester fibers. The high temperature used in the jet-dyeing (120 to 150 °C) eliminated the use of the polluting swelling agents as heat alone was able to swell the fibers effectively to allow dye penetration. In addition, the temperature of the operation needed to exceed the glass transition temperature of polyester (T_g for PET is between 60 to 80 °C) for the swelling to be effective.
At the end of the dyeing cycle, the polyester cools down and returns to its crystalline structure with the dye molecules trapped inside.[233] The unfixed dye is removed by rinsing or by reduction cleaning using alkali chemicals if deeper shades are required.

In the entire supply chain of textile manufacturing, the dyeing step produces the most challenging wastewater stream due to the high complexity and huge variety of fibers , dyes and wide variety of auxiliary chemicals used to aid dyeing (e.g. wetting and swelling agents, dispersants, retardants and softeners).[234] Polyester dyeing discharges wastewater that contains large number of hard-to-destroy surfactants and unused dyes. Newer and tighter environmental regulations have pushed the need to develop ecologically advanced processes to replace or reduce the use of synthetic auxiliary chemicals as well as reduce water footprint in the dyeing process.[235,236] The proposed processes include supercritical CO_2 (sCO_2) dyeing and solvent-assisted dyeing. Dyeing with sCO_2 depends on its unique dissolving power for disperse dyes in addition to its swelling and plasticisation action towards hydrophobic polymers such as PET and other synthetic fibers .[237,238] At the end of the dyeing process, a simple expansion step at common low-pressure allows the solvent to be easily removed and the excess dye to be recovered. The quality of the dyed product is comparable with that obtained in the conventional aqueous process, both in terms of colour yields and fastness properties. In addition to the key advantage of the technology being water-free, sCO_2 dyeing has multiple other advantages such as simpler dye formations (no auxiliary chemicals), shorter dyeing times and elimination of the drying step.[239] However, although each of these advantages hold tremendous environmental saving and, to a lesser extent an economic saving, the commercialization of the sCO_2 dyeing technology has been facing many challenges for the past 30 years. The key challenge is the high CAPEX of the process due the high operational pressure needed (100 to 300 bars), which makes its

penetration in the low-cost dyeing industry highly challenging. In addition to economic obstacles, the migration of oligomers from within the PET to the surface of the PET as well as to the surface of the dyeing equipment presents a major technical challenge with no solution currently.[239,240]

Solvent-assisted dyeing is one of the oldest proposed strategies to minimize water use in the dyeing industry. Chlorinated hydrocarbons such as trichloroethylene, tetrachloroethylene (percholoroethylene) and 1,1,1-trichloroethylene were proposed as dyeing solvents for polyester.[241] The use of chlorinated hydrocarbons for dyeing was not popularized due to their high toxicity and flammability. Alcohol-assisted dyeing started to gain more attention as an alternative. In 1981, Hashimoto investigated the diffusion coefficient of disperse dyes into synthetic fibers in water-alcohol mixtures.[242] The mixtures showed higher diffusion coefficient due to the lowering of the polymer glass transition temperature by solvent absorption (plasticization).[243,244] The use of other alternative solvents compared to the volatile organic alcohol were also recently investigated. Ferrero and Periolatto have found that glycerol can efficiently replace ethanol as an additive to replace auxiliary chemicals.[243] On the other hand, Xu *et al.* investigated the use of liquid paraffin as a dyeing medium for PET and demonstrated that liquid paraffin has higher dye uptake compared to chlorinated hydrocarbons and the dye bath was reused successfully 7 times.[245] An important advantage of solvent dyeing compared to sCO_2 dyeing is that in theory aqueous dyeing machinery can be adapted with minor modifications.[245] When selecting a solvent for fiber dyeing, it is important to demonstrate the reusability of the dye bath and the dye uptake as they both directly relate to the indication of colour fastness and the dyeing cost and effluent control.

1.10.3 Ionic liquid assisted dyeing

The non-volatile nature of ionic liquids offers a key advantage compared to both sCO_2 dyeing and alcohol-based dyeing as the dyeing can operate atmospheric pressure and the potential to use the same aqueous-based dyeing machine with minor modification. Nevertheless, it is important to note that despite the ongoing interest in ILs and their application for various fields, the use of ILs in dyeing processes has been only marginally investigated in literature compared to other research areas. Opwis *et al.* have investigated the use of commonly used aprotic ionic liquids for polyester dyeing using

ionic liquids that are comprised of 1-ethyl-3-methyl-imidazolium cation and various anions, namely acetate, chloride, sulfate, methyl sulfate and phosphate.[246] Dyeing with the methyl sulfate based ionic liquid resulted in best dyeing performance, with better dyeing and darker shades obtained at higher temperatures (140 to 160 °C). In addition, the study showed that dyeing with the IL medium resulted in better quality dyeing in terms of colour shade and similar fastness results to conventional aqueous-based dyeing. Yuan *et al.* showed the use of $[C_4C_1im]Cl$ to improve wool dyeing,[247] Bianchini *et al.* have conducted more comprehensive investigation and screened 8 aprotic ionic liquids to dye cotton, wool and polyester.[248] From the initial screening test, 1-(2-hydroxyethyl)-3-methylimidazolium chloride IL showed the best dyeing result for the different fabrics at atmospheric pressure at 100 °C.

1.10.4 Dye removal methods

Removal of dyes from wastewater and waterways has been under investigation for many decades and it is still an ongoing interest for research and industrial application due to the highly polluting nature of these dyes. However, the removal of dyes from solid substrates or textile fibers have received much less attention simply because there was not a direct application or need for such a technology. In literature, there are no research studies conducted on dyes removal from fibers or solids by solvents. There are, however, few patents that investigated this topic. In 2015 patent, Chin *et al.* investigated a method to decolour polyester fibers use the vapor of organic solvents (xylene, ethylene glycol, ethylene carbonates).[249] The organic solvent vapours at high temperature and pressurized system swells the polyester fiber and extract the dyes. When the vapours of the organic solvent contact the polyester fiber, it condenses. The organic solvent is reused in the process multiple times through vaporization by applying high temperature and low pressures and the dye is kept in the flask. However, no clear explanation or clarification on the status and usability of the isolated dye. In a 2017 patent, the use of organic solvents, namely cycloalkalnes, carbonates, acetone and their combinations was investigated to extract dyestuff from polyester fibers.[250] The process was developed as a pre-treatment step for PET chemical depolymerization process as F2F technology. The investigated organic solvents are highly flammable, and toxic, and have high vapor and low boiling points that range between 77 °C to 120 °C. The high volatility and flammability of the organic solvents makes their use in a large-scale highly challenging.

Organic solvents require high safety measures as well as high-pressure systems to recycle and recover these solvents effectively with minimal losses. Therefore, the use of low-cost protic ionic liquids as alternative solvents seems to be a highly good fit for this application.

1.10.5 Current state of textile industry

The following subsections give brief overview regarding key aspects to understand the textile industry. **Supply chain**: Perhaps the biggest challenge facing the fashion industry is its vertically disintegrated and globally dispersed supply chain, spanning several industries from agriculture (for natural fibers) and petrochemicals (for synthetics) to manufacturing, logistics and retail. What made the supply chain even more complicated and much less transparent was the global shift of garment production in low labor cost countries, causing garment production in many developed countries to become almost extinct. Even the largest retailers and fashion houses are almost never aware of the source of the materials.[251] In recent years, China became the dominant player in the textile market, exporting $109.9 billion USD worth of textiles and $158.4 billion worth of clothing each year.[252] China's textile manufacturing is based on coal as source of energy which significantly contribute to the large carbon footprint associated with textile industry. In fact, textiles produced in China has a 40% larger carbon footprint than textiles made in Turkey or Europe.[253] Figure 1.10 presents an overview of keys stages in garment manufacturing supply chain, highlighting that most of the fiber, yarn and garment manufacturing takes place in developing countries, where highest consumption rate takes place in developed countries.[254]

Often, each step of garment production occurs in a different country, which increases the logistic steps between processes. After manufacturing, garments are shipped in large quantities to central retail distribution centers, followed by smaller retailers where clothing is purchased, often in the UK, EU and USA.[254] Transportation of all these garments takes place by container boats or air cargo, with air cargo having 35% higher carbon emissions compared to boats. At each stage of the manufacturing process of the garment, substantial energy, water and chemical resources are invested. The extreme fragmentation of the entire supply chain around the globe have made it highly

challenging to assess the real environmental impacts associated with textile manufacturing and end-life.[254]

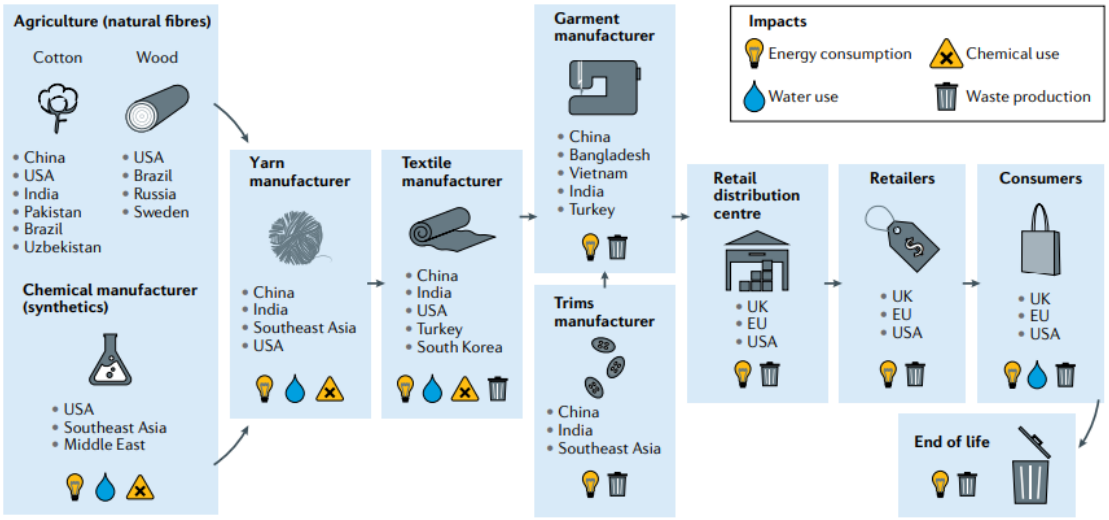

Figure 1.10: The key stages of the fashion supply chain with the geographic location and broad-scale environmental impacts (energy use, water use, waste production and chemical use) for each stage of the process. Taken from reference 242

Chemical and water use: The textile industry uses over 15,000 different chemicals during the manufacturing process, beginning during fiber production.[224] In one example, a single European textile-finishing company uses over 466 g of chemicals per kg of textile. The chemicals include sizing agents, pretreatment auxiliaries, dyestuff, pigments, dyeing auxiliaries, final finishing auxiliaries and basic chemicals.[255] However, approximately 80% of EU-consumed finished textiles are manufactured outside of the EU, making it difficult to confirm total chemical usage. In most of the cases, even some of the "made in EU" textiles are imported as semi-finished textile materials from outside the EU and only finished locally. Hence, the majority of the chemicals use connected to producing textiles for developed countries are made in developing countries.[254] The fashion industry is also a major consumer of water (79 trillion litres per year). The World Bank estimates that 20% of industrial water pollution produced from textile treatment and dyeing.[256] The high pollution level is also attributed to the fact that majority of these operations take place in developing countries where there is huge lack of strict environmental regulations and rigorous wastewater treatment requirement.

In a textile mill, the daily water consumption of an average production (8000 kg fabric/day) is about 1.6 million liters, with 16% of the water consumption attributed to the dyeing phase.[256] As many of these mills are not occupied with advanced wastewater treatment units, millions of liters of the dyeing wastewater containing hazardous dyes, chemicals and salts is discharged to the rivers with no or little treatment.

Textile waste: Textile waste can be classified as pre-consumer and post-consumer. The pre-consumer waste is generated during the production phase of the textile in the form of yarn, fibers or fabrics. As the output of the global fashion system has grown, so have all forms of production waste. A particular type of pre-consumer textile waste referred to as "deadstock" has been under attention in recent years. Deadstock refers to the unsold or returned garment, which is designated as waste. The British luxury house Burberry have incinerated £90 million worth of unsold inventory over five years as of June 2018.[257] The Swedish fast-fashion brand H&M was reported to hold $4.3 billion worth of unsold inventory in warehouses. Following reports indicated that some of the deadstock was diverted to incineration in a waste-to-energy plant in Denmark.[258,259] Incineration should not be a solution for such highly complex waste where substantial amount of water, energy and chemicals were used to make the garment along with carbon footprint, transportation cost/emissions and wastewater produced. On the other hand, post-consumer textile waste is discarded by consumers, and with praise of fast fashion by unaware consumers, the garments lifetime has reduced rapidly. Despite the large differences between the countries' culture, the average lifetime of a garment in China, Germany, Italy, Japan, the UK and the USA is estimated to between 3.1 to 3.5 years on average according to 2019 study.[260] At their end of life, these garments are incinerated or transported to landfills or to developing countries, very often by ship to Africa or east Europe.[261] Current textile recycling rate is still very low with only 15% of post-consumer textile waste were collected for recycling purposes in 2015. From 15%, less than 1% was recycled to textile fibers while the reminder was downgraded to such as insulation material, wiping cloths and mattress stuffing.[261]

Polyester and Disperse dyes: Polyester accounts for 51% of the total textile worldwide production (54 million tonnes) in 2018, followed by cotton at 25% (26 million tonnes). Polyester dominates textile production due to its performance characteristics (strength, durability, elasticity) and cost-efficiency. Polyester production is projected to increase

further due to higher garment consumption rate.[254,262] The high production demand drives high demand and growth for the downstream industry including the $7 billion textile dyes market.[255] Dyeing companies are facing more challenges associated with the acquisition and disposal of these essential raw materials, especially with the increasing government regulation. Innovation in the dyeing industry has been very limited in the past decades, while at the same time, projections s indicate that synthetic dye market will continue to grow as the demand continue to grow. These synthetic dyes are very robust in terms of performance; however, all synthetic dyes are of petroleum-based products and so far, they have been used as a single-use chemical, their service-life ends by the minute the garment is disposed. Disperse dye is a class of sparingly water-soluble dyes and they are used to dye the hydrophobic polyester fibers. Each color of disperse dyes require different raw material, and therefore almost each color has its own manufacturing process. China is dominating the synthetic dye production market, with disperse dyes having the largest share of 49%, followed by 29% for reactive dyes for cotton dyeing.[229] The largest two classes of disperse dye are classified based on their chemical structure as azo-dyes and anthraquinone dye (Figure 1.11). As can be clearly seen for their structure, the production of synthetic disperse dyes depends heavily on petroleum hydrocarbons. For example, a key step in the production of azo-based disperse dyes is the diazotization process which involves the reaction of an aromatic amine with nitrous acid in the presence of excess mineral acid to produce the (-N=N-) compound.[226] There has been growing interest to use natural dyes at-scale with currently few successful product lines. However, the use of natural dyes gives very limited shades and colors and very low color fastness properties such that the color can be washed out after few laundry cycles.

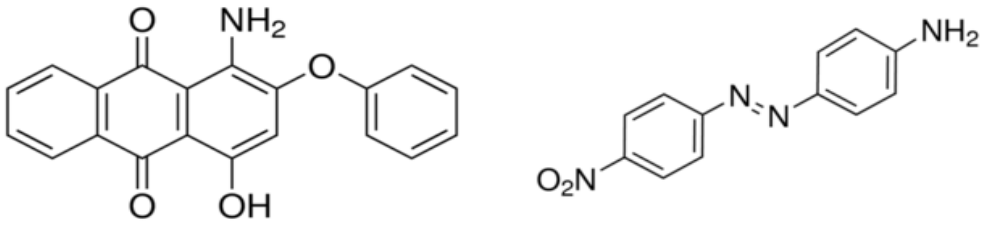

Figure 1.11: Structure of anthraquinone-based (red 60) left. Azo-based dye (orange 3) right.

Circularity and closed-loop processes: To achieve any meaningful impact in the textile industry, the industry as whole from fiber production to retail needs to change their business and manufacturing practices. Unfortunately, businesses are often opposed to change unless there is a government regulation, price to pay or profit to lose. Having to pay for a "cleaner" technology is often associated with large investment, which would necessitate increasing the production cost and subsequently increase the price tag for consumers which harms the business of cheap and fast fashion, eventually leading to a profit decline. The solution for such paradigm requires international collaboration to end the overproduction, fast manufacturing, and low-quality products. The solution does not only depend on the manufacturers and retails, but it also depends on the consumers and their appetite to change their habits. Huge part of consumers unawareness is based on the fact that majority of the textile operations are conducted in developing countries, and therefore large US and EU retailers enjoy the "*out-of-sight-out-of-mind*. If part of the solution is to end manufacturing in developing countries, this would create a wave of economic and social issues in those countries as textile manufacturing is huge part of their economy. For example, half of Pakistan's exports are from textiles and the apparel industry, and 55% of all exports from India are associated with the garment industry.[230] In the recent few years, pressure the textile manufacturing industry witnessed a pressure wave, especially after the 2013 garment factory collapse in Bangladesh, with death toll of 1,134. The customers of the garment factory were high-end brands such as GAP and Calvin Klein. The light at the end of the tunnel is the emergence of new circular technologies such as material recycling mechanically and chemically for polyester and cotton garments. Mechanical recycling is based on shredding the fabrics into small pieces to facilitate their manufacturing to new materials. To overcome the fiber deterioration during shredding, the recycled fibers are often mixed with virgin fibers. Chemical recycling is still at early stage of development and they are meant to retain the structural properties of these fibers, enabling their 100% use without using virgin materials in what is known as fiber-to-fiber (F2F) technologies. Ioncell-F process is an example of under development F2F technology that uses ionic liquid to dissolve cotton fibers from textile waste and re-spun them into cellulosic fibers to create an alternative to virgin cotton or viscose yarns. The recycle and re-use of synthetic dyes as a pretreatment for material recycling methods and their

subsequent reuse to dye new fibers can provide a new circularity dimension in the textile industry; dye recycling, which will be further introduced in Chapter 7.

1.11 Research gaps and thesis objectives

The use of new chemical solvents that are not known to industry (*i.e.* PILs) in a field that has been struggling to take-off (*i.e.* 2nd generation biorefinery) might be seen as double risk that would render commercial deployment. To expedite the industrial development, strategies that de-risk current processing components and open new processing opportunities need to be explored. The work conducted in this thesis aim to explore some of these strategies. The first strategy is to investigate new low-cost feedstocks that fits a niche application, a known supply chain and pre-existing collection infrastructure. The feedstocks that were investigated in this thesis are post-consumer waste wood from construction and demolition activities as well as post-consumer creosote wood from railway sleepers. The use of such highly contaminated waste woods as feedstocks for biorefinery is a novel approach that was not investigated in literature potentially due to their high level of hazardous contamination. The work in thesis explored the ability of the low-cost PILs to valorize and decontaminate waste lignocellulosic biomass for their potential use a negative-cost feedstock in biorefinery. To do so, it is essential to develop an understanding of PILs interactions with the waste wood's biopolymers and the fate of the different contaminants (heavy metals and creosote) in the process. The second strategy is to evaluate the process boundaries and robustness by investigating the water role in the process as i) co-solvent, which impacts the IL use in the process, and ii) an anti-solvent, which impacts the IL dehydration energy. Both IL use and IL dehydration energy are highly important parameters that influence and technoeconomic viability of the process and therefore require careful evaluation and optimization. The third strategy is to develop an in-depth understanding of the fractionation process abilities and limitations. Evaluating the pretreatment at different severity levels can provide a comprehensive understanding about how to better predict process performance, abilities, and limitations. Extrapolating the use of the classical pretreatment severity factor used in aqueous-based pretreatment methods to IL-based methods require incorporation of the IL solution acidity into the severity factor, a method which has not been explored in literature to date.

The ionoSolv process was historically developed as a pretreatment method to produce fermentable sugars using the recovered cellulose-rich pulp. However, ionoSolv process is essentially a new pulping technology, and yet the use of the recovered cellulose pulp for other cellulosic-based applications was not explored to date. Looking into emerging cellulose products market such as nanocellulose can be an easier strategy for technology penetration compared to the struggling cellulosic fuel market. Therefore, it is important to explore the potential use of the recovered cellulose pulps from the as substrate for nanocellulose and highlight whether ionoSolv cellulose pulps can provide any competitive advantage for nanocellulose production relative to commercial pulps. While developing a nanocellulose extraction method, it is important to investigate the current challenges in this field and seek to overcome them. These current challenges include the reduce cellulose substrate preparation steps (e.g. eliminate bleaching) and the use of simpler and environmentally friendly methods that can be adapted to large-scale operation.

Apart from ionoSolv process for biomass fractionation, the use of the low-cost PILs (particularly alkylammonium [HSO_4]-based PILs) remain to be highly unexplored in literature for other applications. From the learnings obtained from this thesis, it was observed that these PILs have high potential to be used as extracting agents. The observation led to the explore the use of [DMBA][HSO_4] to extract synthetic dyes from synthetic fibers, primarily polyester. The dye-rich PIL solution was further used as a dyeing bath for new white polyester fibers. Developing this new circular color extraction-dyeing for synthetic fibers require the evaluation of several process parameters to optimize the dye extraction efficiency and dye-uptake in the subsequent step.

The objectives of this thesis can be summarized as the following:

- Demonstrate the use of the low-cost PILs as viable solvents for fractionation and decontamination of grade C and D post-consumer waste woods.
- Conduct in-depth characterization on the post-consumer waste woods to understand the level and nature of the contaminants.
- Optimize pretreatment solvent (IL selection), time, temperature and solid loading to enable the recovery of highly digestible, contaminant-free cellulose pulps where glucose yield is maximized.

- Investigate the delignification behavior and kinetics of waste wood and compare to virgin biomass and evaluate waste wood lignin recovery and properties.
- Investigate the removal, fractionation and the fate of contaminants in the process streams (cellulose, lignin and IL liquor) and the implications of the fractionation on the process unit operations (electrodeposition and WID boiler use)
- Evaluate the use of various IL/water mixtures to fractionate conventional and non-conventional feedstocks and the impact of water as a co-solvent in the fractionation efficiency and IL use in the process.
- Assess the use of lower water-input on lignin recovery and properties and study the impacts of lower water-input on the fractionation performance and IL dehydration energy.
- Develop a more in-depth understanding on the impact of pretreatment severity on the process performance and outputs using design of experiment approach.
- Evaluate the use of a modified pretreatment severity factor that considers the role of IL medium acidity in ionoSolv biomass fractionation process.
- Examine the potential development of a simple facile nanocellulose extraction method using ionoSolv unbleached cellulose pulps using alkaline-H_2O_2 oxidation.
- Characterize the alkaline-H_2O_2 oxidation outputs (cellulose residues and CNCs). examine links between pretreatment parameters and structural composition, degree of polymerization and crystallinity.
- Evaluate the use of low-cost PILs as solvents for new circular-based processes to decontaminate and valorize waste streams such as textile waste.
- Explore the interaction of synthetic-based fibers (e.g. polyester) and the dye compounds with PILs and the impact of process conditions (temperature, time, solid loading, surface area and PIL concentration) on the interaction.
- Demonstrate the unique advantages PILs can provide for a new process in terms of extraction and solubilization capabilities.

1.12 Thesis structure

This thesis provides insights on few of the knowledge gaps around the ionoSolv lignocellulose fractionation process and highlights the opportunities to expand the feedstock and explore new products. The work in this thesis also led to the potential development of a new process that capitalizes on the use of protic ILs in pre-treating another challenging waste stream, textile waste, while also creating a closed-loop dye recycle process. In the next chapters, the results and discussion are structured as the following:

Highly contaminated waste feedstocks: Chapter 2 investigates the fractionation of highly contaminated grade C post-consumer waste wood using ionoSolv process, providing detail analysis on feedstock composition and evaluating the impact of IL selection and pretreatment conditions on its effective fractionation. Chapter 3 expands the investigation of new and challenging feedstocks to the grade D hazardous creosote-contaminated waste wood and study the fractionation of creosote in the process streams.

Water role in ionoSolv process: Chapter 4 investigates the water role in the process as a co-solvent using different promising feedstocks as well as water use as an anti-solvent for lignin and the energy requirement associated with water use. *Pretreatment severity in ionoSolv process*: Chapter 5 investigates the impact of pretreatment severity on the fractionation behavior of pine softwood through developing a modified pretreatment severity factor and using a design of experiment methodology.

One-step process to nanocellulose: Chapter 6 explores a facile nanocellulose extraction method from unbleached ionoSolv cellulose substrates using a one-step oxidation method, eliminating the need of bleaching as requirement for nanocellulose extraction. The chapter provides a detailed characterization of the cellulose substrates and the extracted nanocellulose.

Novel process Recycled synthetic dyes: Chapter 7 explores a new concept of dyeing with recycled synthetic dyes that were extracted from textile waste, providing a novel circular process for dye recycling using ionic liquids as solvents.

References

(1) Ragauskas, A. J.; Nagy, M.; Kim, D. H.; Eckert, C. a.; Hallett, J. P.; Liotta, C. L. From Wood to Fuels: Integrating Biofuels and Pulp Production. Ind. Biotechnol. 2006, 2 (1), 55–65. https://doi.org/10.1089/ind.2006.2.55.

(2) Tadesse, H.; Luque, R. Advances on Biomass Pretreatment Using Ionic Liquids: An Overview. https://doi.org/10.1039/c0ee00667j.

(3) Brandt, A.; Gräsvik, J.; Hallett, J. P.; Welton, T. Deconstruction of Lignocellulosic Biomass with Ionic Liquids. Green Chem. 2013, 15 (3), 550–583. https://doi.org/10.1039/c2gc36364j.

(4) Ravindran, R.; Jaiswal, A. K. A Comprehensive Review on Pre-Treatment Strategy for Lignocellulosic Food Industry Waste: Challenges and Opportunities. Bioresour. Technol. 2016, 199, 92–102. https://doi.org/10.1016/j.biortech.2015.07.106.

(5) Brandt, A.; Ray, M. J.; To, T. Q.; Leak, D. J.; Murphy, R. J.; Welton, T. Ionic Liquid Pretreatment of Lignocellulosic Biomass with Ionic Liquid-Water Mixtures. Green Chem. 2011, 13 (9), 2489–2499. https://doi.org/10.1039/c1gc15374a.

(6) Brandt-Talbot, A.; Gschwend, F. J. V.; Fennell, P. S.; Lammens, T. M.; Tan, B.; Weale, J.; Hallett, J. P. An Economically Viable Ionic Liquid for the Fractionation of Lignocellulosic Biomass. Green Chem. 2017, 19 (13), 3078–3102. https://doi.org/10.1039/C7GC00705A.

(7) Lynd, L. R. The Grand Challenge of Cellulosic Biofuels. Nat. Biotechnol. 2017, 35 (10), 912–915. https://doi.org/10.1038/nbt.3976.

(8) Perlack, R. D. L. L. W. A. F. T. R. L. G. Biomass as Feedstock for a Bioenergy and Bioproducts Industry: The Technical Feasi- Bility of a Billion-Ton Annual Supply.

(9) Ragauskas, A. J.; Williams, C. K.; Davison, B. H.; Britovsek, G.; Cairney, J.; Eckert, C. A.; Frederick Jr., W. J.; Hallett, J. P.; Leak, D. J.; Liotta, C. L.; Mielenz, J. R.; Murphy, R.; Templer, R.; Tschaplinski, T. The Path Forward for Biofuels and Biomaterials\r10.1126/Science.1114736. Science. 2006, 311 (5760), 484–489. https://doi.org/10.1126/science.1114736.

(10) Brandt, A.; Ray, M. J.; To, T. Q.; Leak, D. J.; Murphy, R. J.; Welton, T. Ionic Liquid Pretreatment of Lignocellulosic Biomass with Ionic Liquid–Water Mixtures, 2011, Vol. 13. https://doi.org/10.1039/c1gc15374a.

(11) Greaves, T. L.; Drummond, C. J. Protic Ionic Liquids: Properties and Applications. Chem. Rev. 2008, 108 (1), 206–237. https://doi.org/10.1021/cr068040u.

(12) Plechkova, N. V; Seddon, K. R. Applications of Ionic Liquids in the Chemical Industry. Chem Soc Rev 2008, 37 (1), 123–150. https://doi.org/10.1039/b006677j.

(13) Hunt, P. A.; Kirchner, B.; Welton, T. Characterising the Electronic Structure of Ionic Liquids: An Examination of the 1-Butyl-3-Methylimidazolium Chloride Ion Pair. Chem. - A Eur. J. 2006, 12 (26), 6762–6775. https://doi.org/10.1002/chem.200600103.

(14) Deetlefs, M.; Seddon, K. R. The Green Synthesis of Ionic Liquids. Handbook of Green Chemistry, Vol.6 Ionic Liquids. Wiley-VCH, 2010, 3–38.

(15) Rogers, R. D.; Seddon, K. R. Ionic Liquids - Solvents of the Future? Science (80-.). 2003, 302 (5646), 792–793. https://doi.org/10.1126/science.1090313.

(16) Hayes, R.; Warr, G. G.; Atkin, R. Structure and Nanostructure in Ionic Liquids. Chem. Rev. 2015, 115 (13), 6357–6426. https://doi.org/10.1021/cr500411q.

(17) Welton, T. Room-Temperature Ionic Liquids. Solvents for Synthesis and Catalysis. Chem. Rev. 1999, 99, 2071–2083. https://doi.org/10.1021/cr980032t.

(18) Dai, C.; Zhang, J.; Huang, C.; Lei, Z. Ionic Liquids in Selective Oxidation: Catalysts and Solvents. Chem. Rev. 2017, 117 (10), 6929−6983. https://doi.org/10.1021/acs.chemrev.7b00030.

(19) Chen, Y.; Zhang, X.; Zhang, D.; Yu, P.; Ma, Y. High Performance Supercapacitors Based on Reduced Graphene Oxide in Aqueous and Ionic Liquid Electrolytes. Carbon N. Y. 2011, 49, 573–580. https://doi.org/10.1016/j.carbon.2010.09.060.

(20) Bates, E. D.; Mayton, R. D.; Ntai, I.; Davis, J. H. CO2 Capture by a Task-Specific Ionic Liquid. J. Am. Chem. Soc. 2002, 124 (6), 926–927. https://doi.org/10.1021/ja017593d.

(21) Humbird, D.; Davis, R.; Tao, L.; Kinchin, C.; Hsu, D.; Aden, A.; Schoen, P.; Lukas, J.; Olthof, B.; Worley, M.; Sexton, D.; Dudgeon, D. Process Design and Economics for Biochemical Conversion of Lignocellulosic Biomass to Ethanol. Renew. Energy, 2011, 303 (147). https://doi.org/10.2172/1013269.

(22) Brodin, M., Vallejos, M., Opedal, M. T., Area, M. C., Chinga-Carrasco, G. Lignocellulosics as sustainable resources for production of bioplastics–A review. J.Clean. Prod, 2017,162, 646-664. https://doi.org/10.1016/j.jclepro.2017.05.209

(23) Li, C.; Tanjore, D.; He, W.; Wong, J.; Gardner, J. L.; Thompson, V. S.; Yancey, N. A.; Sale, K. L.; Simmons, B. A.; Singh, S. Scale-Up of Ionic Liquid-Based Fractionation of Single and Mixed Feedstocks. Bioenergy Res. 2015, 8 (3), 982–991. https://doi.org/10.1007/s12155-015-9587-0.

(24) Fox, D. M.; Awad, W. H.; Gilman, J. W.; Maupin, P. H.; De Long, H. C.; Trulove, P. C. Flammability, Thermal Stability, and Phase Change Characteristics of Several Trialkylimidazolium Salts. Green Chem. 2003, 5 (6), 724. https://doi.org/10.1039/b308444b.

(25) Zhao, D.; Liao, Y.; Zhang, Z. D. Toxicity of Ionic Liquids. Clean - Soil, Air, Water 2007, 35 (1), 42–48. https://doi.org/10.1002/clen.200600015.

(26) Righi, S.; Morfino, A.; Galletti, P.; Samorì, C.; Tugnoli, A.; Stramigioli, C. Comparative Cradle-to-Gate Life Cycle Assessments of Cellulose Dissolution with 1-Butyl-3-Methylimidazolium Chloride and N-Methyl-Morpholine-N-Oxide. Green Chem. 2011, 13 (2), 367–375. https://doi.org/10.1039/C0GC00647E.

(27) Zhang, Y.; Bakshi, B. R.; Demessie, E. S. Life Cycle Assessment of an Ionic Liquid versus Molecular Solvents and Their Applications. Environ. Sci. Technol. 2008, 42 (5), 1724–1730. https://doi.org/10.1021/es0713983.

(28) Tao, L.; Tan, E. C. D.; Aden, A.; Elander, R. T. Techno-Economic Analysis and Life-Cycle Assessment of Lignocellulosic Biomass to Sugars Using Various Pretreatment Technologies. In Biological Conversion of Biomass for Fuels and Chemicals, 2014, No. 10, 358–380.

(29) Clarke, C. J.; Tu, W. C.; Levers, O.; Bröhl, A.; Hallett, J. P. Green and Sustainable Solvents in Chemical Processes. Chem. Rev. 2018, 118 (2), 747–800. https://doi.org/10.1021/acs.chemrev.7b00571.

(30) Yoo, B.; Jing, B.; Jones, S. E.; Lamberti, G. A.; Zhu, Y.; Shah, J. K.; Maginn, E. J. Molecular Mechanisms of Ionic Liquid Cytotoxicity Probed by an Integrated Experimental and Computational Approach. Sci. Rep. 2016, 6 (February), 19889. https://doi.org/10.1038/srep19889.

(31) MacFarlane, D. R.; Seddon, K. R. Ionic Liquids-Progress on the Fundamental Issues. Aust. J. Chem. 2007, 60 (1), 3–5. https://doi.org/10.1071/CH06478.

(32) Deetlefs, M.; Seddon, K. R. Assessing the Greenness of Some Typical Laboratory Ionic Liquid Preparations. Green Chem. 2010, 12 (1), 17–30. https://doi.org/10.1039/B915049H.

(33) Chen, L.; Sharifzadeh, M.; Dowell, N.; Welton, T.; Shah, N.; Hallett, J. P. Inexpensive Ionic Liquids: [HSO4]−-Based Solvent Production at Bulk Scale. Green Chem. 2014, 16(6), 3098-3106. https://doi.org/10.1039/C4GC00016A

(34) Baaqel, H.; Díaz, I.; Tulus, V.; Chachuat, B.; Guillén-Gosálbez, G.; Hallett, J. P. Role of Life-Cycle Externalities in the Valuation of Protic Ionic Liquids-a Case Study in Biomass Pretreatment Solvents. Green Chem. 2020, 22 (10), 3132–3140. https://doi.org/10.1039/d0gc00058b.

(35) Chiappe, C.; Mezzetta, A.; Pomelli, C. S.; Iaquaniello, G.; Gentile, A.; Masciocchi, B. Development of Cost-Effective Biodiesel from Microalgae Using Protic Ionic Liquids. Green Chem. 2016, 18 (18), 4982–4989. https://doi.org/10.1039/C6GC00923A.

(36) Greaves, T. L.; Weerawardena, A.; Krodkiewska, I.; Drummond, C. J. Protic Ionic Liquids: Physicochemical Properties and Behavior as Amphiphile Self-Assembly Solvents. J. Phys. Chem. B 2008, 112 (3), 896–905. https://doi.org/10.1021/jp0767819.

(37) Greaves, T. L.; Weerawardena, A.; Fong, C.; Krodkiewska, I.; Drummond, C. J. Protic Ionic Liquids: Solvents with Tunable Phase Behavior and Physicochemical Properties. J. Phys. Chem. B 2006, 110 (45), 22479–22487. https://doi.org/10.1021/jp0634048.

(38) Yoshizawa, M.; Xu, W.; Angell, C. A. Ionic Liquids by Proton Transfer: Vapor Pressure, Conductivity, and the Relevance of ΔpKa from Aqueous Solutions. J. Am. Chem. Soc. 2003, 125 (50), 15411–15419. https://doi.org/10.1021/ja035783d.

(39) Greaves, T. L.; Drummond, C. J. Protic Ionic Liquids: Evolving Structure-Property Relationships and Expanding Applications. Chem. Rev. 2015, 115 (20), 11379–11448. https://doi.org/10.1021/acs.chemrev.5b00158.

(40) Penttilä, Anne, Petri Uusi-Kyyny, and V. A. Distillable Protic Ionic Liquid 2-(Hydroxy)Ethylammonium Acetate. Ind. Eng. Chem. Res. 2014, 53, 19322−19330. https://doi.org/10.1021/ie503823a

(41) Earle, M. J.; Esperança, J. M. S. S.; Gilea, M. A.; Lopes, J. N. C.; Rebelo, L. P. N.; Magee, J. W.; Seddon, K. R.; Widegren, J. A. The Distillation and Volatility of Ionic Liquids. Nature 2006, 439 (7078), 831–834. https://doi.org/10.1038/nature04451.

(42) Zhang, L.; He, L.; Hong, C. Bin; Qin, S.; Tao, G. H. Brønsted Acidity of Bio-Protic Ionic Liquids: The Acidic Scale of [AA]X Amino Acid Ionic Liquids. Green Chem. 2015, 17 (12), 5154–5163. https://doi.org/10.1039/c5gc01913c.

(43) To, T. Q. 2013, Investigation of the Acidity and Nucleophilicity of Ionic Liquid Mixtures and Their Effects on Reaction Rates, Doctoral dissertation, Imperial College London.

(44) Thomazeau, C.; Olivier-Bourbigou, H.; Magna, L.; Luts, S.; Gilbert, B. Determination of an Acidic Scale in Room Temperature Ionic Liquids. J. Am. Chem. Soc. 2003, 125 (18), 5264–5265. https://doi.org/10.1021/ja0297382.

(45) Belieres, J.-P.; Angell, C. A. Protic Ionic Liquids: Preparation, Characterization, and Proton Free Energy Level Representation. https://doi.org/10.1021/jp067589u.

(46) George, A.; Brandt, A.; Tran, K.; Zahari, S. M. S. N. S.; Klein-Marcuschamer, D.; Sun, N.; Sathitsuksanoh, N.; Shi, J.; Stavila, V.; Parthasarathi, R.; Singh, S.; Holmes, B. M.; Welton, T.; Simmons, B. A.; Hallett, J. P. Design of Low-Cost Ionic Liquids for Lignocellulosic Biomass Pretreatment. Green Chem. 2015, 17 (3), 1728–1734. https://doi.org/10.1039/C4GC01208A.

(47) Wooster, T. J.; Johanson, K. M.; Fraser, K. J.; MacFarlane, D. R.; Scott, J. L. Thermal Degradation of Cyano Containing Ionic Liquids. Green Chem. 2006, 8 (8), 691. https://doi.org/10.1039/b606395k.

(48) Clough, M. T.; Geyer, K.; Hunt, P. A.; Mertes, J.; Welton, T. Thermal Decomposition of Carboxylate Ionic Liquids: Trends and Mechanisms. Phys. Chem. Chem. Phys. 2013, 15 (47), 20480. https://doi.org/10.1039/c3cp53648c.

(49) Klein-Marcuschamer, D. B. A. S.; Blanch, H. W. Techno-Economic Analysis of a Lignocellulosic Ethanol Biorefi Nery with Ionic Liquid Pre-Treatment. Biofuels, Bioprod. Biorefining 2011, 5 (5), 562–569. https://doi.org/10.1002/bbb.

(50) Stark, A. Ionic Liquids in the Biorefinery: A Critical Assessment of Their Potential. Energy Environ. Sci. 2011, 4 (1), 19–32. https://doi.org/10.1039/c0ee00246a.

(51) Mosier, N.; Wyman, C.; Dale, B.; Elander, R.; Lee, Y. Y.; Holtzapple, M.; Ladisch, M. Features of Promising Technologies for Pretreatment of Lignocellulosic Biomass. Bioresour. Technol. 2005, 96 (6), 673–686. https://doi.org/10.1016/j.biortech.2004.06.025.

(52) Tadesse, H.; Luque, R. Advances on Biomass Pretreatment Using Ionic Liquids: An Overview. Energy Environ. Sci. 2011, 4 (10), 3913. https://doi.org/10.1039/c0ee00667j.

(53) George, A.; Brandt, A.; Tran, K.; Zahari, S. M. S. N. S.; Klein-Marcuschamer, D.; Sun, N.; Sathitsuksanoh, N.; Shi, J.; Stavila, V.; Parthasarathi, R.; Singh, S.; Holmes, B. M.; Welton, T.; Simmons, B. a.; Hallett, J. P. Design of Low-Cost Ionic Liquids for Lignocellulosic Biomass Pretreatment. Green Chem. 2015, 17 (3), 1728–1734. https://doi.org/10.1039/C4GC01208A.

(54) Albers, S. C.; Berklund, A. M.; Graff, G. D. The Rise and Fall of Innovation in Biofuels. Nat. Biotechnol. 2016, 34 (8), 814–821. https://doi.org/10.1038/nbt.3644.

(55) Songstad, D. D.; Lakshmanan, P.; Chen, J.; Gibbons, W.; Hughes, S.; Nelson, R. Historical Perspective of Biofuels: Learning from the Past to Rediscover the Future. In Vitro Cellular & Developmental Biology-Plant 45, no. 3 (2009): 189-192. https://doi.org/10.1007/s11627-009-9218-6.

(56) Hammond, G. P.; Kallu, S.; Mcmanus, M. C. Development of Biofuels for the UK Automotive Market. Applied Energy, 2008, 85, 506–515. https://doi.org/10.1016/j.apenergy.2007.09.005.

(57) Ragauskas, A. J.; Beckham, G. T.; Biddy, M. J.; Chandra, R.; Chen, F.; Davis, M. F.; Davison, B. H.; Dixon, R. a; Gilna, P.; Keller, M.; Langan, P.; Naskar, A. K.; Saddler, J. N.; Tschaplinski, T. J.; Tuskan, G. a; Wyman, C. E. Lignin Valorization: Improving Lignin Processing in the Biorefinery. Science 2014, 344 (6185), 1246843. https://doi.org/10.1126/science.1246843.

(58) Searchinger, T.; Heimlich, R.; Houghton, R. A.; Dong, F.; Elobeid, A.; Fabiosa, J.; Tokgoz, S.; Hayes, D.; Yu, T.-H.; Yu4, T.-H. Use of U.S. Croplands for Biofuels Increases Greenhouse Gases through Emissions from Land-Use Change. Science, 2008, 319,(5867), 1238–1240. https://doi.org/10.1126/science.ll52747.

(59) Kang, Q.; Tan, T. Exergy and CO 2 Analyses as Key Tools for the Evaluation of Bio-Ethanol Production. Sustainability, 2016, 8 (1), 1–11. https://doi.org/10.3390/su8010076.

(60) Chen, H.; Liu, J.; Chang, X.; Chen, D.; Xue, Y.; Liu, P.; Lin, H.; Han, S. A Review on the Pretreatment of Lignocellulose for High-Value Chemicals. Fuel Process. Technol. 2017, 160, 196–206. https://doi.org/10.1016/j.fuproc.2016.12.007.

(61) Ignatyev, I. 2011, Cellulose Valorization in Ionic Liquids; Doctoral dissertation, KU Leuven University

(62) Haghighi, S.; Hossein, A.; Tabatabaei, M. Lignocellulosic Biomass to Bioethanol , a Comprehensive Review with a Focus on Pretreatment. Renew. Sustain. Energy Rev. 2013, 27, 77–93. https://doi.org/10.1016/j.rser.2013.06.033.

(63) Sims, R. E. H.; Mabee, W.; Saddler, J. N.; Taylor, M. An Overview of Second Generation Biofuel Technologies. Bioresour. Technol. 2010, 101 (6), 1570–1580. https://doi.org/10.1016/j.biortech.2009.11.046.

(64) Hendriks, A. T. W. M.; Zeeman, G. Pretreatments to Enhance the Digestibility of Lignocellulosic Biomass. Bioresour. Technol. 2009, 100 (1), 10–18. https://doi.org/10.1016/j.biortech.2008.05.027.

(65) Rio, L. F. Del; Chandra, R. P.; Saddler, J. N. The Effect of Varying Organosolv Pretreatment Chemicals on the Physicochemical Properties and Cellulolytic Hydrolysis

of Mountain Pine Beetle-Killed Lodgepole Pine. 2009. https://doi.org/10.1007/s12010-009-8786-6.

(66) Shi, J.; Gladden, J. M.; Sathitsuksanoh, N.; Kambam, P.; Sandoval, L.; Mitra, D.; Zhang, S.; George, A.; Singer, S. W.; Simmons, B. A.; Singh, S. GreenOne-Pot Ionic Liquid Pretreatment and Saccharification of Switchgrass. 2013, 15, 2579–2589. https://doi.org/10.1039/c3gc40545a.

(67) Verdía, P.; Brandt, A.; Hallett, J. P.; Ray, M. J.; Welton, T. Fractionation of Lignocellulosic Biomass with the Ionic Liquid 1-Butylimidazolium Hydrogen Sulfate. Green Chem. 2014, 16 (3), 1617–1627. https://doi.org/10.1039/c3gc41742e.

(68) Gschwend, F. J. V.; Brandt-Talbot, A.; Chambon, C. L.; Hallett, J. P. Ultra-Low Cost Ionic Liquids for the Delignification of Biomass. ACS Symp. Ser. 2017, 1250, 209–223. https://doi.org/10.1021/bk-2017-1250.ch009.

(69) McKendry, P. Energy Production from Biomass (Part 2): Conversion Technologies. Bioresour. Technol. 2002, 83 (1), 47–54. https://doi.org/10.1016/S0960-8524(01)00119-5.

(70) Axelsson, L.; Franzén, M.; Ostwald, M.; Berndes, G.; Lakshmi, G.; Ravindranath, N. H. Lignin Pyrolysis for Profitable Lignocellulosic Biorefineries. Bioffpr 2012, 6 (3), 246–256. https://doi.org/10.1002/bbb.

(71) De Wild, P. J.; Huijgen, W. J. J.; Heeres, H. J. Pyrolysis of Wheat Straw-Derived Organosolv Lignin. J. Anal. Appl. Pyrolysis 2012, 93, 95–103. https://doi.org/10.1016/j.jaap.2011.10.002.

(72) Mohan, D.; Pittman, C. U.; Steele, P. H. Pyrolysis of Wood/Biomass for Bio-Oil: A Critical Review. Energy and Fuels 2006, 20 (3), 848–889. https://doi.org/10.1021/ef0502397.

(73) Kumar, A. K.; Sharma, S. Recent Updates on Different Methods of Pretreatment of Lignocellulosic Feedstocks: A Review. Bioresources and Bioprocessing. Springer, 2017. https://doi.org/10.1186/s40643-017-0137-9.

(74) Usmani, Z.; Sharma, M.; Gupta, P.; Karpichev, Y.; Gathergood, N.; Bhat, R.; Gupta, V. K. Ionic Liquid Based Pretreatment of Lignocellulosic Biomass for Enhanced Bioconversion. Bioresour. Technol. 2020, 304, 123003. https://doi.org/10.1016/j.biortech.2020.123003.

(75) Kumar, A. K.; Sharma, S. Recent Updates on Different Methods of Pretreatment of Lignocellulosic Feedstocks: A Review. Bioresour. Bioprocess. 2017, 4 (1), 7. https://doi.org/10.1186/s40643-017-0137-9.

(76) Li, C.; Sun, L.; Simmons, B. A.; Singh, S. Comparing the Recalcitrance of Eucalyptus , Pine , and Switchgrass Using Ionic Liquid and Dilute Acid Pretreatments. 2013, 14–23. https://doi.org/10.1007/s12155-012-9220-4.

(77) Shi, J.; Thompson, V. S.; Yancey, N. A.; Stavila, V.; Simmons, B. A. Impact of Mixed Feedstocks and Feedstock Densification on Ionic Liquid Pretreatment Efficiency Impact of Mixed Feedstocks and Feedstock Densification on Ionic Liquid Pretreatment Efficiency. Biofuels, 2017, 4(1), 63-72. https://doi.org/10.4155/bfs.12.82.

(78) Sims, R. E. H.; Mabee, W.; Saddler, J. N.; Taylor, M. An Overview of Second Generation Biofuel Technologies. Bioresour. Technol. 2010, 101 (6), 1570–1580. https://doi.org/10.1016/j.biortech.2009.11.046.

(79) Isogai, A.; Hänninen, T.; Fujisawa, S.; Saito, T. Review: Catalytic Oxidation of Cellulose with Nitroxyl Radicals under Aqueous Conditions. Progress in Polymer Science. Elsevier Ltd, 2018, 122–148. https://doi.org/10.1016/j.progpolymsci.2018.07.007.

(80) Moon, R. J.; Martini, A.; Nairn, J.; Simonsen, J.; Youngblood, J. Cellulose Nanomaterials Review: Structure, Properties and Nanocomposites. Chemical Society Reviews. The Royal Society of Chemistry July 20, 2011, pp 3941–3994. https://doi.org/10.1039/c0cs00108b.

(81) Medronho, B., & Lindman, B. Competing forces during cellulose dissolution: from solvents to mechanisms. Curr. Opin. Colloid Interface Sci., 2014, 19(1), 32-40. https://doi.org/10.1016/j.cocis.2013.12.001

(82) Brinchi, L.; Cotana, F.; Fortunati, E.; Kenny, J. M. Production of Nanocrystalline Cellulose from Lignocellulosic Biomass: Technology and Applications. Carbohydrate Polymers. April 15, 2013, pp 154–169. https://doi.org/10.1016/j.carbpol.2013.01.033.

(83) Qian, X.; Ding, S.; Nimlos, M. R.; Johnson, D. K.; Himmel, M. E. Atomic and Electronic Structures of Molecular Crystalline Cellulose I : A First-Principles Investigation. 2005, 10580–10589.

(84) Nechyporchuk, O.; Belgacem, M. N.; Bras, J. Production of Cellulose Nanofibrils: A Review of Recent Advances. Industrial Crops and Products. Elsevier B.V. December 25, 2016, pp 2–25. https://doi.org/10.1016/j.indcrop.2016.02.016.

(85) Kumar, H.; Christopher, L. P. Recent Trends and Developments in Dissolving Pulp Production and Application. Cellulose 2017, 24 (6), 2347–2365. https://doi.org/10.1007/s10570-017-1285-y.

(86) Michud, A.; Tanttu, M.; Asaadi, S.; Ma, Y.; Netti, E.; Kääriainen, P.; Persson, A.; Berntsson, A.; Hummel, M.; Sixta, H. Ioncell-F: Ionic Liquid-Based Cellulosic Textile Fibers as an Alternative to Viscose and Lyocell. Text. Res. J. 2016, 86 (5), 543–552. https://doi.org/10.1177/0040517515591774.

(87) Klemm, D.; Heublein, B.; Fink, H. P.; Bohn, A. Cellulose: Fascinating Biopolymer and Sustainable Raw Material. Angewandte Chemie - International Edition. May 30, 2005, pp 3358–3393. https://doi.org/10.1002/anie.200460587.

(88) Liu, Y.; Shi, L.; Cheng, D.; He, Z. Dissolving Pulp Market and Technologies: Chinese Prospective - a Mini-Review. BioResources 2016, 11 (3), 7902–7916. https://doi.org/10.15376/biores.11.3.Liu.

(89) Chen, C.; Duan, C.; Li, J.; Liu, Y.; Ma, X. Cellulose (Dissolving Pulp) Manufacturing Processes: A Mini Review. Bioresources, 2016, 11 (2), 5553–5564. https://doi.org/10.15376/BOIRES.11.2

(90) Hanabusa, H.; Izgorodina, E. I.; Suzuki, S.; Takeoka, Y.; Rikukawa, M.; Yoshizawa-Fujita, M. Cellulose-Dissolving Protic Ionic Liquids as Low Cost Catalysts

for Direct Transesterification Reactions of Cellulose. Green Chem. 2018, 20 (6), 1412–1422. https://doi.org/10.1039/c7gc03603e.

(91) Girisuta, B.; Janssen, L. P. B. M.; Heeres, H. J. Kinetic Study on the Acid-Catalyzed Hydrolysis of Cellulose to Levulinic Acid. Ind. Eng. Chem. Res, 2007, 1696–1708. https://doi.org/10.1021/ie061186z

(92) Eminov, S.; Brandt, A.; Wilton-Ely, J. D. E. T.; Hallett, J. P. The Highly Selective and Near-Quantitative Conversion of Glucose to 5-Hydroxymethylfurfural Using Ionic Liquids. PLoS One, 2016, 11 (10), e0163835. https://doi.org/10.1371/journal.pone.0163835.

(93) Binder, J. B.; Cefali, A. V.; Blank, J. J.; Raines, R. T. Mechanistic Insights on the Conversion of Sugars into 5- Hydroxymethylfurfural. Energy Environ. Sci. 2010, 3 (6), 765–771. https://doi.org/10.1039/b923961h.

(94) Putten, R. Van; Waal, J. C. Van Der; Jong, E. De; Rasrendra, C. B.; Heeres, H. J.; Vries, J. G. De. Hydroxymethylfurfural , A Versatile Platform Chemical Made from Renewable Resources. Chem. Rev. 2013, 113 (3),1499−1597.

(95) Hu, F.; Jung, S.; Ragauskas, A. Pseudo-Lignin Formation and Its Impact on Enzymatic Hydrolysis. Bioresour. Technol. 2012, 117, 7 -12. https://doi.org/10.1016/j.biortech.2012.04.037.

(96) Willfo, S. Spruce-Derived Mannans – A Potential Raw Material for Hydrocolloids and Novel Advanced Natural Materials. Carbohydr, 2008, 72, 197–210. https://doi.org/10.1016/j.carbpol.2007.08.006.

(97) Binder, J. B.; Blank, J. J.; Cefali, A. V.; Raines, R. T. Synthesis of Furfural from Xylose and Xylan. ChemSusChem, 2010, 3 (11), 1268–1272. https://doi.org/10.1002/cssc.201000181.

(98) Lange, J.; Heide, E. Van Der; Buijtenen, J. Van; Price, R. Furfural — A Promising Platform for Lignocellulosic Biofuels. ChemSusChem, 2012, 150–166. https://doi.org/10.1002/cssc.201100648.

(99) Putten, R. Van; Waal, J. C. Van Der; Jong, E. De; Rasrendra, C. B.; Heeres, H. J.; Vries, J. G. De. Hydroxymethylfurfural , A Versatile Platform Chemical Made from Renewable Resources. Chem Rev, 2013. 113(3), 1499-1597. https://doi.org/10.1021/cr300182k

(100) Pandey, M. P.; Kim, C. S. Lignin Depolymerization and Conversion: A Review of Thermochemical Methods. Chem. Eng. Technol. 2011, 34 (1), 29–41. https://doi.org/10.1002/ceat.201000270.

(101) Xu, C.; Arneil, R.; Arancon, D.; Labidi, J.; Luque, R. Lignin Depolymerisation Strategies: Towards Valuable Chemicals and Fuels. Chem. Soc. Rev. Chem. Soc. Rev 2014, 43 (43), 7485–7500. https://doi.org/10.1039/c4cs00235k.

(102) Mainka, H.; Täger, O.; Körner, E.; Hilfert, L.; Busse, S.; Edelmann, F. T.; Herrmann, A. S. Lignin – an Alternative Precursor for Sustainable and Cost-Effective Automotive Carbon Fiber. Integr. Med. Res. 2015, 4, 283–296. https://doi.org/10.1016/j.jmrt.2015.03.004.

(103) Li, M.; Pu, Y.; Ragauskas, A. J. Current Understanding of the Correlation of Lignin Structure with Biomass Recalcitrance. Front. Chem. 2016, 4, 1–8. https://doi.org/10.3389/fchem.2016.00045.

(104) Alvira, P.; Ballesteros, M.; Negro, M. J. Bioresource Technology Pretreatment Technologies for an Efficient Bioethanol Production Process Based on Enzymatic Hydrolysis : A Review. Bioresour. Technol. 2010, 101 (13), 4851–4861. https://doi.org/10.1016/j.biortech.2009.11.093.

(105) Alvira, P.; Ballesteros, M.; Negro, M. J. Pretreatment Technologies for an Efficient Bioethanol Production Process Based on Enzymatic Hydrolysis : A Review. Bioresour. Technol. 2010, 101 (13), 4851–4861. https://doi.org/10.1016/j.biortech.2009.11.093.

(106) Chen, H.; Liu, J.; Chang, X.; Chen, D.; Xue, Y.; Liu, P.; Lin, H.; Han, S. A Review on the Pretreatment of Lignocellulose for High-Value Chemicals. Fuel Process. Technol. 2017, 160, 196–206. https://doi.org/10.1016/j.fuproc.2016.12.007.

(107) Rahikainen, J.; Mikander, S.; Marjamaa, K.; Tamminen, T. Inhibition of Enzymatic Hydrolysis by Residual Lignins From Softwood — Study of Enzyme Binding and Inactivation on Lignin-Rich Surface. Biotechol. Bioeng. 2011, 108 (12), 2823–2834. https://doi.org/10.1002/bit.23242.

(108) Kai, D.; Tan, M. J.; Chee, P. L.; Chua, Y. K.; Yap, Y. L.; Loh, X. J. Towards Lignin-Based Functional Materials in a Sustainable World. Green Chem. 2016, 18 (5), 1175–1200. https://doi.org/10.1039/c5gc02616d.

(109) Fort, D. A.; Remsing, R. C.; Swatloski, R. P.; Moyna, P.; Moyna, G.; Rogers, R. D. Can Ionic Liquids Dissolve Wood? Processing and Analysis of Lignocellulosic Materials with 1-n-Butyl-3-Methylimidazolium Chloride. Green Chem. 2007, 9 (1), 63–69. https://doi.org/10.1039/B607614A.

(110) Huntley, S. K.; Ellis, D.; Gilbert, M.; Chapple, C.; Mansfield, S. D. Significant Increases in Pulping Efficiency in C4H-F5H-Transformed Poplars: Improved Chemical Savings and Reduced Environmental Toxins. J. Agric. Food Chem. 2003, 51 (21), 6178–6183. https://doi.org/10.1021/jf034320o.

(111) Jawjit, W.; Kroeze, C.; Soontaranun, W.; Hordijk, L. Future Trends in Environmental Impact of Eucalyptus-Based Kraft Pulp Industry in Thailand: A Scenario Analysis. Environ. Sci. Policy 2008, 11 (6), 545–561. https://doi.org/10.1016/j.envsci.2008.03.004.

(112) McKendry, P. Energy Production from Biomass (Part 1): Overview of Biomass. Bioresour. Technol 2002, 83 (1), 37–46. https://doi.org/10.1016/S0960-8524(01)00118-3.

(113) Hongdan, Z.; Shaohua, X.; Shubin, W. Bioresource Technology Enhancement of Enzymatic Saccharification of Sugarcane Bagasse by Liquid Hot Water Pretreatment. Bioresour. Technol. 2013, 143, 391–396. https://doi.org/10.1016/j.biortech.2013.05.103.

(114) Rolly, R.; Sivagurunathan, P.; Kim, S. ScienceDirect Effect of Severity on Dilute Acid Pretreatment of Lignocellulosic Biomass and the Following Hydrogen

Fermentation. Int. J. Hydrogen Energy 2016, 41 (46), 21678–21684. https://doi.org/10.1016/j.ijhydene.2016.06.198.

(115) Bonner, I. J.; Thompson, D. N.; Teymouri, F.; Campbell, T.; Bals, B.; Tumuluru, J. S.; Bonner, I. J.; Thompson, D. N.; Teymouri, F.; Campbell, T.; Bonner, I. J.; Thompson, D. N.; Teymouri, F.; Campbell, T.; Bals, B.; Tumuluru, J. S. Impact of Sequential Ammonia Fiber Expansion (AFEX) Pretreatment and Pelletization on the Moisture Sorption Properties of Corn Stover. Drying Technol. 2015, 33 (14), 1768–1778. https://doi.org/10.1080/07373937.2015.1039127.

(116) Socha, A. M.; Parthasarathi, R.; Shi, J.; Pattathil, S.; Whyte, D. Efficient Biomass Pretreatment Using Ionic Liquids Derived from Lignin and Hemicellulose. Proceedings of the national academy of sciences, 2014, 111 (35), 1–9. https://doi.org/10.1073/pnas.1405685111.

(117) Shi, J.; Gladden, J. M.; Sathitsuksanoh, N.; Kambam, P.; Sandoval, L.; Mitra, D.; Zhang, S.; George, A.; Singer, S. W.; Simmons, B. a.; Singh, S. One-Pot Ionic Liquid Pretreatment and Saccharification of Switchgrass. Green Chem. 2013, 15 (9), 2579. https://doi.org/10.1039/c3gc40545a.

(118) Wijaya, Y. P.; Putra, R. D. D.; Widyaya, V. T.; Ha, J. M.; Suh, D. J.; Kim, C. S. Comparative Study on Two-Step Concentrated Acid Hydrolysis for the Extraction of Sugars from Lignocellulosic Biomass. Bioresour. Technol. 2014, 164, 221–231. https://doi.org/10.1016/j.biortech.2014.04.084.

(119) Li, M.; Tu, M.; Cao, D.; Bass, P.; Adhikari, S. Distinct Roles of Residual Xylan and Lignin in Limiting Enzymatic Hydrolysis of Organosolv Pretreated Loblolly Pine and Sweetgum. J. Agric. Food Chem. 2013, 61 (3), 646–654. https://doi.org/10.1021/jf304517w.

(120) Karimi, K., Shafiei, M., & Kumar, R. Progress in physical and chemical pretreatment of lignocellulosic biomass. In Biofuel technologies, 2013, (pp. 53-96). Springer, Berlin, Heidelberg.

(121) Lin, Z.; Huang, H.; Zhang, H. Ball Milling Pretreatment of Corn Stover for Enhancing the Efficiency of Enzymatic Hydrolysis. Appl. Biochem. Bioetech. 2010, 162, 1872–1880. https://doi.org/10.1007/s12010-010-8965-5.

(122) Sun, N.; Rahman, M.; Qin, Y.; Maxim, M. L. Complete Dissolution and Partial Delignification of Wood in the Ionic Liquid 1-Ethyl-3-Methylimidazolium Acetate Green Chem. 2009, 11 (5), 646–655. https://doi.org/10.1039/b822702k.

(123) Sun, S.; Sun, S.; Cao, X.; Sun, R. The Role of Pretreatment in Improving the Enzymatic Hydrolysis of Lignocellulosic Materials. Bioresour. Technol. 2016, 199, 49–58. https://doi.org/10.1016/j.biortech.2015.08.061.

(124) Online, V. A.; Homepage, J.; Technology, P. Technology Development for the Production of Biobased Products from Biorefinery Carbohydrates — the US Department of Energy ' s " Top 10 " Revisited. Green Chem. 2010, 12 (4). https://doi.org/10.1039/b922014c.

(125) Jørgensen, H.; Jan, K.; Claus, F. Enzymatic Conversion of Lignocellulose into Fermentable Sugars: Challenges and Opportunities. Biofuels, Bioprod. Biorefining 2007, 1 (2), 119–134. https://doi.org/10.1002/bbb.

(126) Oliveira, F. M. V.; Pinheiro, I. O.; Souto-Maior, A. M.; Martin, C.; Gonçalves, A. R.; Rocha, G. J. M. Industrial-Scale Steam Explosion Pretreatment of Sugarcane Straw for Enzymatic Hydrolysis of Cellulose for Production of Second Generation Ethanol and Value-Added Products. Bioresour. Technol. 2013, 130, 168–173. https://doi.org/10.1016/j.biortech.2012.12.030.

(127) Aden, a; Ruth, M.; Ibsen, K.; Jechura, J.; Neeves, K.; Sheehan, J.; Wallace, B.; Montague, L.; Slayton, A.; Lukas, J. Lignocellulosic Biomass to Ethanol Process Design and Economics Utilizing Co-Current Dilute Acid Prehydrolysis and Enzymatic Hydrolysis for Corn Stover. Natl. Renew. Energy Lab. 2002, No. June, Medium: ED; Size: 154 pages. https://doi.org/NREL/TP-510-32438.

(128) Bals, B.; Rogers, C.; Jin, M.; Balan, V.; Dale, B. Evaluation of Ammonia Fiber Expansion (AFEX) Pretreatment for Enzymatic Hydrolysis of Switchgrass Harvested in Different Seasons and Locations. Biotechnol. Biofuels 2010, 3, 1–11. https://doi.org/10.1186/1754-6834-3-1.

(129) Park, N.; Kim, H. Y.; Koo, B. W.; Yeo, H.; Choi, I. G. Organosolv Pretreatment with Various Catalysts for Enhancing Enzymatic Hydrolysis of Pitch Pine (Pinus Rigida). Bioresour. Technol. 2010, 101 (18), 7046–7053. https://doi.org/10.1016/j.biortech.2010.04.020.

(130) Zhao, X.; Cheng, K.; Liu, D. Organosolv Pretreatment of Lignocellulosic Biomass for Enzymatic Hydrolysis. Applied Microbiology and Biotechnology. Springer April 1, 2009, pp 815–827. https://doi.org/10.1007/s00253-009-1883-1.

(131) Zhao, X.; Cheng, K.; Liu, D. Organosolv Pretreatment of Lignocellulosic Biomass for Enzymatic Hydrolysis. Appl. Microbiol. Biotechnol. 2009, 82 (5), 815–827. https://doi.org/10.1007/s00253-009-1883-1.

(132) Chen, M.; Malaret, F.; Firth, A. E. J.; Verdía, P.; Abouelela, A. R.; Chen, Y.; Hallett, J. P. Design of a Combined Ionosolv-Organosolv Biomass Fractionation Process for Biofuel Production and High Value-Added Lignin Valorisation. Green Chem. 2020, 22 (15), 5161–5178. https://doi.org/10.1039/d0gc01143f.

(133) Kilpeläinen, I.; Xie, H.; King, A.; Granstrom, M.; Heikkinen, S.; Argyropoulos, D. S. Dissolution of Wood in Ionic Liquids. J. Agric. Food Chem. 2007, 55 (22), 9142–9148. https://doi.org/10.1021/jf071692e.

(134) Singh, S.; Simmons, B. A.; Vogel, K. P. Visualization of Biomass Solubilization and Cellulose Regeneration during Ionic Liquid Pretreatment of Switchgrass. Biotechnol. Bioeng. 2009, 104 (1), 68–75. https://doi.org/10.1002/bit.22386.

(135) Mäki-Arvela, P.; Anugwom, I.; Virtanen, P.; Sjöholm, R.; Mikkola, J. P. Dissolution of Lignocellulosic Materials and Its Constituents Using Ionic Liquids-A Review. Ind. Crops Prod. 2010, 32 (3), 175–201. https://doi.org/10.1016/j.indcrop.2010.04.005.

(136) Ac, O. F.; For, P. SOLVENTS FOR USE IN THE TREATMENT OF LIGNIN-CONTAINING MATERALS. 2017, 1 (19). https://doi.org/10.1016/j.(73).

(137) Varanasi, S. Biomass Pretreatment. (2011). U.S. Patent No. 8,030,030. Washington, DC: U.S. Patent and Trademark Office.

(138) Brandt, A.; Ray, M. J.; To, T. Q.; Leak, D. J.; Murphyb, R. J. Ionic Liquid Pretreatment of Lignocellulosic Biomass with Ionic Liquid Water Mixtures. Green Chem. 2011, 2489–2499.

(139) Brandt, A.; Gschwend, F.; Fennell, P.; Lammens, T.; Tan, B.; Weale, J.; Hallett, J. P. An Economically Viable Ionic Liquid for the Fractionation of Lignocellulosic Biomass †. Green Chem. 2017. https://doi.org/10.1039/c7gc00705a.

(140) Gschwend, F. J. V.; Brandt-Talbot, A. Rapid Pretreatment of Miscanthus Using the Low-Cost Ionic Liquid Triethylammonium Hydrogen Sulfate at Elevated Temperatures. Green Chem. 2016, 20 (15), 3486–3498. https://doi.org/10.1039/c8gc00837j.

(141) Swatloski, R. P.; Spear, S. K.; Holbrey, J. D.; Rogers, R. D. Dissolution of Cellose with Ionic Liquids. J. Am. Chem. Soc. 2002, 124 (18), 4974–4975. https://doi.org/10.1021/ja025790m.

(142) Li, W.; Sun, N.; Stoner, B.; Jiang, X.; Lu, X.; Rogers, R. D. Rapid Dissolution of Lignocellulosic Biomass in Ionic Liquids Using Temperatures above the Glass Transition of Lignin. Green Chem. 2011, 13 (8), 2038. https://doi.org/10.1039/c1gc15522a.

(143) Doherty, T. V.; Mora-Pale, M.; Foley, S. E.; Linhardt, R. J.; Dordick, J. S. Ionic Liquid Solvent Properties as Predictors of Lignocellulose Pretreatment Efficacy. Green Chem. 2010, 12 (11), 1967. https://doi.org/10.1039/c0gc00206b.

(144) All web-based pricing (http://www.sigmaaldrich.com or http://www.icis.com) were accessed in November 2020.

(145) Chen, L.; Sharifzadeh, M.; Mac Dowell, N.; Welton, T.; Shah, N.; Hallett, J. P. Inexpensive Ionic Liquids: [HSO4] − -Based Solvent Production at Bulk Scale. Green Chem. 2014, 16 (6), 3098–3106. https://doi.org/10.1039/C4GC00016A.

(146) Baaqel, H.; Díaz, I.; Tulus, V.; Chachuat, B.; Guillén-Gosálbez, G.; Hallett, J. P. Role of Life-Cycle Externalities in the Valuation of Protic Ionic Liquids – a Case Study in Biomass Pretreatment Solvents. Green Chem. 2020. https://doi.org/10.1039/D0GC00058B.

(147) Gschwend, F. J. V.; Chambon, C. L.; Biedka, M.; Brandt-Talbot, A.; Fennell, P. S.; Hallett, J. P. Quantitative Glucose Release from Softwood after Pretreatment with Low-Cost Ionic Liquids. Green Chem. 2019, 21 (3), 692–703. https://doi.org/10.1039/c8gc02155d.

(148) Brandt, A.; Chen, L.; Van Dongen, B. E.; Welton, T.; Hallett, J. P. Structural Changes in Lignins Isolated Using an Acidic Ionic Liquid Water Mixture. Green Chem. 2015, 17. https://doi.org/10.1039/c5gc01314c.

(149) Gregorio, G. F. De; Weber, C. C.; Gräsvik, J.; Welton, T. Mechanistic Insights into Lignin Depolymerisation in Acidic Ionic Liquids. Green Chem. 2016. https://doi.org/10.1039/c6gc01295g.

(150) Malaret, F.; Gschwend, F. J. V.; Lopes, J. M.; Tu, W. C.; Hallett, J. P. Eucalyptus Red Grandis Pretreatment with Protic Ionic Liquids: Effect of Severity and

Influence of Sub/Super-Critical CO2 Atmosphere on Pretreatment Performance. RSC Adv. 2020, 10 (27), 16050–16060. https://doi.org/10.1039/d0ra02040k.

(151) Brandt, A.; Ray, M. J.; To, T. Q.; Leak, D. J.; Murphy, R. J.; Welton, T. Ionic Liquid Pretreatment of Lignocellulosic Biomass with Ionic Liquid-Water Mixtures. Green Chem. 2011, 13 (9), 2489–2499. https://doi.org/10.1039/c1gc15374a.

(152) Chambon, C. L.; Chen, M.; Fennell, P. S.; Hallett, J. P. Efficient Fractionation of Lignin- and Ash-Rich Agricultural Residues Following Treatment with a Low-Cost Protic Ionic Liquid. Front. Chem. 2019, 7 (MAR), 1–13. https://doi.org/10.3389/fchem.2019.00246.

(153) Gschwend, F. J. V.; Malaret, F.; Shinde, S.; Brandt-Talbot, A.; Hallett, J. P. Rapid Pretreatment of: Miscanthus Using the Low-Cost Ionic Liquid Triethylammonium Hydrogen Sulfate at Elevated Temperatures. Green Chem. 2018, 20 (15), 3486–3498. https://doi.org/10.1039/c8gc00837j.

(154) Shinde, S. D.; Meng, X.; Kumar, R.; Ragauskas, A. J. Recent Advances in Understanding the Pseudo-Lignin Formation in a Lignocellulosic Biorefinery. Green Chem. 2018, 20 (10), 2192–2205. https://doi.org/10.1039/c8gc00353j.

(155) Kumar, R.; Hu, F.; Sannigrahi, P.; Jung, S.; Ragauskas, A. J.; Wyman, C. E. Carbohydrate Derived-Pseudo-Lignin Can Retard Cellulose Biological Conversion. Biotechnol. Bioeng. 2013, 110 (3), 737–753. https://doi.org/10.1002/bit.24744.

(156) Tu, W. C.; Weigand, L.; Hummel, M.; Sixta, H.; Brandt-Talbot, A.; Hallett, J. P. Characterisation of Cellulose Pulps Isolated from Miscanthus Using a Low-Cost Acidic Ionic Liquid. Cellulose 2020, 1–17. https://doi.org/10.1007/s10570-020-03073-1.

(157) Liang, X.; Liu, J.; Fu, Y.; Chang, J. Influence of Anti-Solvents on Lignin Fractionation of Eucalyptus Globulus via Green Solvent System Pretreatment. Sep. Purif. Technol. 2016, 163, 258–266. https://doi.org/10.1016/j.seppur.2016.03.006.

(158) Zakzeski, J.; Bruijnincx, P. C. A.; Jongerius, A. L.; Weckhuysen, B. M. The Catalytic Valorization of Lignin for the Production of Renewable Chemicals. Chem. Rev. 2010, 110 (6), 3552–3599.

(159) Arora, R.; Manisseri, C.; Li, C.; Ong, M. D.; Scheller, H. V.; Vogel, K.; Simmons, B. A.; Singh, S. Monitoring and Analyzing Process Streams towards Understanding Ionic Liquid Pretreatment of Switchgrass (Panicum Virgatum L.). Bioenergy Res. 2010, 3 (2), 134–145. https://doi.org/10.1007/s12155-010-9087-1.

(160) Modenbach, A. A.; Nokes, S. E. Enzymatic Hydrolysis of Biomass at High-Solids Loadings - A Review. Biomass and Bioenergy 2013, 56, 526–544. https://doi.org/10.1016/j.biombioe.2013.05.031.

(161) Samaniuk, J. R.; Scott, C. T.; Root, T. W.; Klingenberg, D. J. Rheological Modification of Corn Stover Biomass at High Solids Concentrations. J. Rheol. (N. Y. N. Y). 2012, 56 (3), 649–665. https://doi.org/10.1122/1.3702101.

(162) Papa, G.; Feldman, T.; Sale, K. L.; Adani, F.; Singh, S.; Simmons, B. A. Parametric Study for the Optimization of Ionic Liquid Pretreatment of Corn Stover. Bioresour. Technol. 2017, 241, 627–637. https://doi.org/10.1016/j.biortech.2017.05.167.

(163) Wood, A. T.; Augustsson, A.; Louise, S. Persistent Hazardous Waste and the Quest Toward a Circular Economy The Example of Arsenic in Chromated Copper. 2016, 21 (3), 689–699. https://doi.org/10.1111/jiec.12516.

(164) Defra Gov UK. Wood Waste : A Short Review of Recent Research; London, UK, 2012.

(165) Wood Recycler Association. Writing Waste Wood Fire Prevention Plans (FPPs); Worcestershire,UK, 2018.

(166) Krook, J.; Mårtensson, A.; Eklund, M. Sources of Heavy Metal Contamination in Swedish Wood Waste Used for Combustion. Waste Manag. 2006, 26 (2), 158–166. https://doi.org/10.1016/j.wasman.2005.07.017.

(167) Coudert, L.; Blais, J. F.; Mercier, G.; Cooper, P.; Janin, A.; Gastonguay, L. Demonstration of the Efficiency and Robustness of an Acid Leaching Process to Remove Metals from Various CCA-Treated Wood Samples. J. Environ. Manage. 2014, 132, 197–206. https://doi.org/10.1016/j.jenvman.2013.11.028.

(168) Janin, A.; Blais, J. F.; Mercier, G.; Drogui, P. Optimization of a Chemical Leaching Process for Decontamination of CCA-Treated Wood. J. Hazard. Mater. 2009, 169 (1–3), 136–145. https://doi.org/10.1016/j.jhazmat.2009.03.064.

(169) Kramb, J.; Konttinen, J.; Backman, R.; Salo, K.; Roberts, M. Elimination of Arsenic-Containing Emissions from Gasification of Chromated Copper Arsenate Wood. Fuel, 2016, 181, 319–324. https://doi.org/10.1016/j.fuel.2016.04.109.

(170) Edo, M.; Björn, E.; Persson, P.; Jansson, S. Assessment of Chemical and Material Contamination in Waste Wood Fuels – A Case Study Ranging over Nine Years. Waste Manag. 2016, 49, 311–319. https://doi.org/10.1016/j.wasman.2015.11.048.

(171) Nzihou, A.; Stanmore, B. The Fate of Heavy Metals during Combustion and Gasification of Contaminated Biomass — A Brief Review. J. Hazard. Mater. 2013, 256–257, 56–66. https://doi.org/10.1016/j.jhazmat.2013.02.050.

(172) Babel, S.; del Mundo Dacera, D. Heavy Metal Removal from Contaminated Sludge for Land Application: A Review. Waste Manag. 2006, 26 (9), 988–1004. https://doi.org/10.1016/j.wasman.2005.09.017.

(173) Stylianou, M. A.; Kollia, D.; Haralambous, K. J.; Inglezakis, V. J.; Moustakas, K. G.; Loizidou, M. D. Effect of Acid Treatment on the Removal of Heavy Metals from Sewage Sludge. Desalination, 2007, 215 (1–3), 73–81. https://doi.org/10.1016/j.desal.2006.11.015.

(174) Zaier, H.; Ghnaya, T.; Ben Rejeb, K.; Lakhdar, A.; Rejeb, S.; Jemal, F. Effects of EDTA on Phytoextraction of Heavy Metals (Zn, Mn and Pb) from Sludge-Amended Soil with Brassica Napus. Bioresour. Technol. 2010, 101 (11), 3978–3983. https://doi.org/10.1016/j.biortech.2010.01.035.

(175) Babel, S.; del Mundo Dacera, D. Heavy Metal Removal from Contaminated Sludge for Land Application: A Review. Waste Manag. 2006, 26 (9), 988–1004. https://doi.org/10.1016/j.wasman.2005.09.017.

(176) Wu, Q.; Cui, Y.; Li, Q.; Sun, J. Effective Removal of Heavy Metals from Industrial Sludge with the Aid of a Biodegradable Chelating Ligand GLDA. J. Hazard. Mater. 2015, 283, 748–754. https://doi.org/10.1016/j.jhazmat.2014.10.027.

(177) Barakat, M. A. New Trends in Removing Heavy Metals from Industrial Wastewater. Arabian Journal of Chemistry. Elsevier October 1, 2011, pp 361–377. https://doi.org/10.1016/j.arabjc.2010.07.019.

(178) Hanay, O.; Hasar, H.; Kocer, N. N. Effect of EDTA as Washing Solution on Removing of Heavy Metals from Sewage Sludge by Electrokinetic. J. Hazard. Mater. 2009, 169 (1–3), 703–710. https://doi.org/10.1016/j.jhazmat.2009.04.008.

(179) del Mundo Dacera, D.; Babel, S. Use of Citric Acid for Heavy Metals Extraction from Contaminated Sewage Sludge for Land Application. Water Sci. Technol. 2006, 54 (9), 129–135. https://doi.org/10.2166/wst.2006.764.

(180) Gschwend, F. J. V; Hennequin, L. M.; Brandt, A.; Bedoya-Lora, F. E.; Kelsall, G. H.; Polizzi, K.; Fennell, P.; Hallett, J. Towards an Environmentally and Economically Sustainable Biorefinery: Heavy Metal Contaminated Waste Wood as a Low-Cost Feedstock in a Low-Cost Ionic Liquid Process. Green Chem. 2020. https://doi.org/10.1039/D0GC01241F.

(181) Fischer, L.; Falta, T.; Koellensperger, G.; Stojanovic, A.; Kogelnig, D.; Galanski, M.; Krachler, R.; Keppler, B. K.; Hann, S. Ionic Liquids for Extraction of Metals and Metal Containing Compounds from Communal and Industrial Waste Water. Water Res. 2011, 45 (15), 4601–4614. https://doi.org/10.1016/j.watres.2011.06.011.

(182) Zhang, Q.; Wang, Q.; Zhang, S.; Lu, X.; Zhang, X. Electrodeposition in Ionic Liquids. ChemPhysChem 2016, 17 (3), 335–351. https://doi.org/10.1002/cphc.201500713.

(183) Gnansounou, E.; Dauriat, A. Technoeconomic Analysis of Lignocellulosic Ethanol. Biofuels 2011, 101 (13), 123–148. https://doi.org/10.1016/B978-0-12-385099-7.00006-1.

(184) Tao, L.; Aden, A.; Elander, R. T.; Pallapolu, V. R.; Lee, Y. Y.; Garlock, R. J.; Balan, V.; Dale, B. E.; Kim, Y.; Mosier, N. S.; Ladisch, M. R.; Falls, M.; Holtzapple, M. T.; Sierra, R.; Shi, J.; Ebrik, M. A.; Redmond, T.; Yang, B.; Wyman, C. E.; Hames, B.; Thomas, S.; Warner, R. E. Process and Technoeconomic Analysis of Leading Pretreatment Technologies for Lignocellulosic Ethanol Production Using Switchgrass. Bioresour. Technol. 2011, 102, 11105–11114. https://doi.org/10.1016/j.biortech.2011.07.051.

(185) Yu, Y.-S. Uncovering the Cost of Cellulosic Ethanol Production; 2016, Lux Research, Jan 19th

(186) Pedersen, M.; Meyer, A. S. Lignocellulose Pretreatment Severity - Relating PH to Biomatrix Opening. N. Biotechnol. 2010, 27 (6), 739–750. https://doi.org/10.1016/j.nbt.2010.05.003.

(187) Overend, R. P.; Chornet, E. Fractionation of Lignocellulosics by Steam-Aqueous Pretreatments. Philos. Trans. R. Soc. London. 1987, 321 (1561), 523–536. https://doi.org/10.1098/rsta.1987.0029.

(188) Abatzoglou Nicolas, C. E. and B. K. Kinetics of Complex Systems : The Development of a Generalized Severity Parameter and Its Application To. Chem. Eng. Sci. 1992, 47 (5), 1109–1122.

(189) Yang, B.; Wyman, C. E. Effect of Xylan and Lignin Removal by Batch and Flowthrough Pretreatment on the Enzymatic Digestibility of Corn Stover Cellulose. Biotechnol. Bioeng. 2004, 86 (1), 88–98. https://doi.org/10.1002/bit.20043.

(190) Pedersen, M.; Viksø-Nielsen, A.; Meyer, A. S. Monosaccharide Yields and Lignin Removal from Wheat Straw in Response to Catalyst Type and PH during Mild Thermal Pretreatment. Process Biochem. 2010, 45 (7), 1181–1186. https://doi.org/10.1016/j.procbio.2010.03.020.

(191) Cox, B. J.; Jia, S.; Zhang, Z. C.; Ekerdt, J. G. Catalytic Degradation of Lignin Model Compounds in Acidic Imidazolium Based Ionic Liquids: Hammett Acidity and Anion Effects. Polym. Degrad. Stab. 2011, 96 (4), 426–431. https://doi.org/10.1016/j.polymdegradstab.2011.01.011.

(192) Gan, P. G.; Sam, S. T.; Abdullah, M. F. bin; Omar, M. F. Thermal Properties of Nanocellulose-reinforced Composites: A Review. J. Appl. Polym. Sci. 2020, 137 (11), 48544. https://doi.org/10.1002/app.48544.

(193) Brinchi, L.; Cotana, F.; Fortunati, E.; Kenny, J. M. Production of Nanocrystalline Cellulose from Lignocellulosic Biomass: Technology and Applications. Carbohydr. Polym. 2013, 94 (1), 154–169. https://doi.org/10.1016/j.carbpol.2013.01.033.

(194) Chen, M.; Ma, Q.; Zhu, J. Y.; Martin Alonso, D.; Runge, T. GVL Pulping Facilitates Nanocellulose Production from Woody Biomass. Green Chem. 2019, 21 (19), 5316–5325. https://doi.org/10.1039/c9gc01490j.

(195) Shak, K. P. Y.; Pang, Y. L.; Mah, S. K. Nanocellulose: Recent Advances and Its Prospects in Environmental Remediation. Beilstein J. Nanotechnol. 2018, 9 (1), 2479–2498. https://doi.org/10.3762/bjnano.9.232.

(196) Koshani, R.; Van De Ven, T. G. M.; Madadlou, A. Characterization of Carboxylated Cellulose Nanocrytals Isolated through Catalyst-Assisted H2O2 Oxidation in a One-Step Procedure. J. Agric. Food Chem. 2018, 66 (29), 7692–7700. https://doi.org/10.1021/acs.jafc.8b00080.

(197) Cheng, M.; Qin, Z.; Liu, Y.; Qin, Y.; Li, T.; Chen, L.; Zhu, M. Efficient Extraction of Carboxylated Spherical Cellulose Nanocrystals with Narrow Distribution through Hydrolysis of Lyocell Fibers by Using Ammonium Persulfate as an Oxidant. 2014, J.Mater.Chem A, 2(1), 251-258. https://doi.org/10.1039/c3ta13653a.

(198) Chen, D.; van de Ven, T. G. M. Morphological Changes of Sterically Stabilized Nanocrystalline Cellulose after Periodate Oxidation. Cellulose, 2016, 23 (2), 1051–1059. https://doi.org/10.1007/s10570-016-0862-9.

(199) Habibi, Y. Key Advances in the Chemical Modification of Nanocellulosses. Chem. Soc. Rev. 2014, 43(5), 1519–1542. https://doi.org/10.1039/c3cs60204d.

(200) Patel, D. K.; Dutta, S. D.; Lim, K. T. Nanocellulose-Based Polymer Hybrids and Their Emerging Applications in Biomedical Engineering and Water Purification. RSC

Adv. Royal Society of Chemistry June 14, 2019, pp 19143–19162. https://doi.org/10.1039/c9ra03261d.

(201) Habibi, Y.; Lucia, L. A.; Rojas, O. J. Cellulose Nanocrystals: Chemistry, Self-Assembly, and Applications. Chem. Rev. 2010, 110 (6), 3479–3500. https://doi.org/10.1021/cr900339w.

(202) Roman, M.; Winter, W. T. Effect of Sulfate Groups from Sulfuric Acid Hydrolysis on the Thermal Degradation Behavior of Bacterial Cellulose. Biomacromolecules, 2004. 5(5), 1671-1677. https://doi.org/10.1021/BM034519.

(203) Rånby, B. G. The Cellulose Micelles. Tappi 1952, 35, 53–58.

(204) Abdul Khalil, H. P. S.; Bhat, A. H.; Ireana Yusra, A. F. Green Composites from Sustainable Cellulose Nanofibrils: A Review. Carbohydrate Polymers. January 15, 2012, pp 963–979. https://doi.org/10.1016/j.carbpol.2011.08.078.

(205) Habibi, Y.; Chanzy, H.; Vignon, M. R. TEMPO-Mediated Surface Oxidation of Cellulose Whiskers. Cellulose 2006, 13 (6), 679–687. https://doi.org/10.1007/s10570-006-9075-y.

(206) Camarero Espinosa, S.; Kuhnt, T.; Foster, E. J.; Weder, C. Isolation of Thermally Stable Cellulose Nanocrystals by Phosphoric Acid Hydrolysis. Biomacromolecules, 2013, 14 (4), 1223–1230. https://doi.org/10.1021/bm400219u.

(207) Palme, A.; Theliander, H.; Brelid, H. Acid Hydrolysis of Cellulosic Fibers : Comparison of Bleached Kraft Pulp, Dissolving Pulps and Cotton Textile Cellulose. Carbohydr. Polym. 2016, 136, 1281–1287. https://doi.org/10.1016/j.carbpol.2015.10.015.

(208) Gong, J.; Li, J.; Xu, J.; Xiang, Z.; Mo, L. Research on Cellulose Nanocrystals Produced from Cellulose Sources with Various Polymorphs. RSC Adv. 2017, 7 (53), 33486–33493. https://doi.org/10.1039/c7ra06222b.

(209) Neng, W.; Enyong, D.; Rongshi, C. Preparation and Liquid Crystalline Properties of Spherical Cellulose Nanocrystals. Langmuir, 2008, 24 (1), 5–8. https://doi.org/10.1021/la702923w.

(210) Isogai, A.; Saito, T.; Fukuzumi, H. TEMPO-Oxidized Cellulose Nanofibers. Nanoscale. 2011, 3(1), 71–85. https://doi.org/10.1039/c0nr00583e.

(211) Goldstein, S.; Samuni, A. Kinetics and Mechanism of Peroxyl Radical Reactions with Nitroxides. J. Phys. Chem. A 2007, 111 (6), 1066–1072. https://doi.org/10.1021/jp0655975.

(212) Saito, T.; Kimura, S.; Nishiyama, Y.; Isogai, A. Cellulose Nanofibers Prepared by TEMPO-Mediated Oxidation of Native Cellulose. Biomacromolecules, 2007, 8 (8), 2485–2491. https://doi.org/10.1021/bm0703970.

(213) de Nooy, A. E.; Besemer, A. C.; van Bekkum, H. Selective oxidation of primary alcohols mediated by nitroxyl radical in aqueous solution. Kinetics and mechanism. Tetrahedron, 1995, 51(29), 8023-8032. https://doi.org/10.1016/0040-4020(95)00417-7

(214) Sirviö, J. A. Fabrication of Regenerated Cellulose Nanoparticles by Mechanical Disintegration of Cellulose after Dissolution and Regeneration from a Deep Eutectic Solvent. J. Mater. Chem. A 2019, 7 (2), 755–763. https://doi.org/10.1039/c8ta09959f.

(215) Yang, H.; Tejado, A.; Alam, N.; Antal, M.; Van De Ven, T. G. M. Films Prepared from Electrosterically Stabilized Nanocrystalline Cellulose. Langmuir, 2012, 28 (20), 7834–7842. https://doi.org/10.1021/la2049663.

(216) Van De Ven, T. G. M.; Sheikhi, A. Hairy Cellulose Nanocrystalloids: A Novel Class of Nanocellulose. Nanoscale, 2016, 8 (33), 15101–15114. https://doi.org/10.1039/c6nr01570k.

(217) Leung, A. C. W.; Hrapovic, S.; Lam, E.; Liu, Y.; Male, K. B.; Mahmoud, K. A.; Luong, J. H. T. Characteristics and Properties of Carboxylated Cellulose Nanocrystals Prepared from a Novel One-Step Procedure. Small, 2011, 7 (3), 302–305. https://doi.org/10.1002/smll.201001715.

(218) Chen, L.; Zhu, J. Y.; Baez, C.; Kitin, P.; Elder, T. Highly Thermal-Stable and Functional Cellulose Nanocrystals and Nanofibrils Produced Using Fully Recyclable Organic Acids. Green Chem. 2016, 18 (13), 3835–3843. https://doi.org/10.1039/c6gc00687f.

(219) Wang, R.; Chen, L.; Zhu, J. Y.; Yang, R. Tailored and Integrated Production of Carboxylated Cellulose Nanocrystals (CNC) with Nanofibrils (CNF) through Maleic Acid Hydrolysis. Chem. Nano. Mat. , 2017, 3 (5), 328–335. https://doi.org/10.1002/cnma.201700015.

(220) Amass, W.; Amass, A.; Tighe, B. A Review of Biodegradable Polymers: Uses, Current Developments in the Synthesis and Characterization of Biodegradable Polyesters, Blends of Biodegradable Polymers and Recent Advances in Biodegradation Studies. Polym. Int. 1998, 47 (2), 89–144. https://doi.org/10.1002/(SICI)1097-0126(1998100)47:2<89::AID-PI86>3.0.CO;2-F.

(221) Filson, P. B.; Dawson-Andoh, B. E.; Schwegler-Berry, D. Enzymatic-Mediated Production of Cellulose Nanocrystals from Recycled Pulp. Green Chem. 2009, 11 (11), 1808–1814. https://doi.org/10.1039/b915746h.

(222) Ji, H.; Xiang, Z.; Qi, H.; Han, T.; Pranovich, A.; Song, T. Strategy towards One-Step Preparation of Carboxylic Cellulose Nanocrystals and Nanofibrils with High Yield, Carboxylation and Highly Stable Dispersibility Using Innocuous Citric Acid. Green Chem. 2019, 21 (8), 1956–1964. https://doi.org/10.1039/c8gc03493a.

(223) Koshani, R.; Van De Ven, T. G. M.; Madadlou, A. Characterization of Carboxylated Cellulose Nanocrytals Isolated through Catalyst-Assisted H2O2 Oxidation in a One-Step Procedure. J. Agric. Food Chem. 2018, 66 (29), 7692–7700. https://doi.org/10.1021/acs.jafc.8b00080.

(224) House of Commons Environmnetal Audit Committee. Fixing Fashion: Clothing Consumption and Sustainability: Government Respnse to the Committee's Sixteenth Report; 2019.

(225) Samanta, P. A Review on Application of Natural Dyes on Textile Fabrics and Its Revival Strategy. In Chemistry and Technology of Natural and Synthetic Dyes and Pigments. IntechOpen, 2020. https://doi.org/10.5772/intechopen.90038.

(226) . M.; Shukla, S. P.; Mohan, D. Toxicity of Disperse Dyes and Its Removal from Wastewater Using Various Adsorbents: A Review. Res. J. Environ. Toxicol. 2017, 11 (2), 72–89. https://doi.org/10.3923/rjet.2017.72.89.

(227) Klepacz-Smółka, A.; Paździor, K.; Ledakowicz, S.; Sójka-Ledakowicz, J.; Mrozińska, Z.; Zyłła, R. Kinetic Studies of Decolonisation of Concentrates from Nanofiltration Treatment of Real Textile Effluents in Anaerobic/Aerobic Sequencing Batch Reactors. Environ. Prot. Eng. 2009, 35 (3), 145–155.

(228) Ahmad, A.; Mohd-Setapar, S. H.; Chuong, C. S.; Khatoon, A.; Wani, W. A.; Kumar, R.; Rafatullah, M. Recent Advances in New Generation Dye Removal Technologies: Novel Search for Approaches to Reprocess Wastewater. RSC Adv. 2015, 30801–30818. https://doi.org/10.1039/c4ra16959j.

(229) Koh, J. Dyeing with Disperse Dyes. In Textile Dyeing; InTech, 2011. https://doi.org/10.5772/20458.

(230) Teli, M. D. Textile Coloration Industry in India. Color. Technol. 2008, 124 (1), 1–13. https://doi.org/10.1111/j.1478-4408.2007.00114.x.

(231) Shamey, R. Modelling, Simulation and Control of Textile Dyeing. In Modelling and predicting textile behaviour; 2010; pp 322–359. https://doi.org/10.1533/9781845697211.2.322.

(232) Introduction to Dyeing and Dyehouse Automation. In Modelling, Simulation and Control of the Dyeing Process; Elsevier, 2014; pp 1–30. https://doi.org/10.1533/9780857097583.1.

(233) Senthil Kumar, P.; Suganya, S. Introduction to Sustainable Fibers and Textiles. In Sustainable Fibers and Textiles; Elsevier Inc., 2017; pp 1–18. https://doi.org/10.1016/B978-0-08-102041-8.00001-9.

(234) Chattopadhyay, D. P. Chemistry of Dyeing. In Handbook of Textile and Industrial Dyeing: Principles, Processes and Types of Dyes; Elsevier Inc., 2011; Vol. 1, pp 150–183. https://doi.org/10.1533/9780857093974.1.150.

(235) Chico, D.; Aldaya, M. M.; Garrido, A. A Water Footprint Assessment of a Pair of Jeans: The Influence of Agricultural Policies on the Sustainability of Consumer Products. J. Clean. Prod. 2013, 57, 238–248. https://doi.org/10.1016/j.jclepro.2013.06.001.

(236) Jiang, W.; Yuan, Z.; Bi, J.; Sun, L. Conserving Water by Optimizing Production Schedules in the Dyeing Industry. J. Clean. Prod. 2010, 18 (17), 1696–1702. https://doi.org/10.1016/j.jclepro.2010.07.004.

(237) Gao, D.; Yang, D. F.; Cui, H. S.; Huang, T. T.; Lin, J. X. Supercritical Carbon Dioxide Dyeing for PET and Cotton Fabric with Synthesized Dyes by a Modified Apparatus. ACS Sustain. Chem. Eng. 2015, 3 (4), 668–674. https://doi.org/10.1021/sc500844d.

(238) Hou, A.; Chen, B.; Dai, J.; Zhang, K. Using Supercritical Carbon Dioxide as Solvent to Replace Water in Polyethylene Terephthalate (PET) Fabric Dyeing Procedures. J. Clean. Prod. 2010, 18 (10–11), 1009–1014. https://doi.org/10.1016/j.jclepro.2010.03.001.

(239) Banchero, M. Supercritical Fluid Dyeing of Synthetic and Natural Textiles - a Review. Color. Technol. 2013, 129 (1), 2–17. https://doi.org/10.1111/cote.12005.

(240) Montero, G.; Hinks, D.; Hooker, J. Reducing Problems of Cyclic Trimer Deposits in Supercritical Carbon Dioxide Polyester Dyeing Machinery. In Journal of Supercritical Fluids; Elsevier, 2003; Vol. 26, pp 47–54. https://doi.org/10.1016/S0896-8446(02)00187-0.

(241) GEBERT, K. The Dyeing of Polyester Textile Fabric in Perchloroethylene by the Exhaust Process. J. Soc. Dye. Colour. 2008, 87 (12), 509–513. https://doi.org/10.1111/j.1478-4408.1971.tb02997.x.

(242) Hashimoto, I. Rate of Diffusion of Disperse Dye into Synthetic Fibers in Binary Mixed Solvents. Journal of the Textile Machinery Society of Japan, 1981, 6, 50–56.

(243) Ferrero, F.; Periolatto, M. Glycerol in Comparison with Ethanol in Alcohol-Assisted Dyeing. J. Clean. Prod. 2012, 33, 127–131. https://doi.org/10.1016/j.jclepro.2012.04.018.

(244) Ferrero, F.; Periolatto, M.; Rovero, G.; Giansetti, M. Alcohol-Assisted Dyeing Processes: A Chemical Substitution Study. J. Clean. Prod. 2011, 19 (12), 1377–1384. https://doi.org/10.1016/j.jclepro.2011.04.008.

(245) Xu, S.; Chen, J.; Wang, B.; Yang, Y. An Environmentally Responsible Polyester Dyeing Technology Using Liquid Paraffin. J. Clean. Prod. 2016, 112, 987–994. https://doi.org/10.1016/j.jclepro.2015.08.114.

(246) Opwis, K.; Benken, R.; Knittel, D.; Gutmann, J. S. Dyeing of PET Fibers in Ionic Liquids. Int. J. New Technol. 2017, 11, 101–108.

(247) Yuan, J.; Wang, Q.; Fan, X. Dyeing Behaviors of Ionic Liquid Treated Wool. J. Appl. Polym. Sci. 2010, 117 (4), 2278–2283. https://doi.org/10.1002/app.32020.

(248) Bianchini, R.; Cevasco, G.; Chiappe, C.; Pomelli, C. S.; Rodríguez Douton, M. J. Ionic Liquids Can Significantly Improve Textile Dyeing: An Innovative Application Assuring Economic and Environmental Benefits. ACS Sustain. Chem. Eng. 2015, 3 (9), 2303–2308. https://doi.org/10.1021/acssuschemeng.5b00578.

(249) Pang-Chin, L. I. U.; Cheng, H.; Cheng-Ting, W. Method for Decolorization of a Dyed Polyester Fiber, 2015.

(250) Walker, A. Recycling Process, 2017. EU Patent no. EP3172267A1

(251) Karaosman, H.; Perry, P.; Brun, A.; Morales-Alonso, G. Behind the Runway: Extending Sustainability in Luxury Fashion Supply Chains. J. Bus. Res. 2018. https://doi.org/10.1016/j.jbusres.2018.09.017.

(252) Lu, S. Changing trends in world textile and apparel trade | Apparel Industry Analysis | https://www.just-style.com/analysis/changing-trends-in-world-textile-and-apparel-trade_id134353.aspx (accessed May 5, 2020).

(253) Wang, L.; Li, Y.; He, W. The Energy Footprint of China's Textile Industry: Perspectives from Decoupling and Decomposition Analysis. Energies 2017, 10 (10), 1–11.

(254) Niinimäki, K.; Peters, G.; Dahlbo, H.; Perry, P.; Rissanen, T.; Gwilt, A. The Environmental Price of Fast Fashion. Nat. Rev. Earth Environ. 2020, 1 (4), 189–200. https://doi.org/10.1038/s43017-020-0039-9.

(255) Hasanbeigi, A.; Price, L. A review of energy use and energy efficiency technologies for the textile industry. Renew. Sus. Energ. Rev., 2012, 16(6), 3648-3665.

(256) Kant, R. Textile Dyeing Industry an Environmental Hazard. Nat. Sci. 2012, 04 (01), 22–26. https://doi.org/10.4236/ns.2012.41004.

(257) Burberry burns bags, clothes and perfume worth millions - BBC News https://www.bbc.com/news/business-44885983 (accessed May 6, 2020).

(258) Hendriksz, V. H&M accused of burning 12 tonnes of new, unsold clothing per year https://fashionunited.uk/news/fashion/h-m-accused-of-burning-12-tonnes-of-new-unsold-clothing-per-year/2017101726341 (accessed May 5, 2020).

(259) Starn, J. A Power Plant Is Burning H&M Clothes Instead of Coal https://www.bloomberg.com/news/articles/2017-11-24/burning-h-m-rags-is-new-black-as-swedish-plant-ditches-coal (accessed May 5, 2020).

(260) Daystar, J.; Chapman, L.; Moore, M.; Pires, S.; Golden, J. Quantifying Apparel Consumer Use Behavior in Six Countries: Addressing a Data Need in Life Cycle Assessment Modeling. J. Text. Apparel, Technol. Manag. 2019, 11 (1).

(261) Sandin, G.; Peters, G. M. Environmental Impact of Textile Reuse and Recycling – A Review. Journal of Cleaner Production. Elsevier Ltd May 20, 2018, pp 353–365. https://doi.org/10.1016/j.jclepro.2018.02.266.

(262) Ellen MacArthur Foundation. A New Textiles Economy: Redesigning Fashion's Future; 2017.

Chapter 2 : Towards A Circular Economy: Decontamination and Valorization of Post-Consumer Waste Wood Using Low-Cost Protic Ionic Liquids

2.1 Introduction

Capitalizing on the unique structure and properties of the PILs, the use of these solvents to fractionate challenging new feedstocks, namely post-consumer waste wood is investigated in this study. Despite the challenging nature of these feedstocks, if valorized, they provide key economic and ecological advantages as they are negative to low cost, have established supply chain and pre-existing infrastructure and they are diverted from landfill. More importantly, there are currently no viable technologies to treat and/or decontaminate these feedstocks. An in-depth analysis and investigation on the interaction of PILs with these new waste feedstocks and thereby developing an integrated valorization and decontamination processes.

In this study, we explored the potential use of the ionoSolv process as a hybrid decontamination-fractionation process using real post-consumer waste wood collected from waste management companies. This study focused on grade C post-consumer waste which is very small in size (< 1 to 10 mm) relative to waste wood chips (10 – 80 mm), and therefore it is called “waste wood fines”. Waste wood fines are produced during the processing of waste wood in collection facilities after passing through a high-speed shredder, to reduce the particle size of the collected waste wood. Waste wood fines fraction is typically classified as hazardous waste as they are heavily contaminated and presently, they are either landfilled or incinerated in hazardous-waste incinerators.[1] The highly heterogeneous nature and complexity of post-consumer waste wood fines makes it particularly challenging, requiring a comprehensive characterization to its composition and level of contamination. We carried an in-depth analysis on the impact of IL structure on waste wood decontamination efficiency as well as the fractionation of the biomass components. We then further explored the impact of space-time parameters (temperature, time) on the process fractionatative and decontamination performance

using optimal IL candidates. Furthermore, we explored the possibility of recovering and reusing the IL in a cyclic manner by removing dissolved metal contaminants from the IL-stream via electrodeposition. The electrochemistry and electrodeposition of metals[2,3] and alloys[4,5] from IL systems have been studied extensively, but their behavior in mixed IL-water systems is seldom reported. To this end, the effect was investigated of water content on the electrochemistry and deposition morphology of Pb^{II}, the dominant metal contaminant of waste wood fine. Electrodeposition experiments were conducted by the post-doc Sze Tan. These experiments were necessary as part of the process development as the results will guide the decision to locate the electrodeposition unit in the process. Currently, the two potential locations for electrodeposition unit are: location 1 (before lignin precipitation unit) and location 2 (after lignin precipitation unit), as shown in Figure 2.1. The study provides an integrated closed-loop process that valorizes toxic unutilized waste stream to value-added products which can be upgraded to produce biofuels and platform chemicals. The work done in this chapter was peer reviewed and published.[6]

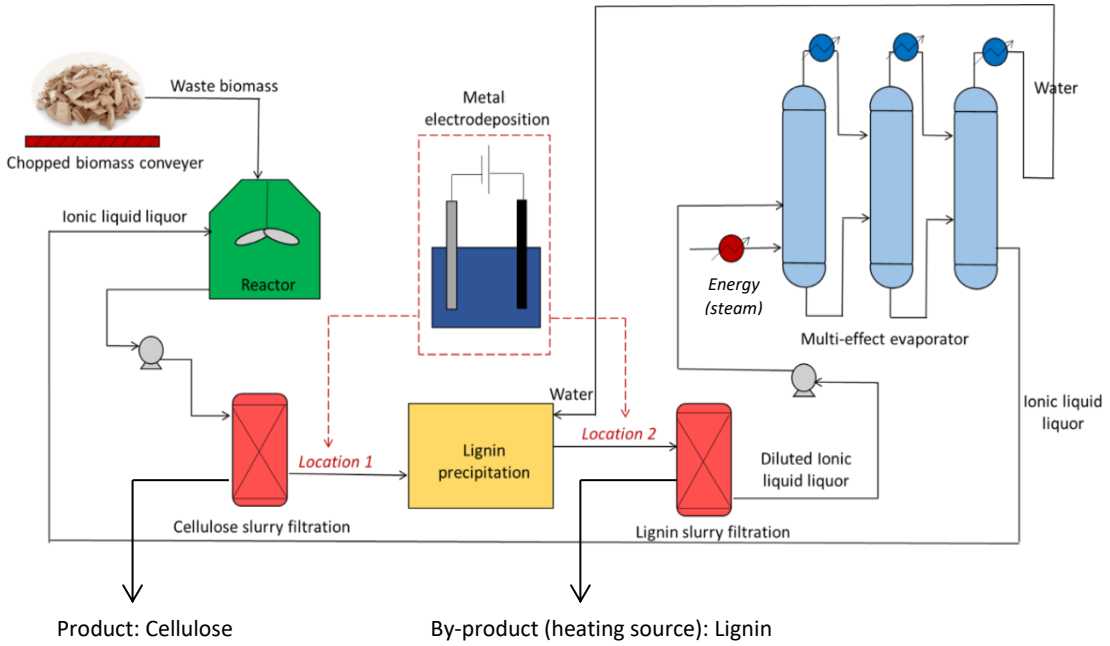

Figure 2.1: Process flow diagram for ionoSolv process highlighting the two potential locations for the metal electrodeposition unit

2.2 Materials & Methods

2.2.1 Materials

Starting materials for ionic liquid synthesis were purchased from Sigma Aldrich and, unless stated otherwise, used as received. Trace metal grade± nitric acid was purchased from Fisher Chemicals. Certified sludge material and ICP mix element standard were purchased from Sigma Aldrich. The certified sludge was used as a trace element reference material to validate the digestion method ICP-MS analysis method. ^{1}H NMR was recorded on a Bruker 400 MHz spectrometer. Chemical shifts (δ) are reported in ppm, the DMSO signal at 2.500 (^{1}H dimension) and 39.520 (13C dimension). ^{1}H, ^{13}C and HMQC NMRs were recorded on a Bruker 400 MHz spectrometer. The Karl-Fisher titrator used in this work was a V20 volumetric Titrator (Mettler-Toledo) and the analytical balance a Sartorius CPA 1003 S balance (±0.001 g). 1-ethyl-3-methylimidazolium acetate [C_2C_1im][OAc] was purchased from Sigma Aldrich and used without further purification, the water content of the ionic liquid was adjusted to be 20 wt% and verified using Karl-Fisher titration.

***Feedstock*:** Waste wood feedstocks were supplied by two waste management companies in the UK (Veolia and Suez). Two feedstocks were defined as waste wood chips and two were waste wood fines. Pine softwood *(Pinus sylvestris)* was sourced from All feedstocks were kept air-dried. Prior to pretreatment, feedstocks were grinded and sieved to achieve particle size of 180–850 μm, 20 + 80 US mesh scale. The biomass was then stored in plastic bags at room temperature in the dark.

2.2.2 Moisture content determination

Moisture contents were determined in triplicate for untreated biomass, and once per sample of recovered pulp sample after pretreatment. The moisture content was determined by wrapping specific amount of biomass or pulp (i.e. 100 mg for air-dried biomass and 0.5 to 1 g for wet pulp) in aluminium foil of known weight. The sample wrapped in foil was dried at 105°C overnight in a convection oven. The samples were transferred into a desiccator with activated silica and the weight was measured after 20 min. The moisture content was calculated as:

$$moisture\ content\ (\%) = \frac{m_{air\ dried\ BM,or\ wet\ pulp} - m_{oven\ dried}}{m_{air\ dried\ BM,wet\ pulp}} \cdot 100\% \qquad (2.1)$$

For all biomass samples, the oven-dried weight (ODW) may then be calculated following Equation:

$$ODW = \frac{Weight_{air\ dry\ sample} x\ (100 - \text{moisture content})}{100} \quad (2.2)$$

2.2.3 Ionic Liquid Synthesis

Synthesis of N, N,N-dimethyl-butylammonium hydrogen sulfate

N,N,N-dimethylbutylamine (101.19 g, 1 mol) was added in 500 mL round-bottom flask and cooled in an ice bath. 200 mL of 5 M H_2SO_4 (1 mol) was added dropwise using a funnel while stirring. The reaction proceeded for at least 5 hours with continuous stirring. Excess water was removed using the rotary evaporator. The ionic liquid was recovered as a clear, viscous liquid. The water content of the IL was adjusted to 20 wt% using Volumetric Karl Fisher Titrator (V20 Mettler-Toledo). ^{1}H NMR: δH (400 MHz, DMSO-d6)/ppm: 9.24 (s, 1H, N–H), 3.02 (dt, J = 12.9, 5.0 Hz, 2H, N–CH_2), 2.76 (d, J = 4.3 Hz, 6H, N–$(CH_3)_2$), 1.64–1.51 (m, 2H, N–CH_2–CH_2), 1.30 (h, J = 7.4 Hz, 2H, N–CH_2–CH_2–CH_2), 0.90 (t, J = 7.4 Hz, 3H, N–CH_2–CH_2– CH_2–CH_3). ^{13}C NMR δC (101 MHz, DMSO-d6)/ppm: 55.92 (N–CH_2), 42.46 (N–CH_3), 25.82 (N–CH_2–CH_2), 19.30 (N–CH_2– CH_2–CH_2), 13.71 (N–CH_2–CH_2–CH_2–CH_3).

Synthesis of 1-methylimidazolium hydrogen sulfate

1-methylimidazol (82.1 g, 1 mol) was added in 500 mL round-bottom flask and cooled in an ice bath. 200 mL of 5 M H_2SO_4 (1 mol) was added dropwise while stirring continuously for 5 to 6 hours. Excess water was removed under reduced pressure using a rotary evaporator at 50°C. The ionic liquid was recovered as a clear liquid. ^{1}H NMR: δH (400 MHz, DMSO-d6)/ppm: 8.92 (s, 1H, C(2)H), 7.61 (m, 1H, C(4)H), 7.54 (m, 1H, C(5)H), 6.17 (br, 1H, $[HSO_4]^-$), 3.84 (s, 3H, N-CH_3). ^{13}C NMR δC (101 MHz, DMSO-d6)/ppm: 136.18 (C2), 123.70 (C4), 120.29 (C5), 35.90 (N-CH_3).

Synthesis of N-methylbutylammonium hydrogen sulfate

N-methybutylamine (87.16 g, 1 mol) was added in 500 mL round-bottom flask and cooled in an ice bath. 200 mL of 5 M H_2SO_4 (1 mol) was added dropwise while stirring for 5 to 6 hours. Excess water was removed under reduced pressure using a rotary

evaporator at 50°C. The ionic liquid was recovered as a clear liquid. 1H NMR: δH (400 MHz, DMSO-d6)/ppm: 8.34 (s, 2H, N-H_2), 6.45 (br, 1H, [HSO_4]-), 2.85 (t, J = 8.0 Hz, 2H, N-CH_2), 2.54 (s, 3H, N-CH_3), 1.53 (tt, J = 8.0, 7.3 Hz, 2H, N-CH_2-CH_2), 1.46-1.32 (m, 2H, N-CH_2-CH_2-CH_2), 0.86 (t, J = 7.4 Hz, 3H, N-CH_2-CH_2—CH_2-CH_3 ^{13}C NMR δC (101 MHz, DMSO-d6)/ppm: 48.98 (N-CH_2), 33.47 (N-CH_3), 28.03 (N-CH_2-CH_2), 19.77 (N-CH_2-CH_2-CH_2), 14.10 (N-CH_2-CH_2—CH_2-CH_3).

Synthesis of 1-methylimidazolium chloride

1-methylimidazole (82.10 g, 1 mol) was added in 500 mL round-bottom flask and cooled with an ice bath. 1 mole (1 equivalent) of aqueous HCl was added dropwise while stirring for 5 to 6 hours. Excess water was removed under reduced pressure using a rotary evaporator at 50°C. The ionic liquid was recovered as pale-yellow liquid. ^{1}H NMR: δH (400 MHz, DMSO-d6)/ppm: 9.16 (s, 1H, H-2), 7.71 (s, ^{1}H, H-4/5), 7.64 (s, 1H, H4/5), 4.5-3.5 (br, H_2O, N-H+), 3.87 (s, 3H, N-CH_3). ^{13}C NMR: δC (101 MHz, DMSO-d6)/ppm: 135.63 (C-2), 123.21 (C-4/5), 119.55 (C-4/5), 35.48 (N-CH_3).

Synthesis of 2-hydroxyethylammonium acetate

2-hydroxyethylamine (61.08 g, 1 mol) was added in 500 mL round-bottom flask and cooed with an ice bath. 1 mol of acetic acid was added dropwise while stirring for 5 to 6 hours. Excess water was removed under reduced pressure using a rotary evaporator at 50°C. The ionic liquid was recovered as pale-yellow liquid. ^{1}H NMR: δH (400 MHz, DMSO-d6)/ppm: 8.83 (br, 3H, N-H), 3.57 (t, J = 5.8 Hz, 2H, N-CH_2), 2.68 (t, J = 5.8 Hz, 2H, N-CH_2-CH_2), 1.79 (s, 3H, $COCH_3$). ^{13}C NMR δC (101 MHz, DMSO-d6)/ppm: 174.84 (CO), 57.32 (N-CH_2-CH_2), 43.87 (N-CH_2), 22.98 ($COCH_3$).

2.2.4 Biomass Fractionation

Pretreatment was conducted according to the standard operating procedure from our laboratory.[7] Determination of oven dried weight of biomass and cellulose pulps (air-dried and wet conditions) were conducted according to the NREL protocol “Determination of Total Solids in Biomass and Total Dissolved Solids in Liquid Process Samples”.[8] For IL screening experiment, IL aqueous solutions were prepared by mixing 8 g of the IL with 2 g of water The water content of the prepared IL solutions was determined using Karl Fisher volumetric Titrator (Mettler-Toledo). The IL solution was then mixed with 2 g of biomass (on an oven-dried weight basis) in a pressure tube, corresponding to a biomass to solvent ratio of 1:5 g g^{-1}. For pretreatment kinetics experiments, the pretreatment

were conducted at oven temperature of 150 °C and 170 °C were pressure tubes out of the oven after specific period of time. For biomass loading experiments, 10 g of the aqueous IL solution (20 wt% water) was mixed with 1, 2 ,3, 4 and 5 g of biomass to achieve 10, 20, 30, 40 and 50 wt% solid loadings, respectively. Throughout the pretreatment experiments with contaminated waste wood samples, extra precautions were taken not to introduce external metal contamination from lab glassware and auxiliaries by using plastic cups, plastic containers and plastic spatulas when possible, and avoid using rare earth stir bars.

After the oven time elapsed, the pressure tube was allowed to cool down for at least 20 minutes. The cellulose-rich pulp was separated from the ionic liquid slurry, washed 3 times using 40 mL of high purity ethanol in 50 mL Falcon tube. The tube was shaken for 1 min and left to settle at room temperature for at least 1 hour. The tube was shaken again for 1 min and centrifuged at 3,000 rpm for 50 min.

Followed, the cellulose pulp was further washed using 24 h Soxhlet extraction with high purity ethanol. Following Soxhlet extraction, the thimbles containing pulp were emptied in pre-weighed falcon tube and washed with 30 mL of water to remove traces of ethanol and ensure that pulp is kept wet in water. After decanting the wash water, the weight of the falcon tube and wet pulp is recorded for pulp yield calculation. Approximately 1 g of the wet pulp was taken for moisture content measurement. Cellulose pulp yield was calculated as follows:

$$Pulp\ yield\ (\%) = \frac{m_{\text{wet pulp}} * (1 - moisture\ content)}{m_{\text{oven dried BM}}} \cdot 100\% \qquad (2.3)$$

Where $m_{\text{oven dried BM}}$ is the weight of the oven dried biomass and moisture content is the water content in the cellulose pulp, determined in the previous section.

The ethanol used for the Soxhlet extraction was combined with the ethanol washings from the previous steps and evaporated under vacuum at 40°C with agitation, leaving a dried ionic liquid/lignin mixture (IL black liquor). 30 mL of distilled water was added to the black IL liquor to precipitate the lignin. The mixture was transferred into a clean 50 mL falcon tube, shaken for one minute and left to settle at room temperature for at least 1 hour. The tube was centrifuged as above and the supernatant decanted and collected in a round bottom flask. This washing step for the recovered solid lignin was repeated

two more times. Lignin was then freeze-dried and dried lignin was weighed to obtain the lignin yield relative to biomass. Lignin yield is calculated using the following Equation:

$$Lignin\ yield\ relative\ to\ biomass\ (\%) = \frac{m_{\text{lignin precipitate}}}{ODW\ x\ \%\ Kalson\ Lignin} \cdot 100\% \qquad (2.4)$$

Where $m_{\text{lignin precipitate}}$ refers to the weight of freeze-dried lignin, ODW refers to the oven dried weight of the biomass and Kalson lignin refers to the percentage of lignin present in the biomass as determined by compositional analysis procedure. To calculate lignin yield based on the original lignin content in the biomass, Equation 2.5 is used:

$$Lignin\ yield\ \text{relative to original lignin}\ (\%) = \frac{m_{\text{lignin precipitate}}}{ODW\ x\ \%\ Kalson\ Lignin\ x\ lignin\ content\ in\ BM} \cdot 100\% \qquad (2.5)$$

2.2.5 Compositional Analysis

Compositional analysis was carried out according to the published procedure Determination of Structural Carbohydrates and Lignin in Biomass by the NREL.[9] The procedure is described in here in short. Compositional analysis determines the following biomass structural components: i) carbohydrates content, namely glucose, xylose, arabinose and mannose, ii) acid insoluble lignin (AIL), iii) acid soluble lignin (ASL), iv) acid insoluble ash. The glucose content determined using this protocol does not distinguish between glucose derived from cellulose or the glucose derived from hemicellulose. Therefore, the glucan content in the pulp and untreated biomass is taken as the total glucose derived from both cellulose and hemicellulose, whereas hemicellulose content in the residue and untreated biomass is taken as the sum of all carbohydrate sugars (xylose, galactose, arabinose, mannose) except glucose.

Ceramic crucibles were placed into a muffle oven (Nabertherm + controller P 330) and ashed 2 to 3 times using a muffle oven at 575°C until a constant weight is reached. 300 mg (calculated on ODW basis) of air-dry biomass or recovered biomass was weighed out into a pressure tube and the weight recorded (Sartoriaum CPA 1003 S balance, ±0.001 g). 3 mL of 72% sulfuric acid was added, the samples stirred using a Teflon stir rod and the pressure tubes placed into a preheated water bath at 30°C. The samples were stirred every 10 min for one hour. Samples were then diluted with 84 mL distilled water and the lids closed. The samples were autoclaved (Sanyo Labo Autoclave ML5 3020 U) for 1 hour at 121°C and left to cool to close to ambient temperature. The samples were then

filtered through filtering ceramic crucibles of a recorded weight. The filtrate was filled in two 15-mL Falcon tubes and the remaining black solid washed with distilled water. The crucibles were placed into a convection oven (VWR Venti-Line 115) at 105°C for 24±2 hours. They were then taken out and placed in a desiccator for 15 min before they were weighed, and the weight of the AIL plus the crucible were recorded. The content of acid insoluble lignin (AIL) was determined according to the following Equation:

$$\%AIL = \frac{(Weight_{crucible\ plus\ AIR} - Weight_{crucible}) - (Weight_{crucible\ plus\ ash} - Weight_{crucible})}{ODW_{sample}} x100 \quad (2.6)$$

The content of one of the Falcon tubes was used for the determination of acid soluble lignin content (ASL) by UV spectrometer (Perkin Elmer Lambda 650 UV/Vis spectrometer) using the UV absorbance at 240 nm. The ASL content was calculated according the following Equation :

$$\%ASL = \frac{UV_{abs} x\ Volume_{filtrate} x Dilution\ factor}{\varepsilon\ x\ ODW_{sample}}\ x\ 100 \quad (2.7)$$

where UV_{abs} is the average UV-vis absorbance for the sample at 240 nm; $V_{filtrate}$ is 86.73 mL; the dilution factor is the ratio of total diluted sample volume to undiluted sample volume as needed to bring the absorbance within the range 0.7-1.0; and ε is the biomass absorptivity at 240 nm (12 L g^{-1} cm^{-1} for pine wood).

The other Falcon tube contents were neutralized by careful addition of calcium carbonate until the pH reached 5. After settling, the liquid was filtered through a 0.2 µm PTFE syringe filter and submitted to HPLC analysis for the determination of total sugar content. HPLC analysis of glucose, xylose, mannose, arabinose and galactose was performed on a Shimadzu HPLC with an AMINEX HPX-87P Column (Biorad, 300 x 7.8 mm, prepacked HPLC carbohydrate analysis column) with refractive index detection. The mobile phase was de-ionized water, the column temperature 85°C and the flow rate was 0.6 mL min^{-1}. Calibration standards with concentrations of 0.1, 1, 2 and 4 mg mL^{-1} of glucose, xylose, mannose, arabinose and galactose and 8 mg mL^{-1} of glucose were used.

Sugar recovery standards were made as 10 mL aqueous solutions close to the expected sugar concentration of the samples and transferred to pressure tubes. The same procedure was applied for SRS standards as for the samples , however instead of adding

3 mL of 72% sulfuric acid, only 278 µL 72% sulfuric acid was added to the sugar-containing solution. The pressure tube closed and autoclaved and the sugar content was determined as described above. The sugar recovery coefficient (SRC) was determined according to the following Equation:

$$SRC\ \% = \frac{C_{HPLC}\ x\ V}{\text{inital weight}} \qquad (2.8)$$

The sugar concentration values of the samples obtained by HPLC were corrected to obtain the percent hydrolyzed sugar recovery values, accounting for any dilution made prior to HPLC analysis, using the following Equation:

$$\%Sugar = \frac{C_{HPLC}\ x\ V\ x\ corr_{hydro}}{\text{SRC x ODW}}\ \text{x100} \qquad (2.9)$$

where C_{HPLC} is the sugar concentration determined by HPLC (mg/mL), V is the dilution factor (86.73 mL for samples and 10 mL for SRC standards). $Corr_{hydro}$ is the correction for the mass increase during hydrolysis of polymeric sugars obtained by dividing the molecular weight of the polymeric sugar by its monomeric weight (0.90 for C6 sugars glucose, galactose and mannose and 0.88 for C5 sugars xylose and arabinose) and ODW is the oven-dried weight of the sample in mg. SRC is the sugar recovery standard value for each sugar. The sugars content in the pulp were normalized based on the pulp yield obtained in the pretreatment as:

$$Glucan_{pulp} = \frac{C_x}{pulp\ yield\ x\ mass\ closure} \qquad (2.10)$$

The glucose content determined using this protocol does not distinguish between glucose derived from cellulose or the glucose derived from hemicellulose. Therefore, the glucan content in the pulp and untreated biomass is taken as the total glucose derived from both cellulose and hemicellulose, whereas hemicellulose content in the residue and untreated biomass is taken as the sum of all carbohydrate sugars (xylose, galactose, arabinose, mannose) except glucose. On this basis, Glucan recovery relative to untreated biomass is calculated as the following:

$$Glucan\ recovery\ = \frac{Glucan_{pulp} x\ Yield_{pulp}}{Glucan_{untreated}} \qquad (2.11)$$

Where $Glucan_{pulp}$ is the glucan content in the cellulose pulp, $Yield_{pulp}$ is the yield of the pulp after ionoSolv processing relative to untreated biomass and $Glucan_{untreated}$ is the glucan content in the untreated biomass.

Hemicellulose extraction is calculated as:

$$Hemicellulose\ extraction = \frac{Hem_{untreated} - Hem_{pulp} x\ Yield_{pulp}}{Hem_{untreated}} \qquad (2.12)$$

Where $Hem_{untreated}$ is the hemicellulose content of untreated biomass calculated as the sum of all sugars (except glucose) and Hem_{pulp} is the hemicellulose content in the cellulose pulp.

Lignin extraction (i.e. delignification) relative to untreated biomass is calculated as the following:

$$Lignin\ extraction = \frac{Lignin_{untreated} - (Lignin_{pulp}\ x\ Yield_{pulp})}{Lignin_{untreated}} \qquad (2.13)$$

Where $Lignin_{untreated}$ is the lignin content in the untreated biomass and $Lignin_{pulp}$ is the lignin content in the recovered cellulose pulp after the ionoSolv pre-treatment.

2.2.6 Enzymatic Saccharification Assay

Saccharification assays of cellulose-pulps and air-dried untreated biomass were carried in triplicate with blanks according to the NREL protocol "Low solids Enzymatic saccharification of lignocellulosic biomass".[10] The saccharification of the cellulose pulps was performed on their wet state to eliminate the hornification effect. All reagents were purchased from Sigma Aldrich. 100±10 mg (on and ODW basis) of air-dried or wet biomass and pulps was placed into a Sterilin tube and the exact weight recorded. 8.5 mL solution consisting of 5 mL 1M sodium citrate buffer at pH 4.8, 40 µL tetracyline antibiotic solution (10 mg/mL in 70% ethanol), 30 µL cycloheximide antibiotic solution (10 mg/mL in purified water), 3.37 mL purified water and 50 µL of CTec2 enzymes was added. For wet cellulose pulps, water content was corrected individually for each sample such that the final volume of the solution is 10 mL. The tubes closed and placed into a Stuart Orbital Incubator (S1500) at 50°C and 250 rpm for 7 days. Saccharification yields were obtained by filtering 1 mL of the saccharification mixture through a PTFE syringe

filter. Samples were run on Shimadzu HPLC with an AMINEX HPX-97P column (Bio rad, 300 x 7.8 mm) with purified water as mobile phase (0.6 mL/min). The column temperature was 85°C and acquisition was run for 20 min. Calibration standards with concentrations of 0.1, 1, 2 and 4 mg/mL of glucose, xylose, mannose, arabinose and galactose and 8 mg/mL of glucose were used.

$$\textbf{Saccharification Yield}\ (\%) = \frac{(\mathbf{C_{sample} - C_{blank}}) \times \mathbf{V_{sample}} \times \mathbf{corr_{anhydro}} \times \mathbf{Pulp\ Yield}}{\mathbf{m_{sample}} \times (\mathbf{1 - mc_{sample}}) \times \mathbf{Glucan_{untreeated}}} \times \mathbf{100} \qquad (2.15)$$

Where C_{sample} is the glucose concentration of the hydrolysis sample as determined by HPLC, C_{blank} is the glucose concentration of the blank control as determined by HPLC , V_{sample} is the volume of the hydrolysis sample (10 mL), $corr_{anhydrous}$ is a correction factor accounting for the increase in mass of sugars during hydrolysis (0.9 for glucose), Pulp Yield is as defined in Eq. 5, m_{sample} is the mass of sample hydrolysed, mc_{sample} is the moisture content of the sample hydrolysed, and $Glucan_{untreated}$ is the glucan content of the untreated biomass

2.2.7 Ash determination

1 g of the cellulose pulp was placed in a pre-weighed marked crucible. The weight of the sample and crucible was recorded to the nearest 0.1 mg. The crucibles were placed in a muffle oven at 575 °C using a muffle oven with a ramping program. At the end of the program, samples were taken from the oven and carefully placed in a desiccator to cool for a specific amount of time, equal to the initial cool time of the empty crucibles (20 minutes). The weight of the crucibles and the ash content was then recorded to the nearest 0.1 mg, and ash content was calculated as the following:

$$Ash\ content = \frac{Weight_{crucible+ash} - Weight_{crucible}}{Weight_{cellulose\ pulp}} \qquad (2.16)$$

2.2.8 CHNS Analysis

Samples for CHNS elemental analysis were sent to MEDAC Ltd, London, United Kingdom. The measurements were conducted in duplicates.

2.2.9 Trace Element Analysis

Samples preparation for microwave-assisted acid digestion were prepared following the EPA standard (Method 3050B) with slight modifications. 500 mg ± 10 of the grounded

homogenized waste wood feedstock, cellulose pulp or lignin samples (oven-dried basis) and 500 ± 10 mg of ionic liquid liquor (oven-dried basis) were weighed using plastic spatula and added to a 250 mL digestion vessels (MARSXpress). 9 mL of trace metal grade nitric acid 69% (HNO_3) and 3 mL of trace metal grade hydrochloric acid 37% (HCl) were added into the Teflon digestion vessel. Digestion vessels were loosely capped with Teflon caps and kept inside the fumehood for 12 hours minimum to allow complete digestion. The vessels were then fully tightened and introduced to microwave for digestion with power/time control by CEM with the following sequence: 300 W at 83% power for 5 min, 600 W at 66% power for 5 min and 1200 W at 58% power for 6 min). The vessels were taken out of the microwave and left to cool down for at least 3 hours at room temperature. Vessels were opened slowly and then each was diluted with 100 mL water and carefully transferred into 100 mL plastic volumetric flasks. The flasks were shaken, and 10 mL aliquots were filtered using a syringe (0.22 μm filter) in 10 mL falcon tubes prepared for ICP analysis. The digestion analysis was conducted in triplicate for each fractionation condition and in at least 5 repeats for waste wood feedstocks. Digestion of sludge certified material (Sigma Aldrich) was conducted in triplicates with every digestion batch to ensure method consistency and repeatability. Standards and microwave digested filtered samples were analyzed using the Agilent 7900 ICP-MS. Multielement standard solutions were prepared for ICP in 5% nitric acid (TraceCERT). Internal standards were used to monitor the response of the elements. Percentage recovery of metal M in the pulp was calculated according to Equation 17 in IL liquor according to Equation 18 and in lignin according to Equation 19:

$$\%M_{pulp} = \frac{c_{M,pulp}}{c_{M,BM} \cdot r_{pulp}} \% \qquad (2.16)$$

$$\%M_{IL} = \frac{c_{M,IL}}{c_{M,BM} \cdot ODW_{BM} / (m_{IL} \cdot (1 - wc_{IL}))} \% \qquad (2.17)$$

$$\%M_{lignin} = \frac{c_{M,lignin}}{c_{M,BM} \cdot r_{lignin}} \% \qquad (2.19)$$

Where $C_{M,x}$ is the concentration of metal M in component x (pulp, IL, lignin or initial biomass) as measured by ICP-MS. ODW_{BM} is the oven-dried weight of the biomass used in pretreatment, m_{IL} is the initial weight of IL solution used for pretreatment and wc_{IL} is

the water content of this solution. Extraction of metal M from the biomass is then calculated as 100-%M_{pulp}.

2.2.10 2D HSQC NMR

50 mg of lignin was dissolved in 0.5 mL of DMSO-d_6 vortexed and left overnight followed by transferring the solution to NMR tube. HSQC NMR spectra were recorded on a Bruker 600 MHz spectrometer -pulse sequence hsqcetgpsi2, spectral width of 10 ppm in F2 (^{1}H) with 2048 data points and 160 ppm in F1 (^{13}C) with 256 data points, 16 scans and 1 s interscan delay. Spectra were analysed using MestReNova (Version 11.0.1, Mestrelab Research 2016). All spectra were referenced to the DMSO peak at 2.500 ppm (^{1}H) and 39.520 ppm (^{13}C). Integral signal intensity values were obtained by simultaneously for integrating the spectra of the same series of experiments to ensure consistency. Integration areas were selected visually according to peak assignments found in literature. Integral sizes are reported with respect to 100 (G_2 +G_{2cond}) signals. All spectra can be found in the Appendix. Integral signal intensity values were obtained by simultaneously for integrating the spectrums of the same series of experiments to ensure consistency. Integration areas were selected visually according to peak assignments found in literature. Integral sizes are reported with respect to 100 (G_2 +G_{2cond}) signals. All spectra can be found in the Appendix (Figures A7-A17) along with the chemical shifts of the investigated bonds and aromatic structure in ionoSolv lignin samples (Table A1).

2.2.11 Electrochemical measurements and surface characterization

Pb-IL solutions were prepared using $PbCO_3$ (99 %, Sigma Aldrich) as the lead source. Solutions of 100, 500 and 1000 mg L-1 Pb^{II} in [H_1Cim]Cl with 20 wt% and 40 wt% water (Millipore Milli-Q purification system, resistivity ca. 18.2 MΩ cm at 25 0C) were used. Pb-IL-lignin solution were prepared by doping a lignin-IL ([H_1Cim]Cl, 20 wt% water) fraction sample to 1000 ppm Pb^{II} mg L^{-1}, mimicking the build-up of Pb^{II} in the sample during IL recycling. Electrochemical measurements were made using a potentiostat (Autolab PGSTAT30) and NOVA software in a three-electrode configuration. A glassy carbon (GC) disk electrode (1.5 mm-radius) served as the working electrode in all cyclic voltammetry experiments. Prior to use, the working electrode was polished with a slurry of 0.05 µm alumina particles on a soft microfiber polishing pad (MicroCloth, Buehler Ltd.) and then on a clean wet microfiber pad. A platinum gauze acted as the counter

electrode, while a Ag/AgCl (3 M NaCl) glass-fritted electrode served as the reference electrode. Electrochemical deposition experiments were conducted where a copper foil (Goodfellow, 99.9%, area = 0.5 cm^2) substrate and a lead wire (Goodfellow, 99.99%, As (0.3 ppm), Bi (2.1 ppm), Cu (0.3 ppm) and Ag (0.9 ppm)) were used as the working electrode and counter electrode, respectively. The surface area of the copper foil electrode is 40 mm^2 and the inter-electrode distance between the working and counter electrode is ~ 1 cm. The electrodeposition experiments were carried out for 1 or 2 hrs at varying electrode potentials (V = -0.80, -0.85, -0.90 and -1.0 V). After electrodeposition, the working electrode was removed from the electrolysis cell and washed with distilled water to remove residual electrolyte from the sample surface. It is subsequently dried in air before surface characterization. The surface morphology of the lead deposits on copper foil is observed with scanning electron microscopy (SEM, JOEL 6010A) coupled with energy dispersive X-ray (EDX) to provide element composition identification of the samples. This part of the experiments (electrochemistry and electrode characterization) was conducted by the post-doc Sze Tan.

2.2.12 Error calculation

In this thesis, all experimental errors were presented as one standard deviation calculated from triplicate measurements (or duplicate measurements at a minimum, in the cases of certain techniques or limited samples, as indicated in the methodology). The error bars shown in all Figures and Tables and reported in the text refer a single standard deviation value.

2.3 Results & Discussion

2.3.1 Waste wood feedstock characterization

The highly heterogeneous nature of waste wood requires rigorous characterization to obtain an average baseline of its structural composition (glucan, hemicellulose, lignin and ash contents), and to assess its level of material and chemical contamination. An untreated sample of pine softwood (*Pinus sylvestris*) was used as a reference for untreated wood as a comparison with waste wood, in terms of structural composition and contamination levels.

2.3.1.1 Structural Composition and Ash content

The waste wood fines sample under investigation contained different contaminants found in the waste wood fines under investigation that were identified by visual inspection. Relatively large (1 to 2 mm) wood chips were the major constituents of the sample. Small parts of engineered wood such as plywood, particleboard and fiberboard were also present in the sample. White and green-painted wood chips as well as glass, stones and polystyrene were the major nonwooden contaminates present. The ash composition of both waste wood fines, and untreated virgin wood was determined by XRF (Table A2 in Appendix). The high abundance of silicon (IV) and iron (III) of 13.6 wt% and 8 wt%, respectively, in the waste wood fine's ash, originated from glass and stones since the ash of untreated virgin wood contained only 0.9 wt% and 1.6 wt% of silicon(IV) and iron(III), respectively. Waste wood fines ash also contained a wide range of metals and heavy metals that were not present in the virgin untreated biomass.

Table 2.1: CHNS elemental analysis, chloride content, direct ash, moisture content and heating values of waste wood fines and untreated wood samples

Feedstock	N	C	H	S	O	Cl	Ash content	LHV	HHV	Moisture content
				%				MJ kg^{-1}		wt%
Waste wood fines	2.56 (0.29)	44.29 (0.83)	6.01 (0.15)	0.05 (0.01)	47.09	0.10	12.83 (1.2)	17.1	18.6	12.2
Untreated Virgin wood	0.46 (0.06)	46.67 (0.8)	6.07 (0.3)	0.00 (0)	46.80	<0.10	0.24 (0.1)	23.0	24.2	6.5

In addition to the high ash content, waste wood fines also showed particularly high nitrogen content of 2.56 wt% (25.6 g kg^{-1}) compared to 0.46% of virgin untreated wood (Table 2.1). This is probably due to the presence of engineered wood such as

particleboard and plywood in this waste wood mix, which usually contain high amount of nitrogen from the urea formaldehyde and melamine formaldehyde resins and binders used in engineered wood. It should be noted that according to a recent French legislation, the nitrogen content should not exceed 1.5 % (15 g kg^{-1}) for the waste wood to be used in combustion facilities.[11] **The results indicate that this waste wood fine would be classified as hazardous and its utilization for WtE application require the installation of specialized and expensive WID boiler.** Trace amounts of sulfur are also present in the waste wood sample where no sulfur was found in the virgin untreated wood. The calorific higher heating value (HHV) content was also calculated based on the experimental CHNS analysis and the lower heating value (LHV) was calculated accordingly by considering the moisture content and heat of vaporization of water. The LHV value of waste wood was 17.1 MJ kg^{-1} which is lower than HHV for untreated pine of 23 MJ kg^{-1}, which could be attributed to the presence of ash and non-carbonaceous material.

Determining the initial composition of the biomass feedstock prior to the pretreatment process is essential to: i) monitor the success of the ionoSolv pretreatment that is quantified by lignin extraction (delignification), ii) determine the initial glucan content which allows quantifying the enzymatic saccharification yield, and iii) monitor glucan losses and recovery after pretreatment. Literature studies concerning post-consumer waste wood to-date are mainly interested in the use of waste wood for WtE applications, and therefore assessing the compositions of structural components (glucan, hemicellulose, lignin) are rarely considered and typically only elemental analysis is conducted. Given the prior knowledge of the heterogenous nature of waste wood, the structural composition of the waste wood fines was determined by four different independent runs, each run having three repeats. The high variability in waste wood composition can be seen from the clear variability in the glucan, acid insoluble lignin content as well as the ash content and is summarized in Table 2.2. Run 1 and 3 had lower glucan and lignin contents and a high ash content while run 2 and 4 had high glucan and lignin contents and a lower ash content. The difference in composition between the runs is clearly due to the different contamination level with run 1 and 3 having higher stones, glass and grit contamination, contributing to the high ash and low glucan and lignin contents. The ash content reported from the compositional analysis procedure is the acid insoluble ash and therefore it is slightly lower compared

to the direct ash from combustion. The composition of waste wood fines was taken as the average of the 4 runs and the values were used to calculate delignification, hemicellulose removal and glucan recovery of the treated cellulose pulps in later sections. Comparing the composition of the waste wood fines to the virgin pine untreated wood, we can see that the compositional difference stems from the glucan and ash contents where waste wood fines contain 36 % glucan and 6.9 % ash, virgin untreated wood contained 42 % glucan and 0 % ash. Comparing hemicellulose non-glucan sugars, waste wood fines have very similar galactose and mannose compositions to virgin pine wood, with slightly higher xylose. This indicates that this waste wood batch contains a high amount of softwoods where glucomannan is the prevalent hemicellulose and smaller proportion of hardwoods where glucuronoxylan is the primary hemicellulose.

Table 2.2: Compositional analysis on waste wood fine sample for (four independent runs) and untreated softwood wood sample

	Glucose	*Xylose*	*Galactose*	*Arabinose*	*Mannose*	*AIL**	*ASL**	*Ash*	*Extractives*
Run 1	36.8	8.0	2.5	-	9.5	24.1	5.4	10.9	2.8
Run 2	39.6	8.1	3.3	-	10.5	28.0	4.3	3.3	2.9
Run 3	31.9	9.4	5.9	-	10.3	26.5	3.2	10.1	2.7
Run 4	39.1	8.7	3.4	-	8.4	29.7	5.0	3.3	2.4
Waste wood (Average)	36.8	8.5	3.8	-	9.6	27.1	4.5	6.9	2.7
Untreated virgin wood	42.5	5.1	3.4	2.7	13.8	28.5	1.4	0.0	2.6

AIL: acid insoluble lignin
ASL: acid soluble lignin

2.3.1.2 Metal concentration in feedstock

Given the anticipated high variability and heterogeneity of the feedstock, several repeats of finely grinded waste wood fines were digested to measure the trace elements metal concentration. Grinding was found to be very important to homogenize the waste wood samples for a more accurate trace elemental analysis. The French legislation on biomass combustion units will be used to discuss and compare the results as a reference.[11] Iron showed the highest average concentration of all metals at 0.11 wt% (1127 mg kg^{-1}). The high iron concentration in waste wood is expected given that ferrous materials (nails, scraps) are one of the main contaminants found in waste wood sourced from demolition and construction activities. In addition, high level of iron oxides-based compounds are also used in pigment formulation which contaminate the surface of the wood permanently unlike the nails and scraps. Lead was the second largest contaminant in

waste wood fines with an average concentration of 484 mg kg^{-1}. The high level of Pb contamination indicates that paints and pigments are potentially a significant source of contamination as Pb compounds (oxides, chromate, nitrate, carbonate and sulfate) were used extensively for decorative paint and pigmentation (i.e. white paint) or as a drying agent (lead naphthenate) before its progressive restriction in the EU by the REACH regulation. This also indicates that this waste wood was probably collected from infrastructure and buildings that were built before the 1970s where the use of lead paints was very common. The concentration of Zn^{II} and Ti^{IV} were also found to be high at 214 and 53 mg kg^{-1}, respectively, likely originating from ZnO and TiO_2 white pigments, which are currently largely used as substitutes for Pb white pigment.[12] Cr^{III}, Cu^{II} and As^{V} were also present at relatively lower concentrations compared to paint- and pigment-associated metals (Pb^{II}, Zn^{II} and Ti^{IV}).

As mentioned before, these three metals are the world's most widely used wood preservative, and although the use of the CCA treated timber is banned in Europe for industrial and commercial building, wood in old infrastructure still contains these preservatives as the life-span of CCA treated wood is around 30 to 40 years.[13] This means that CCA preservatives will continue to be a major contaminate in the waste wood stream for years to come. It is important to note that the bulk amount of CCA treated wood is mechanically separated during the visual inspection step in the waste wood processing as this treated wood has a characteristic green color that makes it easy to distinguish. However, fine residues of CCA treated wood will potentially be present especially in the waste wood fines fraction where the separation of the wood fine is more challenging. Trace amount of Cd of 0.6 mg kg^{-1} was also present which could be from Cd-based compounds that were very commonly used as stabilizers for polymers and plastics.[14] Overall, **the total concentration of heavy metals in this waste wood fine sample was 1.95 g kg^{-1}. The quantity exceeds and nearly is double the authorized value of 1 g kg^{-1} by the French legislation**[11], confirming that this waste wood is heavily contaminated making it unsuitable for use in energy recovery applications, so landfill is the only disposal route.

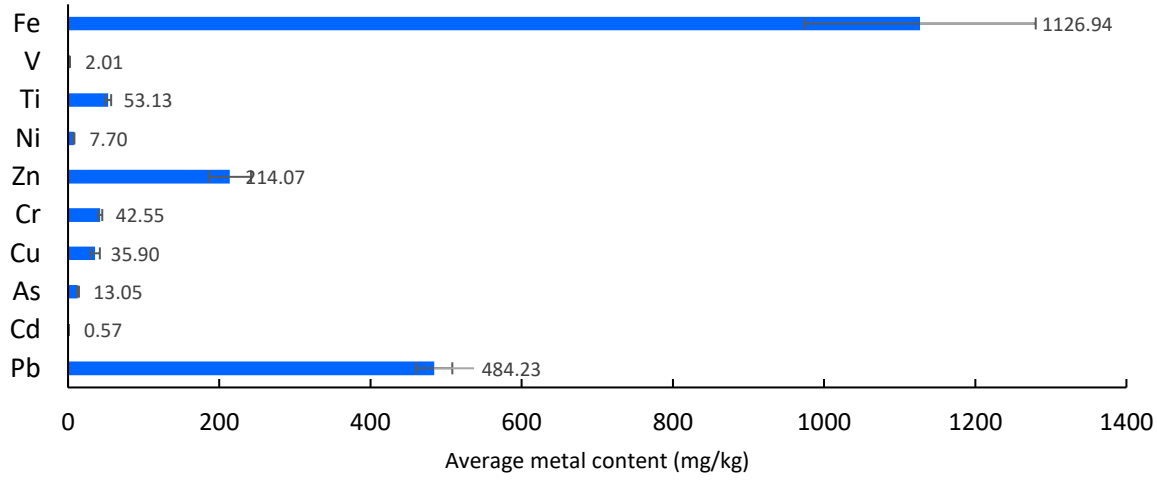

Figure 2.2: Average metal concentration of post-consumer waste wood

To quantify the contribution of paint and pigments on the metal concentration present in the sample, the waste wood fines sample were physically separated into two fractions; painted wood fraction that was a mix of white and green painted wood chips and non-painted wood chips. Figure 2.3 shows the trace element analysis conducted on each fraction separately. Pb concentration in the painted wood reached 1,978 mg kg^{-1} while the non-painted fraction contained only 46 mg kg^{-1}. This confirms that Pb^{II} compounds in paint are the main source of the biomass contamination, making the average value of Pb^{II} concentration in the waste wood fine sample to be 480 mg kg^{-1}. The level of iron contamination was also vastly larger (x 600) in the painted fraction compared to the wood fraction, which highly likely from iron oxides in paint and pigments. The concentrations of Zn^{II} and Ti^{IV} were also significantly higher in the painted fractions which was also expected as these two are the main metals used in paint formulations. The concentrations of Ni^{II}, V^{V} and Cd^{II} were also slightly higher in the painted fraction. Interestingly, that the concentrations of common wood preservatives (Cu^{II}, Cr^{III} and As^{V}) were slightly higher in the wood fraction compared to the painted fraction.

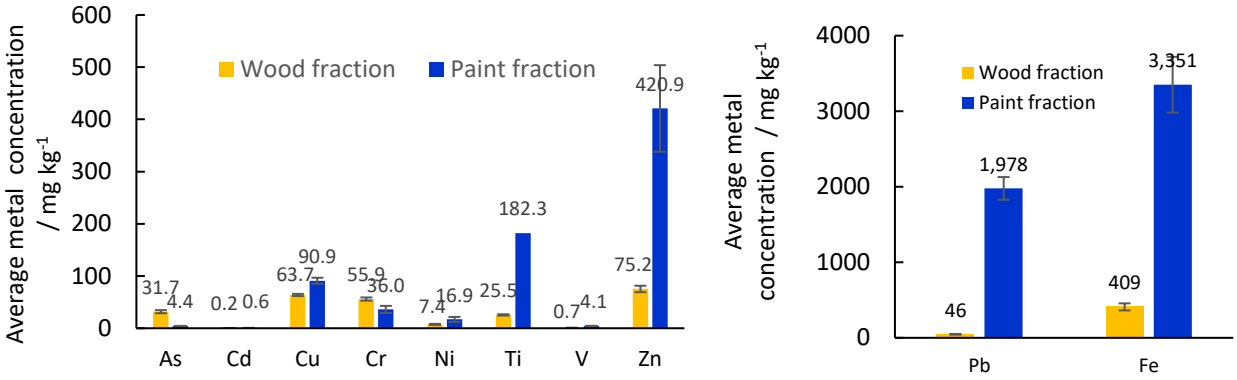

Figure 2.3: Average metal concentration in the wood and painted fractions of the waste wood. Each fraction was separated and processed separately. Raw data was obtained using ICP-MS.

2.3.2 Ionic liquid screening: biomass fractionation and metal extraction

We first investigated the use of different ionic liquids to evaluate their effectiveness in fractionation and decontamination of waste wood fines, simultaneously. For this of experiment, the pretreatment conditions were set to be 170 °C oven temperature for 45 minutes and a biomass to solvent loading of 1:5 g g^{-1} and the water content for all ionic liquids were also fixed at 20 wt%. It is important to note that the temperature of this experimental protocol is not at isothermal conditions as previously discussed in a recent ionoSolv process intensification paper[15] and the temperature of the vessel's content is only reached after 30 minutes. This means that shorter pretreatment times can be achieved under isothermal process conditions.

The structures of the ILs used in this study are shown in Figure 2.4. Herein, 1-ethyl-3-methylimidazolium acetate [C_2C_1im][Oac] was used as this ionic liquid has been considered the classical IL used for biomass dissolution/fractionation (dependent on water content), and it has been used for wide variety of conventional biorefinery feedstocks. Therefore, it was key to investigate the performance of this IL for this new challenging feedstock. (2-hydroxyethylammonium) acetate [2-HEA][OAc] was also tested as acetate-based protic ionic liquids have recently been shown to be effective in fractionating agricultural residues biomass.[16,17] 1-methylimidazolium chloride was investigated as it was recently shown to be highly effective in extracting heavy metals from CCA-treated wood.[13] Further, we explored the use of three protic hydrogen sulfate ionic liquids of different cations; *N*-methylimidazolium hydrogen sulfate [H_1Cim][HSO_4], *N,N,N*-dimethylbutylammonium hydrogen sulfate [DMBA][HSO_4] and *N*-methylbutylammonium hydrogen sulfate [MBHA][HSO_4]. Comparing the performance of [H_1Cim][HSO_4] and [H_1Cim]Cl can provide key insights on the role of anion in the process, while comparing [H_1Cim][HSO_4] with [DMBA][HSO_4] can highlight the role of the cation in the process. In addition, comparing [DMBA][HSO_4] and [MBHA][HSO_4] can provide an interesting insight regarding the impact of the degree of substitution of the ammonium cation on the pretreatment efficiency.

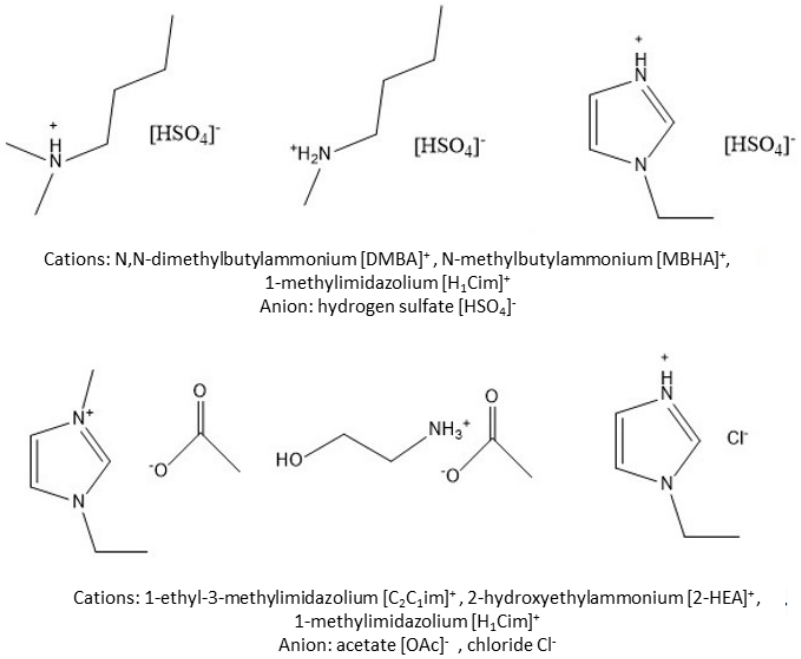

Figure 2.4: Structure of the ILs used in this study

Figure 2.5 shows the key process performance indicators for the ionoSolv pretreatment: glucan recovery, non-glucan hemicellulose removal and delignification were calculated based on values derived from compositional analysis of the cellulose-rich pulps. Lignin yield refers to the recovered precipitated lignin yield from the ionic liquids, and glucose yields are the 7-day enzymatic saccharification yields of the wet cellulose-rich pulps. In this context, glucose yield via enzymatic saccharification yield is taken as the key indicator for the pretreatment effectiveness as glucose is the precursor for biofuel fermentation or chemical transformation into bio-chemicals. **Among the investigated ILs, the highest glucose release was obtained using [H_1Cim]Cl with the glucose yield reaching 80% of the theoretical maximum.** On the other hand, glucose yields of the three [HSO_4]-based ionic liquids were relatively lower with pulps treated with both [DMBA][HSO_4] and [MBHA][HSO_4] achieving similar saccharification yields of 48%, while glucose yields from [H_1Cim][HSO_4] were much lower at only 23%. **This provides a key insight on the significant role the anion plays on the release of glucose from the cellulose-rich pulps when comparing results from [H_1Cim]Cl and [H_1Cim][HSO_4].** Cellulose pulps obtained from [C_2C_1im][OAc] yielded 41% glucose, which is relatively similar to glucose yields from [DMBA][HSO_4] and [MBHA][HSO_4] whereas [2-HEA][OAc] pretreatment have resulted in a low glucose yield of 24%.

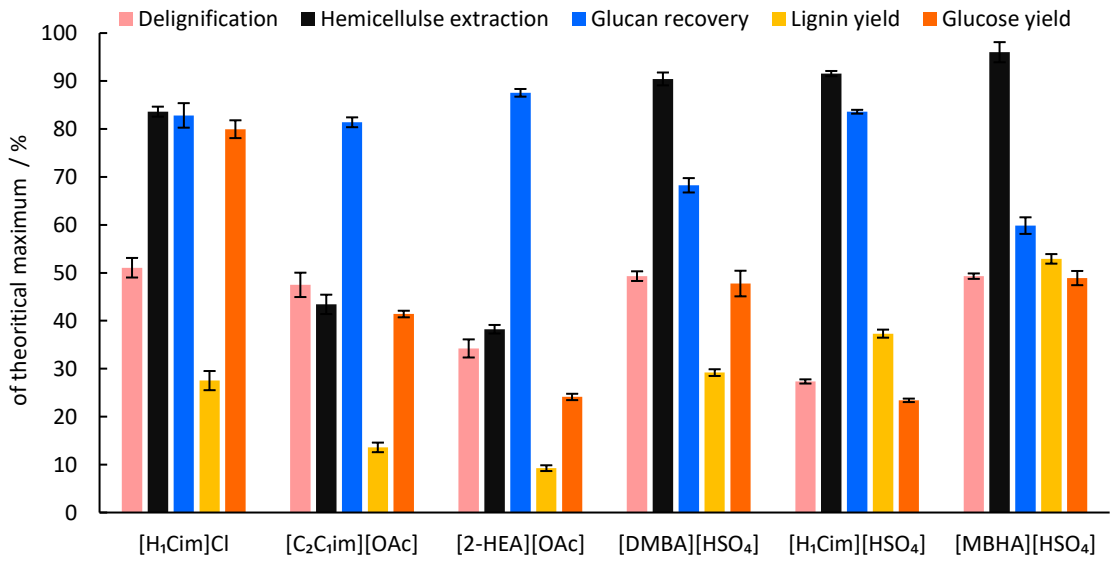

Figure 2.5: Key process performance indicators for ionoSolv pretreatment effectiveness: glucan recovery, non-glucan hemicellulose removal and delignification. Fractionation experiments were conducted at 170 °C for 45 minutes using 1 : 5 g g^{-1} solid loading. Numerical values obtained by compositional analysis procedure.

It is interesting to mention that the average glucose yield of untreated waste wood fines was zero, *i.e.* there was no sugar release after 7-day of enzymatic saccharification. In fact, there was an obvious fungus growing in the saccharification tubes after 7 days of incubation, even though antibiotics (tetracycline and cycloheximide) were added to the mix as part of the enzymatic saccharification protocol. This behavior was observed repeatedly, and a separate enzymatic saccharification test was conducted where the painted fraction of the waste wood was separated from the non-painted fraction. The non-painted fraction showed similar fungus growth as observed with the untreated waste wood, which is an indication of wood-decay microbes and fungi attack favorable at moist conditions. The painted fraction had an average glucose yield of 7.3 % relative to the theoretical maximum. This indicates that that the metal content in the painted fraction was effectively able to prevent fungus growth which helped the enzymes to release small portion of the glucose without it being consumed by the growing fungi. **Overall, the screening of the different ILs highlights the outstanding performance of [H_1Cim]Cl in fractionating waste wood fines where 20-fold increase in glucose yield is achieved relative to the untreated waste wood fines.**

Glucan recovery (*i.e.* % of glucan in cellulose pulp after pretreatment relative to cellulose content in untreated biomass) provides a good indicator of the severity of the pretreatment. Glucan recovery was particularly low for pulps treated with [MBHA][HSO_4] and [DMBA][HSO_4] with values of 59 % and 68 %, respectively, which indicates severe cellulose degradation during the process. On the other hand, glucan recoveries were above 80 % for the other investigated ILs, with [2-HEA][OAc] having the highest glucan recovery of 87 %. The severe degradation of glucan in the acidic $[HSO_4]^-$ PILs indicates that the glucan in waste wood is more susceptible to degradation compared to virgin biomass feedstocks previously investigated using ionoSolv process (glucan recovery ≥ 90%). The degradation of glucan in non-acidic ILs ([H_1Cim]Cl, [C_2C_2im][OAc], [2-HEA][OAc]) also highlights the glucan in waste wood has higher tendency to degrade. This could be due to the age and deterioration of post-consumer waste wood, where glucan is naturally depolymerized and therefore it is easier to degrade during the pretreatment.[18]

Part of the ionoSolv deconstruction process is the effective removal of hemicellulose polysaccharides from the biomass matrix. The three [HSO_4]-based ionic liquids were highly effective in removing more than 90 % of the initial hemicellulose sugars present in the waste wood. [H_1Cim]Cl was slightly less effective, removing 83 % of hemicellulose. Both [C_2C_1im][OAc] and [2-HEA][OAc] ionic liquids were much less effective in removing hemicellulose with 43 % and 38 % removals, respectively. Acetate based ionic liquids are well-known for their ability to preserve the hemicellulose sugars in the cellulose pulps and it is typically highlighted as their one of their key advantages.

Since the ionoSolv process is based on delignification of biomass by depolymerization and subsequent extraction of lignin biopolymer, it was established in a previous study that there is a directly proportional relationship between the enzymatic glucose release and the extent of delignification. Both [H_1Cim][HSO_4] and [2-HEA][OAc] demonstrated poor delignification performance with values of 34 % and 27 %, respectively, which in turn corresponded to low glucose yields of 23 % and 24 %, respectively. However, it was interesting to note that [H_1Cim]Cl, [DMBA][HSO_4], [MBHA][HSO_4] and [C_2C_1im] showed very similar delignification performance with values ranging from 47 to 51 %. While the average delignification of [DMBA][HSO_4], [MBHA][HSO_4] and [C_2C_1im][OAc] can be correlated with the obtained glucose yields, the exceptionally high glucose yields of [H_1Cim]Cl of 80 % cannot be solely explained by the average delignification performance of 51 %. **The finding suggests that while the amount of lignin on the pulp plays a key role in rendering the release of glucose from cellulose, the structure and degree of condensation of the residual lignin in the pulp also plays a key role on the extent of glucose release.** To date, it has been technically challenging to analyze the residual lignin in the cellulose pulp. Under the assumption that the isolated lignin will have similar chemistries to the residual lignin on the pulp, we analyzed the chemical structure of the isolated lignins using HSQC NMR to provide some insights about how each IL solvent impacts the lignin characteristics, reactivity and degree of condensation. To do so, we compared the signal intensities of main ether linkages and aromatic units in softwood and hardwood lignin (Figure 2.6), namely the different positions of the guaiacyl unit (G_2, G_5 and G_6), the syringyl unit intensity (S) and the intensity of the common ether linkages, β-O-4 , β-β and β-5'.

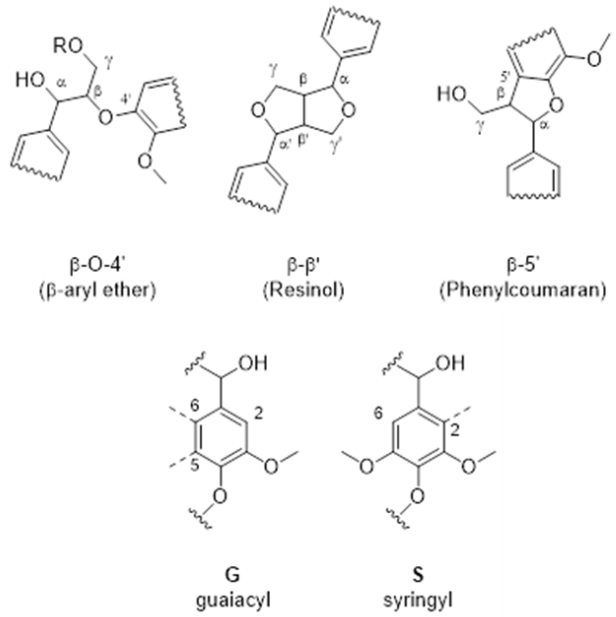

Figure 2.6: The most prominent ether bonds and subunit in softwood and hardwood lignin

Figure 2.7 presents the relative HSQC volume integrals for isolated lignin from pretreatment with different ILs. G_2 signal is typically used as an internal standard as G_2 site in lignin (particularly softwood lignin) does not participate in condensation reactions.[19] However, when G_5 and G_6 sites undergo chemical condensation, the G_2 signal shifts leading to G_{2cond} signal. Therefore, the sum of G_2 and G2cond signal is taken as a reference integral.[19]

The three investigated [HSO_4]-based ILs showed higher degree of lignin condensation and higher extent of ether cleavages compared to [OAc]-based and Cl-based ILs which could be due to the acidic nature of the [HSO_4] anion. Lignin precipitated from the [MBHA][HSO_4] fractionation had the highest degree of condensation reactions (*i.e.* substitution reactions occurring on the aromatic rings) which is evidence by the low G_6 intensity and the high G_{2cond} signal as well as the low intensity of the ether bonds (β-O-4 , β-β and β-5').

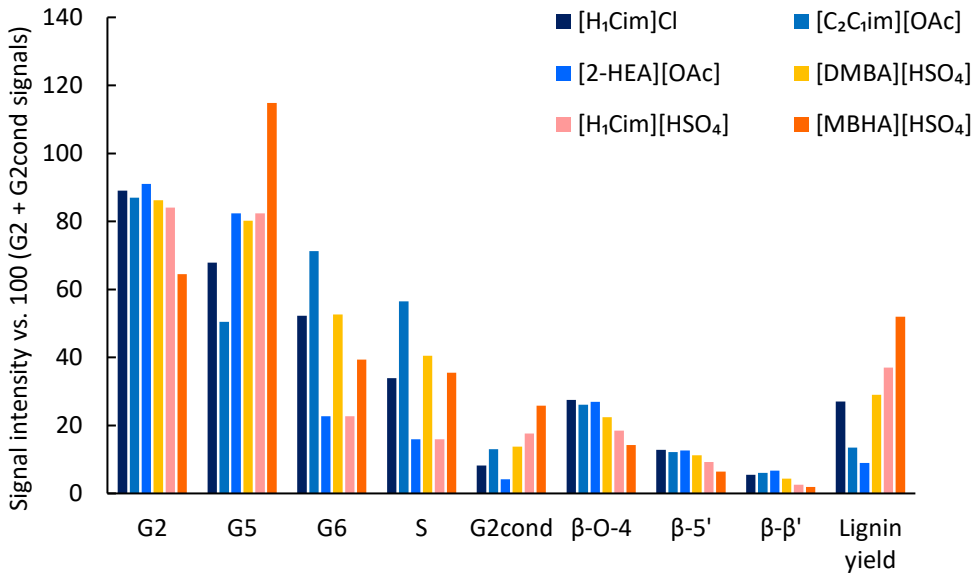

Figure 2.7: Abundance of lignin functionalities according to HSQC NMR spectroscopy for lignin isolated using different ionic liquids (intensity of G2 signal set to 100%). Fractionation experiments conducted at 170 °C for 45 minutes using 1 : 5 g g^{-1} solid loading

This correlates with the high lignin yield from [MBHA][HSO_4] fractionation, which can also indicate the formation of more condensed lignin structures as well as pseudo-lignin. The noticeable large G_5 signal in [MBHA][HSO_4] can be potentially attributed to carbohydrate-derived degradation products that reacts with lignin forming pseudo lignin. [H_1Cim][HSO_4] and [DMBA][HSO_4] also showed relatively high degree of condensation and breakage of ether interlinks, both also correlating with their high lignin yields. Lignin isolated from [H_1Cim]Cl showed only a small degree of condensation compared to [HSO_4]-based ILs and [C_2C_1im][OAc]. [2-HEA][OAc] derived lignin showed the lowest degree of condensation and lowest lignin yield, which aligns with the low delignification using this IL. **Under the assumption that the isolated lignin have relatively similar characteristics to the residual and/or redeposited lignin on the cellulose pulp, the high enzymatic digestibility of [H_1Cim]Cl cellulose pulp could be related to the combined effect of less condensed lignin structure along with relatively high delignification.**

As mentioned above, the potential use of waste wood fines as a biorefinery feedstock requires the use of an ionic liquid that can fractionate the waste wood and enabling the valorization of the cellulose-rich pulp, while also decontaminating the waste wood by

effectively removing the heavy metals. Ionic liquids have been well-known for their ability to extract and chelate metals from aqueous environment using bulky hydrophobic ILs to create biphasic systems.[20–22] The use of hydrophilic ionic liquids to extract heavy metals from solids materials has only been explored recently.[23] To evaluate the effectiveness of the investigated ionic liquids at extracting heavy metals present in the waste wood fines, cellulose-treated pulps were digested followed by ICP-MS trace-element analysis. Figure 2.8 shows the calculated heavy metal extraction of Pb^{II}, Zn^{II}, Cd^{II}, Cu^{II}, Cr^{III}, As^{V}, Ti^{IV}, Ni^{II} and V^{V} using the 6 investigated ionic liquids. Heavy metal extractions were calculated based on the original concentration of these metals in the waste wood fines are presented in Figure 2.2. Interestingly, [**H_1Cim]Cl also showed the highest metal extraction ability of all investigated ionic liquids, with superior extractions of ≥ 90 % for Pb^{II}, Zn^{II}, Cd^{II} and Cu^{II}.** This highlights the outstanding ability of $[H_1Cim]^+$ and Cl^- ions to chelate with the heavy metal presence in the waste wood. With the exception of Cu^{II} and Pb^{II} extractions, $[H_1Cim][HSO_4]$ achieved the 2nd highest extraction for all the other heavy metals, achieving higher extraction efficiencies compared to the $[HSO_4]$-ILs with alkylammonium-based cations. **This finding suggests that cation also play an important role in extracting the heavy metals from the biomass matrix.** The high metal chelating ability of imidazole-based compounds has been well documented since the 1960s.[24] Both acetate-based ionic liquids have also shown high metal extraction ability from waste wood, with the exception of Ti^{IV} where poor extractions of 11 % and 1 % were achieved by $[C_2C_1im][OAc]$ and [2-HEA][OAc], respectively. Extraction of Ti^{IV} was in fact relatively low for all investigated ionic liquids compared to the other investigated metals, with maximum extractions of 50 % and 51 % achieved by $[H_1Cim]Cl$ and $[H_1Cim][HSO_4]$, respectively. Vanadium extraction was also relatively low for all investigated ionic liquids with the highest extraction of 60% achieved by $[MBHA][HSO_4]$, followed by 50 % extraction by $[H_1Cim]Cl$ and lowest extraction of 35 % by $[DMBA][HSO_4]$. Comparing the ability of $[MBHA][HSO_4]$ and $[DMBA][HSO_4]$, it is clear that $[MBHA][HSO_4]$ shows slightly higher extraction ability for all investigated metals, except for Cu^{II}. In fact, extraction of Cu^{II} showed a particularly interesting behavior, where 90 % extraction is achieved with $[H_1Cim]Cl$ followed by 50 % extraction using $[DMBA][HSO_4]$ and then very poor extractions ranging from 22 % with $[C_2C_1im][OAc]$ to 9 % using $[H_1Cim][HSO_4]$. A recent study by Dastyar *et al.* have investigated the use of triethylammonium hydrogen sulfate $[TEA][HSO_4]$ (i.e.

[DMBA][HSO_4] isomer) to extract heavy metals from biomass harvested from a phytoextraction process.[23] Interestingly, the results of the study have shown different trend in metal extraction where Pb^{II} extraction was reported to be negligible, and Cu^{II} extraction was 100%. We are unsure whether the huge difference in behavior is due to the structure of the IL or to the nature of the biomass. Given that we have investigated three [HSO_4]-based protic ILs, it might be unlikely that [TEA][HSO_4] would behave completely different. Therefore, we speculate that the nature of the biomass could be the reason behind the variation in behavior. Future study should focus on comparing the extraction ability of ILs using post-consumer waste wood and harvested biomass from phytoremediation for further confirmation.

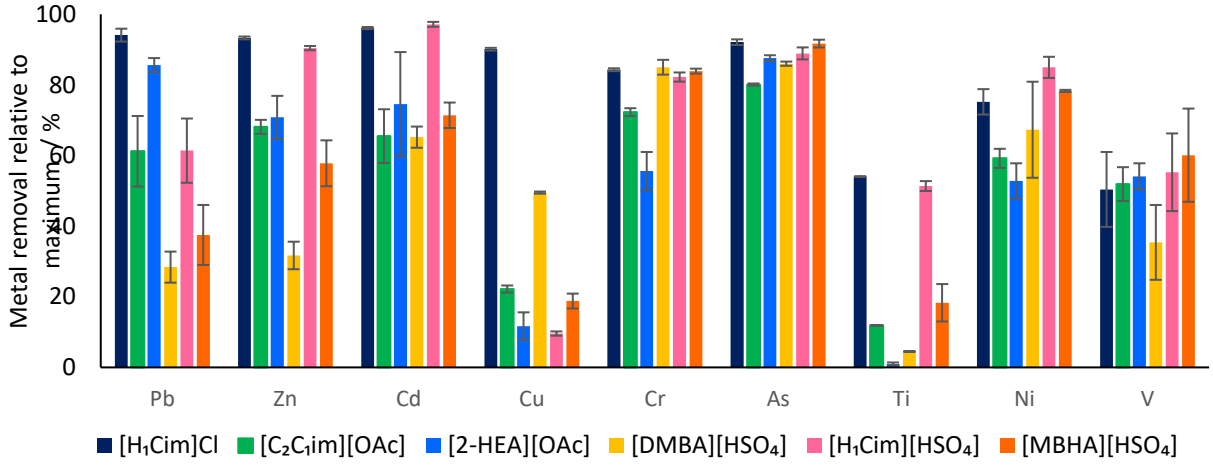

Figure 2.8: Heavy metal extraction during fractionation experiments using different ILs. Fractionation experiments were conducted at 170 °C for 45 minutes using 1 : 5 g g^{-1} solid loading.

The ash content of the biomass and cellulose-rich pulps can give an indication about the level of contamination and potentially the level of metal oxides presence originating from paints and pigments. Figure 2.9 shows the acid-insoluble ash content obtained from compositional analysis of the cellulose-rich pulps for the 6 investigated ionic liquids. **It was interesting to note that the acid-insoluble ash correlates well with ability of ionic liquid to extract heavy metals from biomass.** [H_1Cim]Cl extracted 85 % of the original ash present, followed by [C_2C_1im][OAc], [2-HEA][OAc] and [C_2C_1im][HSO_4], all of which showed very high metal extraction efficiency. On the other hand, both [DMBA][HSO_4] and [MBHA][HSO_4] showed much lower ash extraction of 16 % on average, which reflects their poor ability to extract metals relative to the other investigated ionic liquids.

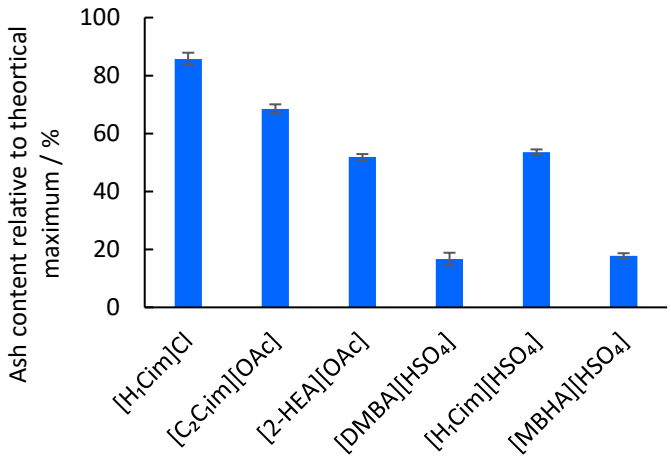

Figure 2.9: Acid insoluble ash content in cellulose-rich pulps from fractionation experiments using different ILs. Data obtained according to compositional analysis procedure. Fractionation experiments conducted at 170 °C for 45 minutes using 1 : 5 g g^{-1} solid loading

2.3.3 Pretreatment kinetics, enzymatic saccharification yield and metal extraction

The fractionation effectiveness of the ionoSolv process with $[HSO_4]^-$-based ionic liquid was studied in a recent process intensification work,[25] mainly aimed at achieving optimized space-time that can be translated to industrial-scale. It was of interest to investigate the impact of pretreatment time on the fractionation of the waste wood fines, especially since delignification did not change considerably with different ionic liquids as discussed previously. Therefore, we conducted space-time optimization to gain further insights on the kinetics of delignification using this new feedstock. Although the IL screening results showed that $[H_1Cim]Cl$ is optimal in terms of fractionation performance and decontamination efficiency, it was still interesting for us to compare the kinetics of delignification of $[H_1Cim]Cl$ with the kinetics of extraction with $[DMBA][HSO_4]$ as the latter has been successfully used to fractionate challenging feedstocks.[26] As glucose yield is taken as the key indicator of waste wood utilization in this study, Figure 2.10-a shows the glucose yields for the cellulose pulps obtained after fractionation using $[DMBA][HSO_4]$ at 170 °C and $[H_1Cim]Cl$ at 150 °C and 170 °C.

Glucose yields of $[H_1Cim]Cl$ at 150 °C and 170 °C increased with pretreatment time with no maxima observed on the investigated time scale, levelling at 80 % relative to theoretical maximum. On the other hand, glucose yields for treated pulps with $[DMBA][HSO_4]$ were lower with an observed optimum of 43% relative to the theoretical

maximum at 45 minutes and it drops down to 38 % at 90 minutes. It is interesting also to highlight that the glucose yield of [H_1Cim]Cl pretreated waste wood pulps reached a plateau after 24 hours (Figure 2.10-b) with a glucose yield of 70 % relative to the theoretical maximum. Figure 2.12 shows the fractionation kinetics of waste wood fines using [H_1Cim]Cl at oven temperatures of 170 °C and 150 °C and [DMBA][HSO_4] at 170 °C by monitoring the key process performance indicators (glucose yield, glucan recovery, delignification and hemicellulose removal) as well as the recovered lignin yields. Glucan recovery for [H_1Cim]Cl treated pulps were relatively higher and remained fairly constant compared to [DMBA][HSO_4] treated pulps where glucan recovery dropped to 63 % at 170 °C for 90 minutes, compared to 80% for [H_1Cim]Cl. However, it is important to note that glucan recovery of waste wood fines at the various conditions were relatively low with approximately 25 % glucan loss after 45 minutes pretreatment, relative to 5 to 10 % glucan loss observed in previous ionoSolv studies using virgin untreated biomass.[39–41]

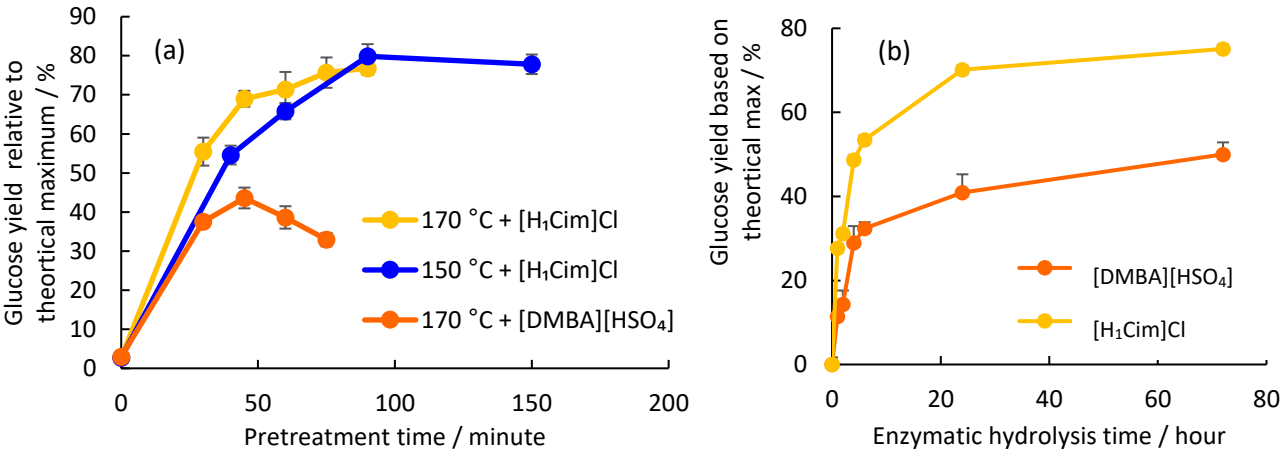

Figure 2.10: (a) 7-day enzymatic hydrolysis glucose yield for fractionation experiment using [DMBA][HSO_4] and [H_1Cim]Cl at different pretreatment time. (b) Enzymatic glucose yields from cellulose-rich pulps obtained from [DMBA][HSO_4] and [H_1Cim]Cl as a function of saccharification time.

As stated above, we speculate that the reason behind this degradation in glucan might be related to the nature of the waste wood and the initial state of cellulose that made it more susceptible to degradation due to ageing. **However, it is still important to note that although the glucan loss was relatively high, it is still fairly reasonable given the heterogenous nature of the feedstock.** In addition, it is important to note that up to 10% of glucan losses could be attributed to the removal of the glucan contained in the hemicellulose in the form of galactoglucomannans and xyloglucans.

Both [DMBA][HSO_4] and [H_1Cim]Cl had very similar performance in removing hemicellulose from waste wood, with higher removals achieved at longer pretreatment time. Comparing the delignification kinetics between 150 °C and 170 °C for [H_1Cim]Cl, it can be observed that slightly higher delignification is achieved at 170 °C compared to 150 °C where for example, at 60 minutes, 50 % delignification is achieved at 150 °C compared to 60 % at 170 °C. It is interesting to note that the delignification behavior by [H_1Cim]Cl remained fairly constant even at high pretreatment severity conditions of 170 °C for 90 minutes or 150 °C for 150 minutes, 50 % delignification was still achieved. In addition, even though the delignification at 170 °C was slightly higher, the glucose yield obtained at 150 °C pretreatment was high reaching 80% relative to theoretical maximum with residence time between 90 to 150 minutes.

On the other hand, delignification by [DMBA][HSO_4] showed a different behavior compared to [H_1Cim]Cl as a clear optimum delignification of 53 % at 45 minutes was achieved before dropping down to 35 % at 170 °C and 90 minutes. Interestingly, a similar delignification of 57% was achieved by [H_1Cim]Cl at 170 °C and 45 minutes. The relatively lower lignin extraction achieved by [DMBA][HSO_4] with waste wood particularly at prolonged pretreatment time is probably due to the fast redeposition of lignin on cellulose pulp promoted by the high acidity of the solvent. As compositional analysis cannot distinguish between native lignin and redeposited lignin, the redeposited condensed lignin is accounted as Kalson lignin, causing a decrease in the delignification value. As an indication of the relative acidity of these ionic liquids, the pH value of the 1 wt% IL solution of [DMBA][HSO_4] is 1.2 while as 1 wt% of [H_1Cim]Cl has a pH value of 4.2. On the other hand, the depolymerized lignin fragments of [H_1Cim]Cl does not seem to undergo condensation reactions to the same level. To have further insights on the structural compositions and degree of condensation of the lignin fragments, we investigated the changes in the recovered lignin structure at different pretreatment time.

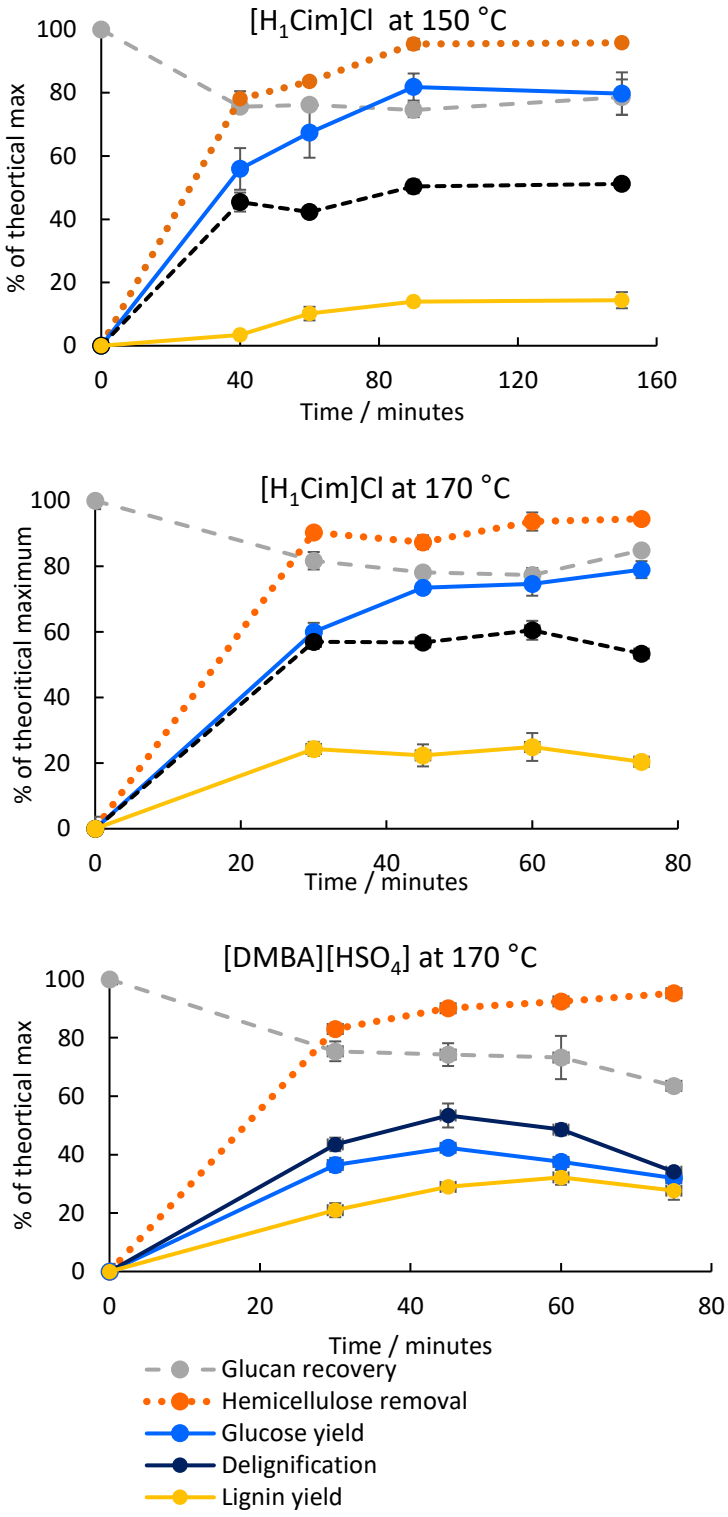

Figure 2.11: Fractionation kinetics of post-consumer waste wood using 1:5 g g^{-1} solid loading. Fractionation experiments were conducted using IL mixed with 20 wt% water as a co-solvent.

Figure 2.12 shows a summary of the HSQC NMR signal intensities for isolated lignin by $[H_1Cim]Cl$ and $[DMBA][HSO_4]$ at different pretreatment times. The main structural change occurred at the aromatic signal G_{2cond} showing the increase level of condensation at longer pretreatment for both $[DMBA][HSO_4]$ and $[H_1Cim]Cl$. However, **the G_{2Cond} signal was almost double the intensity for $[DMBA][HSO_4]$ compared to $[H_1Cim]Cl$, indicating that precipitated lignin with $[DMBA][HSO_4]$ has more condensed structure especially at prolonged pretreatment times. The high degree of *β-O-4* ether linkages cleavage for $[DMBA][HSO_4]$ lignins also indicate the high level of depolymerization, while *β-O-4* ether linkages in $[H_1Cim]Cl$ lignins showing higher intensity, indicating less cleavage and lower overall pretreatment severity**. Therefore, the significant difference in glucose yields between $[H_1Cim]Cl$ and $[DMBA][HSO_4]$ despite their similar delignification performance could be due to the characteristics of the residual lignin on the pulp, as indicated by the precipitated lignin characterization. The results are similar to the findings in the previous section, where the lignin properties showed more coherent explanation to glucose yield trend compared to the delignification values. The higher lignin yields obtained by $[DMBA][HSO_4]$ fractionation particularly at prolong residence time where lower delignification was achieved indicates the formation of more condensed and potentially more hydrophibic lignin structures that easier to precipitate. The higher lignin yield is also partly due to the reaction of extracted lignin fragments with the hemicellulose sugars formation of pseudo lignin structures. It is also interesting to note that syringyl (S) unit was present in the waste wood fines lignin along with G unit, which indicates the presence of hardwoods in the mixture of the waste wood fines. The kinetics of $[H_1Cim]Cl$ fractionation highlight that the IL was effective in fractionating the highly heterogenous waste wood fines over a wide range of time scales without showing a deterioration in the cellulose pulp quality and enzymatic hydrolysis. **This can be a key advantage relative to $[HSO_4]^-$ acidic ionic liquids where the optimal glucose yield can only be achieved at a very narrow time window, requiring a close monitoring for the produced pulp quality and a careful feedstock-dependent kinetics optimization which would be indeed challenging when dealing with highly heterogenous feedstocks such as waste wood.**

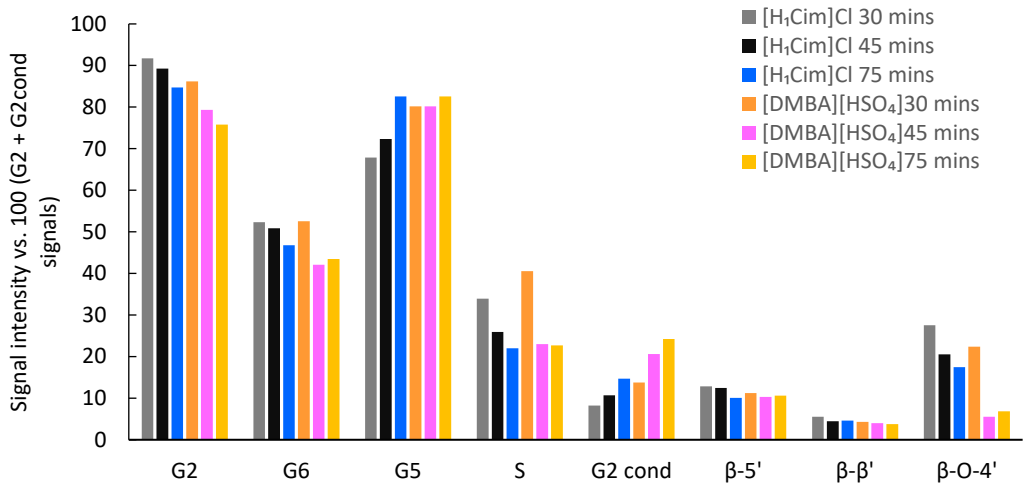

Figure 2.12: Abundance of lignin functionalities according to HSQC NMR spectroscopy for lignin isolated at different pretreatment conditions (intensity of G2 signal set to 100%)

2.3.4 Effect of biomass loading

Studying the fractionation effectiveness of the process at high biomass loading is important as it highlights the process capabilities and potential limitations. Operating the process at high biomass loading provides key economic and process intensification advantages as the loading directly correlates with reactor size, one of the largest contributors to the capital cost of the process. However, it should be also noted that operating the process at high biomass loading can cause multiple operational and economical challenges as higher loading translates to higher power needed for mixing reactor's content in a batch or continuous stirred tank reactor (CSTR) as well as a significant increase in the viscosity of the slurry produced, resulting in more challenging pumping and filtration. Therefore, choosing the appropriate solid loading for the operation should be studied holistically. Figure 2.13 shows waste wood fines fractionation at solid loading ranging from 1:5 g g^{-1} to 1:2 g g^{-1} (i.e. 10 to 50 wt% biomass relative to ionic liquid) using $[H_1Cim]Cl$ at 170 °C for 45 minutes. **Quantitative glucose yield was achieved at the lowest solid loading of 10 wt%, followed by 93 % glucose yield at 20 wt% loading**. The slightly higher glucose release at 20 wt% loading compared to the previously obtained 73 to 79% glucose yield (previous section) is attributed to experimental variation as different batches of $[H_1Cim]Cl$ as well as a new bottle of cellulase enzymes were used. Glucose yield decreased with increasing solid loading with 55 % glucose yield achieved at 50 wt% loading.

The quantitative glucose release from the treated pulp at 10 wt% loading can be attributed to the high achieved delignification of 72 %, showing that a high-quality cellulose pulp can be obtained from such a heavily contaminated waste wood source. It should be noted that this was the highest delignification achieved and increasing in biomass loading to 20 wt% decreased the delignification to 51 % relative to maximum. A further increase in biomass loading only resulted in a minor decrease in delignification where at 50 % loading, 46 % delignification was achieved. It is unclear why the delignification of post-consumer waste wood is not as sensitive to process parameters (time, temperature, solid loading, and to some extent IL!). It is possible that wood age and prolong exposure to UV light might have an impact on lignin structure, making the lignin more condensed, less reactive and therefore more challenging to be removed by the IL. It seems that only a relatively fixed amount of lignin was removed. However, at 10 wt% loading, the high solvent ratio relative to the biomass lignin content could have favored the extraction of lignin. Other IL-based biomass fractionation studies have observed the same effect where optimal delignification was achieved at 10 wt% loading, followed by a decrease at 20 wt% loading. The effect was attributed to the reduced ion mobility at higher biomass loading as well as the increase in available lignin for fixed amount of the IL.[29,30] Glucan degradation at 10 and 20 wt% loading was approximately 15 %, and it was observed that glucan loss gradually increased with increasing solid loading reaching 33 % at 50 wt% loading.

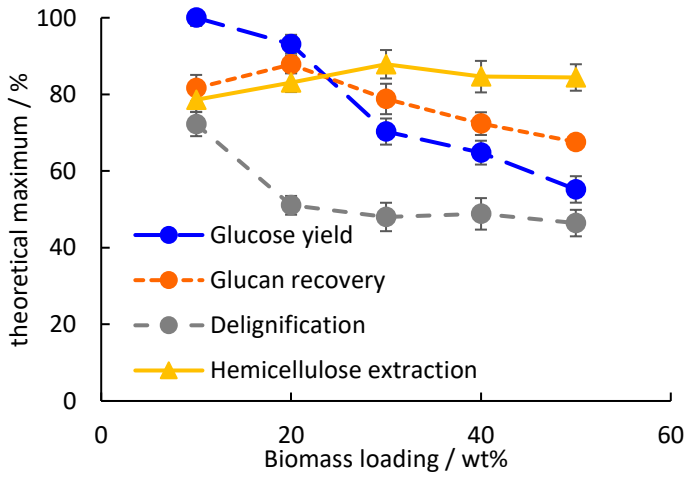

Figure 2.13: Key indicators of biomass fractionation at different biomass loading. Fractionation experiments were conducted using [H_1Cim]Cl mixed with 20 wt% water at 170 °C oven temperature

The effectiveness of [H_1Cim]Cl at extracting metals at high solids loadings was also investigated as presented in Figure 2.14. Extraction of Pb^{II}, the highest heavy metal contaminant in this batch of waste wood fines, decreased gradually from nearly quantitative extraction of 98 % at 10 wt% loading to 84 % extraction at 50 wt% loading. Chromium extraction also decreased from 92 % at 10 wt% loading to 77 % at 50 wt% loading. The extraction of other investigated metals of As^{V}, Cd^{II}, Zn^{II} and Ni^{II} did not change considerably with effective high extraction ranging from 85 to 95 % achieved at the highest investigated loading of 50 wt%. **The ability of [H_1Cim]Cl to effectively extract metals and heavy metals at high substrate loading highlights the high metal solvation and coordination ability of [H_1Cim]Cl.**

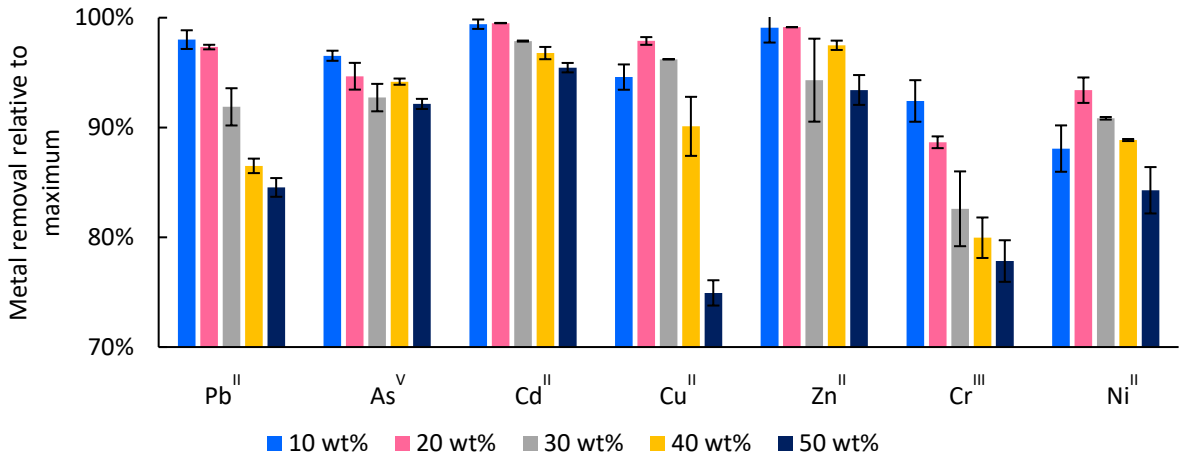

Figure 2.14: Metal extraction during fractionation experiment at different solid loading using [H_1Cim]Cl mixed with 20 wt% water. Fractionation experiments were conducted at 170 °C oven temperature

The results also demonstrate the robustness and effectiveness of the process to simultaneously fractionate and decontaminate post-consumer waste wood fines in a high throughput process, with solid to solvent ratio of 1:2 g g^{-1}. The nearly metal-free cellulose-rich pulp produced can be used as a substrate for glucose production, or alternatively it can be safely used in energy recovery applications as a solid fuel using a regular non-hazardous waste biomass incinerator. The use of 10 wt% solid loading also

provides higher cellulose pulp quality and therefore the cellulose pulp can be upgraded to other cellulose-based products such as paper. However, further characterization needs (e.g. mechanical strength, degree of polymerization) to be conducted to assess quality of the fibers. Overall, fractionation of post-consumer waste wood fines using [H_1Cim]Cl provided very promising results in terms of lignin ad heavy metal extraction as well as cellulose quality and glucose yield.

Recently, there has been an increase interest in using lignin and lignin-based products as bio-sorbents to extract heavy metals from wastewater streams.[31] The application of lignin as bio-sorbent originates from the fact that lignin is highly porous and carbonaceous material that also contain a variety of phenolic and carboxylic functional groups that have high affinity for heavy metals.[32] Therefore, it was essential to assess the potential chelation of metals to the lignin stream in the process. Understanding the partitioning of metals during the process is also of key importance to assess where it is best to locate an electrochemical metal recovery step to clean-up the ionic liquid for reuse. Figure 2.15 shows the trace metals present in the isolated lignin from using 20 wt% and 50 wt% biomass loading. It is evident that lignin does chelate with metals during the fractionation process where for example 3.1 % of Pb^{II} and 9.6% of Cu^{II} relative to the original metal content were found in the isolated lignin at 20 wt% loading. At 50 wt% loading, the amount of metals in the lignin stream increased noticeably indicating the higher chelating tendency of heavy metals with lignin at higher concentration. The current and near-term application of lignin on large-scale chemical plants is solid fuel for energy recovery. Metal chelating with lignin can therefore represent a challenge as a WID boiler might be needed instead of regular boiler, which would increase the process CAPEX. **The finding also indicates that the IL metal clean-up step via electrodeposition is best to be located *prior* to the lignin precipitation step to reduce the possibility of metal chelating in lignin.** However, it should be noted that at steady-state conditions, it might be impossible to completely avoid metal chelation with lignin, and therefore a more extensive assessment on the level of metal contamination in lignin should be conducted. It should be noted that when considering the worst-case scenario of high levels of metal chelation with lignin, **the process can be looked at as waste *minimization* and valorization as the lignin stream represents 7 to 10 wt% of the original waste wood input in the process**.

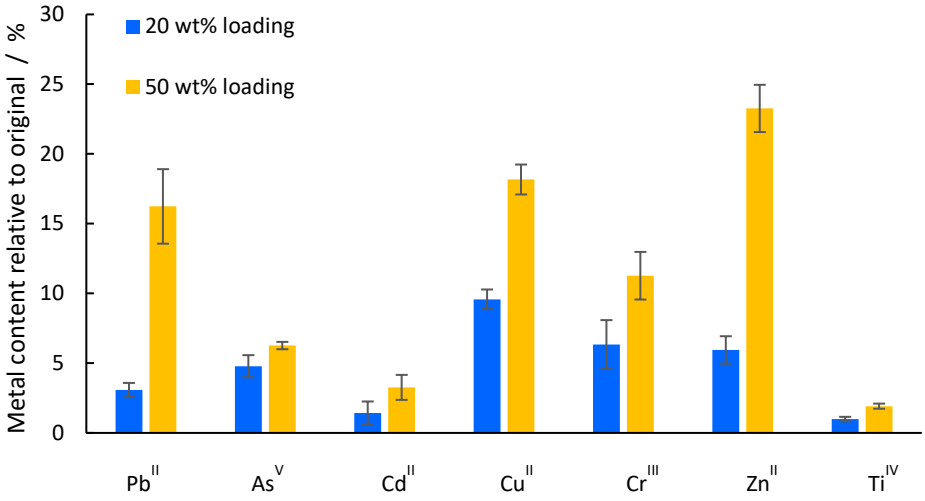

Figure 2.15: Trace metals presence in lignin stream at 20 and 50 wt% loading fractionation experiment. Experiments were conducted using [H_1Cim]Cl mixed with 20 wt% water at 170 °C oven temperature for 45 minutes

Figure 2.16 shows mass balance of Pb and its partitioning in the cellulose pulp, lignin and ionic liquid at 20 wt% and 50 wt% loading. The unaccountable balance was calculated as the difference of the sum of Pb present in the cellulose, lignin and ionic liquid liquor where this percentage probably represent the Pb content in the non-digestible ash silicates such as sand or glass. It is important to note that this glass or sand is still contained in the cellulose-rich pulp, but it is not digested during the ICP-MS trace-element method as the adapted digestion procedure (EPA- Method 3050B) is not a total digestion procedure, so does not dissolve silicate structures. Therefore, Pb^{II} content in the cellulose pulp resembles the Pb^{II} content in the organic digestible fraction, whereas the total maximum Pb^{II} content of cellulose-pulp can be taken as the sum of the Pb^{II} content in the organic pulp fraction and the unaccountable silicate fraction.

The organic fraction of the cellulose pulps contained 2.7 % and 15.5 % of Pb relative to the original Pb^{II} content in the waste wood fines at 20 wt% and 50 wt% loading, respectively. The majority of the extracted lignin remained in the ionic liquid liquor during the fractionation process where **isolated lignins contained only 3.1 % and 16.2 % of the original Pb^{II} present at 20 wt% and 50 wt% loading, respectively.**

This result demonstrates the ability of the fractionation process to be used as an effective waste minimization and valorization approach, where the heavy metals content can be reduced considerably in the organic matter, producing higher-value and cleaner substrates suitable for energy recovery or liquid biofuel production.

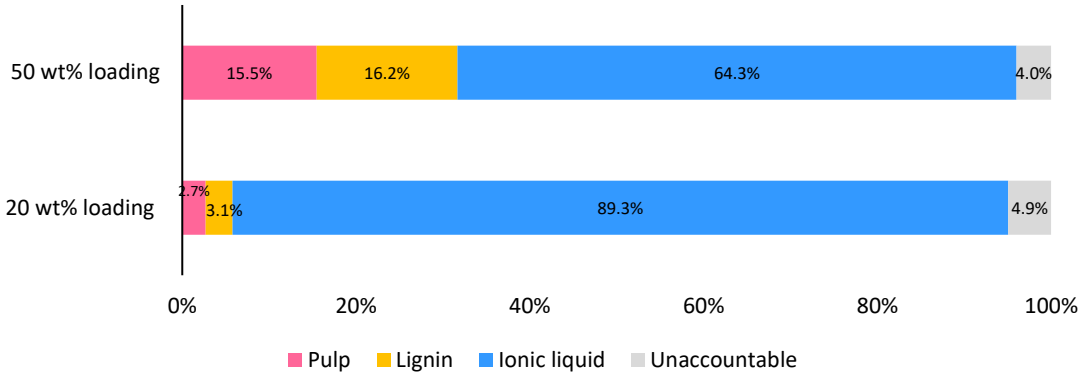

Figure 2.16: Mass balance of Pb content in the cellulose pulp, lignin and ionic liquid at 20 wt% and 50 wt% loading in fractionation experiment using [H1Cim]Cl mixed with 20 wt% water at 170 °C oven temperature.

2.3.5 Waste wood feedstock variability

Given the highly heterogenous nature of waste wood, it was important to investigate the performance of the process using different waste wood batches to assess the effectiveness of the process. Figure 2.17 presents the metals and heavy metals content of four different batches of grade C waste wood obtained from waste management companies. As mentioned earlier, waste wood is typically categorized as waste wood chips and waste wood fines depending on the particle size obtained during the shredding process at the collection facilities. Waste wood chips are the larger size waste wood fraction typically between 10 to 80 mm which is usually less contaminated whereas waste wood fines refer to the smallest size fraction of waste wood (< 1 to 10 mm) produced during the shredding process. It is important to note that these particle sizes reflect the particle size of the waste wood at the collection facilities; however, all the fractionation experiments were conducted using the same particle size of 180 to 850 μm. As shown in Figure 18, the two waste wood fines batches collected from different waste management companies had the same characteristic of being more metal contaminated compared to the waste wood chips.

The higher level of contamination of waste wood fines is clear, specifically the higher concentrations of Pb^{II}, Zn^{II}, Cr^{III} and Ni^{II}.

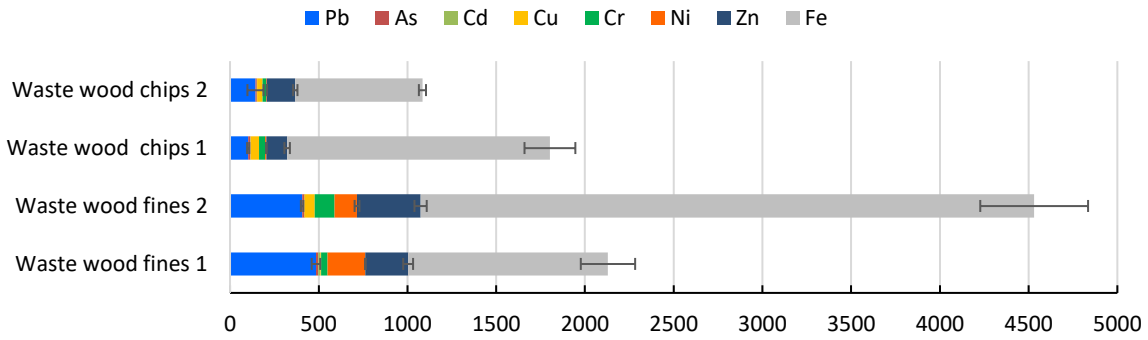

Figure 2.17: Metal contents of post-consumer waste wood chips and waste wood fines collected from waste management companies

The high contamination of waste wood fines with Pb^{II} and Zn^{II} confirm that this fraction contains the bulk of the paint flakes, which is in agreement with the extensive waste wood characterization study over a 9 year period.[33] Figure 2.18 shows the glucose yield of the cellulose-rich pulp obtained by fractionating the four waste wood batches using $[H_1Cim]Cl$ and $[DMBA][HSO_4]$ at 170 °C and 45 minutes. **Glucose yields for cellulose pulps treated with $[H_1Cim]Cl$ were exceptionally high with values ranging from 72 % to 89 % relative to theoretical maximum, with slightly higher glucose yields achieved with waste wood chips compared to waste wood fines**. On the other hand, glucose yields from cellulose pulps treated with $[DMBA][HSO_4]$ were more variable and noticeably lower, ranging from 39 % to 66 % relative to the theoretical maximum. As we observed in the previous section, the residual ash content in the cellulose pulps can provide an indication of the metal removal effectiveness in the process (Figure 2.9). Therefore, we used the direct ash content of the cellulose pulps to compare the metals removal efficiency of $[H_1Cim]Cl$ and $[DMBA][HSO_4]$ from the waste wood chips and waste wood fines. As shown in Figure 2.19, the ash content (and therefore the metal content) of cellulose pulps obtained from $[DMBA][HSO_4]$ fractionation were higher in all investigated post-consumer waste wood samples compared to pulps obtained from $[H_1Cim]Cl$ fractionation. **This confirms that $[H_1Cim]Cl$ has superior metal extraction ability compared to $[DMBA][HSO_4]$.**

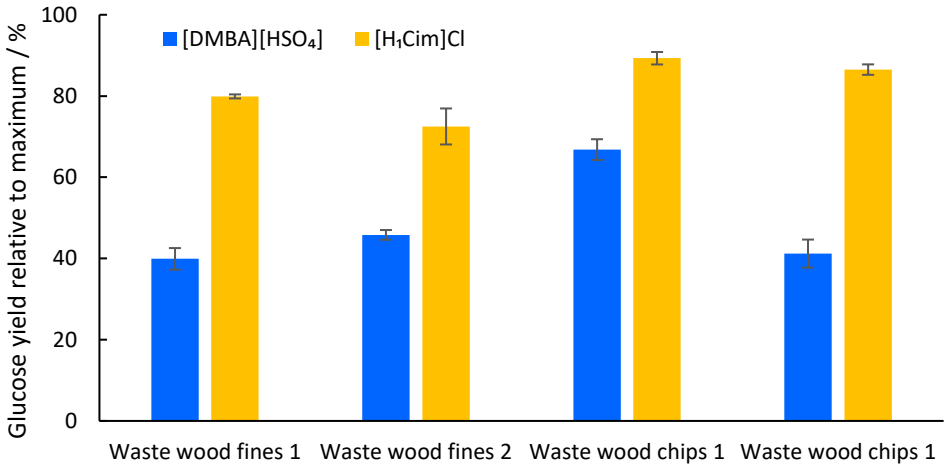

Figure 2.18: Glucose yield of cellulose pulps obtained from fractionation experiments using post-consumer waste wood chips and waste wood fines as feedstock. Fractionation experiments were conducted at 170 °C for 45 minutes and 1 : 5 g g^{-1} solid loading

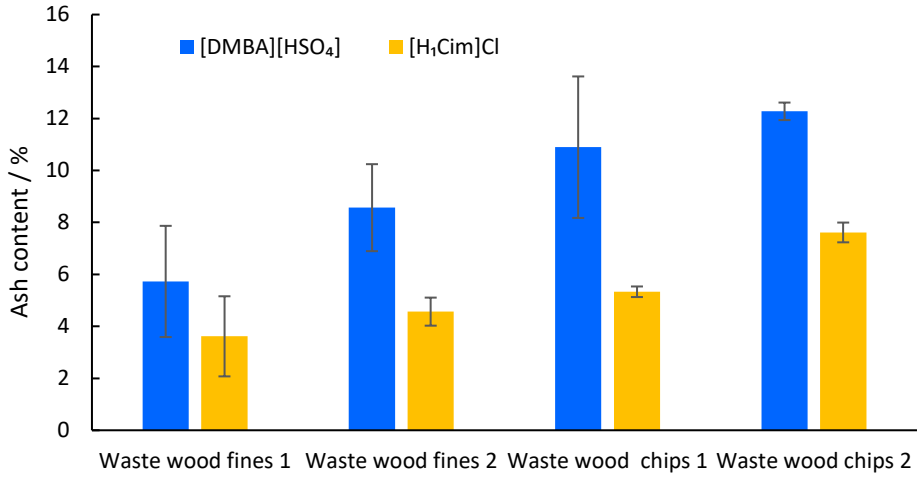

Figure 2.19: Ash content of cellulose pulps obtained from fractionation of waste wood chips and waste wood fines using [H$_1$Cim]Cl and [DMBA][HSO$_4$]

2.3.6 Metal electrodeposition and IL clean-up

For the IL to be used in a cyclic manner, the accumulation of metal ions in the IL-stream needs to be managed. Firstly, the electrodeposition behavior of Pb^{II} in [H$_1$Cim]Cl (lignin-free) was studied to assess the feasibility of using electrochemical strategies for the removal of Pb^{II} from the IL-stream. ILs are very attractive solvents for electrodeposition, due to their high electrochemical stability and innate conductivity, i.e. no addition of supporting electrolyte is required. To illustrate that the ILs can be "cleaned'" up and to further identify where it is best to locate the electrodeposition step in the process,

electrodeposition experiments were conducted by Dr. Sze Tan using the both neat IL and IL liquor after the pretreatment. Figure 2.20i shows cyclic voltammograms for the deposition and dissolution of Pb^{II} in [H_1Cim]Cl with (a) 20 wt% and (b) 40 wt% H_2O, approximating to the water content of the IL-stream before and after lignin precipitation, respectively. A negative-going potential scan produced a reduction current wave and peak.

$$Pb^{II} + 2e^{-} \underset{\text{oxidation}}{\overset{\text{reduction}}{\rightleftharpoons}} Pb$$

This was consistent with the 2-electron reduction of Pb^{II} to deposit Pb^0. The subsequent positive-going potential scan produced a sharp oxidative peak, consistent with the dissolution of deposited Pb^0 from the electrode surface. The potential $E_{I=0}$, at which current, $I = 0$, on the positive-going potential scan can be used as an estimation of the formal potential for the Pb^{II}/Pb^0 redox couple. We note that the potential for the Pb^{II}/Pb^0 redox reaction in [H_1Cim]Cl was -0.72 V and -0.62 V vs AgCl/Ag (3.0 M NaCl) in 20 wt% and 40 wt% H_2O, respectively. The more negative electrode potential indicates the redox reaction Pb^{II}/Pb^0 couple requires more energy in [H_1Cim]Cl with 20 wt% H_2O compared to the 40 wt% H_2O content.

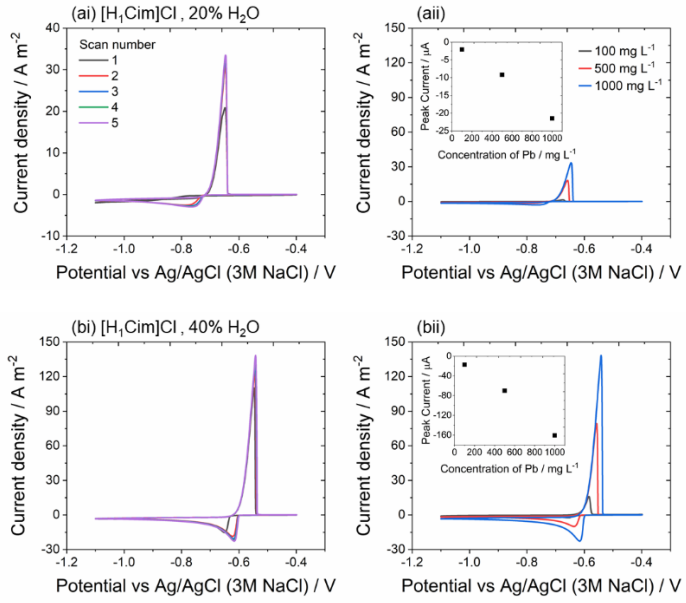

Figure 2.20. Cyclic voltammograms showing (i) repetitive potential cycling of a 3 mm-dia. glassy carbon electrode in 1000 mg L^{-1} Pb^{II} in (a) [H_1Cim]Cl, 20 wt% H_2O and (b) [H_1Cim]Cl, 40 wt% H_2O, and (ii) varying concentration of Pb^{II} (c = 100, 500, 1000 mg L^{-1}). Initial negative-going potential scan from -0.4 to -1.1 V vs Ag/AgCl (3 M NaCl) at a scan rate of 50 mV s^{-1}. Data shown in (ii) was taken from the fifth scan from the repetitive voltammetric scanning procedure.

We also noted that Pb^{II} reduction current response in $[H_1Cim]Cl$ with 20 wt% H_2O was very broad, indicating the kinetically limited electron transfer when compared to Pb deposition in $[H_1Cim]Cl$ with 40 wt% H_2O. Slow kinetics in ILs have been correlated to high viscosity IL as previously reported and is consistent with our findings reported herein.[34] The diffusion coefficients for Pb^{II} in $[H_1Cim]Cl$ with 20 wt% H_2O and 40 wt% H_2O were calculated using Randles–Ševčík Equation to be 7.2×10^{-12} and 7.2×10^{-10} m^2 s^{-1}, respectively.

Figure 2.20ii shows cyclic voltammograms for varying concentrations of Pb^{II} (*c* = 100, 500 and 1000 mg L^{-1}) in $[H_1Cim]Cl$ with 20 wt% and 40 wt% H_2O at a scan rate of 50 mV s^{-1}. It is clear that Pb^{II} can be deposited from $[H_1Cim]Cl$ with 40 wt% H_2O has faster kinetics than from $[H_1Cim]Cl$ with 20 wt% H_2O. However, as discussed earlier, $[H_1Cim]Cl$ with 20 wt% and 40 wt% H_2O approximate to the water content of the IL-stream before and after lignin precipitation, respectively. As it has been shown that lignin may chelate and precipitate Pb^{II} from the IL, it is desirable to remove Pb^{II} from the IL-stream *before* the lignin precipitation step in the ionoSolv process. Therefore, to define optimal electrodeposition conditions, the effects of cathode potential on current densities and electrodeposit morphologies were determined for Pb^{II} reduction to Pb^0 on copper electrodes in $[H_1Cim]Cl$ with 20 wt% H_2O, as shown in Figure 2.22. The electrodeposition potential at the working electrode acts as the main driving force for the nucleation and growth of Pb^0 deposits on the copper electrode.

Figure 2.21(a) shows the time dependences of current densities , for Pb electrodeposition on Cu from 1000 mg L^{-1} Pb^{II} in $[H_1Cim]Cl$ with 20 wt% H_2O at various potentials (-0.80, -0.85, -0.90 and -1.0 V vs. AgCl/Ag). In this electrochemical system, the magnitude of current measured at the electrode is controlled by the rate of the reaction and the mass transport of Pb^{2+} to the electrode surface. The rate of reaction is controlled by the potential applied and mass transport is controlled by the diffusion of Pb^{2+} to the electrode surface. At the more positive applied potential of -0.8 V vs. AgCl|Ag, the measured current was a quasi-steady-state current of -0.98 A m^{-2}. Increasing the driving force of reduction to -0.85 produced quasi-steady-state current density of -1.19 A m^{-2} and further increase to the driving force to -0.95 V produced the same current density value of -1.19 A m^{-2}. This implies that the reaction is kinetically controlled at -0.8 V, but transport control at both -0.85 and -0.9 V vs. AgCl|Ag as the current value did not change, indicating that it is limited to Pb^{+2} diffusion. When -1.0 V vs. AgCl|Ag was

applied, a quasi-steady-state current density of -1.43 A m^{-2}. The observed increase in current density is attributed to the additional hydrogen evolution reaction, $2H^+ + 2e^- \rightarrow H_2$, producing the bubbles observed on the working electrode surface. Applied potentials where hydrogen evolution starts are typically avoided for electrodeposition applications as the evolution of hydrogen can cause hydrogen embrittlement of the deposits. In addition, hydrogen evolution is a side reaction which is a waste of the energy input. Scanning electron microscopy (SEM) images shown in Figure 2.21(b-d) are for a sequence of deposits at increasingly negative applied potential. Comparing Figure 2.21(b) and (c), it is evident that the density of the plate-like crystal grains increased with decreasing more negative electrode potential.

Figure 2.21(d) shows the deposition morphology of Pb^0 when accompanied by hydrogen evolution resulting in porous network clusters due to the formation of bubbles on the electrode surface.[34]

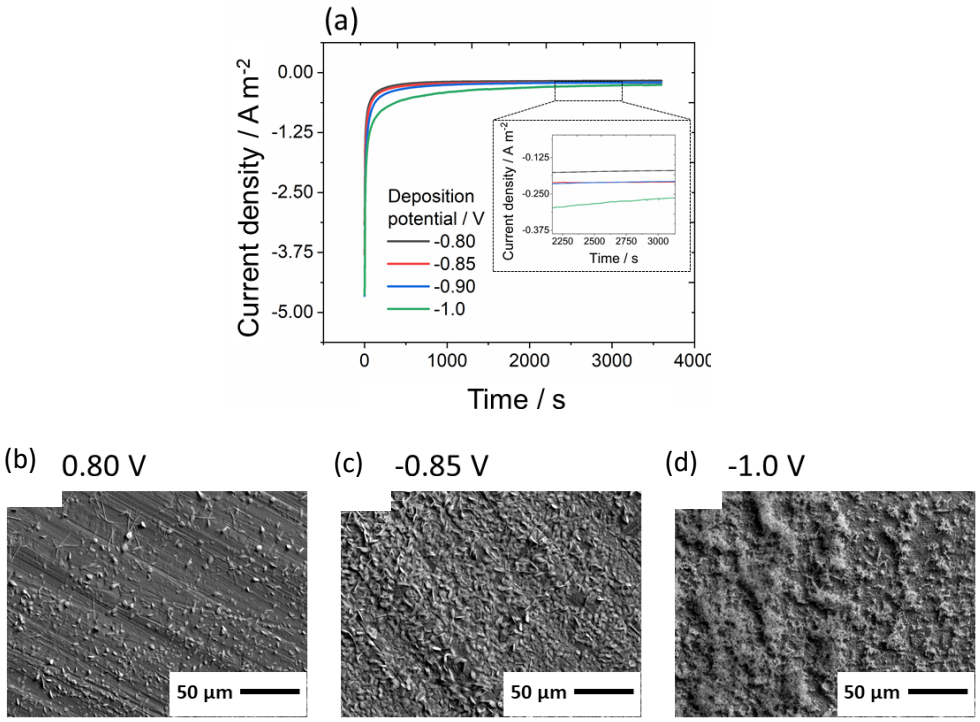

Figure 2.21. Time dependences of: (a) Measured current densities and for electrodeposition of Pb onto Cu from 1000 mg L^{-1} Pb^{II} in $[H_1Cim]Cl$ with 20 wt% H_2O at varying potentials (-0.80, -0.85, -0.90 and -1.0 V) for 1 hr. SEM images of Pb deposition at (b) -0.80, (c) -0.85 and (d) -1.0 V vs. AgCl/Ag.

When -1.0 V vs. AgCl|Ag was applied, a quasi-steady-state current density of -1.43 A m^{-2}. The observed increase in current density is attributed to the additional hydrogen evolution reaction, $2H^+ + 2e^- \rightarrow H_2$, producing the bubbles observed on the working electrode surface. Applied potentials where hydrogen evolution starts are typically avoided for electrodeposition applications as the evolution of hydrogen can cause hydrogen embrittlement of the deposits. In addition, hydrogen evolution is a side reaction which is a waste of the energy input. Scanning electron microscopy (SEM) images shown in Figure 2.21(b-d) are for a sequence of deposits at increasingly negative applied potential. Comparing Figure 2.21(b) and (c), it is evident that the density of the plate-like crystal grains increased with decreasing more negative electrode potential. Figure 2.21(d) shows the deposition morphology of Pb^0 when accompanied by hydrogen evolution resulting in porous network clusters due to the formation of bubbles on the electrode surface.[34]

Figure 2.22(a) shows voltammograms of a Cu electrode in lignin-containing $[H_1Cim]Cl$-20 wt% water sample, taken from the process and spiked with 1000 mg L^{-1} Pb^{II}. Based on the previous findings, the applied potential was chosen to be -0.85 V vs. *AgCl|Ag* to avoid hydrogen evolution. Compared to the lignin-free Pb^{II}-IL counterpart, the reduction process was more complex, the voltammograms exhibiting a broad reduction peak and significant contributions from non-faradaic background currents. This was attributed to side reactions of other metals in the process solution (C_{Fe} = 42 mg L^{-1}, C_{Cu} = 1.8 mg L^{-1}), which can catalyze hydrogen evolution, as well as organic components. Furthermore, both the deposition and dissolution peak currents decreased monotonically with repetitive potential cycles, consistent with surface fouling of the electrode from adsorbed organic compounds.[35,36] Figure 2.23(b) and (c) show SEM images of Pb^0 electrodeposited on Cu from the Pb^{II}-lignin-$[H_1Cim]Cl$, 20 wt% water solution. They show plate-like deposit morphologies, similar to Pb^0 deposits from Pb^{II}-$[H_1Cim]Cl$, 20 wt% water mixtures. Energy dispersive X-ray (EDX) spectra of the deposits from Pb^{II}-$[H_1Cim]Cl$ and Pb^{II}-lignin-$[H_1Cim]Cl$ mixtures confirmed pure Pb^0 deposits in both cases.

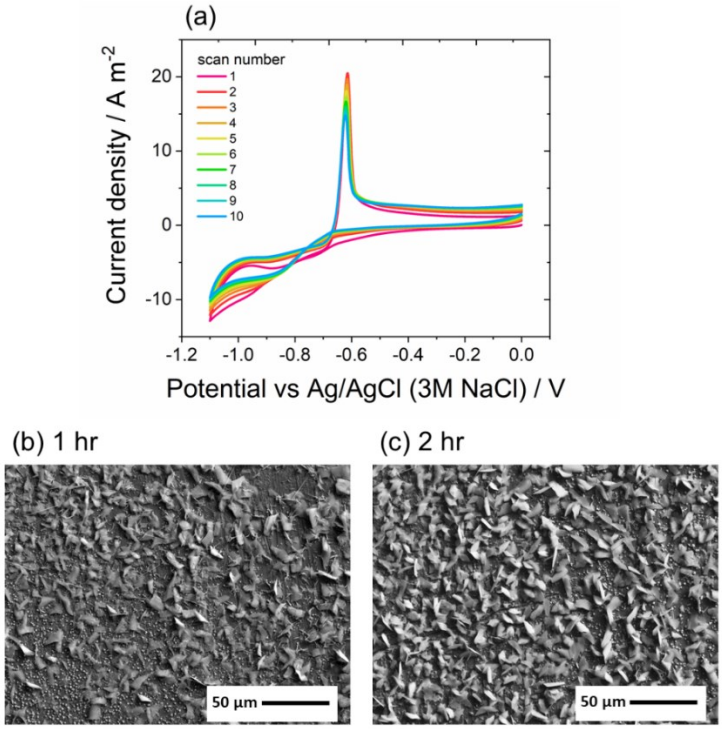

Figure 2.22. (a) Cyclic voltammograms of GC electrode in 1000 mg L^{-1} Pb^{II}-lignin-[H_1Cim]Cl with 20 wt% water. SEM images of Pb^0 deposits on Cu foil after (b) 1 hr and (c) 2 hr electrodeposition at -0.85 V vs. AgCl|Ag.

These preliminary experiments highlight that electrodeposition can be applied as an efficient way to clean-up the IL liquid liquor before the lignin precipitation step to prevent metals chelating with lignin. However, we can clearly see that the presence of lignin and other soluble organic compounds and oligomers represent a challenge to perform an energy efficient electrodeposition due to issues such as the promoted hydrogen evolution reaction and electrode fouling. Therefore, an independent in-depth study needs investigate this complex system to optimize energy use and improve the kinetically limited reaction due to the high viscous nature of the process stream. Purification and filtration processes prior to electrodeposition needs to be investigated as well to reduce the total organic content.

2.4 Conclusions

The study demonstrates the first example of valorizing and fractionating of hazardous post-consumer waste wood from construction and demolition activities to high value-added products of cellulose pulp and lignin. We investigated the role of the different variables on the fractionation and metal decontamination performance (ionic liquid, temperature, time, solid loading) in terms of cellulose-pulp quality, enzymatic digestibility and trace metal content. By screening different ionic liquids, we showed that the cellulose accessibility to enzymatic hydrolysis is not entirely governed by the extent of delignification achieved by the ionic liquid, but also to the degree of condensation of the lignin fragments during the fractionation. At optimal fractionation conditions using $[H_1Cim]Cl$, we showed that we can achieve quantitative to near-quantitative glucose yield, providing a 100-fold increase over untreated waste wood fines, in addition to over 90% removal of heavy metal contamination. We also demonstrated the tendency of some heavy metals to chelate with lignin and showed that electrodeposition can be used to effectively deposit Pb^0 and potentially other metals from the ionic liquid liquor. The study highlights the potential use of ionoSolv technology as an integrated strategy to solve two grand environmental challenges: waste remediation sustainable production of fuels and chemicals.

References

(1) Krook, J.; Mårtensson, A.; Eklund, M. Sources of Heavy Metal Contamination in Swedish Wood Waste Used for Combustion. Waste Manag. 2006, 26 (2), 158–166. https://doi.org/10.1016/j.wasman.2005.07.017.

(2) Hsieh, L.-Y.; Fong, J.-D.; Hsieh, Y.-Y.; Wang, S.-P.; Sun, I.-W. Electrodeposition of Bismuth in a Choline Chloride/Ethylene Glycol Deep Eutectic Solvent under Ambient Atmosphere. J. Electrochem. Soc. 2018, 165 (9), D331–D338. https://doi.org/10.1149/2.0411809jes.

(3) Ru, J.; Hua, Y.; Xu, C.; Li, J.; Li, Y.; Wang, D.; Qi, C.; Gong, K. Electrochemistry of Pb(II)/Pb during Preparation of Lead Wires from PbO in Choline Chloride—Urea Deep Eutectic Solvent. Russ. J. Electrochem. 2015, 51 (8), 773–781. https://doi.org/10.1134/S1023193515080108.

(4) Xie, X.; Zou, X.; Lu, X.; Lu, C.; Cheng, H.; Xu, Q.; Zhou, Z. Electrodeposition of Zn and Cu-Zn Alloy from ZnO/CuO Precursors in Deep Eutectic Solvent. Appl. Surf. Sci. 2016, 385, 481–489. https://doi.org/10.1016/j.apsusc.2016.05.138.

(5) Tsai, R.-W.; Hsieh, Y.-T.; Chen, P.-Y.; Sun, I.-W. Voltammetric Study and Electrodeposition of Tellurium, Lead, and Lead Telluride in Room-Temperature Ionic Liquid 1-Ethyl-3-Methylimidazolium Tetrafluoroborate. Electrochim. Acta 2014, 137, 49–56. https://doi.org/10.1016/j.electacta.2014.05.099.

(6) Abouelela, A. R.; Tan, S.; Kelsall, G. H.; Hallett, J. P. Toward a Circular Economy: Decontamination and Valorization of Postconsumer Waste Wood Using the IonoSolv Process. ACS Sustain. Chem. Eng. 2020, 8 (38), 14441–14461. https://doi.org/10.1021/acssuschemeng.0c04365.

(7) Brandt, A.; Gschwend, F.; Fennell, P.; Lammens, T.; Tan, B.; Weale, J.; Hallett, J. P. An Economically Viable Ionic Liquid for the Fractionation of Lignocellulosic Biomass. Green Chem. 2017. https://doi.org/10.1039/c7gc00705a.

(8) Sluiter, A.; Hames, B.; Hyman, D.; Payne, C.; Ruiz, R.; Scarlata, C.; Sluiter, J.; Templeton, D.; Nrel, J. W. Determination of Total Solids in Biomass and Total Dissolved Solids in Liquid Process Samples; 2008.

(9) Sluiter, a.; Hames, B.; Ruiz, R.; Scarlata, C.; Sluiter, J.; Templeton, D.; Crocker, D. Determination of Structural Carbohydrates and Lignin in Biomass; 2012.

(10) Shu, Z.; Xie, C.; Zhou, J.; Li, T.; Chen, Y.; Wang, W.; Tan, Y.; Zhao, Z. Low Solids Enzymatic Saccharification of Lignocellulosic Biomass Laboratory; 2015.

(11) DEVP1405250A. Ixant Les Critères de Sortie Du Statut de Déchet Pour Les Broyats d'emballages En Bois Pour Un Usage Comme Combustibles de Type Biomasse Dans Une Installation de Combustion. 2014.

(12) Huron, M.; Oukala, S.; Lardière, J.; Giraud, N.; Dupont, C. An Extensive Characterization of Various Treated Waste Wood for Assessment of Suitability with Combustion Process. Fuel 2017, 202, 118–128. https://doi.org/10.1016/j.fuel.2017.04.025.

(13) Gschwend, F. J.; Hennequin, L. M.; Brandt, A.; Bedoya-Lora, F. E.; Kelsall, G. H.; Polizzi, K.; Fennell, P.; Hallett, J. Towards an Environmentally and Economically

Sustainable Biorefinery: Heavy Metal Contaminated Waste Wood as a Low-Cost Feedstock in a Low-Cost Ionic Liquid Process. Green Chem. 2020. https://doi.org/10.1039/d0gc01241f.

(14) ECHA. Cadmium and Cadmium Compounds in Plastics; 2012.

(15) Weigand, L.; Mostame, S.; Brandt-Talbot, A.; Welton, T.; Hallett, J. P. Effect of Pretreatment Severity on the Cellulose and Lignin Isolated from: Salix Using IonoSolv Pretreatment. Faraday Discuss. 2017, 202, 331–349. https://doi.org/10.1039/c7fd00059f.

(16) Rocha, E. G. A.; Pin, T. C.; Rabelo, S. C.; Costa, A. C. Evaluation of the Use of Protic Ionic Liquids on Biomass Fractionation. Fuel 2017, 206, 145–154. https://doi.org/10.1016/j.fuel.2017.06.014.

(17) Reis, C. L. B.; Silva, L. M. A. e.; Rodrigues, T. H. S.; Félix, A. K. N.; Santiago-Aguiar, R. S. de; Canuto, K. M.; Rocha, M. V. P. Pretreatment of Cashew Apple Bagasse Using Protic Ionic Liquids: Enhanced Enzymatic Hydrolysis. Bioresour. Technol. 2017, 224, 694–701. https://doi.org/10.1016/j.biortech.2016.11.019.

(18) Zervos, S.; Moropoulou, A. Cotton Cellulose Ageing in Sealed Vessels. Kinetic Model of Autocatalytic Depolymerization. Cellulose 2005, 12 (5), 485–496. https://doi.org/10.1007/s10570-005-7131-7.

(19) Sette, M.; Wechselberger, R.; Crestini, C. Elucidation of Lignin Structure by Quantitative 2D NMR. Chem. - A Eur. J. 2011, 17 (34), 9529–9535. https://doi.org/10.1002/chem.201003045.

(20) De Los Ríos, A. P.; Hernández-Fernández, F. J.; Lozano, L. J.; Sánchez, S.; Moreno, J. I.; Godínez, C. Removal of Metal Ions from Aqueous Solutions by Extraction with Ionic Liquids. J. Chem. Eng. Data 2010, 55 (2), 605–608. https://doi.org/10.1021/je9005008.

(21) Keppler, B.; Stojanovic, A.; Fuerhacker, M.; Kogelnig, D.; Haile, T. M. Application of Ionic Liquids for the Removal of Heavy Metals from Wastewater and Activated Sludge. Water Sci. Technol. 2012, 65 (10), 1765–1773. https://doi.org/10.2166/wst.2012.907.

(22) Pirkwieser, P.; López-López, J. A.; Kandioller, W.; Keppler, B. K.; Moreno, C.; Jirsa, F. Novel 3-Hydroxy-2-Naphthoate-Based Task-Specific Ionic Liquids for an Efficient Extraction of Heavy Metals. Front. Chem. 2018, 6 (MAY), 1–11. https://doi.org/10.3389/fchem.2018.00172.

(23) Dastyar, W.; Zhao, M.; Yuan, W.; Li, H.; Ting, Z. J.; Ghaedi, H.; Yuan, H.; Li, X.; Wang, W. Effective Pretreatment of Heavy Metal-Contaminated Biomass Using a Low-Cost Ionic Liquid (Triethylammonium Hydrogen Sulfate): Optimization by Response Surface Methodology-Box Behnken Design. ACS Sustain. Chem. Eng. 2019, 7 (13), 11571–11581. https://doi.org/10.1021/acssuschemeng.9b01457.

(24) Drey, C. N. C.; Fruton, J. S. Metal Chelates of a Bis-Imidazole. Biochemistry 1965, 4 (7), 1258–1263. https://doi.org/10.1021/bi00883a007.

(25) Gschwend, F. J. V.; Brandt-Talbot, A. Rapid Pretreatment of Miscanthus Using the Low-Cost Ionic Liquid Triethylammonium Hydrogen Sulfate at Elevated

Temperatures. Green Chem. 2018, 20 (15), 3486–3498. https://doi.org/10.1039/c8gc00837j.

(26) Gschwend, F. J. V.; Chambon, C. L.; Biedka, M.; Brandt-Talbot, A.; Fennell, P. S.; Hallett, J. P. Quantitative Glucose Release from Softwood after Pretreatment with Low-Cost Ionic Liquids. Green Chem. 2019, 21 (3), 692–703. https://doi.org/10.1039/c8gc02155d.

(27) Verdía, P.; Brandt, A.; Hallett, J. P.; Ray, M. J.; Welton, T. Fractionation of Lignocellulosic Biomass with the Ionic Liquid 1-Butylimidazolium Hydrogen Sulfate. Green Chem. 2014, 16 (3), 1617. https://doi.org/10.1039/c3gc41742e.

(28) Brandt-Talbot, A.; Gschwend, F. J. V.; Fennell, P. S.; Lammens, T. M.; Tan, B.; Weale, J.; Hallett, J. P. An Economically Viable Ionic Liquid for the Fractionation of Lignocellulosic Biomass. Green Chem. 2017, 19 (13), 3078–3102. https://doi.org/10.1039/C7GC00705A.

(29) Pinkert, A.; Goeke, D. F.; Marsh, K. N.; Pang, S. Extracting Wood Lignin without Dissolving or Degrading Cellulose: Investigations on the Use of Food Additive-Derived Ionic Liquids. Green Chem. 2011, 13 (11), 3124–3136. https://doi.org/10.1039/c1gc15671c.

(30) Rashid, T.; Gnanasundaram, N.; Appusamy, A.; Kait, C. F.; Thanabalan, M. Enhanced Lignin Extraction from Different Species of Oil Palm Biomass: Kinetics and Optimization of Extraction Conditions. Ind. Crops Prod. 2018, 116, 122–136. https://doi.org/10.1016/j.indcrop.2018.02.056.

(31) Nasrullah, A.; Bhat, A. H.; Isa, M. H. Lignin: A Sustainable Biosorbent for Heavy Metal Adsorption from Wastewater, a Review. AIP Conf. Proc. 2016, 1787 (November 2016). https://doi.org/10.1063/1.4968080.

(32) Naseer, A.; Jamshaid, A.; Hamid, A.; Muhammad, N.; Ghauri, M.; Iqbal, J.; Rafiq, S.; Khuram, S.; Shah, N. S. Lignin and Lignin Based Materials for the Removal of Heavy Metals from Waste Water - An Overview. Zeitschrift fur Phys. Chemie 2019, 233 (3), 315–345. https://doi.org/10.1515/zpch-2018-1209.

(33) Edo, M.; Björn, E.; Persson, P.; Jansson, S. Assessment of Chemical and Material Contamination in Waste Wood Fuels – A Case Study Ranging over Nine Years. Waste Manag. 2016, 49, 311–319. https://doi.org/10.1016/j.wasman.2015.11.048.

(34) Bentley, C. L.; Li, J.; Bond, A. M.; Zhang, J. Mass-Transport and Heterogeneous Electron-Transfer Kinetics Associated with the Ferrocene/Ferrocenium Process in Ionic Liquids. J. Phys. Chem. C 2016, 120 (30), 16516–16525. https://doi.org/10.1021/acs.jpcc.6b05545.

(35) Patel, A. N.; Tan, S. Y.; Miller, T. S.; MacPherson, J. V.; Unwin, P. R. Comparison and Reappraisal of Carbon Electrodes for the Voltammetric Detection of Dopamine. Anal. Chem. 2013, 85 (24), 11755–11764. https://doi.org/10.1021/ac401969q.

(36) Patel, A. N.; Tan, S. Y.; Unwin, P. R. Epinephrine Electro-Oxidation Highlights Fast Electrochemistry at the Graphite Basal Surface. Chem. Commun. 2013, 49 (78), 8776–8778. https://doi.org/10.1039/c3cc45022h.

Chapter 3 : Use of a Low-cost Protic Ionic Liquid for Creosote Wood Fractionation and Simultaneous Extraction of Polycyclic Aromatic Hydrocarbons

3.1 Introduction

Oil-borne chemicals such as creosote and pentachlorophenol are used as wood preservatives.[1] Creosote is one of the oldest historically used heavy duty wood preservative used in non-residential applications where long service life is essential. (e.g. more than 40 years). The first large-scale use of creosote started in the 19th century as preservative for the wooden railroad ties to avoid serious depletion of forests during the massive construction of national railways in countries such as the United Kingdom and United States.[2] Today creosote treated wood is now widely used in railway sleepers, electricity and telecommunication poles and fence panels.[3] Creosote is a complex mixture of heavy oils produced by the distillation of coal-tar or wood-tar at temperatures above 200 to 350 °C.[4] Creosote is added to the wood using specialized vacuum-pressure treatment cylinders, and once it is added, creosote acts as a highly effective fungicide, insecticide, miticide, and sporicide. About 85% of the compounds in creosote derived from coal-tar are polycyclic aromatic hydrocarbons (PAHs) such as naphthalene, quinoline, acenaphthene, dibenzofurane, pyrene, phenanthrene and fluorene whereas the remaining 10 to 15% consists of simpler phenolic compounds.[5] Around 20 to 40 wt% of the total weight of creosote wood is attributed to 16 PAH compounds, all of which defined as priority pollutants by the Environmental Protection Agency (EPA).[4] Moret *et al.* have shown the large presence of PAH compounds to the surrounding soil and nearby vegetation from creosote-treated railway tiles.[6]

Concerns regarding the carcinogenic potential of coal tar creosote have increased over the past decades, leading to banning of its use by the general public (UK ban took place in 2003).[7] Emissions of PAHs and phenolic compounds from creosote treated wood was reported to have adverse impact on air quality.[4,5] The contact of telecommunication poles or railway sleepers with rainwater or humidity also lead to the leaching of PAH compounds to the groundwater.[8] Despite the increasing health, safety and

environmental regulations concerning the use of creosote treated wood, it is anticipated that its industrial will continues in the future due to the high protection level it provides and the low-cost of the treatment method. In the UK, the authorized sale, supply and use of creosote treated wood is allowed as per 2020 for railway sleepers, highway fencing and overhead electricity and telecommunication poles, with the possibility to extend this period for longer.[9] Creosote treated wood is classified as a hazardous waste in the UK and categorized as grade D waste wood with current disposal routes limited to specialist landfill sites or, to smaller extent, combustion in specialized WID-compliant boilers.[10] It is important to note that data on the quantities of creosote wood waste generated are scarce and available data should be used with caution due to high uncertainty.[3] As of 2009, it was estimated that hazardous waste arising from railway sleepers and utility poles is approximately 60,000 tonnes/year in the UK alone.[11]

It is anticipated that the amount of creosote-treated wood requiring disposal will continue to increase in the future, particularly as creosote treated wood is manufactured to extend the service life of wood. The demand for circular-based chemical processes that can divert hazardous contaminated waste such as creosote wood from landfill will also continue to increase in the near future. The objective of this study was to extend our investigation on the use of ionoSolv process to fractionate and decontaminate the hazardous creosote treated wood.

It is important to note that although $[H_1Cim]Cl$ was the solvent of choice for heavy metal contaminated waste wood in Chapter 2, [DMBA][HSO_4] is the more preferable solvent choice in ionoSolv fractionation process as it is cheaper to synthesize relative to $[H_1Cim]Cl$ as both the cation and the anion precursors are cheaper making it more cost-effective. The initial experiments using creosote treated wood and [DMBA][HSO_4] showed high level of success and therefore the evaluation continued using this PIL. This is the first study that attempts to decontaminate and valorise the hazardous creosote treated wood using ionic liquids to high value-added products of cellulose and lignin, while simultaneously extract the PAH compounds present in the creosote preservatives.

3.2 Materials & Methods

Materials: Chemicals used for IL synthesis, compositional analysis and enzymatic saccharification were purchased from Sigma Aldrich and used as received with no further purification. **Feedstock:** Creosote feedstock was provided by London Reclaimed Brick Merchant Company. The bricks were reclaimed from Europe (Belgium, Poland or the Czech Republic). The wood was provided as large brick of 1.5 x 0.4 x 0.5 m dimensions. The bricks were cut in the Mechanical Engineering Department in Imperial College London, then further chopped, sieved to particle size of 180 to 850 μm and stored in aplastic bag in a dark place. The creosote timber wood species was confirmed using HSQC NMR spectroscopy on the isolated lignin which showed the predominance of guaiacyl unit in the aromatic structure of lignin and the absence of p-hydroxyphenyl (H) and syringyl (S) units, confirming that creosote timber is from softwood species such as pine or spruce. Handling of creosote treated wood should be conducted in the fume hood at all times due its highly toxic and hazardous nature and the high potential exposure of PAHs.

3.2.1 Moisture content determination

For untreated biomass as well as recovered pulp the moisture content was determined according to the NREL protocol 'Determination of Total Solids in Biomass and Total Dissolved Solids in Liquid Process Samples.[12] Refer to Section 2.2.2 for more details.

3.2.2 Ionic Liquid Synthesis

N,*N*,*N*-dimethylbutylamine (75.9 g, 750 mmol) was cooled with an ice bath in a round-bottom flask. 150 mL of 5 M H_2SO_4 (750 mmol) was added dropwise while stirring. The reaction proceeded for at least 5 hours with continuous stirring. Excess water was removed using the rotary evaporator. The water content of the IL was adjusted to 20 wt% using Volumetric Karl Fisher Titrator (V20 Mettler-Toledo). Further details on the procedure is described in Section 2.2.3.

3.2.3 Biomass pretreatment

Pretreatments, determinations of oven dried weight and ionic liquid water content measurements were conducted according to the standard operating procedures from our laboratory, in triplicate.[13] All fractionation experiments in this study used 2 g of the air-dried chopped and sieved (180 – 850 μm) biomass mixed with an IL solution comprising 8 g of [DMBA][HSO_4] and 2 g of water (10 g solution, corresponding to 1 : 5

g g^{-1} solid loading on oven-dried basis) in a pressure tube. Detailed procedure of the fractionation experiments can in Section 2.2.4. The logarithmic value of the pretreatment severity factor which combines temperature and residence time was calculated based on the following equation:

$$\log R_0 = \log(t\ x \exp\left[\frac{T-T_0}{\omega}\right]) \qquad (3.1)$$

where ω is the fitted parameter which is assigned the value of 14.75; t is the duration of pretreatment (min); T is the pretreatment temperature (°C); T_b is the base temperature (100°C). For more details regarding the derivation of the equation and the physical meaning of the pretreatment severity factor please refer to Section 1.8 in Chapter 1.

3.2.4 Compositional analysis

Structural composition of the feedstocks and cellulose pulps were determined according to the published procedure Determination of Structural Carbohydrates and Lignin in Biomass by NREL.[14] Details of the procedure is found Section 2.2.5.

3.2.5 Enzymatic Saccharification

Saccharification assays were carried out according to an adapted procedure the Low Solids Enzymatic Saccharification of Lignocellulosic Biomass protocol published by NREL.[13] Details of the procedure can be found in Section 2.2.6.

3.2.6 Elemental analysis

Samples for CHNS elemental analysis were sent to MEDAC Ltd, London, United Kingdom. The measurements were conducted in duplicate.

3.2.7 Toluene extraction for solids and liquids

Toluene Soxhlet extraction for creosote treated wood and pine wood was conducted using a Soxhlet apparatus, heating plate and chiller. 1 g of the wood was placed in a cellulose thimble using 200 mL of toluene (Sigma Aldrich-GC grade). The extraction was carried out for 24 hours. After the extraction, the cellulose thimbles contenting the samples were left to the air-dry for two days. Extraction for each feedstock was conducted in triplicate. For cellulose pulps and lignin samples, 0.25 g of the sample was used in 50 mL of toluene, analysis was conducted in duplicates. For ionic liquid liquor

samples, liquid-liquid extraction was conducted using 15-mL centrifuge tubes. The ionic liquid liquor was mixed with toluene in 1:2 ratio at 500 rpm for 24 hours at room temperature. Samples of the toluene were taken from the top layer by using syringe filtration (0.22 μm) to ensure no IL residue in the sample.

3.2.8 Fourier-transform infrared spectroscopy

A PerkinElmer Spectrum 100 FT-IR spectrometer with a diamond germanium ATR single reflection crystal was used on lignin, feedstock, as well as cellulose pulps. The spectra were recorded between 500 cm^{-1} and 4000 cm^{-1} using 32 scans with a resolution of 2 cm^{-1}.

3.2.9 Lignin 2D HSQC NMR

For HSQC analysis 50 mg of lignin was dissolved in 0.5 mL of DMSO-d^6 vortexed and left overnight followed by transferring the solution to NMR tube. HSQC NMR spectra were recorded on a Bruker 600 MHz spectrometer -pulse sequence hsqcetgpsi2, spectral width of 10 ppm in F2 (^1H) with 2048 data points and 160 ppm in F1 (^{13}C) with 256 data points, 16 scans and 1 s interscan delay. Spectra were analysed using MestReNova (Version 11.0.1, Mestrelab Research 2016). All spectra were referenced to the DMSO peak at 2.500 ppm (^1H) and 39.520 ppm (^{13}C).

3.2.10 Qualitative and quantitative analysis of PAH

Qualitative determination of PAH compounds was conducted using GC-MS (Agilent intuvo 9000 GC coupled to 5977 MSD mass spec) by Dr. Lisa Haigh (Imperial College London, Chemistry Department). The temperature program starts at 50 °C, ramp 5 °C/min to 290 °C, isothermal for 2 minutes. Helium gas flow of 1.2 mL/min using a column of 30m in length and 0.25mm i.d. For quantification, a Varian 3400 GC/FID system was employed. The compounds were quantified using external prepared standards. An Agilent DB 5-ms UI column of 15 m length and 0.25 mm i.d. was used with 0.25 µm film thickness was used with flow of helium 1.2 mL/min. The temperature program was 35°C for 1 min, then 15°C/min to 100°C, 1 min isothermal, then 10°C/min to 320°C, isothermal for 5 min.

3.3 Results and Discussion

3.3.1 Feedstock Characterization

Visual examination of the creosote treated railway sleepers showed a highly visible creosote contamination as creosote appeared as dark brown impregnated strips. The creosote wood exhibited a strong, characteristic coal-tar smell of creosote. During the cutting of the contaminated creosote area showed more visible layering of the embedded creosote (Figure 3.1). The creosote-treated wood was labelled as “creosote wood mixed” and “creosote wood dark”, depending on the degree of creosote contamination present in the sample. Creosote wood mixed refers to the wood sample obtained by grinding the entire block of wood composed of light brown wooden areas and dark brown creosote treated areas. Creosote treated dark refers to the wood samples obtained by cutting and grinding the heavily creosote contaminated section from the block. In this study, pine softwood sample was used as a reference for baseline comparison to evaluate the degree of creosote wood contamination and structural composition.

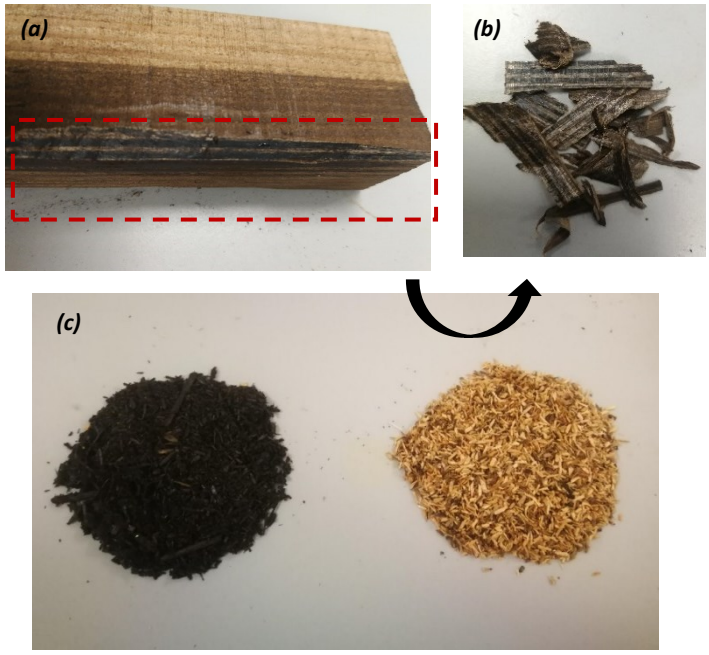

Figure 3.1: (a) creosote wood block showing the impregnation of creosote in the timber, (b) strips of creosote-rich samples cut from the block, (c) creosote wood block by grinding the creosote-rich contaminated area (left) creosote wood mixed from grinding the entire creosote wood block (right)

Table 3.1 presents the elemental analysis and toluene extractives of the creosote wood mixed, dark samples, and pine wood. Elemental CHNS analysis showed a particularly high carbon content of the creosote wood dark of 60.5% compared to 48% and 46% for

the creosote wood mixed and pine wood samples, respectively. The high carbon content in the creosote wood dark indicates the presence of significant carbonaceous compounds, which is expected as creosote is primarily composed of heavy oils and aromatic hydrocarbons. The high carbon content of the creosote wood dark resulted in a higher heating value (HHV) of 24.9 MJ/kg compared to 18.5 MJ/kg and 17.0 MJ/kg for creosote mixed wood and pine wood, respectively. Creosote wood dark also contained a higher nitrogen content compared creosote wood mixed sample which can be attributed to the presence of nitrogen-containing aromatics in the creosote, such as quinolines and pyridine-based compounds.

Table 3.1: Elemental analysis and toluene extractives of the creosote wood mixed and dark

Feedstock type	C	H	N	S	O	HHV	Moisture content	Toluene extractives
	(%)					(MJ/kg)	(wt%)	(wt%)
Creosote wood mixed	48.15	6.52	0.24	0.24	48.5	18.5	9.0	21.14
Creosote wood dark	60.49	6.78	0.53	0.13	32.1	24.9	15.0	41.91
Pine wood	46.67	6.07	0.46	0.00	46.8	17.0	7.0	12.61

The 24 h toluene Soxhlet extraction for the three feedstocks showed a noticeable variation in the percentage of extractives as was clearly seen by the colour of the solvent (Figure A18 in Appendix). Toluene extractives for creosote wood dark was the highest, accounting for 41 wt%, whereas toluene extractives for creosote wood mixed and pine wood were 21% and 12%, respectively. The high percentage of toluene extractives in creosote wood dark highlights the significant concentration of PAH compounds originating from creosote. Creosote wood mixed, which represents the entire block of creosote wood, had x2 the toluene extractives compared to pine wood, indicating the high level of PAH compounds relative to untreated virgin pine wood.

The structural composition of carbohydrates, lignin, ash and extractives of creosote treated wood compared to virgin pine wood are presented in Figure 3.2. It is important

to determine the structural composition of creosote wood as a feedstock to evaluate the pretreatment effectiveness in terms of delignification and hemicellulose removal.

Determination of ethanol-soluble extractives is an important sample preparation step prior compositional analysis procedure. It is important to remove the non-structural ethanol extractives to prevent their interference in proceeding analytical steps, particularly during the determination of acid-soluble lignin. In this step, the sample is subjected to 24 hours of Soxhlet extraction with ethanol to remove extractable organic compounds such as waxes, fats, resins, phenols, alcohols or other minor components.[15] Similar to the toluene extraction step, there was a noticeable difference between pine wood and both creosote-treated samples is the ethanol-soluble extractives. Extractives in pine wood accounted for 5.0% (by mass) of the sample, which is within the expected range of extractives in virgin pine softwood.[16,17] **On the other hand, ethanol extractives from creosote mixed wood and creosote dark wood were significantly higher, at 41.9% and 42.4%, respectively.** The high level of ethanol extractives in both the highly concentrated creosote sample (creosote wood dark) and the mixed whole block sample (creosote wood mixed) indicates the significant presence of waxes, oils, hydrocarbons and alcohols. It is interesting to note that for the creosote wood mixed sample, the percentage of ethanol extractives were twice as high as toluene extractives whereas for the creosote wood dark sample, the percentage of ethanol extractives were very close to toluene extractives. This indicates that the creosote mixed sample is rich not only in aromatics, and hydrocarbons, but potentially also in waxes, alcohols and other compounds that seem to have higher affinity and solubility in ethanol compared to toluene. The results of this analysis were confirmed using three repeats per sample.

Glucan contents for the creosote wood samples accounted for 28-29% of the sample which was significantly lower compared to virgin pine wood where the glucan content was 43%. This is in agreement with literature reporting since creosote-PAH compounds account for 20 to 40 wt% of the total weight of creosote treated wood.[4] Therefore, the relative glucan content on mass basis is lower. Acid insoluble lignin content (AIL) for the creosote wood dark sample was 15.9%, which is slightly higher than the AIL content for the creosote wood mixed sample at 11.7%. The AIL contents for both of creosote samples were lower compared with the AIL in pine wood (27.1%). The hemicellulose sugar content in creosote wood samples encompassed xylan, galactan and mannan, which are

identical and similar in compositions to hemicellulose sugars found in pine softwood, reflecting galactoglucomannan and glucuronoxylan branched polysaccharides.

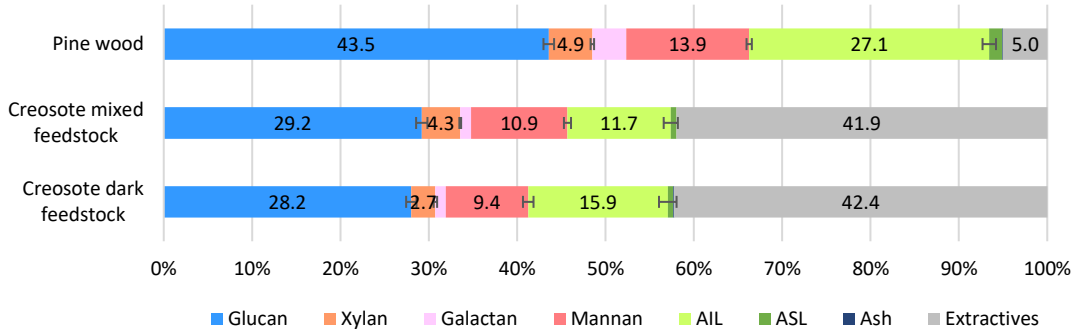

Figure 3.2: Compositional analysis of pine wood and creosote wood feedstock (mixed and dark)

3.3.2 Analysis of surface chemical functionalities

ATR FT-IR spectroscopy was used to compare the surface of the creosote wood to virgin pine wood biomass and identify any differences in absorption bands due to the presence of creosote-based aromatic compounds. Figure 3.3 presents the overlay of the four spectra: i) creosote wood dark sample, ii) pine wood sample, iii) cellulose pulp sample and, iv) creosote wood dark sample after toluene extraction. In this analysis, creosote wood dark sample was used as it is more enriched with creosote, which facilitates identifying unique absorption bands related to creosote and aromatic compounds. The spectrum of the cellulose pulp was also obtained from analysing a cellulose pulp obtained from fractionating a creosote wood dark sample, for the same reasons. The spectra of pine wood displayed bands that are typically seen in lignocellulosic biomass such as at 1051 cm^{-1} (C–O stretching in cellulose and hemicellulose), and 1503 cm^{-1} (aromatic skeleton of lignin) and 1650 cm^{-1} for C-C stretching in aromatic rings of lignin.[18] Apart from the prominent polysaccharides and lignin bands found in lignocellulosic biomass, there were four strong to medium bands that appeared in the creosote wood feedstock only. A strong band at 1600 cm^{-1} was identified in creosote wood feedstock which can be attributed to aromatic vibrations plus C-O stretching.[18] It is important to note that this band in lignocellulosic biomass are often attributed to the skeletal nature of aromatic lignin. However, since the band shows a very strong absorbance, it is more likely that the band is dominated by the vibration due to the

presence of creosote-based aromatic compounds. Another strong absorption band found at 1456 cm^{-1} was observed which are indicative of aromatic C=C stretching vibrations in aromatic compounds.[19] Two strong to medium absorption bands at 738 cm^{-1} and 700 cm^{-1} appeared in the creosote wood dark spectrum and both bands are typical for benzene-derived compounds for out-of-plane C-H bending.[19] The spectrum for the creosote wood dark feedstock after 24 hr Soxhlet toluene extraction clearly shows that the bands attributed to the presence of benzene-derived compounds (700 cm^{-1} and 738 cm^{-1}) are no longer present, indicating their effective removal by toluene. The strong bands shown in creosote wood dark at 1600 cm^{-1} band and 1456 cm^{-1} were also reduced significantly as PAH compounds were extracted into toluene. The spectrum for creosote dark pulp was very similar to the spectrum of creosote wood dark after toluene extraction where the strong aromatic bands no longer showed. This indicates that creosote polyaromatic compounds were extracted by [DMBA][HSO_4] during the fractionation process, which will be further investigated in the following sections.

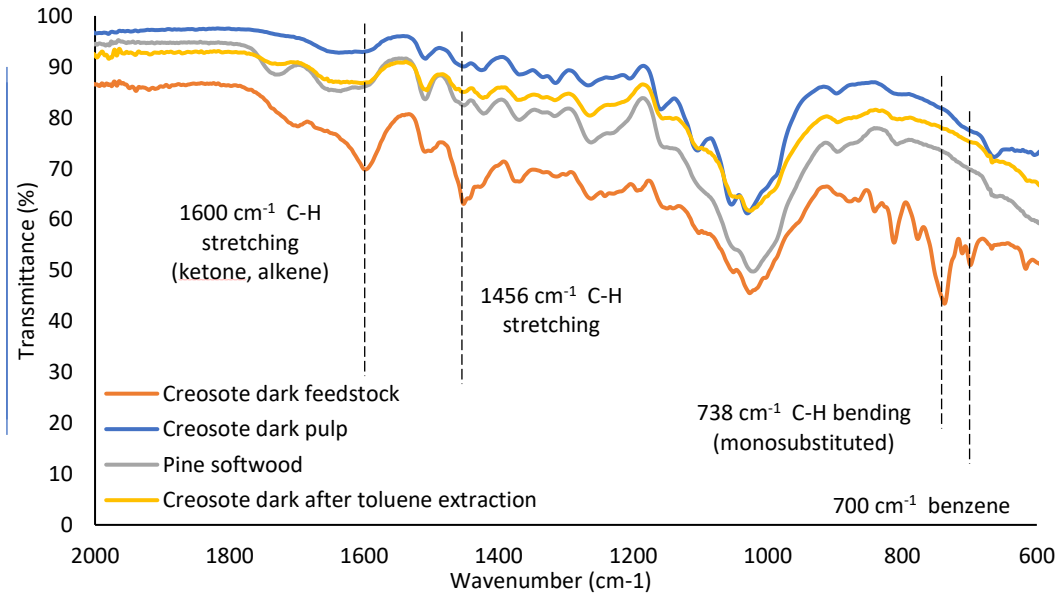

Figure 3.3: FTIR spectra of creosote treated wood, creosote dark pulp, pine wood and creosote wood dark after toluene extraction

3.3.3 Polyaromatic hydrocarbon analysis

Table 3.2 presents the compounds found in the toluene Soxhlet extract from the creosote wood dark sample identified using GC-MS. The compounds span a range of C_{10}

to C_{14} polycyclic and heterocyclic aromatic hydrocarbons. Figure 3.4 shows the structures of naphthalene (a simple polycyclic aromatic hydrocarbon), dibenzofuran (an oxygen-containing heterocyclic hydrocarbon), fluorene (a heterocyclic hydrocarbon) and anthracene (a tricyclic aromatic hydrocarbon), compounds present in creosote.

Table 3.2: Polycyclic aromatic hydrocarbon compounds detected in the toluene extract from the creosote wood dark sample

Retention time (minute)	Compound – Molecular formula	Boiling point (°C)
9.8	Naphthalene ($C_{10}H_8$)	218
11.8	Methyl Naphthalene ($C_{11}H_{10}$)	240
13.9	Ethyl Naphthalene ($C_{12}H_{12}$)	258
15.6	Acenaphthene ($C_{12}H_{10}$)	279
16.1	Dibenzofuran ($C_{12}H_8O$)	285
17.5	Fluorene ($C_{13}H_{10}$)	295
18.4	4-Methyl Dibenzofuran ($C_{13}H_{10}O$)	306
21	Anthracene ($C_{14}H_{10}$)	340

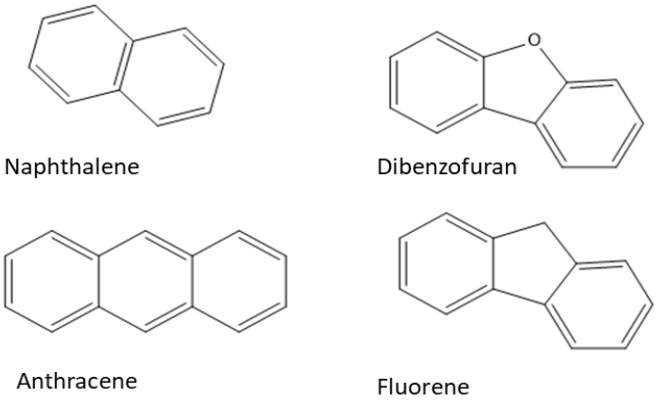

Figure 3.4: Structure of polyaromatic and heterocyclic aromatic compounds quantified the in creosote wood feedstock

Table 3.3 presents the concentration of these compounds in the toluene extracts of creosote dark and creosote mixed samples quantified using GC-FID. As expected, the concentrations of the polyaromatic compounds in the toluene extract from the creosote dark sample were significantly higher than their concentrations in the creosote mixed sample. **Anthracene is present in the highest concentration in the creosote dark sample as well as the highest concentration in the creosote wood mixed sample**

with concentrations of 27,647 mg/kg and 3,957 mg/kg, respectively. The creosote sample is very rich in anthracene, reflecting a key characteristic of creosote and its production process from coal-tar distillation. As mentioned above, creosote is typically produced from the distillation of coal-tar, specifically the heavy fraction of the distillate (boiling points 300 to 400 °C) and is referred to as "heavy oils" or "anthracene oils" as anthracene accounts for 40 to 70% of the constituents.[5]

Table 3.3: Concentrations of selected compounds in the toluene extract of creosote wood

	Naphthalene	Dibenzofuran	Fluorene	Anthracene
Feedstock	(mg/kg)			
Creosote dark wood	4,242 ±128	9,417 ±395	12,388 ±546	27,647 ±1380
Creosote mixed wood	2,454 ±26	3,112 ±49	1,655 ±21	3,957 ±35

3.3.4 Effect of pretreatment time and temperature on fractionation

Since post-consumer creosote-treated wood will be disposed of as the whole block of railway sleepers, fences or utility poles, the fractionation experiments were conducted on the creosote wood mixed samples, representing the entire block of creosote-treated wood. Glucose yield via enzymatic hydrolysis of the cellulose-rich pulp was taken as the key parameter to measure the pretreatment effectiveness in this context. To study the impact of pretreatment severity in pretreating the newly challenging feedstock, we conducted the pretreatment at three severity levels of $\log R_0$ 2.84, 3.25 and 3.71, which corresponds to processing conditions of 120 °C and 180 minutes, 150 °C and 60 minutes and 170 °C and 45 minutes, respectively. These severity levels were chosen to represent low, medium and high severity conditions using 80 wt% [DMBA][HSO_4] as pretreatment medium and the $\log R_0$ values were calculated using the classical severity factor Equation (Equation 3.1).

Figure 3.5 shows the process performance indicators, namely i) cellulose pulp yield and isolated lignin yields obtained gravimetrically from the pretreatment experiments, ii) glucose yield from 7-day enzymatic hydrolysis of the cellulose pulp, and iii) cellulose pulp quality parameters of delignification, hemicellulose extraction and glucan recovery calculated from the compositional analysis results. Hemicellulose extraction is also considered a key process performance indicator and it is also important in assessing the pulp quality, particularly with regards to materials applications. Hemicellulose

extraction is calculated based on the removal of all non-glucan sugars (*i.e.* xylan, mannan and galactan) relative to the untreated creosote wood feedstock.

We observe a mild increase in hemicellulose extraction with increasing pretreatment severity, with the extraction increasing from 83.2 % to 87.4% at pretreatment severities of 2.84 and 3.71, respectively. This also indicates that at low pretreatment severity, the ionoSolv process is still highly effective in removing the majority of the hemicellulose present, while it is more challenging to extract lignin, likely due to the low operating temperature compared to the T_g of lignin. Glucan recovery remained high, ranging between 92.5 % to 85.6 % with a mild decrease when increasing the pretreatment severity. It is interesting to note that glucan recovery was high, opposite to expectations for a weathered feedstock, indicating that glucan losses during the ionoSolv process is at a similar level for creosote-treated wood and virgin wood. The observed loss in glucan is likely related to the hydrolysis of the amorphous parts of the cellulose as well as the hydrolysis of the glucan associated with the hemicellulose polymers. Overall, it is key to highlight the high effectiveness of [DMBA][HSO_4] in delignifying creosote-treated wood at high pretreatment severity, producing highly digestible cellulose-rich pulps.

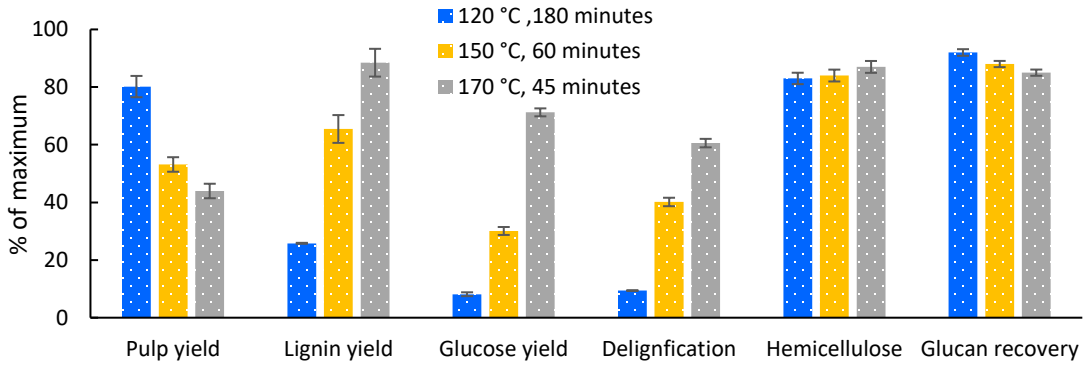

Figure 3.5: Key performance indicators of ionoSolv fractionation process at different pretreatment severity using creosote wood mixed feedstock treated with [DMBA][HSO_4] at 20 wt% H_2O biomass loading of 1:5 g g^{-1}

Cellulose pulp yields showed a significant decrease from 80.1% to 53.1% when increasing the pretreatment severity from 2.84 to 3.25 whereas further increasing the severity from 3.25 to 3.71 showed a less significant decrease in pulp yield from 53.1% to 46.5%. It was reported that effective lignin extraction from softwood requires performing the pretreatment experiment at temperatures higher than the glass transition of lignin (T_g of 130 to 150 °C).[20] Therefore, the significant drop in pulp yield

at higher temperatures (specifically from 120 to 150 °C) reflect the effective lignin extraction achieved. This is confirmed by the delignification values obtained from compositional analysis, where delignification increased significantly from 9.4% to 40.1% relative to the theoretical maximum upon increasing the pretreatment severity from 2.84 to 3.25. Isolated lignin yields consequently increased with pretreatment severity due to the increase in lignin extraction during the pretreatment. Interestingly, we note that lignin yields were consistently higher than the corresponding delignification values. This was also the case at the lowest pretreatment severity (120 °C and 180 minutes) where the amount of lignin precipitated represents 35% of the original amount of lignin present in the biomass, while the actual lignin extracted from biomass was only 9% of the original total amount. The lignin precipitation yield often exceeds the delignification value at high pretreatment severity when the liquor is overcooked, promoting the repolymerization of more condensed lignin or the formation of lignin-like structures (*i.e.* pseudo-lignin).[21] **However, in this case, the high lignin precipitation even at low pretreatment severity indicates the potential co-precipitation of high molecular weight PAH compounds present in the creosote wood.** This will be discussed further in the following section. Further increasing the pretreatment severity to 3.71 (*i.e.* 170 °C, 45 minutes) increased the delignification to 60.5% relative to the maximum, indicating that a relatively high cellulose-pulp quality can be achieved from creosote-treated wood feedstocks. The ionoSolv process is a lignin-extraction process and previous studies demonstrated a positive correlation between delignification and glucose yield from enzymatic hydrolysis. **We observe here the same strong correlation where the higher delignification achieved at 3.71 pretreatment severity resulted in a significant increase in glucose yield, reaching 71.2% relative to the theoretical maximum.** This demonstrates the high capability of ionoSolv process in fractionating wide variety of lignocellulosic biomass to highly digestible cellulose pulps, including a highly contaminated feedstock such as creosote-treated wood.

Figure 3.6 details the ionoSolv fractionation kinetics at 170 °C in terms of pulp yield, lignin yield and 7-day enzymatic hydrolysis glucose yield. Cellulose pulp yields initially decreased from pretreatment times of 30 minutes to 45 and 60 minutes as longer pretreatment time allows more lignin to be extracted, reflected by the increase in the isolated lignin yield. Glucose yields also increased remarkably with increasing pretreatment time as higher lignin extraction (delignification) allows higher exposure of

the cellulose fibers , facilitating its enzymatic hydrolysis of cellulose to glucose. **At 45 minutes pretreatment time, enzymatic glucose yield increased by 20-fold relative to the untreated creosote treated wood.** Cellulose pulp yields eventually started increasing again after 60 minutes while both lignin yields and glucose yields decreased.

The synergistic effect between pulp yield, lignin yield and glucose yield at prolonged pretreatment times at 170 °C has been attributed to the deposition of condensed lignin and lignin-like structures (*pseudo-lignin*) on the cellulose-pulp surface, causing unproductive binding to enzymes and also physically hindering their binding to cellulose surface.[28] The present kinetic experiments confirm the similar fractionation behaviour of creosote treated wood and softwood using [DMBA][HSO_4] as the ionic liquid, mixed with 20 wt% water.[29]

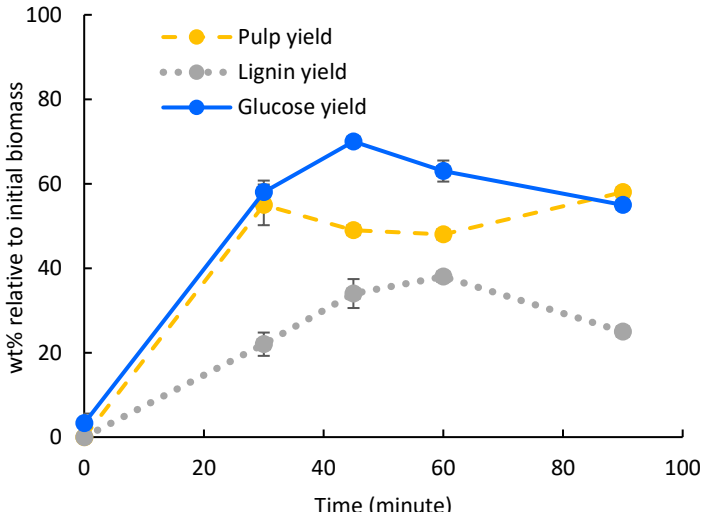

Figure 3.6: Kinetics of creosote wood mixed fractionation at 170 °C using [DMBA][HSO_4] at 20 wt% H_2O and biomass loading of 1:5 g g^{-1}

3.3.5 Effect of biomass fractionation on the extraction of PAH compounds

The use of ILs for PAH extractions from aqueous environment using biphasic systems have been explored in several studies before. [30,31] These studies mainly considered the distribution ratios of PAHs between hydrophobic ILs and aqueous environments. However, no previous studies have investigated the extraction of PAH compounds using ILs from solid PAH contaminated substrates such as creosote wood. We therefore investigated the efficiency of [DMBA][HSO_4] in extracting these compounds and their partitioning between the cellulose pulp, ionic liquid liquor and lignin streams. We

conducted the biomass fractionation experiments using [DMBA][HSO_4] with the creosote wood dark as feedstock as it contains higher concentrations of PAHs, making it easier to monitor PAH partitioning between the three process streams. In addition, we conducted a recycling experiment to verify the quality of the cellulose pulps and the fate of PAHs in the process after multiple solvent uses. The toluene extracts of creosote wood feedstock as well as cellulose pulps, lignins and ionic liquid liquors obtained from the two fractionation cycles were analysed by GC-FID and the chromatograms are presented in Figure 3.7. It is important to note that the toluene extraction for IL liquors were conducted after adding water as an anti-solvent to precipitate extracted lignin and then re-concentrating the IL liquor back to 20 wt% water content. The retention times of the four investigated PAH compounds are 10.1 for naphthalene, 13.9 for dibenzofuran, 14.9 for fluorene and 17.2 for anthracene and the peaks can be clearly identified in the creosote wood dark chromatogram (Figure 3.7-a). Figure A20 shows the toluene extract from pine wood as baseline for comparison where no trace of PAH compounds detected, confirming that all detected peaks originate entirely from creosote. After the fractionation experiments, the obtained cellulose pulps from cycle 1 and cycle 2 displayed no trace of PAH compounds as can be clearly seen in the chromatogram (Figure 3.7-b). **The outcomes clearly indicate that pretreatment of creosote treated wood using aqueous [DMBA][HSO_4] can effectively extract the PAHs present in creosote wood, producing a cellulose pulp free of creosote hydrocarbon contamination.** The ionic liquid liquor chromatogram (Figure 3.7-c) revealed the presence of the investigated PAH compounds, particularly naphthalene and fluorene in the 1st fractionation cycle. In the 2nd fractionation cycle anthracene started appearing in the IL liquor, along with naphthalene and fluorene.

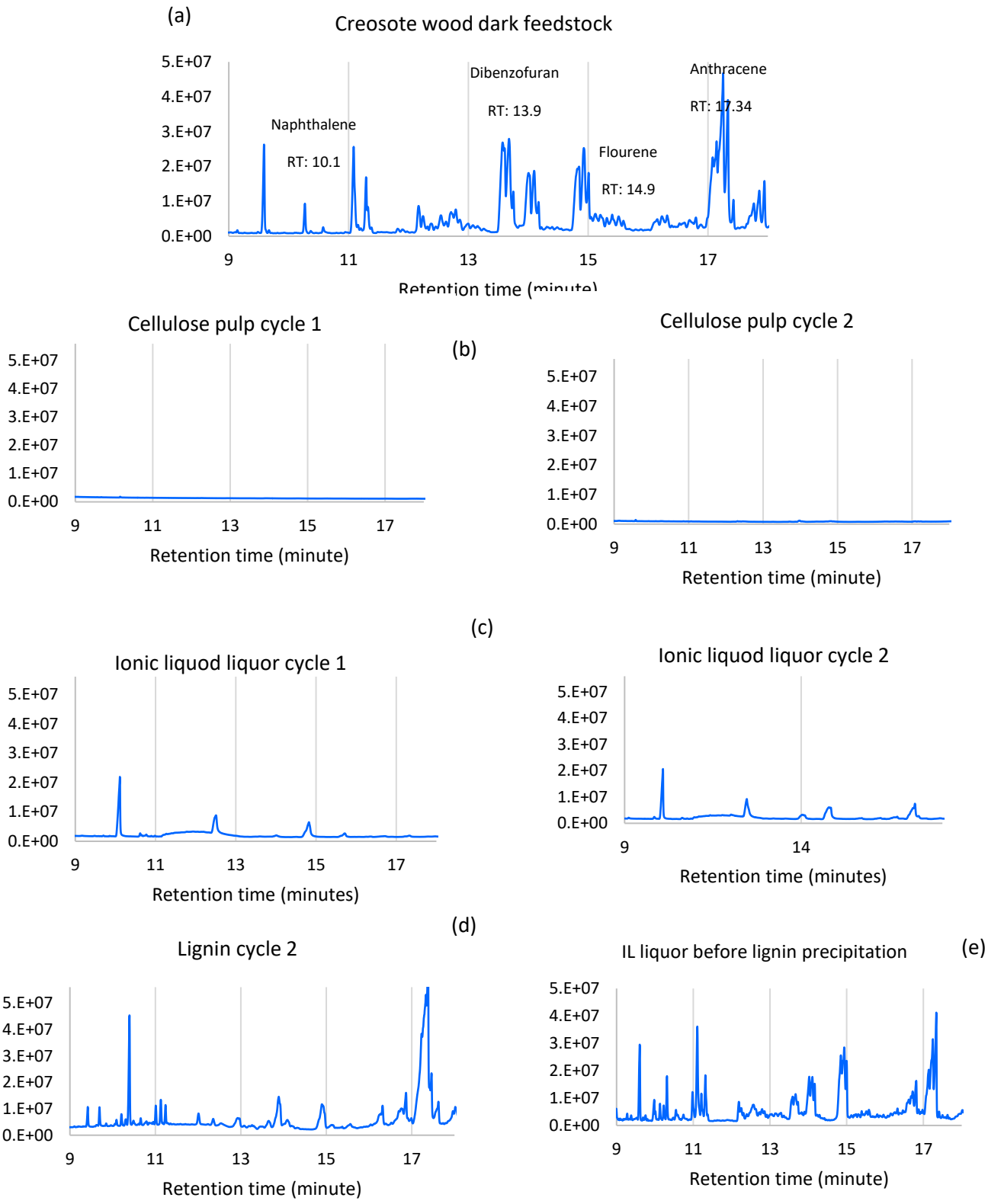

Figure 3.7: GC-FID chromatograms of toluene extracts from (a) creosote wood dark , (b) cellulose pulps , (c) ionic liquid liquors, (d) lignin sample and (e) IL liquid before lignin precipitation. Fractionation experiments using 80 wt% [DMBA][HSO_4] mixed with 20 wt%

As stated above, the IL liquor samples from the 1st and 2nd fractionation cycles were analysed after the addition of water to precipitate lignin and re-concentration of the IL back to 20 wt% water. Since PAHs are naturally hydrophobic and have very low solubility in water, these compounds are very likely to precipitate with the lignin. **Analysing the toluene extract from the isolated lignin from the 2nd fractionation cycle, we observed the presence of the investigated PAHs compounds with medium intensity for naphthalene, dibenzofuran and fluorene and particularly high intensity for anthracene** (Figure 3.6-d). We also analysed the pine-lignin to establish a baseline comparison and to account for potential interference from signals originating from aromatic-lignin (Figure A21). The analysis showed that there is only one peak overlapping between the pine wood lignin and creosote wood lignin chromatograms at the naphthalene peak, however the naphthalene peak at creosote wood lignin had 8-fold higher intensity.

It is interesting to note that the partitioning of PAHs between IL liquor and lignin correlate with their degree of hydrophobicity and solubility in water, where the tricyclic anthracene showed particularly high partitioning with lignin due to its high aromaticity and extremely low solubility in water (0.29 mg/L at 50 °C), compared to naphthalene with a water solubility of 81 mg/L at 50 °C. **This indicates that PAH compounds present in creosote wood are more likely to precipitate with the lignin fraction in the ionoSolv process, where lignin would likely be used as a heating source for energy recovery.[6]** The presence of PAH compounds in lignin increases the hazard level of the lignin stream and would therefore require the installation of a more expensive WID compliant waste boiler rather than a standard industrial boiler. **However, since the volume of recovered lignin is approximately 1/3 of the feed biomass, the size of the WID compliant boiler will be smaller compared to the WID compliant boiler size to recover energy from the creosote wood as a feedstock.** Therefore, the process can be applied for waste remediation - particularly minimization – in addition to valorisation, producing highly digestible cellulose-rich pulps whilst reducing incinerated waste by 60-70%. Figure 3.7-e shows the intensity of the PAH compounds in the IL liquor before the addition of water to precipitate lignin. It can be clearly seen that PAH compounds are present at much higher concentrations than prior to lignin precipitation (Figure 3.7-c).

This confirms the extraction of PAH compounds by the hydrophilic [DMBA][HSO_4] ionic liquid during the fractionation process and their subsequent precipitation with lignin after water addition.

3.3.6 Appearance of PAH in lignin structure

To further confirm the presence of PAH in the isolated lignin, Figure 3.8 presents the FT-IR spectrum of the precipitated lignin from recycling experiments using creosote wood dark as a feedstock as well as the FT-IR spectrum of precipitated pine wood lignin. Lignin samples were generated at the optimum fractionation conditions of 170 °C and 45 minutes. Pine wood lignin showed medium to high absorption bands at 1135 cm^{-1} and 1030 cm^{-1}, which are bands that typically found in the molecular spectra softwood lignin.[18] The spectra of creosote lignin recovered from the 1st pretreatment cycle did not show any noticeable difference compared to pine wood lignin. On the other hand, a medium-strong absorption band at 744 cm^{-1} appeared in the creosote lignin recovered from the 2nd pretreatment cycle, indicating the presence of benzene-derived compounds. As FT-IR may not a very sensitive measurement method to identify compounds, particularly due to the similar structure of aromatic lignin and PAH compounds, we further analysed the recovered lignin structure using HSQC NMR spectroscopy. Figure 3.9 shows the aromatic region of HSQC spectra of recovered lignin from creosote-treated wood (cycle 1) and from pine softwood. The spectra of creosote lignin show no presence of syringyl (S) unit in its structure (typically found at ^{13}C 104.4 and ^{1}H 6.68), which confirms that the creosote treated timber is made of softwood timber where lignin aromatic structure is predominantly made of guaiacyl (G) unit. However, we note the appearance of new peaks in the creosote wood lignin with chemical shifts of ^{13}C 124 – 130 and ^{1}H 6.9 – 8.9. Chemical shifts in this region are typically attributed to a wide range of PAH compounds, including those investigated in this study (naphthalene, anthracene and dibenzofuran).[27,28] This confirms the co-precipitation of PAH compounds with lignin upon water addition. The co-precipitation of PAHs with lignin provides a self-cleaning route in the process as no additional processing unit is required to clean-up and recover the IL for recycling (e.g. adsorption columns or a liquid-liquid extraction unit).

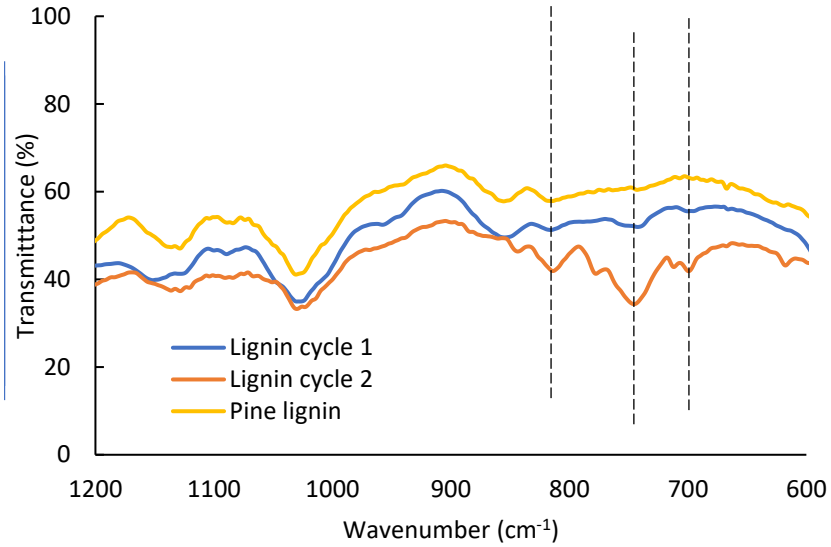

Figure 3.8: FTIR spectra of creosote treated lignin recovered from pretreatment cycle 1 and 2 and pine lignin

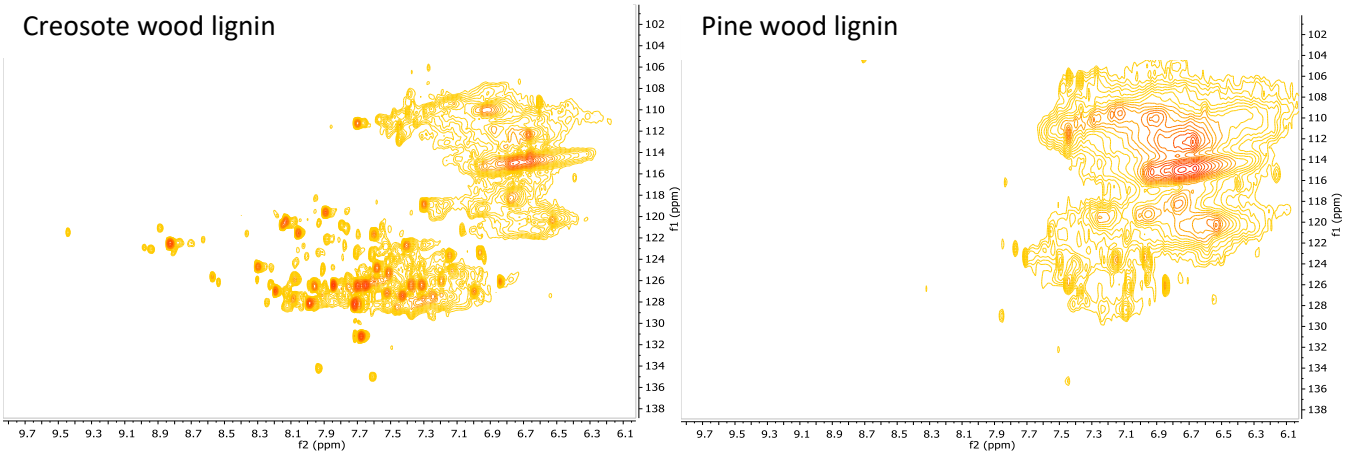

Figure 3.9: Aromatic region of HSQC NMR spectra showing creosote wood lignin (left) and pine wood lignin (right)

3.4 Conclusion

Coal-derived creosote is one of the most widely used wood preservatives that protects timber from all types of fungus attack. Polycyclic aromatic hydrocarbons (PAHs) are the largest constituents of creosote, making creosote-treated timber a hazardous waste by the end of its service life with landfill and specialized incineration being the only current disposal routes. This study investigates the use of the low-cost ionic liquid *N,N,N*-dimethylbutylammonium hydrogen sulphate [DMBA][HSO_4] to effectively valorize the hazardous creosote treated timber using ionoSolv as an integrated biomass

fractionation and waste remediation process. We found that [DMBA][HSO_4] mixed with 20 wt% water is capable of fractionating creosote treated timber into a cellulose-rich pulp and lignin stream at high solids loading of 1:5 g g^{-1}. Pretreatment severity plays an essential role in the process fractionation performance with delignification reaching 60% and enzymatic saccharification of cellulose-rich pulps exceeding 70% of theoretical maximum achieved at the highest investigated pretreatment severity condition (170 °C, 45 minutes, 20 wt% water content as co-solvent). We report for the first time that the non-hydrophobic protic ionic liquid [DMBA][HSO_4] is highly effective in extracting PAHs from the creosote embedded in the timber, producing a highly digestible PAH-free cellulose-rich pulp. Analysis of the fate of PAH compounds in the process streams (feedstock, IL liquor, cellulose pulp and lignin) showed the high tendency of PAH compounds to precipitate with lignin upon water addition as anti-solvent. The study demonstrates a novel application of low-cost protic [HSO_4]-based ionic liquid in fractionating and decontaminating creosote-rich, underutilized hazardous biomass waste to economically produce inexpensive cellulose substrate for the production of 2nd generation biofuels, bioproducts and biomaterials.

References

(1) Freeman, M. C.; O'Dowd, W. J.; Brown, T. D.; Hargis, R. A.; James, R. A.; Plasynski, S. I.; Walbert, G. F.; Lowe, A. F.; Battista, J. J. Pilot-Scale Air Toxics R&D Assessment of Creosote-Treated and PCP-Treated Wood Cofiring for Pulverized Coal Utility Boiler Applications. Biomass and Bioenergy 2000, 19 (6), 447–456. https://doi.org/10.1016/S0961-9534(00)00055-6.

(2) Murphy, B. L.; Brown, J. Environmental Forensics Aspects of PAHs from Wood Treatment with Creosote Compounds; 2005; Vol. 6. https://doi.org/10.1080/15275920590952829.

(3) Murphy, B. L.; Brown, J. Environmental Forensics Aspects of PAHs from Wood Treatment with Creosote Compounds. Environ. Forensics 2005, 6 (2), 151–159. https://doi.org/10.1080/15275920590952829.

(4) Kohler, M.; Kunniger, T.; Schmid, P.; Gujer, E.; Crockett, R.; Wolfensberger, M. Inventory and Emission Factors of Creosote, Polycyclic Aromatic Hydrocarbons (PAH), and Phenols from Railroad Ties Treated with Creosote. Environ. Sci. Technol. 2000, 34 (22), 4766–4772. https://doi.org/10.1021/es000103h.

(5) Gevao, B.; Jones, K. C. Kinetics and Potential Significance of Polycyclic Aromatic Hydrocarbon Desorption from Creosote-Treated Wood. Environ. Sci. Technol. 1998, 32 (5), 640–646. https://doi.org/10.1021/es9706413.

(6) Moret, S.; Purcaro, G.; Conte, L. S. Polycyclic Aromatic Hydrocarbon (PAH) Content of Soil and Olives Collected in Areas Contaminated with Creosote Released from Old Railway Ties. Sci. Total Environ. 2007, 386 (1–3), 1–8. https://doi.org/10.1016/j.scitotenv.2007.07.008.

(7) Williams, I. D. A Change of Emphasis: Waste to Resource Management; 2015; Vol. 2015-Janua. https://doi.org/10.1039/9781782622178-00207.

(8) Becker, L.; Matuschek, G.; Lenoir, D.; Kettrup, A. Leaching Behaviour of Wood Treated with Creosote. Chemosphere 2001, 42 (3), 301–308. https://doi.org/10.1016/S0045-6535(00)00071-0.

(9) Wood Protection Association, Use of Creosote and Creosote-Treated Wood; UK, 2019.

(10) Defra., An Assessment of the Environmental Impact of Management Options for Waste; UK, 2012

(11) WRAP. Wood Waste Market in the UK; Oxon, UK, 2009.

(12) Sluiter, A.; Hames, B.; Hyman, D.; Payne, C.; Ruiz, R.; Scarlata, C.; Sluiter, J.; Templeton, D.; Nrel, J. W. Determination of Total Solids in Biomass and Total Dissolved Solids in Liquid Process Samples; 2008.

(13) M. G. Resch, J. O. Baker, and S. R. D. Low Solids Enzymatic Saccharification of Lignocellulosic Biomass Laboratory; 2015

(14) Sluiter, a.; Hames, B.; Ruiz, R.; Scarlata, C.; Sluiter, J.; Templeton, D.; Crocker, D. Determination of Structural Carbohydrates and Lignin in Biomass; 2012.

(15) Rosendahl, L. Direct Thermochemical Liquefaction for Energy Applications; Woodhead publishing, 2017.

(16) Lan, Y.; Li, J.; Tang, Y.; Liu, C.; Li, S.; Li, R.; Dong, L.; Bao, J.; Dai, Z.; Mater, J.; Chem, A.; Li, J.-S.; Tang, Y.-J.; Liu, C.-H.; Li, S.-L.; Li, R.-H.; Dong, L.-Z.; Dai, Z.-H.; Bao, J.-C.; Lan, Y.-Q. Quantitative Sugar Release from Softwood after Pretreatement with Low-Cost Ionic Liquids. J. Mater. Chem. A Mater. energy Sustain. 2013, 00, 1–6. https://doi.org/10.1039/x0xx00000x.

(17) Gschwend, F. J. V.; Chambon, C. L.; Biedka, M.; Brandt-Talbot, A.; Fennell, P. S.; Hallett, J. P. Quantitative Glucose Release from Softwood after Pretreatment with Low-Cost Ionic Liquids. Green Chem. 2019, 21 (3), 692–703. https://doi.org/10.1039/c8gc02155d.

(18) Casas, A.; Alonso, M. V.; Oliet, M.; Rojo, E.; Rodríguez, F. FTIR Analysis of Lignin Regenerated from Pinus Radiata and Eucalyptus Globulus Woods Dissolved in Imidazolium-Based Ionic Liquids. J. Chem. Technol. Biotechnol. 2012, 87 (4), 472–480. https://doi.org/10.1002/jctb.2724.

(19) Traoré, M.; Kaal, J.; Martínez Cortizas, A. Application of FTIR Spectroscopy to the Characterization of Archeological Wood. Spectrochim. Acta - Part A Mol. Biomol. Spectrosc. 2016, 153, 63–70. https://doi.org/10.1016/j.saa.2015.07.108.

(20) Li, W.; Sun, N.; Stoner, B.; Jiang, X.; Lu, X.; Rogers, R. D. Rapid Dissolution of Lignocellulosic Biomass in Ionic Liquids Using Temperatures above the Glass Transition of Lignin. Green Chem. 2011, 13 (8), 2038. https://doi.org/10.1039/c1gc15522a.

(21) Gschwend, F. J. V.; Brandt-Talbot, A. Rapid Pretreatment of Miscanthus Using the Low-Cost Ionic Liquid Triethylammonium Hydrogen Sulfate at Elevated Temperatures. Green Chem. 2016, 20 (15), 3486–3498. https://doi.org/10.1039/c8gc00837j.

(22) Shinde, S. D.; Meng, X.; Kumar, R.; Ragauskas, A. J. Recent Advances in Understanding the Pseudo-Lignin Formation in a Lignocellulosic Biorefinery. Green Chem. 2018. https://doi.org/10.1039/C8GC00353J.

(23) Gschwend, F. J. V.; Chambon, C. L.; Biedka, M.; Brandt-Talbot, A.; Fennell, P. S.; Hallett, J. P. Quantitative Glucose Release from Softwood after Pretreatment with Low-Cost Ionic Liquids. Green Chem. 2019, 21 (3), 692–703. https://doi.org/10.1039/c8gc02155d.

(24) Liu, J. F.; Chi, Y. G.; Peng, J. F.; Jiang, G. Bin; Jönsson, J. Å. Ionic Liquids/Water Distribution Ratios of Some Polycyclic Aromatic Hydrocarbons. J. Chem. Eng. Data 2004, 49 (5), 1422–1424. https://doi.org/10.1021/je049879e.

(25) Liu, J. F.; Jiang, G. Bin; Chi, Y. G.; Cai, Y. Q.; Zhou, Q. X.; Hu, J. T. Use of Ionic Liquids for Liquid-Phase Microextraction of Polycyclic Aromatic Hydrocarbons. Anal. Chem. 2003, 75 (21), 5870–5876. https://doi.org/10.1021/ac034506m.

(26) Brandt-Talbot, A.; Gschwend, F. J. V.; Fennell, P. S.; Lammens, T. M.; Tan, B.; Weale, J.; Hallett, J. P. An Economically Viable Ionic Liquid for the Fractionation of Lignocellulosic Biomass. Green Chem. 2017, 19 (13), 3078–3102. https://doi.org/10.1039/C7GC00705A.

(27) Thonhauser, T.; Ceresoli, D.; Marzari, N. NMR Shifts for Polycyclic Aromatic Hydrocarbons from First-Principles. Int. J. Quantum Chem. 2009, 109 (14), 3336–3342. https://doi.org/10.1002/qua.21941.

(28) Ruiz-Morales, Y.; Miranda-Olvera, A. D.; Portales-Martínez, B.; Domínguez, J. M. Determination Of13C NMR Chemical Shift Structural Ranges for Polycyclic Aromatic Hydrocarbons (PAHs) and PAHs in Asphaltenes: An Experimental and Theoretical Density Functional Theory Study. Energy and Fuels 2019, 33 (9), 7950–7970. https://doi.org/10.1021/acs.energyfuels.9b00182.

Chapter 4 : Evaluating the Dual Water Role in ionoSolv Fractionation Process as a Co-Solvent and Anti-Solvent

4.1 Introduction

IonoSolv is an emerging chemical technology in the sphere of biomass pretreatment that has proved to be highly effective in fractionating wide variety of biomass in recent years. Water has a dual role in the ionoSolv process, acting as both an anti-solvent and a co-solvent, as shown in Figure 4.1. As a co-solvent, water is mixed with the IL to form the pretreatment medium as it early studies demonstrated that adding a small amount of water to the IL medium improves biomass fractionation.[4] Water is also used as anti-solvent to precipitate the extracted lignin from the IL liquor, an essential step to recover and "clean" the IL before the next biomass delignification cycle. Previous ionoSolv related studies have typically used 20 wt% water as co-solvent and high amounts of water, namely 3 g of water per g of IL (defined as 3 equivalent) for lignin precipitation.[18,19] In IL fractionation process such as ionoSolv, studies have shown that cellulose crystallinity plays a minor role in cellulose digestibility whereas delignification plays a major role in liberating the glucose sugar. Increasing water concentration as a co-solvent in the pretreatment medium reduces the IL use in the process, which translates to major reduction in the process operating cost (OPEX) as IL costs typically account for 40% of the process OPEX.[5] Other advantages of higher water concentration as a co-solvent in the process include lower viscosity of produced slurry, lower pumping energy, easier filtration and therefore less intensive washing of the IL liquor off the cellulose pulp.[8] However, high water concentrations would eliminate the active role of IL in the fractionation process as the process start to behave as an auto-hydrolysis process where water becomes the main pretreatment medium.

Therefore, finding the optimal balanced IL/water mixture where the advantage of each pretreatment solvent is maximized in the mixture is important during the process development phase.

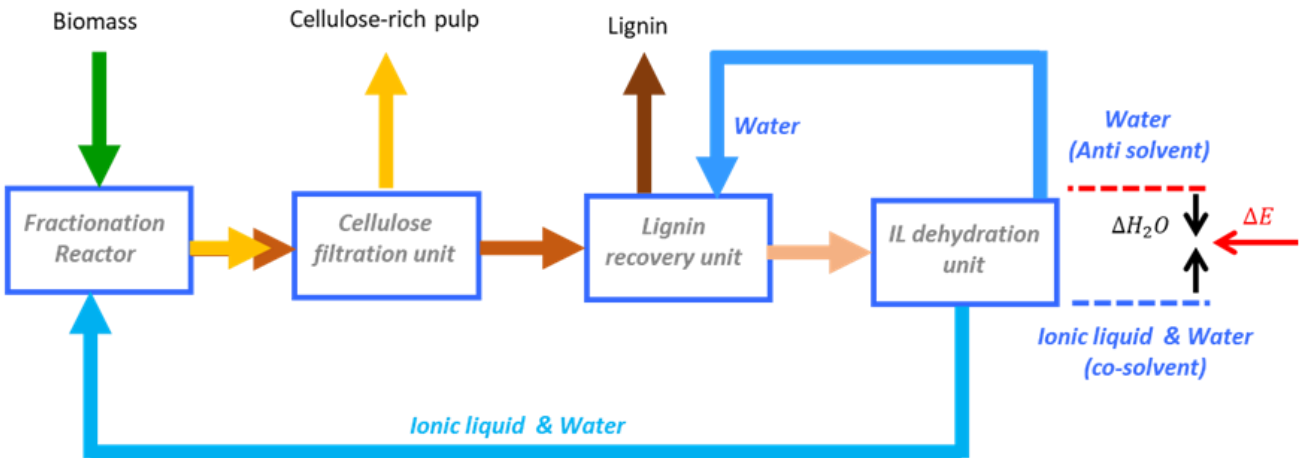

Figure 4.1: Process flow diagram of the ionoSolv fractionation process highlighting water use as co-solvent in the IL pretreatment medium and anti-solvent for lignin precipitation

Water added during the lignin precipitation step results in significant dilution of the IL medium. For example, the current use of 3 equivalent of water for lignin precipitation results in diluting the IL medium from 80 wt% to 20 wt%.[9] The regeneration of the IL to the initial concentration requires the incorporation of a drying step before the next pretreatment cycle. It is expected that the high energy requirement to regenerate the ILs can hinder their application in the large-scale.[9,10] This challenge is not unique to the ionoSolv process as the dehydration of ILs for their effective recovery and recycling has been identified as a key challenge in other IL-based processes such as biomass dissolution and sugar valorisation.[29–32] Thermal-based evaporation technologies such as multi-effect evaporators and vapor compression evaporators are well-established and can potentially be employed for efficient IL dehydration. Those evaporators are essential part of the Kraft pulp and paper process to concentrate the black liquor for chemical recycling.[14] However, thermal evaporation technologies are known to be highly energy intensive.[15] In India, the energy requirement for black liquor evaporators consumes ~24 to 30 % of the total boiler steam, making it the 6th largest energy consuming industrial sector in India.[16]

Membrane-based processes have been proposed as potentially lower cost processes for IL recycle and dehydration.[12,17] However, the use of pressure-driven membrane processes for IL recovery has its own technical challenges due to the high osmotic pressure of ILs, resulting in poor selectivity and low steady-state flux.[28] Pervaporation and membrane distillation (MD) are two membrane-based technologies that are independent of the osmotic pressure. Due to the low operating temperatures, both technologies have been remarked as potential alternatives to distilling highly saline solutions. The distinct difference between pervaporation and membrane distillation is the type of membrane used in the process. Organic solvents such as acetone, hexane and ethanol can be used as anti-solvent alternatives to water to recover lignin from the IL liquor.[19–21] However, the use of large volumes of organic solvents in ionoSolv process will counterbalance a key advantage of the process which is the use of the non-volatile ILs. Therefore, although water brings a challenging dehydration issue due to its non-volatile nature, it remains an ideal anti-solvent as its non-hazardous, low-cost and high efficiency in precipitating lignin.[22,23] Efforts to reduce the IL dehydration energy in the ionoSolv process is directly linked to the water use in the process, an area that has not been thoroughly studied in any of the previous ionoSolv studies.[24] Therefore, the optimization of water content allows for a more critical assessment of how "green" the process is in terms of scalability, energy use and economics, three inseparable aspects that are often overlooked by researchers during the development of new sustainable chemical technologies.[10]

This study defines the water role in the ionoSolv process using the protic IL [DMBA][HSO_4], both as co-solvent and anti-solvent. First, we investigated the impact of the pre-treatment severity controlled by IL solvent concentration on the effectiveness of biomass fractionation. As different types of biomass have different fractionation behaviour during the pretreatment process, our investigation included the use of four types of lignocellulose biomass. First we used *Miscanthus x giganteus*, the most commonly studied *Miscanthus* variant, a non-invasive dedicated energy grass that is particularly of interest to produce liquid biofuels.[25] We also used pine wood, a forest residue softwood biomass that is the dominant lignocellulosic feedstocks in the Northern hemisphere.[26] The recent success of ionoSolv process to fractionate pre and post-consumer waste wood have also inspired to use i) treated timber, a chemically

treated wood with copper preservative used extensively in the construction industry, one of the largest sectors to produce wood waste;[27] and ii) post-consumer waste wood collected from a waste management company. Second, the study investigates the role of water as anti-solvent for lignin precipitation in terms of lignin yield and properties. To develop a more in-depth understanding of the process delignification performance in a near steady-state conditions, 6 consecutive recycling experiments were conducted using optimized amount of water as anti-solvent. To highlight the importance of water, use as a co-solvent and anti-solvent in the process, the process energy consumption was estimated using 3-effects thermal evaporation process using Aspen plus coupled with COSMOtherm to estimate the thermodynamic properties of the ILs. The study demonstrates the key importance of optimizing new chemical processes based on the chemical product yield and composition as well as the energy consumption in the process. The outcomes of this study will provide key insights on the dual water role in the process and establish a more comprehensive design basis for the process performance in terms of the designing the pretreatment medium and evaluating the technoeconomic viability of the process.

4.2 Materials & Methods

Materials: Starting materials for the ionic liquid synthesis were purchased from Sigma Aldrich and, unless stated otherwise, used as received. The Karl-Fisher titrator used in this work was a V20 volumetric Titrator (Mettler-Toledo) and the analytical balance a Sartorius CPA 1003 S balance (±0.001 g). *Miscanthus* × *giganteus* was obtained from the Silwood Park campus (Imperial College London, UK). Pine wood was obtained from Metla (Finnish Forest Research Institute). Treated timber was obtained from Travis Perkins and post-consumer waste wood was provided by a waste management company in the UK (Suez). By visual inspection, waste wood contained small amount of sand and glass, common contaminates of post-consumer waste wood. The waste wood was used as received without separating these contaminants. All feedstocks were air-dried, chopped and sieved (180–850 μm, 20 + 80 US mesh scale) prior to use and stored in plastic bags at room temperature in the dark.

4.2.1 Ionic Liquid Synthesis

N,N,N-dimethylbutylamine (252.9 g, 2.5 mol) was weighed into a 1000 mL round-bottom flask and cooled in an ice bath. Under stirring, 500 mL of 5 M H_2SO_4 (2.5 mol) were

added dropwise to form *N,N,N*-dimethylbutylammonium hydrogen sulfate [DMBA][HSO_4]. The IL solution was recovered as a colourless liquid. The water content of the recovered IL was measured using volumetric Karl Fisher titration and adjusted as needed for each sample. This was achieved by either water addition or water removal by heating at 45 ºC under reduced pressure. [DMBA][HSO_4]/water mixtures with the desired water contents (5 wt%, 10 wt%, 20 wt %, 30 wt%, 40 wt% and 50 wt%) were obtained and confirmed by triplicate measurements with the Karl Fisher titrator.

4.2.2 Biomass fractionation and Recycling

Pretreatment was conducted according to the standard operating procedure from our laboratory.[7] Determination of oven dried weight of biomass and cellulose pulps (air-dried and wet conditions) were conducted according to NREL protocol.[28] Aqueous solutions of [DMBA][HSO_4] with water contents of 5, 10, 20, 30, 40 and 50 wt%, respectively, were mixed with 2 g of biomass (on an oven-dried weight basis), corresponding to a biomass to solvent ratio of 1:5 $g \cdot g^{-1}$. Pre-treatment experiments were conducted at an oven temperature of 170 °C for 30 minutes at non-isothermal conditions using an oven of known heating profile.[5] The detailed experimental procedure is described in Section 2.2.4. For recycling experiments, the IL liquor with residual lignin obtained after the pre-treatment and the water collected from lignin washing (approximately 120 mL) were combined in a pre-weighted round bottom flask and dried in a rotary evaporator. The weight of the flask was recorded, and the wet yield of IL determined. Based on the wet yield of IL and the residual water content measured using Karl Fisher titrator, water was added to achieve 20 wt% and the mixture stirred until a homogenous solution formed. The recovered IL liquor was then transferred into a pressure tube and mixed with a new batch of air-dried pine wood (20 wt% of the transferred solution's weight) to be used for the new pretreatment cycle. Recycling experiments were conducted at 150 °C oven temperature for 1 hour and this condition is equivalent in severity to 170 °C and 30 minutes according to our laboratory protocol.[29]

4.2.3 Compositional Analysis

Compositional analysis was carried out according to a published procedure by the National Renewable Energy Laboratory (NREL) Version 54.[28] Compositional analysis determines the following structural components: i) carbohydrates content, namely glucose, xylose, arabinose and mannose, ii) acid insoluble lignin, iii) acid soluble lignin, iv) acid insoluble ash. The detailed procedure is described in Section 2.2.5.

4.2.5 Enzymatic Saccharification Assay

Saccharification assays were conducted according to the NREL protocol "Low solids Enzymatic saccharification of lignocellulosic biomass".[30] The saccharification of the cellulose pulps was performed on their wet state to eliminate the hornification effect. The determination of the moisture content of wet pulps was conducted based on NREL protocol [31] and ranged from 89 to 90 wt%. All reagents and enzymes were purchased from Sigma Aldrich and used as received. All samples were conducted in triplicates with blanks. Blanks are used to correct for residue sugars presence in the enzyme solution. The detailed experimental procedure is described in Section 2.2.6.

4.2.5 Lignin Molecular weight and 2-D HSQC NMR

Samples were prepared by dissolving 20 mg of lignin in 1 mL GPC grade DMSO containing LiBr (1 $g \cdot L^{-1}$) and filtered through a 0.2 μm Syringe filter. GPC measurements were performed using an Agilent 1260 Infinity instrument equipped with a Viscotek column set (AGuard, A6000 M and A3000 M) and using GPC grade DMSO used as eluent at a flow rate of 0.4 $mL \cdot min^{-1}$ at 60 °C. The Agilent 1260 Infinity RID detector was used for detection. Calibration of the instrument was conducted using 10 pullulan standards (Agilent calibration kit, 180 < Mp < 780 000).

For HSQC analysis 50 mg of lignin was dissolved in 0.5 mL of DMSO-d_6 vortexed and left overnight followed by transferring the solution to NMR tube. HSQC NMR spectra were recorded on a Bruker 600 MHz spectrometer -pulse sequence hsqcetgpsi2, spectral width of 10 ppm in F2 (^1H) with 2048 data points and 160 ppm in F1 (^{13}C) with 256 data points, 16 scans and 1 s interscan delay. Spectra were analysed using MestReNova (Version 11.0.1, Mestrelab Research 2016). All spectra were referenced to the DMSO peak at 2.500 ppm (^1H) and 39.520 ppm (^{13}C).

4.2.6 Quantum chemical calculations by TURBOMOLE and COSMO

The chemical structure of the ionic liquid [DMBA][HSO_4] was created and optimised using TURBOMOLE v7.02 (with TmoleX v4.2.1 graphic interface) software.

Molecular structures of ILs were described by an ion-pair [CA] model. Quantum chemical calculations were carried out to generate a COSMO file containing energies, geometries and polarization charge of the σ-surface. The standard method used in COSMOtherm is B88-P86 (bp) functional[32] and TZVP basis with RI approximation[33] using COSMO solvation model. The COSMO-RS method program package (version C30_1801) and its parametrization BP_TZVP_C30_18 was used in COSMOtherm software. In this work, COSMO-RS method was used to create ILs pseudocomponents into Aspen Properties. COSMOtherm was used to carry out the normal boiling point, density, σ-profile and COSMO-volume calculations (the last two to use the COSMOSAC model from Aspen Properties).[34] This work was conducted by the visiting researcher Dr. Jesús Lemus.

4.2.7 Process Simulation by ASPEN PLUS

A property package was created in Aspen Properties v9.0. where [DMBA][HSO_4] was defined as a pseudocomponent. Normal boiling point, density and molecular weight were imported from COSMOtherm to create the pseudocomponent. The COSMOSAC model was selected as the thermodynamic model and a gamma method was modified to use COSMOSAC-Mathias modification. The σ-profile was specified as pure component properties SGPRF1-5 and the COSMO-volume as the CSACVL component parameter. This work was conducted by the visiting researcher Dr. Jesús Lemus.

4.3 Results and Discussions

4.3.1 Water as a co-solvent on biomass fractionation

Pretreatment experiments were conducted using different [DMBA][HSO_4]/water mixtures with water contents ranging from 5 wt% to 50 wt%. All pretreatments were carried out at 170 °C for 30 minutes using biomass to solvent loadings of 1:5 g g^{-1}. Figure 4.2 shows the raw biomass composition of the four biomass types used in this study.

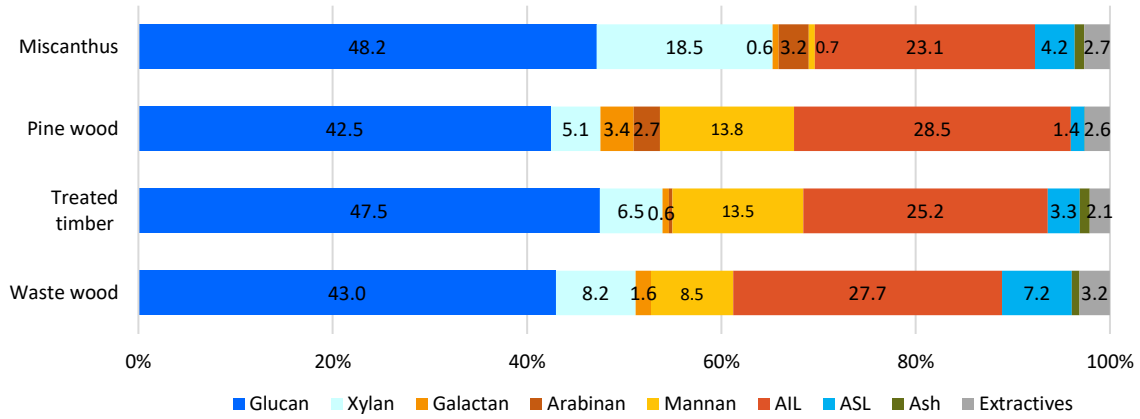

Figure 4.2: Structural composition of the investigated untreated biomass

Figure 4.3 shows the key changes in the cellulose-rich pulp compositions (lignin extraction, hemicellulose removal and glucan recovery) for the four investigated biomass types after fractionation using different [DMBA][HSO_4]/water mixtures. These parameters are calculated based on the compositions of the cellulose-rich pulp obtained by compositional analysis, while the pulp yield is calculated gravimetrically. Lignin extraction (delignification) is taken as the key performance indicator to assess the process effectiveness. Figure 4.3-a shows that lignin extraction from *Miscanthus* remained high and constant (86 % on average) with a very mild decrease observed across the different [DMBA][HSO_4]/water mixtures. A similar trend of high and consistent delignification of *Miscanthus* was also reported in organoSolv and combined ionoSolv/organoSolv processing when varying the concentration of ethanol as pretreatment medium.[35] **The result highlight that *Miscanthus* fractionation does not require extensive organic or ionic solvent use, representing an important economic advantage, in particular taking into account that *Miscanthus* is a key candidate as energy crop**.[36] This highlights that only temperature and time have significant impact on *Miscanthus* delignification as reported by Gschwend *et al.* whereas IL concentration have a minor impact.[37] On the other hand, lignin extraction from pine wood and treated timber (both classified as softwoods) decreased significantly when increasing the water concentration in the pretreatment medium, achieving the highest lignin extraction at the lowest water concentration of 5 wt%. **This highlights that IL concentration plays a significant role in determining the pretreatment severity when using softwood-based feedstocks.**

The highly recalcitrant behaviour of softwood towards delignification compared to grassy biomass is typically attributed to the difference in their lignin structures.[38] Softwood lignin consist predominantly of guaiacyl (G) units (95 %) that is more prone to chemical condensation compared to grass lignin that contains a mixture of guaiacyl (G), synrigyl (S) and p-hydroxyphenyl (H) units.[25] A kinetic study using lignin model compound (guaiacylglycerol-β-guaiacol ether) that represents the β-*O*-4 ether linkage found in softwoods lignin showed that the cleavage of these β-*O*-4 linkages to depolymerize lignin requires the initiation of a dehydration reaction which is inhibited by the addition of water.[4] The initial dehydration of the model compound was in fact shown to be the rate-determining step in the overall hydrolysis reaction rate of β-*O*-4 ether linkage. The results here indicate that efficient delignification (and ether linkage cleavage) occurs when IL is mixed with small water, allowing sufficient hydrolysis to occur whilst limiting the impeding effects of water on dehydration. This could explain our experimental observation where effective delignification of softwood only being achieved at high pretreatment severity as dictated by high solvent concentration.

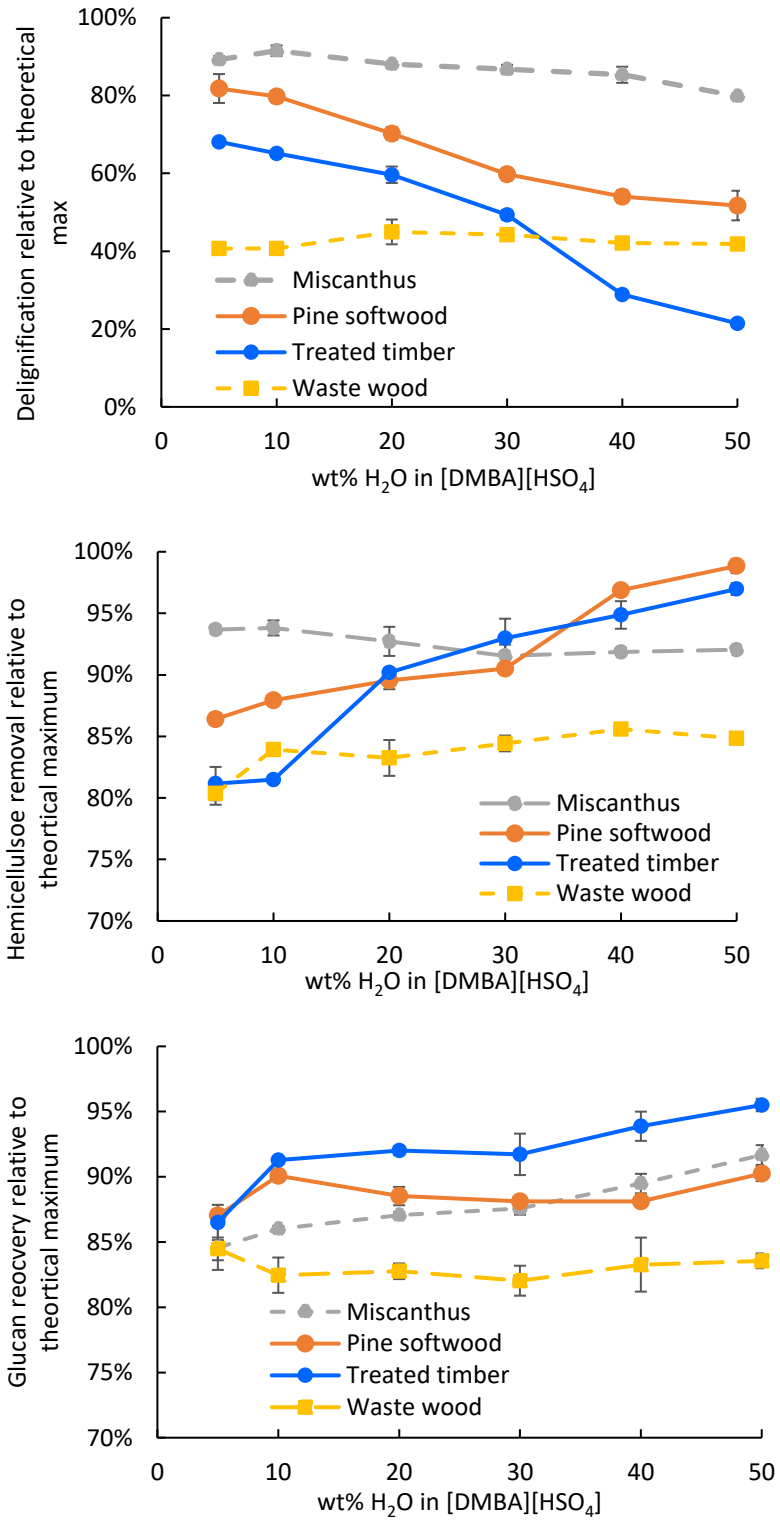

Figure 4.3: Key performance indicators of ionoSolv fractionation process. Fractionation experiments conducted using [DMBA][HSO4] at 170 °C for 30 minutes using a 1:5 g·g^{-1} solids loading

Post-consumer waste wood is a newly explored negative cost feedstock that has been fractionated successfully using ionoSolv process. **As in the case of grassy biomass, the delignification of waste wood was also found to be almost independent of the water concentration in the pretreatment medium. However, in this case, delignification remained low compared to the other feedstocks (44% on average).** The relatively low delignification of waste wood is a recurring phenomenon that has observed in the previous chapters, although the waste wood used in this study was from a different batch and a different source. The results provide further confirmation that extent of lignin extraction that can be achieved from post-consumer wood is limited. It is important to highlight that waste wood has a higher initial Klason lignin content, 34.8 %, compared to pine wood, treated timber and *Miscanthus,* which lignin contents are 29.9, 28.5 and 27.1 %, respectively (Figure 4.2). This can also have a role in the low lignin extraction achieved relative to the fixed amount of IL available.

Hemicellulose removal increased with increasing water concentration in the pretreatment medium for treated timber and pine wood from 81 % and 86 % at 5 wt% water to 97 % and 98 % at 50 wt% water, respectively (Figure 4.3-b). This suggests that water plays a more dominant role than [DMBA][HSO_4] in extracting and solubilizing the hemicellulose sugars of softwoods. The effect can be attributed to an auto-hydrolysis effect that is also seen in hydrothermal pretreatment methods where hemicellulose depolymerization and solubilization is the main deconstruction mechanism, whereas lignin and cellulose remain highly intact.[39,40] The near-quantitative hemicellulose removal (98 %) for softwoods at high water concentrations can be also an advantage even if the lignin extraction is lower, as selective lignin removal can be achieved in a subsequent bleaching step.[41] Effective removal of hemicellulose sugars from the biomass matrix is considered one of the main challenges in the current industrial pulping processes (Kraft and Acid Sulfite pulping), where an extra processing stage is needed to ensure effective extraction of hemicellulose sugars such as pre-hydrolysis for Kraft pulping or alkali extraction purification for Acid Sulfite pulping.[42] On the other hand, extraction of hemicellulose seems to be unaffected by water concentration in [DMBA][HSO_4] for *Miscanthus* and waste wood with average removals of 92.6 % and 83.7 %, respectively.

A noticeable increase in glucan recovery was also observed when increasing water concentration as a co-solvent in the pretreatment medium for pine wood, treated timber and *Miscanthus*. **The results indicate that glucan degradation and losses during pretreatment are mainly impacted by the IL concentration, where water higher concentrations help to preserve the glucan.** For softwood feedstocks this could be also related to the low delignification of biomass at high water concentration, leaving the glucan highly intact with only selective extraction of hemicellulose sugars. Glucan recovery for waste wood seemed to remain unaffected by changes in the water concentration in the pretreatment medium. The independency of the pretreatment outcomes (delignification, glucan recovery, hemicellulose removal) of post-consumer waste wood at various pretreatment conditions of different severities was communicated in more detail in the Chapter 2. Similar trends are observed in this study, where delignification, hemicellulose removal and glucan recovery remained fairly constant when varying the concentration of water. Regardless, **the independency of waste wood fractionation on pretreatment conditions can be an advantage as it gives more flexibility in altering the conditions of the process without causing a significant change in the product composition**. For example, in this case we can reduce IL use in the process without significantly impacting the composition of the cellulose pulp generated.

Figure 4.4 presents the isolated lignin yields from the fractionation process. The highest lignin yields for the four investigated feedstocks were obtained with water contents of 10 and 20 wt%. As discussed earlier, higher water concentrations in the pretreatment medium decreased the delignification ability of [DMBA][HSO_4], particularly for softwoods. Therefore, lignin precipitation yield decreased with increasing water concentration as less lignin was extracted in the process. We note that lignin yields using 95 wt% [DMBA][HSO_4] were slightly lower compared to lignin yields obtained at 90 and 80 wt% [DMBA][HSO_4] for all investigated feedstocks. This could be related to the effect of lignin solubility in [DMBA][HSO_4], where it seems that lignin fragments are more soluble in the 95 wt% [DMBA][HSO_4] solution compared to the 90 wt% [DMBA][HSO_4]. Table 4.1 presents the average molecular weight (M_w), number molecular weight (M_n) and polydispersity index (PDI) for isolated lignins using different [DMBA][HSO_4]/H_2O mixtures for all investigated feedstocks. Lignin isolated at 5 wt%

water showed the highest M_w and the highest PDI for all investigated feedstocks. A decrease in M_w and PDI was observed at 10 wt% water, followed by a milder increase in M_W and a decrease in PDI as the water concentration increased further. The relatively high M_w and PDI of lignin obtained after pretreatments at 5 wt% water in [DMBA][HSO_4] suggests that the lignin isolated under these conditions had the most modified and condensed structure compared to the other isolated lignin. **We observe that the pretreatment medium at higher water concentration tends to extract smaller and less condensed lignin fragments as indicated by the steady decrease in the M_w and PDI of precipitated lignin for the four investigated feedstocks.**

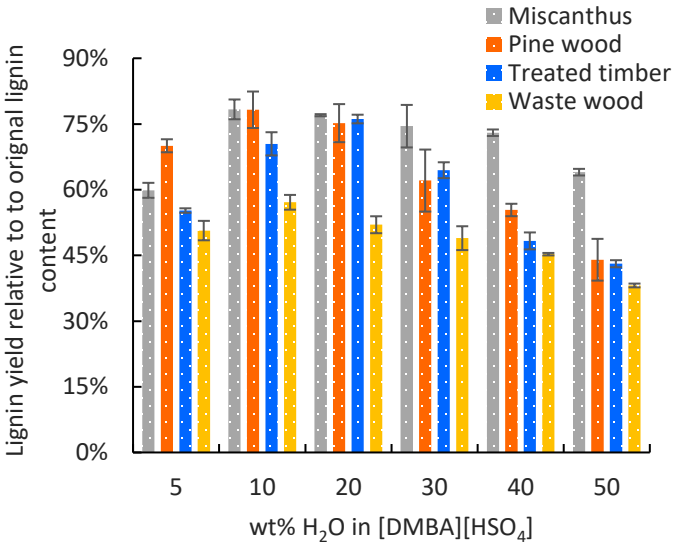

Figure 4.4: Lignin yield obtained from fractionating biomass using different [DMBA][HSO_4]-water mixtures. Fractionation experiments conducted at 170 °C for 30 minutes using 1:5 g·g^{-1} solids loading. Lignin precipitation was conducted using 3 water equivalents.

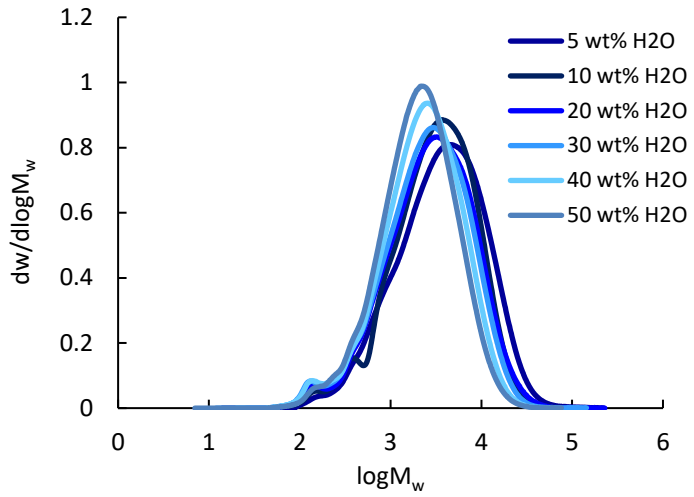

Figure 4.5: Molecular weight profiles for isolated lignin obtained from fractionating pine wood using different [DMBA][HSO_4]-water mixtures. Lignin precipitation was conducted using 3 water equivalents

Figure 4.6 shows the glucose yields obtained from enzymatic hydrolysis of the cellulose pulps. The cellulose pulps were used in their "wet" state (*i.e.* without air drying and moisture content 89-90 wt%) to avoid the hornification effect that can cause the collapse of the cellulose pores and hinder the enzymatic hydrolysis process.[43] Glucose yield is a valuable indicator of the performance of the process, as glucose can be further fermented to biofuels (e.g. bioethanol, lactic acid) or chemically transformed to produce other value-added bio-based chemicals (e.g. furfural and HMF).[44–46]

Table 4.1: Average molecular weights and polydispersity of isolated lignin from pre-treatments at different water/[DMBA][HSO_4] mixtures. Pretreatments were conducted at 170 °C and 30 minutes using 1:5 g·g^{-1} solid loading.

H_2O (wt%)	Waste wood			Treated timber			Pine wood			Miscanthus		
	Mn	Mw	PDI	Mn	Mw	PDI	Mn	Mw	PDI	Mn	Mw	PDI
5	1260	6708	5.34	1825	6115	3.35	1315	6435	4.89	3080	17200	5.58
10	1100	3319	3.02	1565	4810	3.07	1188	4672	3.93	1980	10400	5.25
20	1042	3415	3.28	1372	4592	3.35	1025	5325	5.20	1432	4554	3.18
30	922	3141	3.41	1232	4047	3.28	991	4251	4.29	1276	4010	3.14
40	948	2848	3.00	1182	3405	2.88	1175	3384	2.88	1440	3979	2.76
50	996	2925	2.94	1183	3024	2.56	1025	2682	2.62	1590	3400	2.13

Glucose yields for the cellulose pulps of *Miscanthus* were largely unaffected by the change in the [DMBA][HSO_4]/water ratios, with a relatively high glucose yield of 72% on average.

On the other hand, glucose yields from pine wood and treated timber pulps were the highest between 10 and 20 wt% water (an average of 74% relative to theoretical maximum) with a significant drop in glucose yield at 50 wt% H_2O to 30% and 20%, respectively. **The dramatic drop in glucose yields for softwood feedstocks directly correlates to the low delignification of biomass at high water concentrations.** On the other hand, **glucose yields from waste wood decreased mildly at higher water concentrations,** compared to softwood. It was interesting to note that for the four investigated feedstocks there was an obvious decrease in the glucose yield when only a 5 wt% of water was employed. As the delignification for all investigated biomass were similar when using 5 and 10 wt% water in [DMBA][HSO_4], it is less likely that this drop is caused by the formation of pseudo-lignin, a phenomenon that has been previously reported to have adverse impact on the glucose yields obtained when using acidic [HSO_4]-based ILs at severe pretreatment conditions.[5,7,47] **We speculate that this decrease can be attributed to the change in the cellulose fiber morphology, causing fibers to be less accessible to enzymes.** Cellulose pulp fibers obtained from the 95 wt% [DMBA][HSO_4] pretreatment appeared to be more agglomerated compared to cellulose pulps obtained from pretreatment using higher water concentrations. This change in the morphology of the fibers was more apparent when the cellulose pulps were air dried (Figure A22) and the same effect was observed for the four investigated feedstocks.

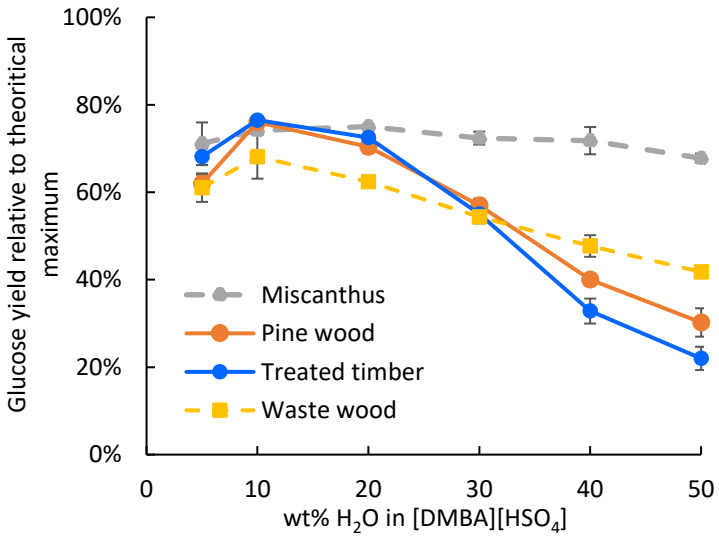

Figure 4.6: Glucose yield relative to maximum after 7 days of enzymatic saccharification of cellulose-rich pulps. Fractionation experiments were conducted at 170 °C for 30 minutes using a 1:5 g·g^{-1} solid loading

Since ionoSolv pretreatment is based on the delignification mechanism for biomass deconstruction, glucose yields are expected to correlate with the extent of delignification achieved (Figure 4.7). **The positive linear correlation between delignification and saccharification is clear with all the investigated feedstocks except for post-consumer waste wood, where delignification had little to no impact on the extent of glucose release from the cellulose-rich pulps.**

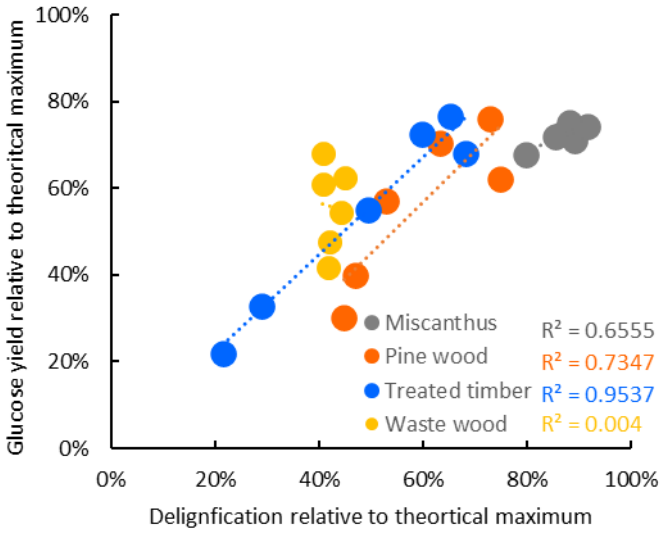

Figure 4.7: Correlation between enzymatic glucose yield and delignification across the four investigated feedstocks. Fractionation experiments were conducted at 170 °C for 30 minutes using a 1:5 g·g^{-1} solid loading using different [DMBA][HSO$_4$] concentrations

4.3.2 Water as an anti-solvent for lignin precipitation

The high lignin extracting power of protic [HSO$_4$]-based ILs demonstrates the high solubility of lignin in these ILs.[4] In previous ionoSolv studies, a ratio of 3 g of water per g of IL-water mixture (referred to as "equivalents") was added to recover the lignin from protic [HSO$_4$] ILs, which is an equivalent to diluting the IL by a factor of 4.[9,47] As previously mentioned, reducing the amount of water during this step is highly important as it correlates directly to the energy needed to dehydrate the IL back to its initial concentration for the next deconstruction cycle. Figure 4.8 shows the impact of reducing the water equivalents on lignin precipitation using pine wood as feedstock. Reducing water equivalents from 3 g g^{-1} to 1.5 g g^{-1} had no impact on lignin yields, remaining relatively constant at 80% relative to initial lignin content. Reducing the equivalents of

water to 1 g g^{-1} lowered the lignin yield for pine wood from ~80% to 65%, further reduction to 0.75 g g^{-1} decreased the lignin yield to 35% and when only 0.5 g g^{-1} of water were added the lignin yield was 10 %. These changes in lignin yields upon the addition of different amounts of water is typically related to the structural properties of the recovered lignin, such as the abundance of sub-unit ether linkages and the degree of condensation in the aromatic rings (Figure 4.9).[48]

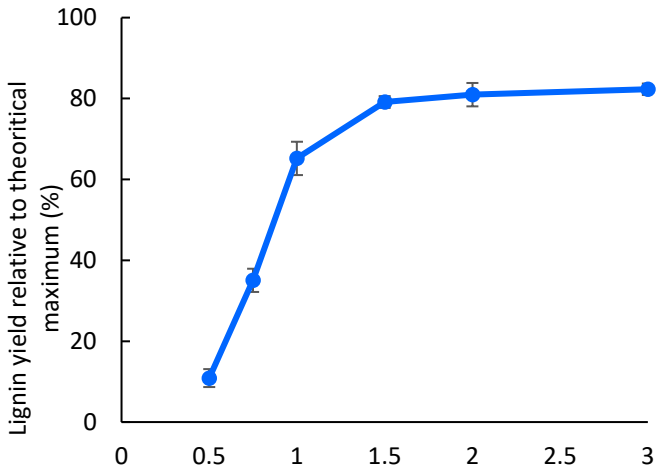

Figure 4.8: Lignin yield at different water equivalents. Fractionation experiments were conducted using 80 wt% [DMBA][HSO_4] and 20 wt% wtaer at 170 °C for 30 minutes using a 1:5 g·g^{-1} solids loading

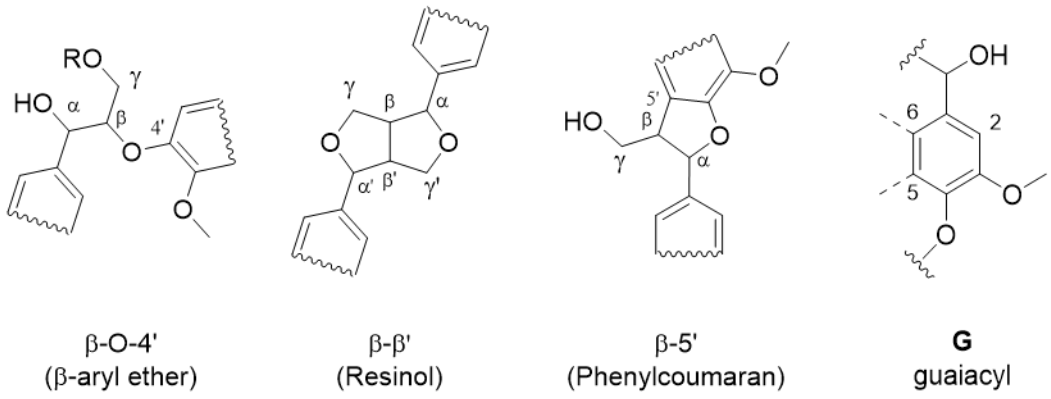

Figure 4.9: Key Ether linkages and aromatic rings found in pine wood lignin

Figure 4.10 shows the signal intensities using 2D HSQC NMR analysis to estimate the subunit compositions of the recovered lignin fractions, the degree of condensation of the

aromatic rings and the cleavage of common ether linkages. The degree of condensation in the aromatic lignin rings can be evaluated based on the signal intensity of G_{2cond}. Lignin precipitated using 3, 2 and 1:5 g g^{-1} water equivalent showed the same signal intensity in the aromatic region. On the other hand, the degree of condensation was higher when using lower amounts of water equivalents (1, 0.75 and 0.5 g g^{-1}), as evidenced by the lower G_6 and G_2 signal intensities and the higher G_{2cond} signal. This indicates that the chemically modified and cross-linked lignin fragments are more prone to precipitation upon the addition of small water equivalents.[48] **As fewer water equivalents were added, the precipitated lignin fractions showed a lower abundance of common interunit linkages β-*O*-4', phenylcoumaran (β-5) and resinol (β–β′), also indicating a higher degree of modification and condensation.** The molecular weights of the recovered fractions were also measured using gel permeation chromatography (GPC). Table 4.2 shows the average molecular weight of lignin recovered using different water equivalents.

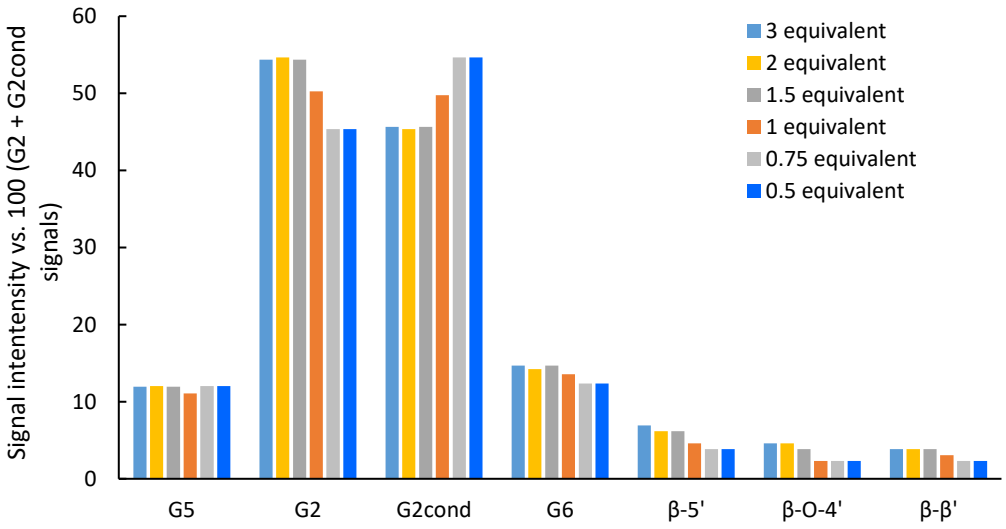

Figure 4.10: Abundance of lignin functionalities according to HSQC NMR spectroscopy for lignins isolated using different equivalents of water (intensity of G2 signal set to 100%). Fractionation experiments conducted at 170 °C for 30 minutes using softwood pine as feedstock

As anticipated, the amount of the water equivalents added influenced the properties of the lignin fraction precipitated. **Lower water equivalents of 0.5 and 0.75 g g^{-1} promoted the precipitation of the most hydrophobic, non-uniform lignin macromolecules as indicated by the large molecular weight of 7,700 to 9000 g·mol-**

[1] and the relatively high PDI of value of 4.9 to 5.4. Using higher water equivalent, 1 and 1.5 g g^{-1}, caused the precipitation of more hydrophilic smaller fragments of lignin along with large macromolecules, reducing the M_W of the recovered lignin to 5,400 and 6,500 g/mol and the PDI to be ~4. Higher water equivalents of 3 and 2 g g^{-1} resulted in the precipitation of the more hydrophilic monodisperse small lignin fragments that required the addition of a higher amount of water to precipitate. **Based on the lignin yields, chemical functionality and molecular weight, it was decided that reducing the use of water as anti-solvent in the process from 3 to 1 equivalents is more reasonable compared to using 0.75 or 0.5 water equivalents**. Using 1 water equivalent achieved a high degree of precipitation and the isolated lignin showed lesser signs of chemical condensation and lower polydispersity.

Table 4.2: Average molecular weight and polydiserpsity index of lignin isolated using different equivalents of water. Fractionation experiments were conducted at 170 °C for 30 minutes using softwood pine as a feedstock and a 1:5 g·g^{-1} solid loading.

Water Equivalent (g·g^{-1})	M_w	M_n	PDI
3	4,592	1,372	3.3
2	4,506	1,432	3.1
1.5	5,490	1,356	4.0
1	6,520	1,604	4.1
0.75	7,743	1,576	4.9
0.5	9,055	1,671	5.4

Mw: weight average molar mass (Da); Mn: number average molar mass (Da); PDI: polydispersity index.

4.3.4 Water impact on fractionation performance after solvent recycling

Reducing the water amount needed to precipitate lignin means that a higher concentration of dissolved lignin in the IL liquor will be present during the next delignification cycle. This has the potential to negatively impact the pretreatment performance as with higher amounts of dissolved lignin fragments there is a higher

possibility for the lignin undergo further reactions in the IL liquor. The residual lignin fragments in the liquor can potentially undergo one of the following reactions pathways i) re-polymerization reactions during the next pretreatment cycle, forming more condensed lignin structures that can deposit on the pulp surface;[49] or ii) reactions with degradation products formed during pretreatment, such as furfural and 5-HMF, that can form lignin-like structures known as pseudo-lignin, which also has high tendency to deposit on the cellulose-pulp surface.[50,51] The compositional analysis of the cellulose pulps is unable to distinguish between freshly extracted lignin from the biomass and re-polymerized condensed lignin fragments or pseudo-lignin. Condensed lignin and pseudo-lignin structures have adverse impact on the cellulose-pulp quality (*i.e.* high lignin content) and on its enzymatic hydrolysis through unproductive binding to the enzymes and physical hindrance to enzymes to access cellulose.[49,52] As discussed in the previous section, reducing the amount of precipitated lignin fragments using only 1 equivalent of water leads to slightly more condensed structures than lignin precipitated using 3 water equivalents. Herein, we investigated the impact of reducing the amount of water spent for lignin precipitation and its effect on the lignin properties, the delignification performance and the cellulose pulp quality.

Two sets of recycling experiments using 3 and 1 water equivalents for lignin precipitation were performed. For each set of experiments, 6 pretreatment cycles were conducted using pine wood as feedstock using a 20 wt% solid loading at 150 °C for 1 hour. Figure 4.11 presents the delignification and enzymatic glucose yields across the 6 cycles for both sets of experiments (numerical pulp composition values can be found in Table A2). Both parameters, delignification and glucose yields, followed the same pattern across the 6 cycles for both set of experiments, indicating that reducing the amount of water from 3 to 1 equivalent did not alter the performance of the process. **These results show that the performance of the delignification process is robust, and that cellulose pulp composition and quality remains unaffected by the higher proportion of dissolved lignin remaining in the IL across the six cycles.**

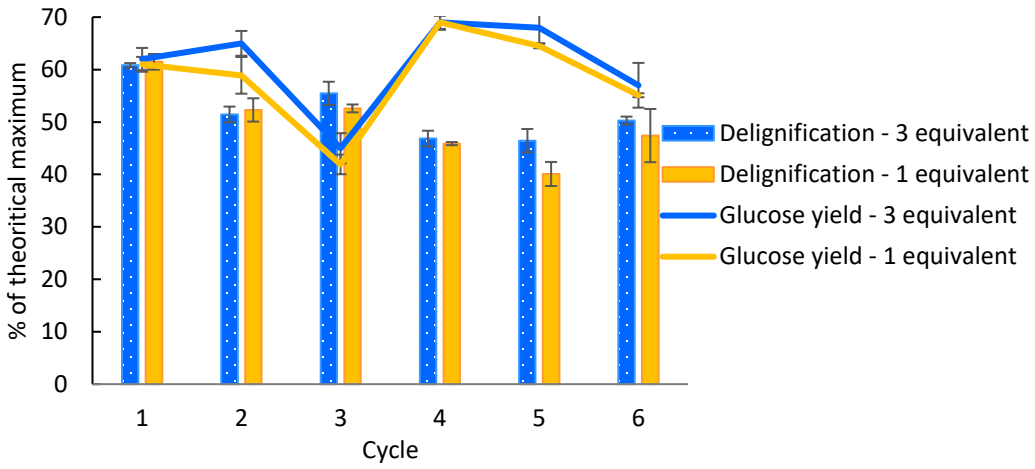

Figure 4.11: Delignification and 7-day enzymatic glucose yield obtained across 6 pretreatment cycles using 3 and 1 water equivalent as anti-solvent. Fractionation experiments were conducted at 150 °C for 1 h using 1:5 g·g^{-1} solid loading

There was a clear drop in the glucose yield obtained in the third cycle for the two sets of conditions, indicating that the decrease is not related to the change in the equivalents of water, especially since the delignification performance remained unchanged. The mass balance of lignin for the two sets of conditions (Figure 4.12) was performed in order to have a better insight on the reason behind glucose yield drop at the 3rd cycle. The mass balance includes the precipitated lignin yield, the residual lignin on pulp as quantified by compositional analysis and the dissolved lignin in the IL liquor. It is important to note that it has not been possible so far to quantify the concentration of the dissolved lignin fragments in the IL solution. Therefore, the dissolved lignin is calculated based on the difference between the initial lignin content in the biomass and the sum of the lignin found in the two solid fractions. The lignin fragments that remain in the IL liquor are typically the fragments with lower molecular weight and higher solubility in water, whereas the larger and more condensed fragments precipitate upon water addition.

The first pretreatment cycle using 1 water equivalent resulted in lower lignin yields and higher dissolved lignin compared to 3 water equivalents. For the 2nd cycle, higher lignin yields were obtained for both water equivalents, accompanied by a decrease in the dissolved lignin. For the 3rd pretreatment cycle, lignin precipitation reached to a peak for both water equivalents. Lignin yield exceeded 100 % when using 1 water equivalent

and reached 84% at 3 water equivalents. The high lignin yield at the third cycle, especially when using 1 equivalent of water, might be an indication that the lignin precipitate contained fragments of pseudo-lignin formed via polycondensation reactions of sugar degradation products that formed and accumulated in the IL liquor over the course of the pretreatment cycles. It should be noted that pseudo-lignin is usually defined as a lignin-like structure that results in positive Kalson lignin (*i.e.* higher lignin content in the pulp relative to untreated material). At cycle 3, the delignification and consequently the residual lignin on the cellulose pulp did not change dramatically compared to cycle 1 and 2, showing no indication of positive Kalson lignin in the cellulose pulp. However, the fact that the glucose yield of cellulose pulps in cycle 3 showed significant decrease when using 3 or 1 water equivalent indicates that structure of the residual "lignin" on the pulp is potentially more condensed causing unproductive binding with enzymes and inhibiting the enzymatic hydrolysis, a well-known effect of pseudo-lignin.[50] The slight or incomplete deposition of pseudo lignin on the cellulose pulp surface during pretreatment is probably due to the mild pretreatment condition, which allowed the pseudo lignin structures to remain soluble in the IL during the course of pretreatment, then precipitated later upon water addition resulting in mass balance that exceeds 100%. More severe pretreatment condition would have accelerated the subsequent deposition on the cellulose pulp.[5]

precipitated lignin yields decreased at the 4th cycle, after the precipitation of the accumulated lignin in cycle 3. For the 5th and 6th cycles, we observed a similar effect of gradual increase in lignin precipitation yield as more lignin is extracted, with the effect being more pronounced when using 1 water equivalent. Figure 4.13 shows the average M_W and PDI of the precipitated lignin across the 6 pretreatment cycles using 3 and 1 water equivalent as anti-solvent. In the 1st pretreatment cycle, lignin precipitated using 1 water equivalent showed slightly higher M_w and higher monodispersity compared to lignin precipitated using 3 water equivalents, indicating that higher water input tends to precipitate more diverse lignin polymer chains. The 2nd pretreatment cycle showed the same trend of high polydisperse lignin at higher water input while the average M_W of lignin for both water equivalents was lower compared to the 1st cycle. The 3rd cycle showed a noticeable increase in the M_W of lignin precipitated using 1 water equivalent and slightly higher PDI. The M_W of recovered lignin decreased steadily in the following pretreatment cycles until the M_w of both lignin recovered using 3 and 1 water equivalent

reached a nearly identical value of ~4,700 g/mol. The decrease in M_W of lignin could be due the precipitation of the low M_w small lignin fragments that accumulated across the cycles. These results suggest that reducing the equivalents of water used as anti-solvent for lignin precipitation can alter the properties of the recovered lignin fragments. However, **as the process continues to reach steady state after multiple pretreatment cycles, the fraction of lignin recovered by water precipitation using 3 or 1 water equivalent does not have an adverse impact on the cellulose-pulp quality.**

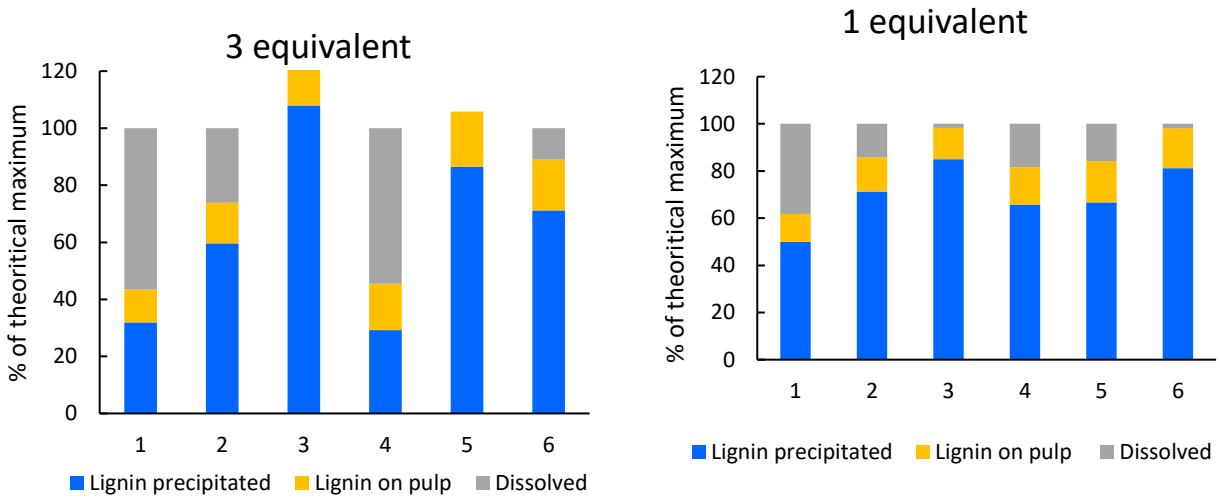

Figure 4.13: Lignin mass balance across 6 pretreatment cycles using 1 water equivalent as anti-solvent and right using 3 water equivalents as anti-solvent.

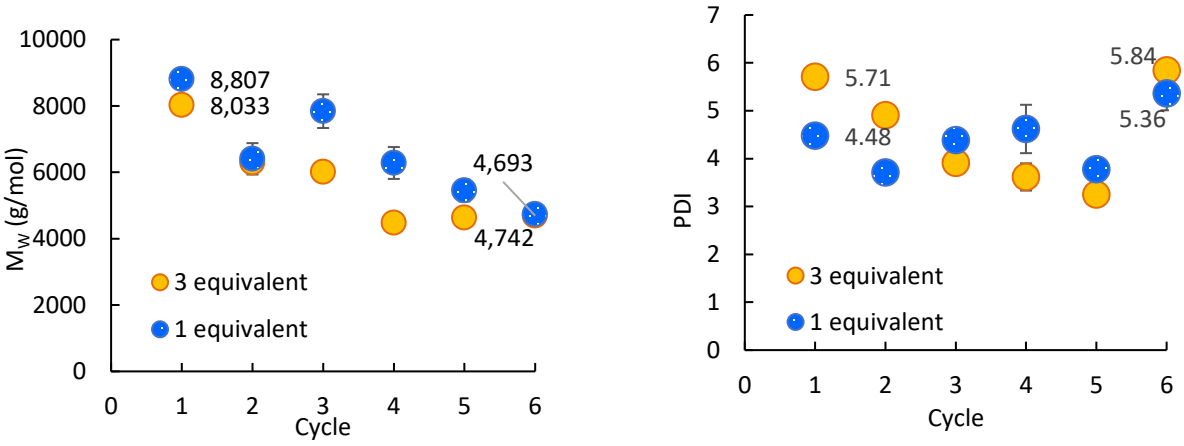

Figure 4.12: Average molecular weight and polydispersity index of isolated lignin across 6 pretreatment cycles using 3 water equivalent (Left) and 1 water equivalent (Right) as anti-solvent.

4.3.5 Impact of water use on IL dehydration energy

As mentioned earlier, the addition of water as anti-solvent in the process has a significant impact on the energy requirement of the process, due to the combined effect of the high heat of vaporization of water (2260 KJ/kg), and the boiling point elevation phenomena caused by the high IL concentration.[53] It was demonstrated that it is possible to reduce the amount of water required to precipitate lignin by one-third without impacting the fractionation performance of the process. This section higlights the impact of reducing the water use as an anti-solvent on the energy requirement of the process, focusing on the IL dehydration section which was identified as the most energy intensive part in the process.[9]

Figure 4.14 shows the vapor-liquid equilibrium diagram for [DMBA][HSO_4] at different water concentrations. **The boiling point of [DMBA][HSO_4]/water mixtures increases more noticeably at water concentrations below 40 wt%, which is within the operating concentration range of the process (initial water content in IL is 20 wt%).** The increase in the boiling point elevation is potentially due to the stronger hydrogen bond interactions between the water molecules and the protic [DMBA][HSO_4] and between the anion and the cation themselves at lower water concentrations, which will make the dehydration process more challenging.[54]

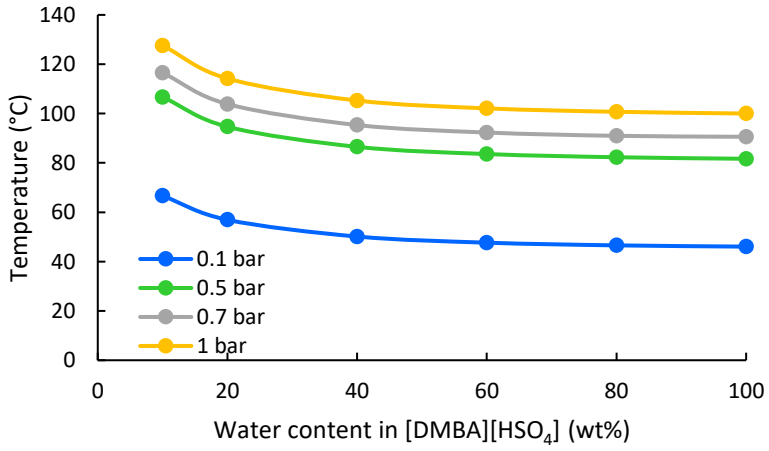

Figure 4.14: Vapor-liquid equilibrium diagram for [DMBA][HSO_4]-water at different water concentrations

The IL dehydration process was simulated using multi-effect evaporation, typically used in industrial applications such as Kraft pulping as a highly efficient method to concentrate solutions.[15] The multi-effect evaporation process is based on the use of the steam generated at high pressures in an evaporator (i) to supply the heat required for the thermal separation in the subsequent evaporator (i+1) operating at lower pressure, therefore reducing the amount of the external utility steam supplied in the first evaporator (i-1) to initiate the separation (Figure A23). The multi-effect evaporation process was simulated using 4 evaporators and 3 evaporators. It was found that using 3 evaporators (operating pressures of 0.7, 0.4 and 0.1 bar) is sufficient to dehydrate the IL to 80 wt% without operating at very low pressures. Figure 4.15 shows the impact of the equivalents of water added during the lignin precipitation step on the dehydration energy required to concentrate [DMBA][HSO_4] back to the initial water concentration of 20 wt%

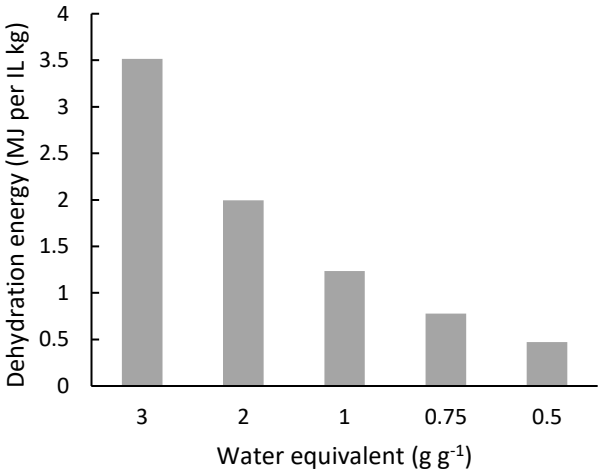

Figure 4.15: Dehydration energy required to concentrate [DMBA][HSO_4] using different water equivalents as anti-solvent, back to the initial water concentration of 20 wt%.

Reducing the amount of water from 3 equivalents to 1 equivalent reduces the dehydration energy significantly from 3.52 to 1.25 MJ per kg of IL. Lignin produced in the ionoSolv process has a higher heating value of approximately 22 MJ/kg, which corresponds to 1.26 MJ per kg of IL. **The outcomes indicate that the 65% decrease in the dehydration energy enables the process to satisfy its largest portion of the total energy requirement by integrating the energy of lignin combustion**Further reducing the water equivalent as anti-solvent to 0.75 and 0.5 g g^{-1} also reduces the dehydration energy needed to re-concentrate the IL as the IL is less diluted. However, as demonstrated in the previous section, it is very likely that the fractionation performance will be negatively impacted, resulting in a lower quality cellulose pulp. **This heat balance on the IL dehydration is another step that demonstrates the technoeconomic viability of the process, not only from a glucose yield perspective, but from an energy use point-of-view.**

4.4 Conclusions

The important dual role of water as both co-solvent and anti-solvent in the ionoSolv biomass fractionation process has been evaluated using the low-cost protic ionic liquid [DMBA][HSO_4], as a solvent. The effectiveness of biomass fractionation using [DMBA][HSO_4] mixed with different concentrations of water on conventional biorefinery feedstocks (*Miscanthus* and pine wood) and non-conventional low-cost lignocellulosic biomass waste (treated timber and post-consumer waste wood) was investigated. Cellulose pulp composition, lignin extraction and enzymatic hydrolysis of the cellulose pulps were analyzed after pretreatments carried out at 170 °C for 30 minutes. The study showed that it is possible to reduce the PIL use in the process by increasing the water concentration as a co-solvent, while still maintaining effective biomass delignification for *Miscanthus* and post-consumer waste wood. However, softwood biomass showed higher resistance to fractionation at higher water concentrations in the pretreatment medium, highlighting the necessity to use high IL concentration to achieve effective delignification. We also investigated the impact of reducing the amount of water used as anti-solvent for lignin precipitation in terms of lignin yields and properties. The robust performance of the fractionation process at optimized anti-solvent use was demonstrated using the challenging feedstock pine softwood over 6 pretreatment cycles. Finally, we demonstrated the significance of evaluating water-use on the energy requirements of the process, particularly in the ionic liquid regeneration step, achieving a 65% saving. This highlights the importance of optimizing new chemical processes not only based on product yield (e.g. glucose yield), but also for the water use, which has a direct impact on process sustainability, energy, economics and scalability.

References

(1) Gregorio, G. F. De; Weber, C. C.; Gräsvik, J.; Welton, T. Mechanistic Insights into Lignin Depolymerisation in Acidic Ionic Liquids. Green Chem. 2016. https://doi.org/10.1039/c6gc01295g.

(2) Gschwend, F. J. V.; Brandt-Talbot, A. Rapid Pretreatment of Miscanthus Using the Low-Cost Ionic Liquid Triethylammonium Hydrogen Sulfate at Elevated Temperatures. Green Chem. 2016, 20 (15), 3486–3498. https://doi.org/10.1039/c8gc00837j.

(3) Verdía, P.; Brandt, A.; Hallett, J. P.; Ray, M. J.; Welton, T. Fractionation of Lignocellulosic Biomass with the Ionic Liquid 1-Butylimidazolium Hydrogen Sulfate. Green Chem. 2014, 16 (3), 1617–1627. https://doi.org/10.1039/c3gc41742e.

(4) Brandt-Talbot, A.; Gschwend, F. J. V.; Fennell, P. S.; Lammens, T. M.; Tan, B.; Weale, J.; Hallett, J. P. An Economically Viable Ionic Liquid for the Fractionation of Lignocellulosic Biomass. Green Chem. 2017, 19 (13), 3078–3102. https://doi.org/10.1039/C7GC00705A.

(5) Shi, J.; Balamurugan, K.; Parthasarathi, R.; Sathitsuksanoh, N.; Zhang, S.; Stavila, V.; Subramanian, V.; Simmons, B. A.; Singh, S. Understanding the Role of Water during Ionic Liquid Pretreatment of Lignocellulose: Co-Solvent or Anti-Solvent? Green Chem. 2014, 16 (8), 3830–3840. https://doi.org/10.1039/c4gc00373j.

(6) Brandt, A.; Gräsvik, J.; Hallett, J. P.; Welton, T. Deconstruction of Lignocellulosic Biomass with Ionic Liquids. Green Chem. 2013, 15 (3), 550–583. https://doi.org/10.1039/c2gc36364j.

(7) Clarke, C. J.; Tu, W. C.; Levers, O.; Bröhl, A.; Hallett, J. P. Green and Sustainable Solvents in Chemical Processes. Chem. Rev. 2018, 118 (2), 747–800. https://doi.org/10.1021/acs.chemrev.7b00571.

(8) Sun, J.; Shi, J.; Murthy Konda, N. V. S. N.; Campos, D.; Liu, D.; Nemser, S.; Shamshina, J.; Dutta, T.; Berton, P.; Gurau, G.; Rogers, R. D.; Simmons, B. A.; Singh, S. Efficient Dehydration and Recovery of Ionic Liquid after Lignocellulosic Processing Using Pervaporation. Biotechnol. Biofuels 2017, 1 (1), 1–14. https://doi.org/10.1186/s13068-017-0842-9.

(9) Wu, H.; Shen, F.; Wang, J.; Luo, J.; Liu, L.; Khan, R.; Wan, Y. Separation and Concentration of Ionic Liquid Aqueous Solution by Vacuum Membrane Distillation. J. Memb. Sci. 2016, 518, 216–228. https://doi.org/10.1016/j.memsci.2016.07.017.

(10) Al Ghatta, A.; Wilton-Ely, J. D. E. T.; Hallett, J. P. Strategies for the Separation of the Furanic Compounds HMF, DFF, FFCA, and FDCA from Ionic Liquids. ACS Sustain. Chem. Eng. 2019. https://doi.org/https://doi.org/10.1021/acssuschemeng.9b03613.

(11) Jyoti, G.; Khanam, S. Simulation of Heat Integrated Multiple Effect Evaporator System. Int. J. Therm. Sci. 2014, 76, 110–117. https://doi.org/10.1016/j.ijthermalsci.2013.08.016.

(12) Verma, O. P.; Mohammed, T. H.; Mangal, S.; Manik, G. Minimization of Energy Consumption in Multi-Stage Evaporator System of Kraft Recovery Process Using Interior-Point Method. Energy 2017, 129, 148–157. https://doi.org/10.1016/j.energy.2017.04.093.

(13) Pharande, V. A.; Asthana, S. R.; Saini, D. R.; Kaul, S. N. Energy Optimization in Integrated Pulp and Paper Mills with Recourse to Environmental Benefits. J. Sci. Ind. Res. (India). 2011, 70 (12), 1061–1069.

(14) Huang, S.-Y.; Fedkiw, P. S. Pervaporation Removal of Water from Ionic Liquid Solutions Using Nafion Membranes. Sep. Sci. Technol. 2016, 51 (18), 2932–2939. https://doi.org/10.1080/01496395.2016.1236816.

(15) Haerens, K.; Van Deuren, S.; Matthijs, E.; Van der Bruggen, B. Challenges for Recycling Ionic Liquids by Using Pressure Driven Membrane Processes. Green Chem. 2010, 12 (12), 2182–2188. https://doi.org/10.1039/c0gc00406e.

(16) Wang, G.; Chen, H. Fractionation and Characterization of Lignin from Steam-Exploded Corn Stalk by Sequential Dissolution in Ethanol-Water Solvent. Sep. Purif. Technol. 2013, 120, 402–409. https://doi.org/10.1016/j.seppur.2013.10.029.

(17) Li, M. F.; Sun, S. N.; Xu, F.; Sun, R. C. Sequential Solvent Fractionation of Heterogeneous Bamboo Organosolv Lignin for Value-Added Application. Sep. Purif. Technol. 2012, 101, 18–25. https://doi.org/10.1016/j.seppur.2012.09.013.

(18) Cui, C.; Sun, R.; Argyropoulos, D. S. Fractional Precipitation of Softwood Kraft Lignin: Isolation of Narrow Fractions Common to a Variety of Lignins. ACS Sustain. Chem. Eng. 2014, 2 (4), 959–968. https://doi.org/10.1021/sc400545d.

(19) Liang, X.; Liu, J.; Fu, Y.; Chang, J. Influence of Anti-Solvents on Lignin Fractionation of Eucalyptus Globulus via Green Solvent System Pretreatment. Sep. Purif. Technol. 2016, 163, 258–266. https://doi.org/10.1016/j.seppur.2016.03.006.

(20) Chambon, C. L.; Fitriyanti, V.; Verdía, P.; Yang, S. M.; Hérou, S.; Titirici, M. M.; Brandt-Talbot, A.; Fennell, P. S.; Hallett, J. P. Fractionation by Sequential Antisolvent Precipitation of Grass, Softwood, and Hardwood Lignins Isolated Using Low-Cost Ionic Liquids and Water. ACS Sustain. Chem. Eng. 2020, 8 (9), 3751–3761. https://doi.org/10.1021/acssuschemeng.9b06939.

(21) Brandt, A.; Ray, M. J.; To, T. Q.; Leak, D. J.; Murphy, R. J.; Welton, T. Green Chemistry Ionic Liquid Pretreatment of Lignocellulosic Biomass with Ionic Liquid–Water Mixtures. https://doi.org/10.1039/c1gc15374a.

(22) Merten Morales, Thomas Pielhop, Philippe Saliba, Konrad Hungerbühler, P. R. von R. Sustainability Assessment of Glucose Production Technologies from Highly Recalcitrant Softwood Including Scavengers. Biofuels, Bioprod. Biorefining 2016, 6 (3), 441–453 (2017). https://doi.org/10.1002/bbb.

(23) NNFCC. Lignocellulosic Feedstock in the UK A Report for the Lignocellulosic Biorefinery Network. 2014, No. November.

(24) WRAP. Realising the Value of Recovered Wood; UK, 2011.

(25) Sluiter, A.; Hames, B.; Ruiz, R.; Scarlata, C.; Sluiter, J.; Templeton, D.; Crocker, D. Analytical Procedure - Determination of Structural Carbohydrates and Lignin in Biomass; 2008. https://doi.org/NREL/TP-510-42618.

(26) Gschwend, F. J. V.; Chambon, C. L.; Biedka, M.; Brandt-Talbot, A.; Fennell, P. S.; Hallett, J. P. Quantitative Glucose Release from Softwood after Pretreatment with

Low-Cost Ionic Liquids. Green Chem. 2019, 21 (3), 692–703. https://doi.org/10.1039/c8gc02155d.

(27) Shu, Z.; Xie, C.; Zhou, J.; Li, T.; Chen, Y.; Wang, W.; Tan, Y.; Zhao, Z. Low Solids Enzymatic Saccharification of Lignocellulosic Biomass Laboratory; 2015; Vol. 747. https://doi.org/10.1016/j.jallcom.2018.03.019.

(28) Sluiter, A.; Hames, B.; Hyman, D.; Payne, R.; Scarlata, C.; Sluiter, J.; Templeton, D.; Wolfe, J. Determination of Total Solids in Biomass and Total Dissolved Solids in Liquid Process Samples; 2008; Vol. XXV. https://doi.org/NREL/TP-510-42621.

(29) Perdew, J. P.; Yue, W. Accurate and Simple Density Functional for the Electronic Exchange Energy: Generalized Gradient Approximation. Phys. Rev. B 1986, 33 (12), 8800–8802. https://doi.org/10.1103/PhysRevB.33.8800.

(30) Eichkorn, K.; Treutler, O.; Öhm, H.; Häser, M.; Ahlrichs, R. Auxiliary Basis Sets to Approximate Coulomb Potentials. Chem. Phys. Lett. 1995, 240 (4), 283–290. https://doi.org/10.1016/0009-2614(95)00621-A.

(31) Santiago, R.; Bedia, J.; Moreno, D.; Moya, C.; de Riva, J.; Larriba, M.; Palomar, J. Acetylene Absorption by Ionic Liquids: A Multiscale Analysis Based on Molecular and Process Simulation. Sep. Purif. Technol. 2018, 204, 38–48. https://doi.org/10.1016/j.seppur.2018.04.060.

(32) Bauer, S.; Sorek, H.; Mitchell, V. D.; Ibáñez, A. B.; Wemmer, D. E. Characterization of Miscanthus Giganteus Lignin Isolated by Ethanol Organosolv Process under Reflux Condition. J. Agric. Food Chem. 2012, 60 (33), 8203–8212. https://doi.org/10.1021/jf302409d.

(33) Axelsson, L.; Franzén, M.; Ostwald, M.; Berndes, G.; Lakshmi, G.; Ravindranath, N. H. Perspective: Jatropha Cultivation in Southern India: Assessing Farmers' Experiences. Biofuels, Bioprod. Biorefining 2012, 6 (3), 246–256. https://doi.org/10.1002/bbb.

(34) Gschwend, F. J. V.; Malaret, F.; Shinde, S.; Brandt-Talbot, A.; Hallett, J. P. Rapid Pretreatment of: Miscanthus Using the Low-Cost Ionic Liquid Triethylammonium Hydrogen Sulfate at Elevated Temperatures. Green Chem. 2018, 20 (15), 3486–3498. https://doi.org/10.1039/c8gc00837j.

(35) Sadeghifar, H.; Cui, C.; Argyropoulos, D. S. Toward Thermoplastic Lignin Polymers. Part 1. Selective Masking of Phenolic Hydroxyl Groups in Kraft Lignins via Methylation and Oxypropylation Chemistries. Ind. Eng. Chem. Res. 2012, 51 (51), 16713–16720. https://doi.org/10.1021/ie301848j.

(36) Chiaramonti, D.; Prussi, M.; Ferrero, S.; Oriani, L.; Ottonello, P.; Torre, P.; Cherchi, F. Review of Pretreatment Processes for Lignocellulosic Ethanol Production, and Development of an Innovative Method. Biomass and Bioenergy 2012, 46, 25–35. https://doi.org/10.1016/j.biombioe.2012.04.020.

(37) Oliveira, F. M. V.; Pinheiro, I. O.; Souto-Maior, A. M.; Martin, C.; Gonçalves, A. R.; Rocha, G. J. M. Industrial-Scale Steam Explosion Pretreatment of Sugarcane Straw for Enzymatic Hydrolysis of Cellulose for Production of Second Generation Ethanol and Value-Added Products. Bioresour. Technol. 2013, 130, 168–173. https://doi.org/10.1016/j.biortech.2012.12.030.

(38) Weinstock, I. A.; Atalla, R. H.; Reiner, R. S.; Moen, M. A.; Hammel, K. E.; Houtman, C. J.; Hill, C. L.; Harrup, M. K. A New Environmentally Benign Technology for Transforming Wood Pulp into Paper, Engineering Polyoxometalates as Catalysts for Multiple Processes. J. Mol. Catal. A Chem. 1997, 116 (1–2), 59–84. https://doi.org/10.1016/S1381-1169(96)00074-X.

(39) Liu, Y.; Shi, L.; Cheng, D.; He, Z. Dissolving Pulp Market and Technologies: Chinese Prospective - a Mini-Review. BioResources 2016, 11 (3), 7902–7916. https://doi.org/10.15376/biores.11.3.Liu.

(40) Fernandes Diniz, J. M. B.; Gil, M. H.; Castro, J. A. A. M. Hornification - Its Origin and Interpretation in Wood Pulps. Wood Sci. Technol. 2004, 37 (6), 489–494. https://doi.org/10.1007/s00226-003-0216-2.

(41) Wasewar, K. L.; Yawalkar, A. A.; Moulijn, J. A.; Pangarkar, V. G. Fermentation of Glucose to Lactic Acid Coupled with Reactive Extraction: A Review. Ind. Eng. Chem. Res. 2004, 43 (19), 5969–5982. https://doi.org/10.1021/ie049963n.

(42) Tabah, B.; Pulidindi, I. N.; Chitturi, V. R.; Reddy Arava, L. M.; Varvak, A.; Foran, E.; Gedanken, A. Solar-Energy-Driven Conversion of Biomass to Bioethanol: A Sustainable Approach. J. Mater. Chem. A 2017, 5 (30), 15486–15506. https://doi.org/10.1039/c7ta03083e.

(43) Al Ghatta, A.; Wilton-Ely, J. D. E. T.; Hallett, J. P. Efficient Formation of 2,5-Diformylfuran in Ionic Liquids at High Substrate Loadings and Low Oxygen Pressure with Separation through Sublimation. ACS Sustain. Chem. Eng. 2020. https://doi.org/10.1021/acssuschemeng.9b06691.

(44) Gschwend, F. J. V.; Chambon, C. L.; Biedka, M.; Brandt-Talbot, A.; Fennell, P. S.; Hallett, J. P. Quantitative Glucose Release from Softwood after Pretreatment with Low-Cost Ionic Liquids. Green Chem. 2019, 21 (3), 692–703. https://doi.org/10.1039/c8gc02155d.

(45) Chambon, C. L.; Fitriyanti, V.; Verdia, P.; Yang, S. M.; Herou, S.; Titirici, M.-M.; Brandt-Talbot, A.; Fennell, P. S.; Hallett, J. P. Fractionation by Sequential Anti-Solvent Precipitation of Grass, Softwood and Hardwood Lignins Isolated Using Low-Cost Ionic Liquids and Water. ACS Sustain. Chem. Eng. 2020. https://doi.org/10.1021/acssuschemeng.9b06939.

(46) Kumar, R.; Hu, F.; Sannigrahi, P.; Jung, S.; Ragauskas, A. J.; Wyman, C. E. Carbohydrate Derived-Pseudo-Lignin Can Retard Cellulose Biological Conversion. Biotechnol. Bioeng. 2013, 110 (3), 737–753. https://doi.org/10.1002/bit.24744.

(47) Shinde, S. D.; Meng, X.; Kumar, R.; Ragauskas, A. J. Recent Advances in Understanding the Pseudo-Lignin Formation in a Lignocellulosic Biorefinery. Green Chem. 2018, 20 (10), 2192–2205. https://doi.org/10.1039/C8GC00353J.

(48) Hu, F.; Jung, S.; Ragauskas, A. Pseudo-Lignin Formation and Its Impact on Enzymatic Hydrolysis. 2012. https://doi.org/10.1016/j.biortech.2012.04.037.

(49) Hoerning, A.; Ribeiro, F. R. G.; Cardozo Filho, L.; Lião, L. M.; Corazza, M. L.; Voll, F. A. P. Boiling Point Elevation of Aqueous Solutions of Ionic Liquids Derived from Diethanolamine Base and Carboxylic Acids. J. Chem. Thermodyn. 2016, 98, 1–8. https://doi.org/10.1016/j.jct.2016.02.017.

(50) Greaves, T. L. D. C. Protic Ionic Liquids- Properties and Applications. Chem. Rev. 2008, 108, 206–237.

Chapter 5 : Evaluation of Softwood Fractionation behavior in [HSO_4]-based Protic Ionic Liquid Using Modified Pretreatment Severity Factor

5.1 Introduction

As was presented in the previous chapters, the fractionation mechanism of protic [HSO_4]-based IL pretreatment is based on the ability of the ILs to depolymerize and solubilize the lignin macromolecules along with the removal of hemicellulose polysaccharides shielding the cellulose polymer. The efficiency of the fractionation mechanism depends on the feedstock used, and more importantly on the fractionation conditions employed.[1]

Softwood is one of the key feedstocks for a 2nd generation biorefinery as it is sustainably produced for timber, pulp and paper production globally. Softwood is available from forestry residues or in the form of waste streams from timber production (i.e. sawdust).[2] In the UK, it is estimated that 1.3 million tons of softwood forest residues can be collected annually at a cost of £18 to £50 per dry tonne.[3] Despite the high availability of softwoods at low cost, softwoods are more challenging to fractionate as they are well known for their high resistance to fractionation compared to hardwoods and grasses.[4] The challenging nature of softwood fractionation stems from the relatively high lignin content (up to 35%) and the structure of the lignin that is predominantly made of the guaiacyl (G) units (up to 95%).[3,4] Guaiacyl units are more prone to condensation reactions during the fractionation forming more complex and condensed structures that deposit on the cellulose surface.[2,5] The high recalcitrance of softwood biomass makes low-cost aqueous-based pretreatment methods such as steam explosion or dilute acid highly ineffective.[6] More successful fractionation attempts were reported using alkaline-based pretreatments[7] and Organosolv pretreatments[8], however these methods suffer from the high recovery cost of the solvents and high capital investment.[9]

The work conducted in this chapter aims to develop a more comprehensive understanding on the fractionation of softwood in protic [HSO_4]-based IL, focusing on the role of temperature, time, IL concentration and corresponding acidity using what is known as pretreatment severity factor[10] (refer to section 1.8 in Chapter 1). The use of pretreatment severity factor in ILs-based pretreatment is very limited compared to its use in aqueous-based pretreatment. Malarat *et al.* have recently investigated the impact of pretreatment severity in terms of temperature and time on the fractionation of *Eucalyptus* using triethylammonium hydrogen sulfate [TEA][HSO_4].[11] The severity factor R_0 was used to evaluate the pretreatment severity where it was found that the glucan solubilization followed a linear trend with R_0. Hemicellulose removal from the biomass also increased with increasing the pretreatment severity and 100% was achieved at severity levels ~1300 min. Delignification showed maximum values of above 90% in the range of R_0 1300– 6900 min, below or above this range lower delignification is achieved. The role that IL medium's acidity play in the deconstruction of the biomass was given even smaller attention. Weigand *et al.* investigated the impact of pretreatment severity in terms of temperature, time and protic IL acidity using [TEA][HSO_4] as a medium and hardwood willow as a feedstock.[12] The acidity of the protic IL was altered using different acid base ratios during the IL synthesis, and the corresponding pH of the 1 wt% of the solution was used as an indication of the medium's acidity. Higher pretreatment severity levels which corresponded to higher temperatures, prolonged cooking times or higher solution's acidity shown to be more aggressive in terms of cellulose degradation and pseudo-lignin deposition on the pulp surface. Although the use of pH and the acid : base ratio can give an indication about the IL acidity, exact quantification of the IL acidity was not conducted nor incorporated in the pretreatment severity factor.

In this study, a modified pretreatment severity factor that considers the variation of the IL solution acidity based on its composition in the pretreatment medium was used to express and predict the fractionation efficiency of pine softwood *(Pinus sylvestris)*. The modified factor incorporates the Hammett acidity function (H_0) of the IL/H_2O mixture into the classical pretreatment severity factor. The use of the modified severity factor as a tool to predict delignification, hemicellulose removal, glucan degradation and subsequent cellulose susceptibility towards enzymatic hydrolysis using [DMBA][HSO_4] as pretreatment medium is discussed in detail.

A Box-Behnken Design (BBD) response surface methodology (RSM) was applied as a tool to design experiments of different severity levels using the three key process variables: temperature, time, IL concentration. The BBD-RSM is one of the most common design of experiments (DOE) tools to evaluate the significance and the interaction of process variables and identify optimal conditions simultaneously using minimum and well-defined experiments.[13–15]

5.2 Materials & Methods

Materials and IL synthesis: Chemicals used for IL synthesis, compositional analysis and enzymatic saccharification were purchased from Sigma Aldrich and used as received with no further purification. The synthesis procedure of *N,N,N*-dimethyl-butylammonium hydrogen sulfate [DMBA][HSO_4] was described in details in section 2.2.3 in Chapter 2. **Feedstock:** Pine softwood *(Pinus sylvestris)* was obtained from Metla (Finnish Forest Research Institute. The feedstock was air-dried (7 wt% moisture content), chopped and sieved (180–850 μm, 20 + 80 US mesh scale) prior to use and stored in plastic bags at room temperature in the dark.

5.2.1 Biomass fractionation

Pretreatment, determination of oven dried weight and ionic liquid water content measurements were conducted according to the standard operating procedure from our laboratory. In short, aqueous solutions of [DMBA][HSO_4] of pre-determined water content is mixed with 2 g of biomass (on an oven-dried weight basis), corresponding to a biomass to solvent ratio of 1 : 5 $g.g^{-1}$. The cellulose rich pulp was washed thoroughly with ethanol followed by 24-hours Soxhlet extraction. Lignin was precipitated from the IL liquor, washed thoroughly with water and freeze-dried. A more detailed description of the biomass fractionation experiments can be found in section 2.2.4 in Chapter 2.

The pretreatment severity factor to disintegrate lignocellulosic biomass has been calculated according to the method developed by Chornet and Overend[10] which considers the pretreatment temperature and holding time as in the following Equation:

$$R_0 = \int_0^t e^{\frac{(T-T_0)}{14.75}} dt \qquad (5.1)$$

Under isothermal conditions, the Equation becomes:

$$R_0 = te^{\frac{(T-T_{ref})}{14.75}} \qquad (5.2)$$

where R_0 is the severity factor that has the unit of time, T is the temperature of the reaction medium in °C, T_0 is a reference temperature in °C, t is the time in minutes. The fitted value 14.75 originates from the arbitrary constant ω which is based on the activation energy when assuming pseudo first order reaction kinetics.[6] The logarithmic term of Equation 5.2 (i.e. $\log R_0$) is typically used to express the severity factor for easier expressions of numerical values.

Since catalyst and acids are typically used in aqueous based pretreatment, it was important to consider their role in the disintegration process, particularly for hemicellulose hydrolysis.[6] Therefore, an extended version of the severity factor that combines severity parameters R^0 and solution acidity $[H]^+$ was later introduced as the modified severity factor[16] calculated as:

$$\log R_0' = logR_0 - pH \qquad (5.3)$$

5.2.2 Hammett acidity measurements

IL Hammett acidity was measured using UV-Vis, combining the Beer-Lambert law (Eq. 5.5) and a modified form of the Henderson-Hasselbalch[17] (Eq. 5.6)

$$A = \varepsilon \times c \times l \qquad (5.5)$$

Where A is absorbance, ε is absorptivity, c is concentration, l is path length.

$$H_0 = pK_{BH^+} - log\left(\frac{[\varepsilon_0]-[\varepsilon]}{[\varepsilon]}\right) \qquad (5.6)$$

Where H_0 is Hammett acidity, $pK_{BH^+}$is the basicity constant of the Hammett base, ε_0 is the absorptivity of the fully unprotonated Hammett base, and ε is the absorptivity of the partially protonated Hammett base.

The pK_{BH^+} value of 4-nitroaniline is 1.00, obtained from literature.[17], The Hammett base used was selected to be 4-nitroaniline as it is suitable for the range of Hammett acidities investigated.[17,18] To determine the extinction coefficient of the fully unprotonated 4-nitroaniline $\boldsymbol{\varepsilon_0}$, six concentrations of 4-nitroaniline between 0.1mM to 1mM were prepared in anhydrous DCM. The UV-Vis spectra of these solutions were measured and using the Beer-Lambert law (Eq. 5.5), the extinction coefficient of the 4-nitroaniline $\boldsymbol{\varepsilon_0}$

was calculated using the maximum absorbance at 350 nm. The calculated coefficient in this study was 15,572 which is fairly consistent with what was reported by Grasvik *et al.*[17] To measure the extinction coefficient (ε) for each [DMBA][HSO_4]/water mixture, 1mL of 4-nitroaniline solution was transferred to a 5mL round bottom flask. The DCM was removed through rotatory evaporation and 1mL of the [DMBA][HSO_4] was added. By this method, a series of different 4-nitroaniline concentration was added for each aqueous IL solution, and a sample for the UV-Vis was prepared (total of 5 4-nitroaniline concentrations per each IL solution). The solutions were left overnight to ensure that all the 4-nitroaniline is dissolved in the IL solution. The UV-Vis spectrum of the solutions was later measured and the absorbance of the unprotonated peak at 350 nm was recorded. All Hammett acidity measurements were repeated twice, *i.e.* preparing new stock solutions of 4-nitroaniline in DCM and ionic liquid which were then diluted to the desired concentrations. All UV-Vis measurements were performed using a Perkin Elmer Lambda 650, with solutions pipetted into sealed UV-clear quartz cuvettes with a path length of 0.5 cm. A sample of the UV-vis spectrum for 80 wt% IL solution and the corresponding linear correlation are shown in the Appendix (Figure A24 and A25).

5.2.3 Box-Behnken Design

A 3-level of BBD-RSM was conducted using the three key fractionation variables using [HSO_4]-based protic ionic liquids: pretreatment time, temperature and IL concentration. The response variable was the lignin extraction or delignification. A set of 15 trials with 3 replicates at the centre point was designed using JMP-Pro. All experiments were carried out in randomized order and each of the trial point was conducted in duplicates. Table 5.1 shows the Box-Behnken design matrix of the experiment of 15 trials along with the coded (-1,0,1) and uncoded values to create the statistical design. The design of experiment, data fitting and analysis of regression model was conducted using JMP Pro software. The fit model was evaluated based on the analysis of variance (ANOVA) results of R^2 and R^2 adjusted.

Table 5.1 Experimental factors, levels and code of variables chosen for Box-Behnken design

Variable	*Coded Levels*		
	Low level (-1)	Central level (0)	High level (+1)
A: Temperature (° C)	160	170	180
B: Time (minute)	20	30	40
C: IL concentration (wt%)	70	80	90

5.2.4 Feedstock and pulp characterization

Compositional analysis was carried out according to a published procedure by the National Renewable Energy Laboratory (NREL). Compositional analysis was carried out according to a published procedure by the National Renewable Energy Laboratory (NREL) Version 54. The detailed procedure can be found in section 2.2.5 in Chapter 2. Enzymatic saccharification assays were carried out according to a protocol published by the NREL55 in duplicate with blanks. All reagents were purchased from Sigma Aldrich. The detailed procedure can be found in section 2.2.6 in Chapter 2.

5.2.5 Lignin characterization

GPC measurements were performed using an Agilent 1260 Infinity instrument equipped with a Viscotek column set (AGuard, A6000 M and A3000 M). The Agilent 1260 Infinity RID detector was used for detection. GPC grade DMSO containing LiBr (1 g L/) was used as eluent at a flow rate of 0.4 mL min^{-1} at 60 °C. Samples were prepared by dissolving 20 mg lignin in 1 mL eluent and filtering through a 0.2 μm Syringe filter. Ten pullulan standards (Agilent calibration kit, 180 < Mp < 780 000) were used to calibrate the instrument.

5.2.6 IL liquor characterization

Ionic liquid solutions were analysed by removing 200 mg of the solution with a pipette into an Eppendorf micro centrifuge tube. The exact weight was recorded, ca. 600 mg of water added and the exact weight recorded again. The tube was shaken and centrifuged with a VWR MICRO STAR 17R centrifuge at 4 °C and 13.3 G for 10 min to remove any water- insoluble material. The supernatant was pipetted off into a HPLC vial and

submitted for analysis on a Shimadzu HPLC system with RI and UV/Vis detector and an Aminex HPX-87H column (BioRad, 300 × 7.8 mm) with 0.01 M H_2SO_4 as mobile phase (0.6 mL min^{-1}). The column temperature was 55 °C and acquisition was run for 55 min. Calibration was carried out using standards with concentrations of 0.01, 0.02, 0.1, 0.2 and 0.4, 1, 2 and 4 mg mL^{-1} of glucose, xylose, galactose, arabinose, furfural and 5-HMF. Analyte concentrations in the HPLC sample were calculated using the resulting calibration curves. The mass fraction w/w of analytes detected in the ionic liquid solution (in mg g^{-1} of dried biomass) was determined using Equation:

$$w/w = \frac{c_{HPLC}.(m_{sample+}\, m_{water}).m_{IL}}{\rho_{HPLC}.m_{sample}.(1-wc_{sample}).ODW} \qquad (5.7)$$

where C_{HPLC} is the concentration of the analyte calculated using HPLC data in mg mL^{-1}, m_{sample} is the weight of the IL solution sample added in mg, m_{water} is the weight of the water added to dilute the sample in mg, m_{IL} dry IL weight added during the pretreatment in g, ρ_{HPLC} density of HPLC sample (used value is 1.045 g mL^{-1}), wc_{sample} is water content of the sample.

5.3 Results and Discussion

5.3.1 Model fitting and impact of severity variables on delignification

The values of the design parameters, experimental and predicted delignification response for pine softwood are presented in Table 5.2. The results of the ANOVA analysis are also presented in Table 5.3, highlighting that the model has a P value of <0.0001 and F value of 74. This demonstrates that the model with 99% level of confidence ($\alpha = 0.01$) and all effects can be described with a quadratic model. The model fitted the data with R^2 of 0.986 for delignification response, suggesting that there is a strong correlation coefficient between the data. The model also exhibits high adjusted R^2 and predicted R^2 values of 0.973 and 0.965, respectively, suggesting that the model has a high predictive ability and that it is unsuitable to explain only 3% variation in response. The highly comparable results in each run between the experimental and predicted delignification values can be seen in Table 5.2.

Table 5.2: Operating conditions determined by RSM-BBD method, composition and enzymatic hydrolysis yield for biomass pretreatment using [DMBA][HSO_4] and corresponding experimental and predicted delignification response

	Operating conditions			Delignification (%)	
Run	T (°C)	t (minute)	C (wt%)	Exp[b]	Pred[c]
1	170	20	90	73.74	73.36
2	180	20	80	70.27	67.51
3	180	40	80	62.74	60.20
4	170	30	80	88.68	88.39
5	160	30	70	38.41	36.16
6	160	20	80	40.43	43.17
7	160	40	80	57.98	60.77
8	160	30	90	68.85	67.24
9	170	20	70	34.11	34.27
10	180	30	90	65.01	67.81
11	170	30	80	89.07	88.39
12	170	40	90	59.35	59.19
13	180	30	70	56.28	59.36
14	170	40	70	58.59	58.74
15	170	30	80	88.10	88.39

Table 5.3: ANOVA results for model fit

Significant model terms	*All terms are significant - Quadratic model*
F - value	74
P - value	<0.0001
Lack of fits	3
R^2	0.986
R^2 *Adjusted*	0.973
R^2 *predicted*	0.965

The synergetic effect of each two variable is illustrated by the 3D response surfaces and the contour plots as shown in Figure 5.1 (A-C). The 3D delignification responses of T-t and T-C variables exhibited steep curved surfaces, which highlights the sensitivity of the response in the design space. This is also evidenced by the values in Table 5.2 where the experimental and predicted delignification efficiency varied from 35% to 88%, depending on the process variable combination (*i.e.* pretreatment severity). The contour plots highlight the regions where maximum delignification response (≥70%) is predicted. We can see that the region where high delignification is achieved is small, suggesting the sensitivity of the model to the design variables.[19] This is in alignment with the results of the 3D response surface. The results reflect that optimal fractionation in acidic [HSO_4] PILs can only be achieved in narrow window particularly at high temperatures (>120

°C). The statistical significance of the model term coefficients is presented in Table A2 in the Appendix along with the model equation to predict delignification of softwood biomass using [DMBA][HSO_4]. The analysis shows that all the quadratic model terms are statistically significant ($p < 0.01$) and therefore no term can be eliminated.

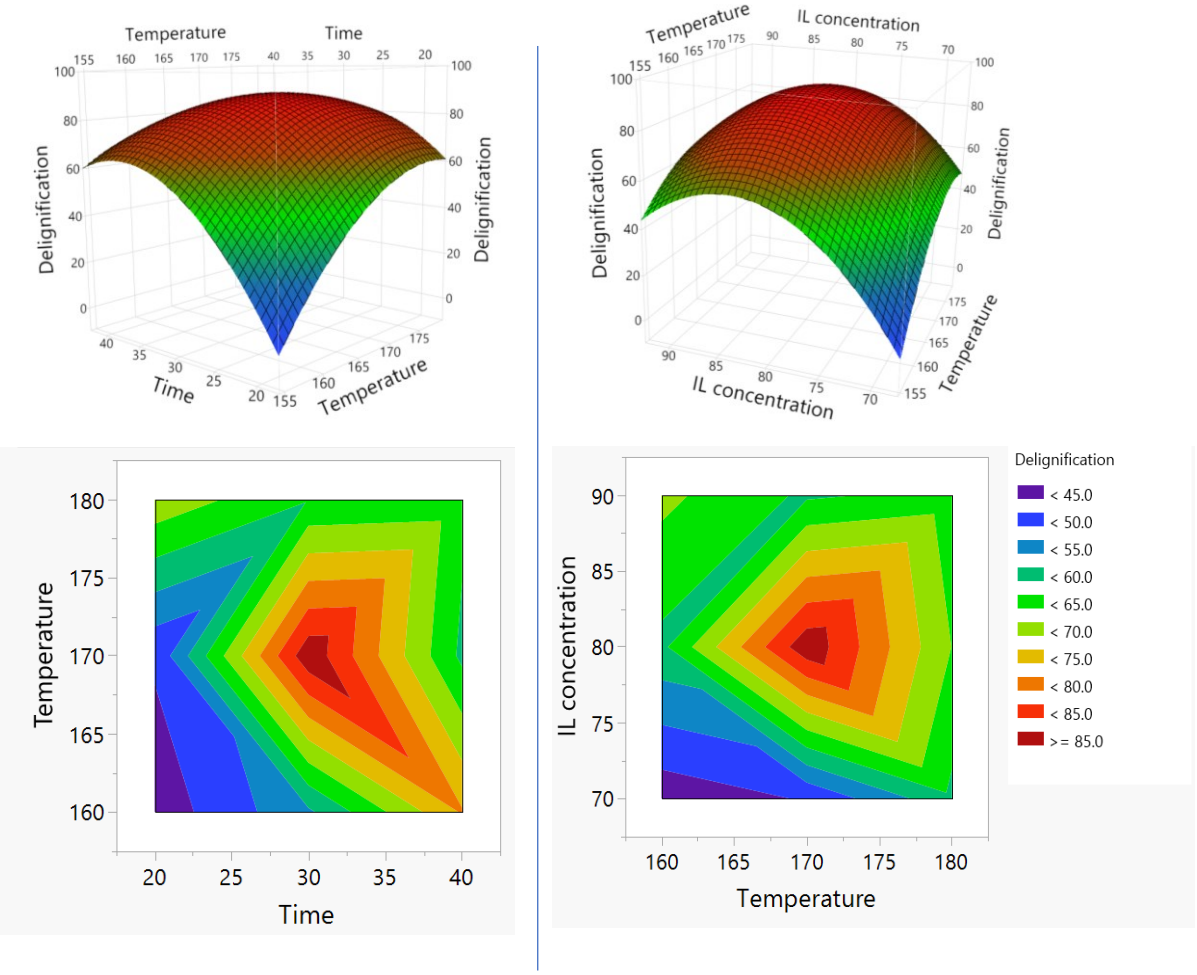

Figure 5.1: (a) BBD-RSM response surface graph (b) corresponding counter plots at the centre point – IL concentration = 80 wt% (left) Time = 30 minutes (right)

In [HSO_4]-based protic IL biomass fractionation process, low delignification is typically achieved under two operating conditions: i) low pretreatment severity where the process variables are not severe enough to effectively extract the native lignin from the biomass, or ii) very high pretreatment severity conditions used where the biomass is "overcooked" allowing the re-deposition of extracted lignin fragments and sugar dehydration products

on the cellulose surface in the form of pseudo-lignin.[20] The formation of pseudo-lignin at high severity condition is typically also associated with hemicellulose sugar dehydration products which undergo polycondensation reactions forming complex high molecular weight high aromaticity structures that are easily redeposit on the cellulose fibers .[21] Optimal delignification is achieved when the process variables are in a delicate balance to achieve the sweet spot where enough native lignin is extracted from the biomass with minimal deposition of pseudo-lignin on the cellulose surface. Runs 6 and 9 demonstrate low severity conditions where a combination of low temperature, short residence time or low IL concentration resulted in low delignification values of 40.4% and 34.1%, respectively. Runs 3, 10 and 12 illustrates how high severity conditions due to prolong residence time, high temperature or high IL concentration results in 59 % to 62% delignification response. **The design parameters that provide the optimal delignification of ~88% for pine softwood were at 170 °C for 30 minutes and using 80 wt% [DMBA][HSO_4], which represents the central point in the BBD design (run 4, 11, 15).** However, other process conditions had also achieved high delignification performance (>70%) using 170 °C, 20 minutes and 90 wt% [DMBA][HSO_4] (run 1) and 180 °C, 20 minutes and 80 wt% (run 2).

5.3.3 Modified pretreatment severity factor and its impact on fractionation

In protic ionic liquid systems such as [DMBA][HSO_4], the acidity of the medium, and therefore the severity of pretreatment, can be controlled by adjusting the acid/base ratio during synthesis or by changing the amount of water mixed with ionic liquid.[12] As part of the BBD experimental design, different IL concentrations were used. It was important to scrutinize the impact of water concentration on the acidity behavior of the pretreatment medium. Therefore, we measured the acidity of [DMBA][HSO_4] at various water concentrations. The Hammett acidity measurements were conducted by UROP student Subhashree Balaji under my supervision. Hammett acidity is a function that is typically used to measure acidity of non-aqueous media. It must be noted that a lower H_0 value means the solution is more acidic due to the higher tendency for the solution to donate protons, and thus a "higher" solution acidity (H_0 is analogous to pH, as the two scale converge in aqueous solutions). The H_0 values of [DMBA][HSO_4]/water mixtures (x_{H_2O}= 5 to 50 wt%) are reported in Figure 5.2. **[DMBA][HSO_4]/water mixtures were the least acidic with 20 to 30 wt% water and H_0 of 1.64 and 1.68, respectively. Increasing water concentration above 30 wt% showed a dramatic**

decrease in the H_0, indicating that excess amount of water increased the proton transfer ability of the medium (more acidic). At 5 wt% water in [DMBA][HSO_4], the medium acidity also increased noticeably. The effect is attributed to the lower solvation of the ILs ions at low water content (solvation limit around x_{H_2O}=20 wt%, corresponding to 75 mol%) which increases the proton chemical activity of sulfuric acid non-linearly due to a significantly reduced proton solvation energy in the absence of more basic water molecules.[22] Extremely high chemical activity of protons is associated with the relatively weak solvation in comparison with solvation by the more basic water molecules. It is interesting to note that the acidity trend of [DMBA][HSO_4] water mixtures matches the reported results by Gregorio *et al.* using 1-butyl-3-methylimidazolium hydrogen sulfate [C_4C_1im][HSO_4], an aprotic ionic liquid, when 10 and 20 mol% excess amount of acid was used during the synthesis step (i.e. acid/base ratio of 1.1 and 1.2).[23]

To calculate the pretreatment severity, it is common to use the R_0 expression which is a function of the pretreatment temperature and holding time. Fewer acid-based pretreatment studies incorporated what is called as the combined pretreatment severity factor R_0' (or $\log R_0'$ for easier use of numerical values) where the pH of the solution is also taken into consideration such that $\log R_0' = \log R_0 - pH$.[24,25] In this study, the IL concentrations used were 90, 80 and 70 wt% which corresponds to solution acidities of H_0 = 1.50, 1.64, and 1.68, respectively. It is important to express the variation in IL/H_2O mixture's acidity into the classical definition of the pretreatment severity factor to better represent and predict the severity conditions in protic [HSO_4]-based ILs pretreatment. For this reason, Hammett acidity function of the IL solutions (which is already in a logarithm format – Equation 5.6) was incorporated into the classical logarithm Equation of the pretreatment severity factor ($\log R_0$). The resulting expression is referred to as the modified pretreatment severity factor in its logarithmic format ($\log R_0^*$) calculated according to Equation 5.8:

$$\log R_0^* = \log R_0 - H_0 \qquad (5.8)$$

It should be emphasized that classical and modified severity factors are R_0 and R_0^*, respectively, however, the logarithm values will be used throughout the study to easily compare the numerical numbers.

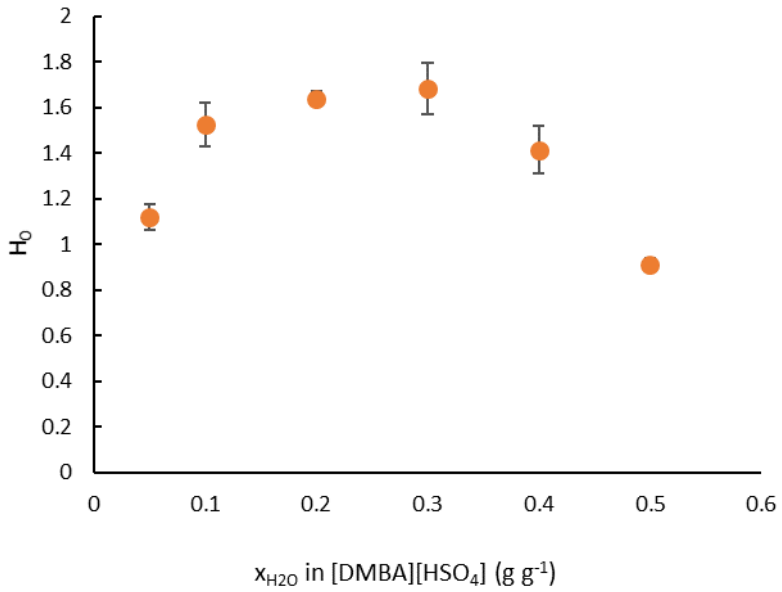

Figure 5.2: Hammett acidity value for [DMBA][HSO_4]/water mixtures

Table 5.4 presents the modified pretreatment severity factor $logR_0^*$, the severity factor $logR_0$, cellulose pulp yield, structural composition of the recovered cellulose pulps (normalized), experimental delignification values obtained by compositional analysis, as well as the enzymatic hydrolysis of the cellulose pulps to glucose. The BBD-RSM experimental runs presented in Table 5.2 were re-numbered in Table 5.4 based on the modified pretreatment severity factor $logR_0^*$ to facilitate comparison and result interpretation.

Table 5.4: Cellulose pulp structural composition after pretreatment with [DMBA][HSO_4], IL liquor composition and enzymatic hydrolysis glucose yield

#	Operating conditions			Severity factors		Cellulose pulp yield (wt%)	Cellulose pulp structural composition (%)			IL Liquor sugar and dehydration product concentration (mg.g^{-1} of biomass)					Delignification (%)	Glucose yield (%)
	T (° C)	t (min)	C (wt%)	log R_0^*	log R_0		Glucan	Hemicellulose	Lignin*	Glucose	Xylose	Mannose	Furfural	HMF		
1	180	40	80	2.32	3.96	27.1	16.8	0	10.3	50.2	70.2	4.7	16.0	23.9	62.7	64.5
2	180	30	90	2.31	3.83	34.8	23.1	0	11.7	33.1	3.0	1.5	6.7	33.1	65.01	61.8
3	180	30	70	2.15	3.83	39.1	24.2	0	14.9	60.2	15.4	8.9	9.5	20.0	56.3	77.7
4	170	40	90	2.14	3.66	37.8	25.6	0	12.2	32.3	14.9	8.6	22.4	28.6	59.4	66.7
5	180	20	80	2.02	3.66	42	34.3	0	7.8	38.7	49.8	29.2	17.7	21.2	70.3	55.2
6	170	40	70	1.98	3.66	43.8	30.1	1.6	12.1	49.2	29.7	17.3	15.2	23.0	58.6	68.6
7	170	30	80	1.90	3.54	43.4	39.1	0.7	3.6	48.2	66.8	39.1	26.6	31.6	88.10	94.9
8	170	30	80	1.90	3.54	43.4	39.8	0.6	3	48.8	67.9	39.5	25.7	33.4	88.7	95.1
9	170	30	80	1.90	3.54	43.9	39.7	0.7	3.2	48.6	67.5	39.8	26.0	32.5	89.1	94.1
10	170	20	90	1.84	3.36	50.5	37.6	0	12.9	24.9	46.0	27.0	16.1	17.9	73.7	90.1
11	160	40	80	1.73	3.37	44.6	34.2	1.3	9.1	24.7	31.0	18.2	13.4	14.6	57.9	80.5
12	160	30	90	1.72	3.24	47.5	39.1	0.8	7.5	19.0	32.1	16.4	15.2	16.4	68.8	87.6
13	170	20	70	1.68	3.36	60.7	38.2	2.9	19.7	26.4	87.0	51.1	13.8	16.1	34.1	32.7
14	160	30	70	1.56	3.24	57.1	36.8	3.6	16.7	29.3	74.0	43.5	11.5	11.8	38.4	44.4
15	160	20	80	1.43	3.07	64.6	42.2	4	18.4	16.8	66.9	39.3	10.1	6.3	40.4	23.1
UB*	-	-	-	-		-	44.5	25	29.9	-	-	-	-	-	-	1.97

[a]sum of acid insoluble lignin (AIL) and acid soluble lignin (ASL) obtained from compositional analysis
* Untreated pine softwood

Based on the different combinations of process variables used in BBD-RSM experiments, the modified pretreatment severity factor $logR_0^*$ spanned from 1.4 to 2.3, representing the lowest and highest severity conditions, respectively. On the other hand, the pretreatment severity factor spanned from $logR_0$ from 3.1 to 4. The incorporation of the IL medium's acidity (H_0) into the classical severity factor created a variation in the pretreatment severity level between experimental runs were temperature and time remained constant. For example, run 2 and 3 both operated at 180 °C and 30 minutes and therefore both runs had an identical $logR_0$ of 3.83 despite the difference in the IL concentrations 90 wt% and 70 wt% and corresponding medium acidity of 1.50 and 1.68, respectively. Similarly, run 12 and 14, 10 and 13, run 4 and 6 had identical severity factors of 3.24, 3.36 and 3.66, respectively as temperature and time remained constant using the classical severity factor Equation. Despite the identical severity conditions, the runs have resulted in vastly different delignification responses due to the different medium acidity (*i.e.* wt% IL concentration used). For example, run 10 and 13 both had an identical $logR_0$ of 3.36 whereas the corresponding delignification varied significantly from 73% to 34%, respectively. **Using $logR_0^*$ which incorporates the IL acidity corrected the severity factor for the run 10 and 13 to 1.84 and 1.68 better reflect and the large difference in delignification performance**. Cellulose pulp yield (*i.e.* recovered cellulose-rich residues after pretreatment) was highly variable ranging from 27 wt% to 60 wt% depending on the modified severity factor and delignification efficiency. The highest severity conditions were runs 1 and 2 ($logR_0^*$ of 2.32 and 2.31) resulting in the lowest cellulose pulp yields of 34.8 and 27.1 wt%, respectively and delignification of 65 and 61%, respectively. **The low cellulose pulp yields despite the relatively high delignification reflect the severe degradation of cellulose along with extraction of hemicellulose and lignin.** It should be noted that the remaining ~30% lignin on the cellulose pulp at such high severity conditions reflects both the non-extracted native lignin as well as the redeposited pseudo lignin. From the residual lignin content in the recovered cellulose pulps, we can clearly see that only few operating conditions effectively extracted lignin, achieving ≥70% delignification (*i.e.* runs 5, 10 and 12 the central BBD runs 7 to 9). High severity experiments with $logR_0^*$ 2.14 to 2.32 resulted in a milder delignification of 55 to 65%.

The fit of the classical severity factor $logR_0$ and the modified severity factory $logR_0^*$ with delignification, hemicellulose removal/solubilization and glucan solubilization obtained

from the compositional analysis data as presented in Figure 5.3. The correlations of the two severity factors with delignification were expressed as quadratic fitting considering the results obtained by the BBD-RSM analysis where delignification showed a steep curvature and an optimal point given the low biomass delignification obtained at low and high severity conditions. On the other hand, the severity factors correlated linearly with the polysaccharide (cellulose and hemicellulose). Comparing the fittings between $logR_0^*$ and $logR_0$, we can see that fitting the data against $logR_0^*$ improved the fitting for hemicellulose solubilization and delignification whereas the fitting for glucan solubilization seemed to be largely unchanged between the classical and the modified severity factors. **The more significant improvement in hemicellulose removal and delignification fittings upon introducing H_0 reflects the higher sensitivity of hemicellulose and lignin removal by the acidity of the medium, while glucan losses and degradation seem to be less affected with variation in medium acidity, at least within the design space investigated. The outcomes also indicate the modified severity factor can be used to better predict the pretreatment outcomes relative to the classical expression.**

From Figure 5.3-a, we can see that there is a clear-cut of required $logR_0^*$ 1.8 to 1.9 to achieve ~70 to 90% delignification for pine softwood whereas $logR_0^*$>1.9 result in lower delignification of ~55 to 65% and $logR_0^*$<1.7 shows low delignification of ~35 to 40%. Hemicellulose solubilization fitted data showed that hemicellulose is more effectively solubilized when the modified severity factor is at 1.98 and higher with complete solubilization at severity factors of ~ 2.3. Glucan solubilization ranged between 5 to 20% when the pretreatment severity was <1.9. At severity levels >1.9, we notice a significant increase in glucan degradation in the IL liquor reaching up to 60% losses at the highest severity of 2.32**.** As mentioned in earlier chapters, glucan losses up to 10% is normal as glucan is considered one of the hemicellulose polymers. However, higher amounts of glucan losses to the IL liquor indicates that the cellulose is being attacked and started to hydrolyse due to the high severity conditions. At the optimal conditions identified earlier of 170 °C, 30 minutes and 20 wt%, delignification corresponded to 88%, hemicellulose removal 97% and glucan solubilization 10% and the conditions correspond to $logR_0^*$ of 1.9.

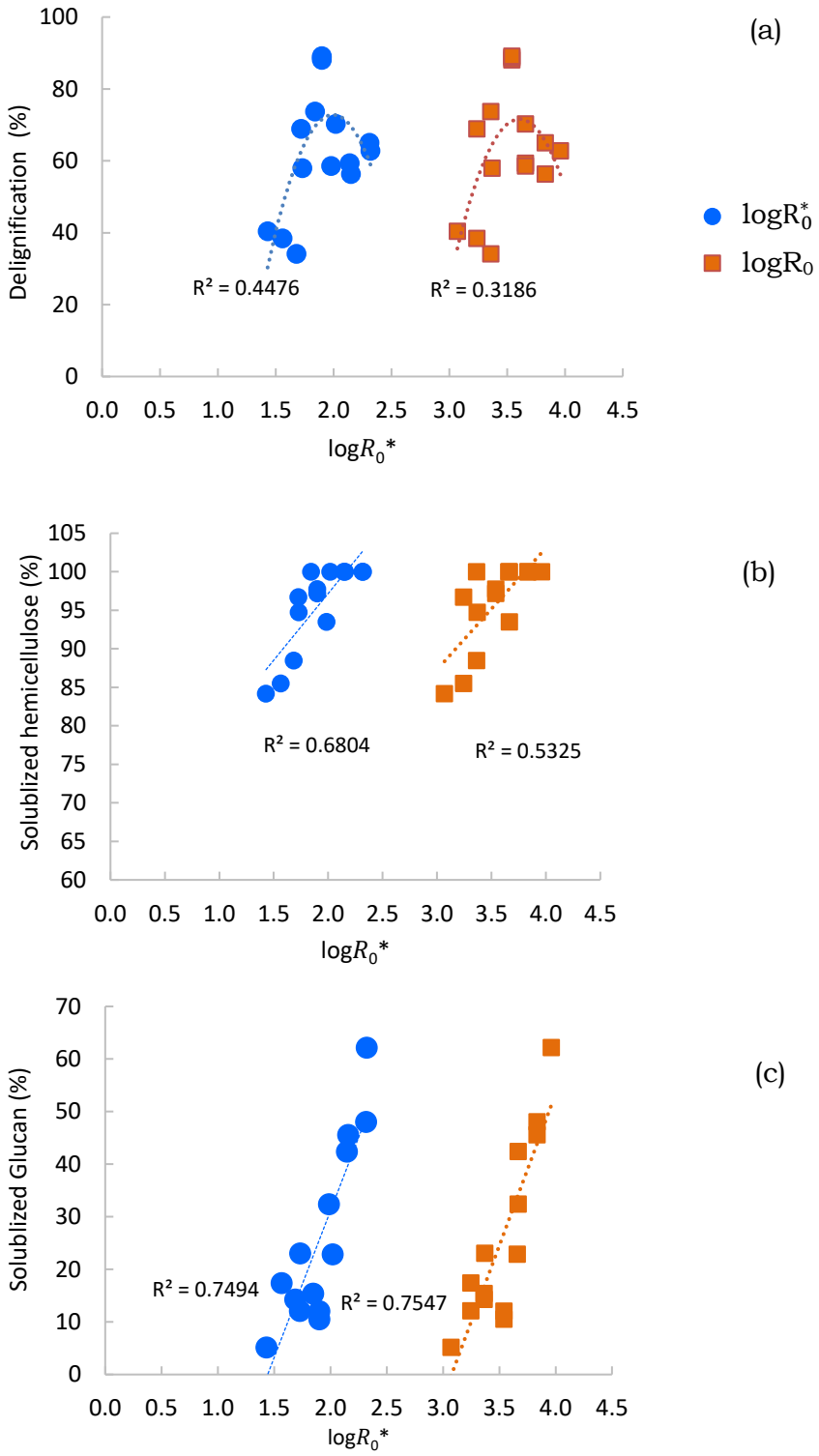

Figure 5.3: Pretreatment severity factor correlation with a) lignin removal, b) solubilized hemicellulose, c) solubilized glucan using $\log R_0$ and $\log R_0^*$ terms

Glucose yields from enzymatic hydrolysis of recovered cellulose pulps show a high variation in response ranging between 23% to 95% relative to theoretical maximum (Figure 5.4-a). There is an overall positive correlation between glucose yield and lignin extraction which was also observed in the previous chapter as well as previous studies.[26] The reason behind the positive correlation is generally related to the higher surface area exposure of cellulose substrate, allowing easier access to enzymes to hydrolyse it. The variation in glucose yield depending on the modified severity factor is presented in Figure 5.4-b. Similar to delignification trend with $\log R_0^*$, glucose release from cellulose pulps were the highest at $\log R_0^*$ 1.7 to 1.9 ranging between 80 to 90% relative to theoretical maximum. At high severity factor, the glucose yield drops to <70% whereas at low severity factor glucose yield are <40%.

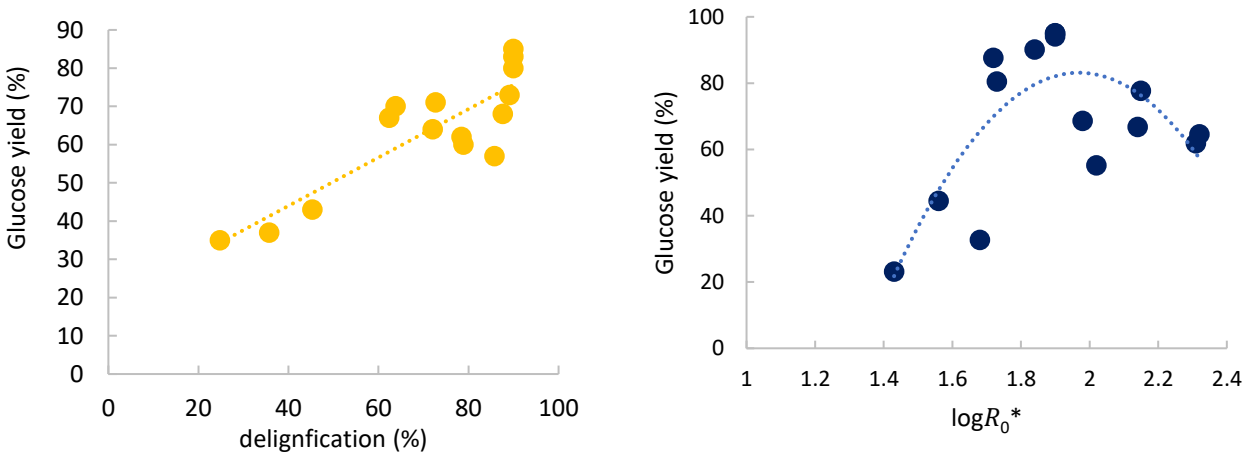

Figure 5.4: Correlation between glucose yield and lignin extraction. Enzymatic hydrolysis was conducted for 72 hours and pretreatment conditions are summarized in Table 5.5

However, it is important to note that there are experimental conditions where delignification values alone do not entirely reflect and explain the glucose yield obtained. For example, runs 14 and 15 resulted in very similar delignification values of 38% and 40%, respectively, whereas the glucose yields corresponded to 44% and 23%, respectively. Similarly, the central point condition (170 °C, 30 minutes, 80 wt% IL) resulted in a near-quantitative glucose yield of ~95% ($\log R_0^*$ of 1.9, delignification 88%) and run 10 (170 °C, 20 and 90 wt% IL) also resulted in a 90% glucose yield, despite the slightly lower delignification achieved of 73%. **This variation in glucose yield despite**

the similar level of delignification, or vice versa, highlights the important influence other factors could have on glucose yield such as the characteristics of the residual lignin on the cellulose pulp impacted by the pretreatment severity level. A similar effect was also observed in the previous chapters (Chapter 2 and Chapter 4) where it was evidenced that lignin properties had strong impact on the release of glucose from cellulose, under the assumption that recovered lignin have similar characteristics to residual lignin on pulp. Figure 5.5 shows a real image of the air-dried cellulose recovered fibers after the pretreatment. There is a clear variation in the cellulose fiber brightness and color which reflects in a visual way the impact of pretreatment severity on the amount and characteristics of residual lignin in (or on) the recovered cellulose.

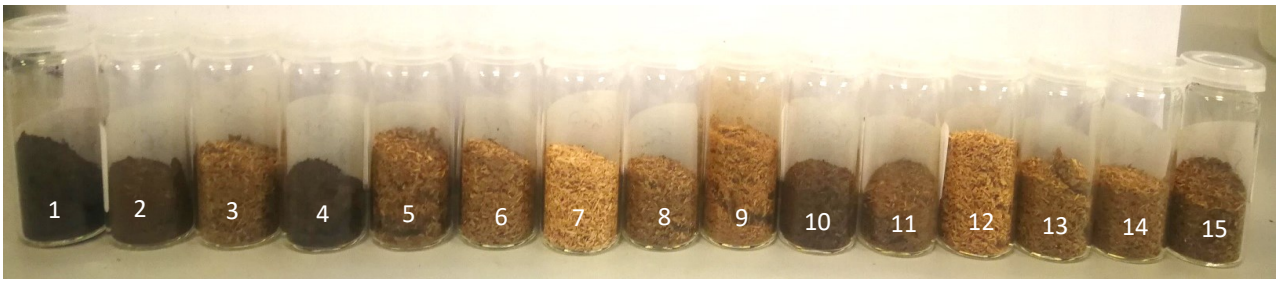

Figure 5.5: images of recovered cellulose fibers from BBD-RSM experiments. The numbering of the vials follows the same order as the numbers in Table 5.4

The composition of the soluble sugar monomers, furfural and 5-HMF found in the IL liquor relative to the biomass (mg g^{-1}) is presented in Table 5.4. **Optimal delignification conditions (*i.e.* central point run 7 to 9) have yielded 2.5 wt% furfural and 3.2 wt% 5-HMF relative to untreated biomass. Although these yields are low, they are still promising especially as the process is not optimized to produce these compounds.** Current industrial furfural production processes depend on the use of agricultural residues (corncobs in China and bagasse in South Africa). Quaker Oats Technology in China uses continuous fixed bed reactors followed by azeotropic distillation to isolate the furfural.[27] The yield of furfural in the process is 4 to 12% with respect to the dry weight biomass. Other more advanced processes such as SupraYield yields 50 to 70% furfural, however the process uses higher operating temperatures (240 °C) which allows more efficient conversion of sugars to furfural.[27] Therefore, with slight modification and

optimization of operating conditions, the ionoSolv process show high promise to be used for furfural production. 5-HMF is also a key platform chemical in the biorefinery, however, the production of 5-HMF in high yield as well as its separation from the reaction medium is far more challenging than furfural (b.p 114 °C at 1 mbar), and therefore industrial production of 5-HMF remains at an early stage of development.[28,29] It is important to note that furfural and 5-HMF are considered as fermentation inhibitors in aqueous-based pretreatment processes such as steam explosion and dilute acid pretreatment as cellulose is not isolated/filtered prior to the enzymatic hydrolysis or fermentation step. Therefore, fractionation methods such as [HSO4]-based PIL offer a key advantage in this regard, where fermentation inhibitors (i.e. sugar dehydration products) are formed during the pretreatment, however they do not enter the downstream steps.[5]

Figure 5.6 also shows the yield of hemicellulose components calculated based the initial composition of each component precursor in untreated biomass. It is important to note that the yield of furfural (dehydration product of C5 sugars) was calculated based on the initial composition of xylose and arabinose whereas the yield of 5-HMF (dehydration product for C6 sugars) was calculated based on the initial composition of glucose and galactose in the untreated biomass. The largest component of hemicellulose polymer in pine softwood used in this study is mannan where it composed of 13.5% (55% of total hemicellulose polymer), followed by xylan with 5.1% (*i.e.* 20% of total hemicellulose) with arabinan and galactan accounting equally for the balance remaining.

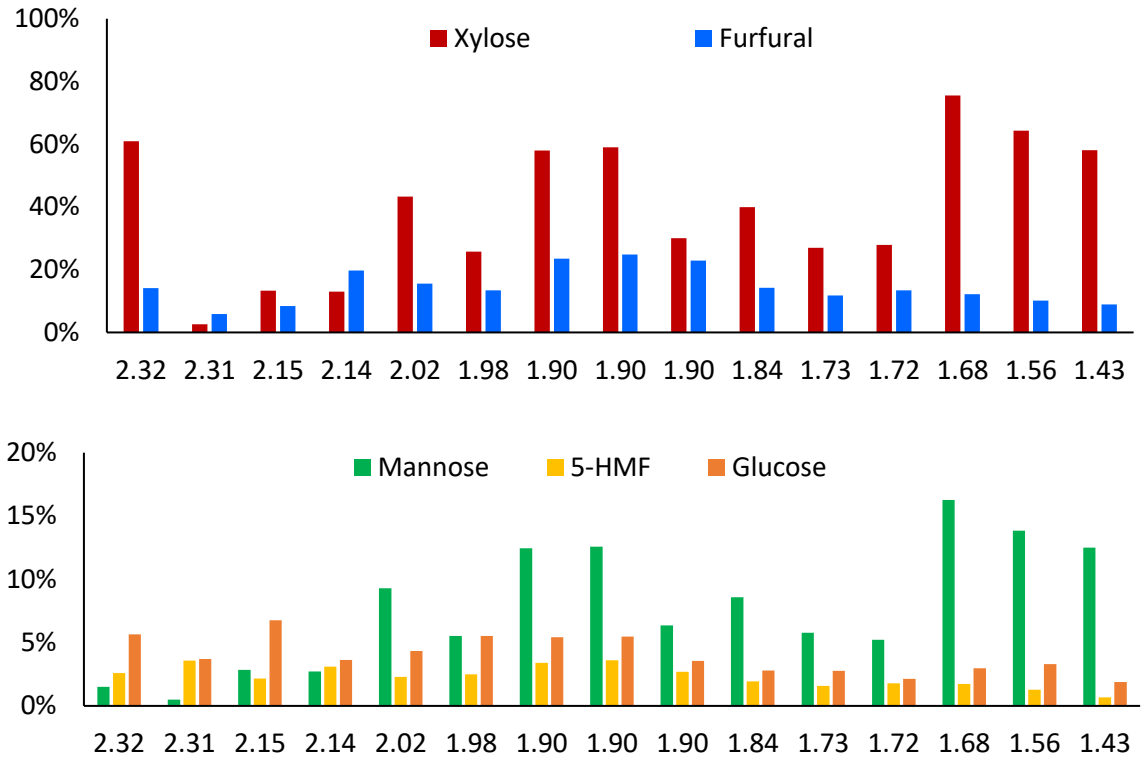

Figure 5.6: Hemicellulose component in IL liquid liquor. Pine softwood was pre-treated according to the conditions presented in Table 5. Values were calculated relative to total amount of biomass added (20 wt% relative to IL); monomer sugars (glucose, xylose, mannose) were calculated based on their initial amount in untreated softwood pine. Furfural based on initial xylose and arabinose in untreated biomass and 5-HMF based on initial glucose and mannose in untreated biomass.

From Table 5.4 and Figure 5.6, it was observed that although pretreatment with [DMBA][HSO_4] resulted in removing >80% of hemicellulose at all operating conditions with quantitative removal under several conditions, the detected mannose sugar did not exceed 18% of the maximum whereas xylose sugar monomers were detected at higher quantities. Even when considering the dehydration product yields, there is still a high discrepancy between the hemicellulose removal and the detected soluble sugar monomers in the IL medium. **This indicates that there is a high portion of the hemicellulose that cannot be detected in monomeric form or as dehydration products.** To have a clearer picture of the fate of the hemicellulose components and partitioning in the process streams, it is important to perform mass balance for the hemicellulose component. Table 5.5presents the numerical values for the mass balance related to the detected hemicellulose components in the IL liquor in mol% relative to the initial hemicellulose content in the biomass. The undetected fraction is calculated based

on the balance difference between the sum of hemicellulose residual in the cellulose pulp and detected hemicellulose compounds in the liquor. **It can be clearly seen that across all operating conditions, the "undetected" hemicellulose accounted for the most significant part of the mass balance, ranging between 67 to 91%.** Brandt *et. al* have also observed that a significant portion of the hemicellulose was missing while performing mass balances particularly at high severity conditions (*i.e.* 120 °C , 20 wt% [TEA][HSO_4] for 24 hours, *Miscanthus* feedstock) with "undetected" hemicellulose corresponding to 60%.[20]

Table 5.5: Hemicellulose mass balance in IL liquor in the form of dissolved sugar monomers and dehydration products, residual hemicellulose in the recovered cellulose pulp and the balance

Run	logR_0*	Conditions			Dissolved hemicellulose sugars[2]	Dissolved dehydration products[3]	Hemicellulose in pulp[4]	Undetected[5]
		T (° C)	t (min)	C[1] (wt%)				
1	2.32	180	40	80	13.00%	8.50%	1.40%	77.10%
2	2.31	180	30	90	0.78%	7.60%	0.00%	91.62%
3	2.15	180	30	70	4.22%	6.10%	0.00%	89.68%
4	2.14	170	40	90	4.08%	11.00%	4.50%	80.42%
5	2.02	180	20	80	13.72%	8.50%	0.00%	77.78%
6	1.98	170	40	70	8.16%	8.10%	1.00%	82.74%
7	1.90	170	30	80	18.39%	12.70%	0.80%	68.11%
8	1.90	170	30	80	18.65%	12.80%	1.10%	67.45%
9	1.90	170	30	80	18.55%	12.40%	1.10%	67.95%
10	1.84	170	20	90	12.67%	7.50%	0.00%	79.83%
11	1.73	160	40	80	8.55%	6.20%	0.00%	85.25%
12	1.72	160	30	90	8.43%	7.00%	5.50%	79.07%
13	1.68	170	20	70	23.98%	6.50%	2.70%	66.82%
14	1.56	160	30	70	20.41%	5.20%	2.30%	72.09%
15	1.43	160	20	80	18.43%	3.80%	6.60%	71.17%

[1]H_0 values for 90, 80 and 70 wt% aqueous [DMBA][HSO_4] solution is 1.50, 1.64 and 1.68, respectively. [2]sum of xylose and mannose sugars in IL liquor, [3]sum of furfural and 5-HMF in IL liquor, [4]sum of hemicellulose components in pulp, [5]reminder balance

A potential reason for the significant undetected portions of hemicellulose in this study could be due to the solubilization of hemicellulose polymers in the form of large oligomers in the IL liquor. For example, Kabel *et al.* investigated the xylan solubility after wheat straw pretreatment using mild acid pretreatment medium (1 to 2 wt% H_2SO_4) and detected various amounts of xylan oligomers in the pretreatment medium depending on the pretreatment severity level.[31] However, Brandt *et al.* reported that it is unlikely for sugar oligomers to have high solubility in protic [HSO_4] IL liquors as hemicellulose components were able to be detected in their monomeric form with 100% mass balance

closure when low severity pretreatment is performed (*i.e.* 120 °C , 20 wt% [TEA][HSO_4] for 1 hour).[20] In addition, the high acidity of the medium should also promote the hydrolysis of these large oligomers. **This leaves us with the second more plausible route for the fate of solubilized hemicellulose sugars in protic [HSO_4]-based ILs, which is their transformation to soluble and insoluble humin/pseudo lignin structures.**[32] The soluble structures remain in the IL liquor during the course of pretreatment whereas the insoluble part redeposits onto the cellulose surface. Figure 5.7 presents a hypothesized reaction pathway for pseudo lignin formation starting from the dehydration of C5 and C6 sugars to furfural and 5-HMF.[33] Both furfural and 5-HMF can be converted to aromatic compounds which are key precursors for pseudo lignin formation via polymerization reactions.

According to the mass balance, the two conditions with the highest modified severity factors are: $\log R_0^*$ 2.32 (180 °C, 30 mins, 80 wt% IL) and $\log R_0^*$ 2.31 (180 °C, 30 mins, 90 wt% IL) resulted with the "undetected" hemicellulose fraction of 77% and 91%, respectively, with the main variation stemming from the dissolved sugar in the IL medium. The discrepancy is also clear when comparing the detected soluble sugars in the IL medium between the two runs (Figure 5.6). This result highlights that despite the similarity of the resultant $\log R_0^*$ between two experimental runs, the combinations of parameters of temperature, time and IL concentrations have huge impact on the chemistry and fate of the hemicellulose components in the system, and therefore the value of $\log R_0^*$ alone cannot be used to predict the fate of dissolved hemicellulose sugars in the IL medium. The medium with higher acidity (*i.e.* 90 wt% IL, H_0 1.50) resulted in less detectable sugars in the IL medium and therefore a higher "undetected" portion in the mass balance. This agrees with the with the more prompted polymerization of hemicellulose derived components (furfural and 5-HMF) at high severity conditions to form pseudo lignin in acidic pretreatment. The impact of the IL medium acidity on the hemicellulose components seems to be more pronounced in lower severity conditions. For example, comparing run 10 (170 °C, 20 mins, 90 wt%, $\log R_0^*$ = 1.84) and run 13 (170 °C, 20 mins, 70 wt%, $\log R_0^*$ = 1.68), there is a noticeable variation between the "undetected" hemicellulose, with higher severity and more acidic IL resulting in higher unaccountable portion of hemicellulose, indicating higher formation of pseudo lignin production.

On other hand, leaving the pretreatment for longer time (*i.e.* increasing the severity level) tends to mask the effect of the IL acidity as run 4 and 6 both had very similar fraction of undetected hemicellulose of 80 and 82%, respectively. **It is very interesting to note that the conditions where optimal delignification was achieved (*i.e.* central point, 88% delignification) corresponded to the lowest "undetected" hemicellulose**, **indicating the lowest formation of pseudo lignin products.**

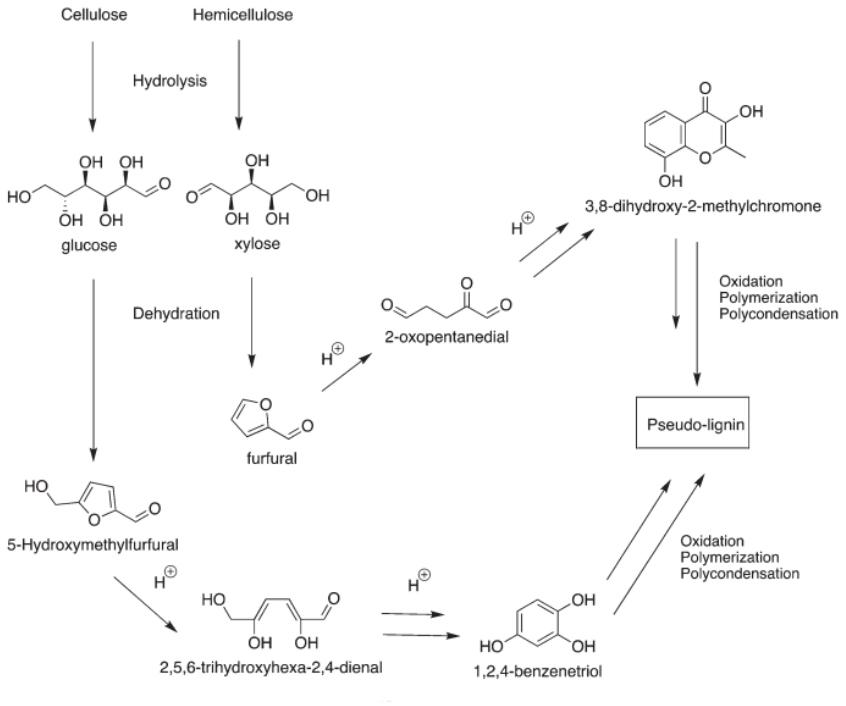

Figure 5.7: Proposed mechanism for pseudo lignin formation in acidic pretreatment mediums based on furfural and 5-HMF sugar dehydration products formed in the pretreatment medium. Taken from reference 35

At lower or higher severity conditions than 1.9, there was less of the dehydration products found in the IL liquor which is either due to less initial extraction of hemicellulose (low severity conditions) or polycondensation reactions of these products (high severity conditions). For example, 20% of hemicellulose was quantified as sugar monomers (xylose and mannose) at run 13 and 14 ($logR_0^*$ of 1.68, 1.56), however only 5-6% dehydration products were formed as formation of furfural and 5-HMF typically requires high severity conditions. The dehydration reaction to produce furfural typically requires high temperatures/severity conditions.[34] On the other hand, high severity condition where $logR_0^* > 1.9$, the dehydration products yield varied from 6 to 11%. Run 4 ($logR_0^*$ of 2.14) has the 2nd highest dehydration product yield after the central point,

however there was only 4% detectable monosaccharide sugars in the IL liquor. This indicates the excess of the sugars formed dehydration which subsequently were polymerized and condensed, forming pseudo lignin.

Sipponen and co-workers studied the impact of hot water pretreatment severity on the generation of pseudo lignin from wheat straw, and their study elucidated that higher severity induced the accumulation of more pseudo-lignin within the temperature range of 170–200 °C.[35] Ma *et al.* also reported that high severity conditions promoted the formation of aromatic-rich pseudo lignin structures from the aliphatic structures at lower severity.[36] Hu and Ragauskas investigated introducing DMSO during dilute acid pretreatment to supress the formation of 5-HMF, a key intermediate in pseudo lignin formation, without impacting the pretreatment severity conditions. They found that introducing dimethyl sulfoxide (DMSO) successfully reduced pseudo lignin by 30% due to the stronger coordination of 5-HMF with DMSO rather than 5-HMF with water.[37] Since the formation of pseudo lignin structures is associated with oxidation-polymerization reactions (Figure 5.7), the study also examined the role of oxygen in pseudo lignin formation during dilute acid pretreatment. High severity experiments conducted under an oxygen environment resulted in 89% formation of pseudo-lignin vs. 49% under an inert nitrogen environment and 42% under air. These results suggest that N_2 can supress oxidative reactions leading to pseudo lignin formation however it cannot eliminate other non-oxidative reaction pathways that also lead to pseudo lignin formation.[37]

As evidenced by the delignification values, using [HSO_4]-based protic ILs provides a narrow window for optimal delignification. Therefore, it might be necessary to investigate methods to supress pseudo lignin formation in the ionoSolv process during the pretreatment in the future, particularly if high or low severity conditions are needed to be used without compromising cellulose quality. Alternatively, it might be also worth considering using multi-stage extractions that aim to maximize delignification and remove hemicellulose components in the first stage followed by a second extraction stage. By removing the hemicellulose in the first stage at low severity conditions, pseudo lignin formation should be significantly suppressed in the second stage of extraction. Re-evaluating the severity conditions will also change slightly based on the reactor design and configuration.

The formation of pseudo lignin is typically associated with excess Kalson lignin (acid insoluble lignin) relative to the untreated biomass. In addition to the Kalson lignin values, pseudo lignin can also be indicated with a noticeable increase in the precipitated lignin upon water addition, which can also exceed the initial lignin content in the biomass. Figure 5.8 presents the lignin mass balance considering the residual lignin remaining in the pulp, the precipitated recovered lignin fraction after water addition, and the remaining lignin fragments in the IL liquor. **The lignin that remains in the IL liquor even after the addition excess amount of water as anti-solvent (3 equivalent) must have low molecular weight and large number of hydrophilic groups to retain high solubility in water**. **Comparing the values of residual lignin in the pulp with the initial lignin content in the biomass (29.9%), we can clearly see that there were two runs that corresponded to the highest severity (logR_0^* 2.32 and 2.31) and yielded Kalson lignin > 29.9% as well as exceptionally high lignin yields of >80%.** This clearly indicates the formation of pseudo lignin, as 18 wt% of pseudo lignin structures were formed at those high severity conditions. The formed pseudo lignin partitioned between i) soluble fraction that remained in the IL liquid during the course of the pretreatment and precipitated along with extracted lignin upon the addition of water, and ii) insoluble fraction that redeposited on the cellulose fibers during the course of the pretreatment. The lignin yield obtained during optimal delignification conditions (logR_0^* 1.9) was 42% whereas lignin yield obtained in the severe pretreatment conditions were 81 to 85%. Therefore, we can see that most of the pseudo lignin structures remained soluble in the IL liquor and then precipitated with extracted lignin upon water addition due to its high polyaromaticity structural features and insolubility in water. On the other hand, a smaller fraction of higher molecular weight (M_w) pseudo lignin structures redeposited on the solid cellulose fibers during the course of the pretreatment, decrease cellulose accessibility to enzymes and blocking the active binding site.[33] At the optimal conditions, 88% delignification was achieved and out of this only 42% of lignin precipitated, and the remaining lignin fragments remained soluble in the IL liquor after diluting the IL solution substantially. This is further evidence that the lignin fragments during these conditions were not modified and less aromatic and therefore remained soluble in the diluted IL solution.

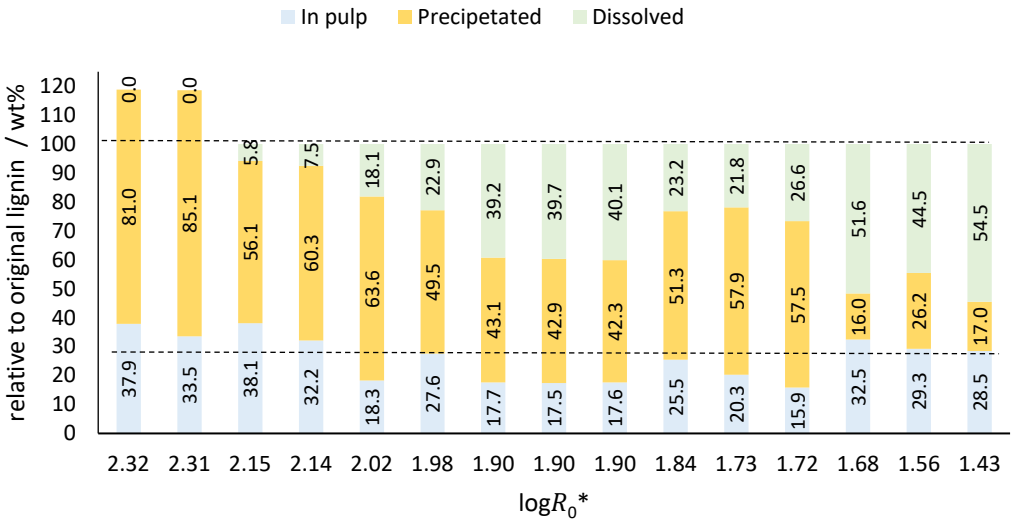

Figure 5.8: Lignin mass balance. Pine softwood was pre-treated according to the conditions presented in Table 5. Values were calculated relative to the initial lignin content in the untreated biomass. Pulp lignin is the sum of acid insoluble lignin and acid soluble lignin obtained from compositional analysis. Precipitated lignin is the lignin obtained after water addition as anti-solvent. Dissolved lignin is the lignin remaining in the IL liquor calculated as the remaining balance. Dotted lower line represents the initial lignin in the untreated biomass (29.9%) and dotted upper line represent the 100% balance closure

Table 5.6 presents the molecular weight characterization of the precipitated lignin. Runs 1 and 2 have highly polydisperse lignins with PDI of 8.5 and 8.3, respectively. The high PDI values indicate the highly diverse and branched structure of the lignin and pseudo lignin formed via polycondensation reactions of sugar intermediates, causing broad molecular weight distributions. Interestingly, the average M_w of the lignin produced in runs 1 and 2 was 62,000 g mol^{-1}, which is lower than the average Mw of the lignin extracted at the optimal delignification conditions of 69,000 g mol^{-1}. However, the PDI of the precipitated lignin at the optimal condition was ~5 , indicating that the lignin is less modified compared the lignin/pseudo lignin precipitated at high severity conditions. On the other hand, low severity conditions such as runs 11 and 13 showed a low PDI of 3 and 2.7, respectively. It is interesting to note that when the pretreatment was conducted at 180 °C or 160 °C, the number average molecular weight M_n was <1000 for all runs. At 180 °C, the lignin chains were short, yet they had high M_w due to the high severity conditions ($logR_0^*$ > 2) and the competing polycondensation and fragmentation reactions of the extracted lignin/pseudo lignin. On the other hand, at 160 °C fractionation runs ($logR_0^*$1.4 to 1.7), the lignin chains also had low M_n which reflects the extraction of smaller polymer chains due to the low delignification, or similarly, competing polycondensation and fragmentation reactions.

Table 5.6: Mw, Mn and PDI for extracted precipitated lignin at different severity conditions

Run	T (° C)	t (min)	IL (wt%)	$logR_0^*$	M_n (Da)	M_w (Da)	PDI (M_w/M_n)
1	180	40	80	2.32	754	6256	8.3
2	180	30	90	2.31	736	6229	8.5
3	180	30	70	2.15	685	2904	4.2
4	170	40	90	2.14	1457	6864	4.7
5	180	20	80	2.02	706	3960	5.6
6	170	40	70	1.98	1356	5490	4.0
7	170	30	80	1.90	1435	6803	4.7
8	170	30	80	1.90	1337	6832	5.1
9	170	30	80	1.90	1453	7266	5.0
10	170	20	90	1.84	1332	4019	3.0
11	160	40	80	1.73	882	5695	6.5
12	160	30	90	1.72	732	4506	6.2
13	170	20	70	1.68	1272	3372	2.7
14	160	30	70	1.56	705	2623	3.7
15	160	20	80	1.43	838	3143	3.8

5.4 Conclusion

The impact of pretreatment severity in acidic protic [DMBA][HSO_4] IL using pine softwood was investigated using a modified severity factor that takes into account IL solution's acidity. A BBD-RSM method was used as a tool to design the experimental space of various severity levels considering pretreatment time, pretreatment temperature and IL concentration as process variables. The modified severity factor was correlated with fractionation process indicators (delignification, hemicellulose removal and glucan solubilization). The use of the modified severity factor showed an improved correlation with the fractionation indicators relative to the classical pretreatment severity factor, indicating it can better predict the pretreatment outcomes, particularly for delignification and hemicellulose removal. The fate of hemicellulose components and their conversion to pseudo lignin structures and its impact on the precipitated lignin properties was also investigated and correlated to the modified pretreatment severity factor. It was found that the use of $logR_0^*$ alone cannot be used to predict the fate of dissolved hemicellulose sugars in the IL medium given the complex reaction pathways wit dissolved lignin fragments.

References

(1) Gschwend, F. J. V.; Brandt-Talbot, A. Rapid Pretreatment of Miscanthus Using the Low-Cost Ionic Liquid Triethylammonium Hydrogen Sulfate at Elevated Temperatures. Green Chem. 2016, 20 (15), 3486–3498. https://doi.org/10.1039/c8gc00837j.

(2) Satari, B.; Karimi, K.; Kumar, R. Cellulose Solvent-Based Pretreatment for Enhanced Second-Generation Biofuel Production: A Review; Royal Society of Chemistry, 2019; Vol. 3. https://doi.org/10.1039/c8se00287h.

(3) Gschwend, F. J. V.; Chambon, C. L.; Biedka, M.; Brandt-Talbot, A.; Fennell, P. S.; Hallett, J. P. Quantitative Glucose Release from Softwood after Pretreatment with Low-Cost Ionic Liquids. Green Chem. 2019, 21 (3), 692–703. https://doi.org/10.1039/c8gc02155d.

(4) Sadeghifar, H.; Wells, T.; Le, R. K.; Sadeghifar, F.; Yuan, J. S.; Jonas Ragauskas, A. Fractionation of Organosolv Lignin Using Acetone:Water and Properties of the Obtained Fractions. ACS Sustain. Chem. Eng. 2017, 5 (1), 580–587. https://doi.org/10.1021/acssuschemeng.6b01955.

(5) Balan, V. Current Challenges in Commercially Producing Biofuels from Lignocellulosic Biomass. ISRN Biotechnol. 2014, 2014 (i), 1–31. https://doi.org/10.1155/2014/463074.

(6) Pedersen, M.; Meyer, A. S. Lignocellulose Pretreatment Severity - Relating PH to Biomatrix Opening. N. Biotechnol. 2010, 27 (6), 739–750. https://doi.org/10.1016/j.nbt.2010.05.003.

(7) Alvarez-Vasco, C.; Zhang, X. Alkaline Hydrogen Peroxide (AHP) Pretreatment of Softwood: Enhanced Enzymatic Hydrolysability at Low Peroxide Loadings. Biomass and Bioenergy 2017, 96, 96–102. https://doi.org/10.1016/j.biombioe.2016.11.005.

(8) Agnihotri, S.; Johnsen, I. A.; Bøe, M. S.; Øyaas, K.; Moe, S. Ethanol Organosolv Pretreatment of Softwood (Picea Abies) and Sugarcane Bagasse for Biofuel and Biorefinery Applications. Wood Sci. Technol. 2015, 49 (5), 881–896. https://doi.org/10.1007/s00226-015-0738-4.

(9) Rastogi, M.; Shrivastava, S. Recent Advances in Second Generation Bioethanol Production: An Insight to Pretreatment, Saccharification and Fermentation Processes. Renewable and Sustainable Energy Reviews. Elsevier Ltd 2017, pp 330–340. https://doi.org/10.1016/j.rser.2017.05.225.

(10) Overend, R. P.; Chornet, E. Fractionation of Lignocellulosics by Steam-Aqueous Pretreatments. Philos. Trans. R. Soc. London. 1987, 321 (1561), 523–536. https://doi.org/10.1098/rsta.1987.0029.

(11) Malaret, F.; Gschwend, F. J. V.; Lopes, J. M.; Tu, W. C.; Hallett, J. P. Eucalyptus Red Grandis Pretreatment with Protic Ionic Liquids: Effect of Severity and Influence of Sub/Super-Critical CO2 Atmosphere on Pretreatment Performance. RSC Adv. 2020, 10 (27), 16050–16060. https://doi.org/10.1039/d0ra02040k.

(12) Weigand, L.; Mostame, S.; Brandt-Talbot, A.; Welton, T.; Hallett, J. P. Effect of Pretreatment Severity on the Cellulose and Lignin Isolated from: Salix Using IonoSolv

Pretreatment. Faraday Discuss. 2017, 202, 331–349. https://doi.org/10.1039/c7fd00059f.

(13) Usmani, Z.; Sharma, M.; Gupta, P.; Karpichev, Y.; Gathergood, N.; Bhat, R.; Gupta, V. K. Ionic Liquid Based Pretreatment of Lignocellulosic Biomass for Enhanced Bioconversion. Bioresour. Technol. 2020, 304, 123003. https://doi.org/10.1016/j.biortech.2020.123003.

(14) Da Costa Lopes, A. M.; Lins, R. M. G.; Rebelo, R. A.; Łukasik, R. M. Biorefinery Approach for Lignocellulosic Biomass Valorisation with an Acidic Ionic Liquid. Green Chem. 2018, 20 (17), 4043–4057. https://doi.org/10.1039/c8gc01763h.

(15) Sasikumar, E.; Viruthagiri, T. Optimization of Process Conditions Using Response Surface Methodology (RSM) for Ethanol Production from Pretreated Sugarcane Bagasse: Kinetics and Modeling. BioEnergy Res. 2008, 1 (3–4), 239–247. https://doi.org/10.1007/s12155-008-9018-6.

(16) Abatzoglou Nicolas, C. E. and B. K. Kinetics of Complex Systems : The Development of a Generalized Severity Parameter and Its Application To. Chem. Eng. Sci. 1992, 47 (5), 1109–1122.

(17) Gra, J.; Hallett, J. P.; To, T. Q.; Welton, T. A Quick, Simple, Robust Method to Measure the Acidity of Ionic Liquids. Chem Comm 2014, 50, 7258–7261. https://doi.org/10.1039/c4cc02816c.

(18) Hammett, L.; Deyrup, A. A Series of Simple Basic Indicators. I. The Acidity Functinos of Mixtures of Sulfuric and Perchloric Acids with Water. J. Am. Chem. Soc. 1932. https://doi.org/10.1021/ja01346a015.

(19) Zhang, L.; Liu, Y.; Li, Z. Effects of Reduced Severity of Ammonium Sulfite Pretreatment on Bamboo for High Cellulose Recovery. RSC Adv. 2019, 9 (52), 30489–30495. https://doi.org/10.1039/c9ra06475c.

(20) Brandt-Talbot, A.; Gschwend, F. J. V.; Fennell, P. S.; Lammens, T. M.; Tan, B.; Weale, J.; Hallett, J. P. An Economically Viable Ionic Liquid for the Fractionation of Lignocellulosic Biomass. Green Chem. 2017, 19 (13), 3078–3102. https://doi.org/10.1039/C7GC00705A.

(21) Shinde, S. D.; Meng, X.; Kumar, R.; Ragauskas, A. J. Recent Advances in Understanding the Pseudo-Lignin Formation in a Lignocellulosic Biorefinery. Green Chem. 2018. https://doi.org/10.1039/C8GC00353J.

(22) Yalcin, D.; Christofferson, A. J.; Greaves, T. L. Solvation Properties of Protic Ionic Liquid–Molecular Solvent Mixtures. PCCP 2020, No. 22, 10995–11011. https://doi.org/10.1039/d0cp00201a.

(23) Gregorio, G. F. De; Weber, C. C.; Gräsvik, J.; Welton, T. Mechanistic Insights into Lignin Depolymerisation in Acidic Ionic Liquids. Green Chem. 2016. https://doi.org/10.1039/c6gc01295g.

(24) Yang, B.; Wyman, C. E. Effect of Xylan and Lignin Removal by Batch and Flowthrough Pretreatment on the Enzymatic Digestibility of Corn Stover Cellulose. Biotechnol. Bioeng. 2004, 86 (1), 88–98. https://doi.org/10.1002/bit.20043.

(25) Chum, H. L.; Johnson, D. K.; Black, S. K.; Overend, R. P. Pretreatment-Catalyst Effects and the Combined Severity Parameter. Appl. Biochem. Biotechnol. 1990, 24–25 (1), 1–14. https://doi.org/10.1007/BF02920229.

(26) Hu, F.; Jung, S.; Ragauskas, A. Pseudo-Lignin Formation and Its Impact on Enzymatic Hydrolysis. 2012. https://doi.org/10.1016/j.biortech.2012.04.037.

(27) Dashtban, M.; Gilbert, A.; Fatehi, P. Production of Furfural: Overview and Challenges. J-for 2012, 2 (4), 44–53.

(28) Wang, H.; Liu, S.; Zhao, Y.; Zhang, H.; Wang, J. Molecular Origin for the Difficulty in Separation of 5-Hydroxymethylfurfural from Imidazolium Based Ionic Liquids. ACS Sustain. Chem. Eng. 2016, acssuschemeng.6b01652. https://doi.org/10.1021/acssuschemeng.6b01652.

(29) Hu, S.; Zhang, Z.; Zhou, Y.; Han, B.; Fan, H.; Li, W.; Song, J.; Xie, Y. Conversion of Fructose to 5-Hydroxymethylfurfural Using Ionic Liquids Prepared from Renewable Materials. Green Chem. 2008, 10 (12), 1280. https://doi.org/10.1039/b810392e.

(30) Agbor, V. B.; Cicek, N.; Sparling, R.; Berlin, A.; Levin, D. B. Biomass Pretreatment: Fundamentals toward Application. Biotechnol. Adv. 2011, 29 (6), 675–685. https://doi.org/10.1016/j.biotechadv.2011.05.005.

(31) Kabel, M. A.; Bos, G.; Zeevalking, J.; Voragen, A. G. J.; Schols, H. A. Effect of Pretreatment Severity on Xylan Solubility and Enzymatic Breakdown of the Remaining Cellulose from Wheat Straw. Bioresour. Technol. 2007, 98 (10), 2034–2042. https://doi.org/10.1016/j.biortech.2006.08.006.

(32) Aarum, I.; Devle, H.; Ekeberg, D.; Horn, S. J.; Stenstrøm, Y. Characterization of Pseudo-Lignin from Steam Exploded Birch. ACS Omega 2018, 3, 4924–4931. https://doi.org/10.1021/acsomega.8b00381.

(33) Hu, F.; Jung, S.; Ragauskas, A. Pseudo-Lignin Formation and Its Impact on Enzymatic Hydrolysis. Bioresour. Technol. 2012, 117, 7–12. https://doi.org/10.1016/j.biortech.2012.04.037.

(34) Lange, J.; Heide, E. Van Der; Buijtenen, J. Van; Price, R. Furfural — A Promising Platform for Lignocellulosic Biofuels. 2012, 150–166. https://doi.org/10.1002/cssc.201100648.

(35) Sipponen, M. H.; Pihlajaniemi, V.; Pastinen, O.; Laakso, S. Reduction of Surface Area of Lignin Improves Enzymatic Hydrolysis of Cellulose from Hydrothermally Pretreated Wheat Straw. RSC Adv. 2014, 4, 36591–36596. https://doi.org/10.1039/c4ra06926a.

(36) Guo, G.; Li, S.; Wang, L.; Ren, S.; Fang, G. Separation and Characterization of Lignin from Bio-Ethanol Production Residue. Bioresour. Technol. 2013, 135, 738–741. https://doi.org/10.1016/j.biortech.2012.10.041.

(37) Hu, F.; Ragauskas, A. Suppression of Pseudo-Lignin Formation under Dilute Acid Pretreatment Conditions. RSC Adv. 2014, 4, 4317. https://doi.org/10.1039/c3ra42841a.

Chapter 6 : Efficient Extraction of Carboxylated Nanocellulose using ionoSolv process with Alkaline H_2O_2 assisted Oxidation

6.1 Introduction

It has been over 200 years since Payen had first used the term "cellulose" to describe the delignified plant tissues, what would be later to known as the world's most abundant natural biopolymer.[1] The extraction of the fibrous cellulose polymer from the complex hierarchical lignocellulosic biomass matrix required the deconstruction of its robust structure using mechanical or chemical disintegration methods.[2] In the early 20th century, the Sulfite process and Kraft process became increasingly popular as efficient chemical pulping processes that extract high-purity cellulose from wood timber, primarily to produce paper and paperboard.[3] Today, the applications and market of different grades of cellulose has expanded massively to include textile production, composites, pharmaceuticals and consumables.[4] More recently, cellulose has started to attract growing attention at the nanoscale, particularly to isolate or extract cellulosic nanomaterials (CNMs) in the form of microfibrillated cellulose (MFC), cellulose nanofibers (CNFs), cellulose nanocrystals (CNCs) or cellulose spherical nanoparticles (CNPs).[5,6] The nanoscale of CNMs make them exhibit numerous unique properties such as large surface area, tunable morphology (hydrophobicity and hydrophilicity), low density, high specific strength and high reactivity.[7,8] These characteristics unlocked tremendous potential applications for CNMs such as transparent films for food packaging[9] and electronics[10] reinforcement fillers for composites and polymers[11], rheology modifiers for cosmetics[12], films and aerogels for energy storage[13] and lubrication agent for drilling fluids.[14]

To a varying extent, many of the conventional CNCs extraction methods suffer from requiring multiple complex treatment and purification steps, highly purified cellulose substrates (i.e. bleached) and production of a large amount of challenging waste streams. For example, CNC extraction using mineral acid hydrolysis method requires 9 kg of H_2SO_4 per kg of CNCs produced, which translates into the disposal of 12 kg of Na_2SO_4 per kg of CNC after acid neutralization.[15]

Similarly, conventional oxidation reactions are also often carried using very low solid loadings (1 to 5%) and prolonged reaction times. These factors hinder the progress towards efficient process scale-up and commercial use of CNCs. The need to develop more facile, environmentally friendly methods for CNC extraction with minimal processing steps has started to receive more attention in the past few years. For example, in efforts to eliminate the use of chlorine-containing oxidizing agent in a conventional TEMPO-mediated oxidation method, electro-mediated TEMPO oxidation for CNC extraction was proposed an alternative.[16] However, the method required prolonged reaction times (48 hours) compared to using NaClO as an oxidizing agent (<90 minutes). Ji *et al.* recently investigated the use of the non-toxic and easy-to-recover citric acid to prepare carboxylic CNCs, however the obtained yields were relatively low (10 to 33%), similar to those obtained by mineral acid hydrolysis. [17]

Another environmentally friendly alternative method involves the use of H_2O_2 for effective isolation and extraction of CNCs. H_2O_2 is a commonly used oxidizing agent in the pulp and paper industry as an environmentally friendly bleaching alternative to chlorine-containing chemicals as it decomposes inevitably to oxygen and water.[18] It is approved for use by the Joint Food and Agriculture Organization of the United Nations (FAO)/World Health Organization (WHO) Expert Committee on Food Additives (JECFA) as a multipurpose food additive.[19] The use of catalyst-assisted H_2O_2 mediated oxidation has been only recently explored to isolate carboxylated CNCs from bleached softwood pulp and MCC.[20] The CNC isolation procedure involved mixing the softwood pulp in 30 wt% H_2O_2 in the presence of a copper-based catalyst at 60 °C for 72 hours. The use of extremely long reaction times translates directly into very large reactor volume, which counterbalance the benefits of using the relatively safe and environmentally friendly H_2O_2 oxidizing agent as a cost-effective isolation of CNCs. The use of alkaline H_2O_2 oxidation and ultrasonication for facile extraction of CNCs from ethanol treated cellulose pulps was explored recently by Li *et al.*[21] Wood flour fine powder of 60-mesh particle size was used as a feedstock with a low solid to liquid ratio of 1: 20 g g^{-1} during the alkaline H_2O_2 oxidation (50 °C for 90 minutes) . The above processing conditions were successful in the extraction of CNCs at lab-scale, however they are economically unfeasible when considering large scale CNC production.

Here, we explore a simple procedure to produce carboxylated CNCs from unbleached cellulose pulps, obtained by ionoSolv fractionation process followed by a 1-hour alkaline H_2O_2 oxidation. Since cellulose substrates are known to resist oxidation due to the high crystallinity and low accessibility to reagents, an alkali NaOH solution was used in conjunction with H_2O_2 oxidation to improve the cellulose pulp accessibility via the well-known fiber-swelling phenomenon.[22,23] The two-step process (Figure 6.1) involved the use of the low-cost *N*,*N*,*N*-dimethylbutylammonium hydrogen sulfate [DMBA][HSO_4] to fractionate *Miscanthus* × *giganteus* (particle size of 1 – 3 mm) to produce cellulose-rich pulps followed by alkaline H_2O_2 oxidation of the obtained pulps at solid loading of 1 : 10 g g^{-1} to produce i) a highly pure, low degree of polymerization (DP) cellulose residue that can be further tailored and processed to produce CNFs or CNCs and ii) a functionalized carboxylated CNC suspension. We investigated the impact of controlling ionoSolv fractionation severity on the cellulose (pulp and oxidation residue) composition, crystallinity and degree of polymerization as well as on the properties of the carboxylated CNCs in terms of structure, size and stability. We showed that using low and high fractionation severity during ionoSolv biomass fractionation had a significant impact on the cellulose-rich pulp as well as on the alkaline H_2O_2 cellulose residue in terms of chemical structure and degree of polymerization; however, the fractionation conditions had only a minor impact on the properties of the carboxylated CNCs produced. This is the first study to demonstrate the successful production of functionalized negatively charged carboxylic-CNCs from unbleached ionoSolv cellulose pulps with 10 to 30% lignin content.

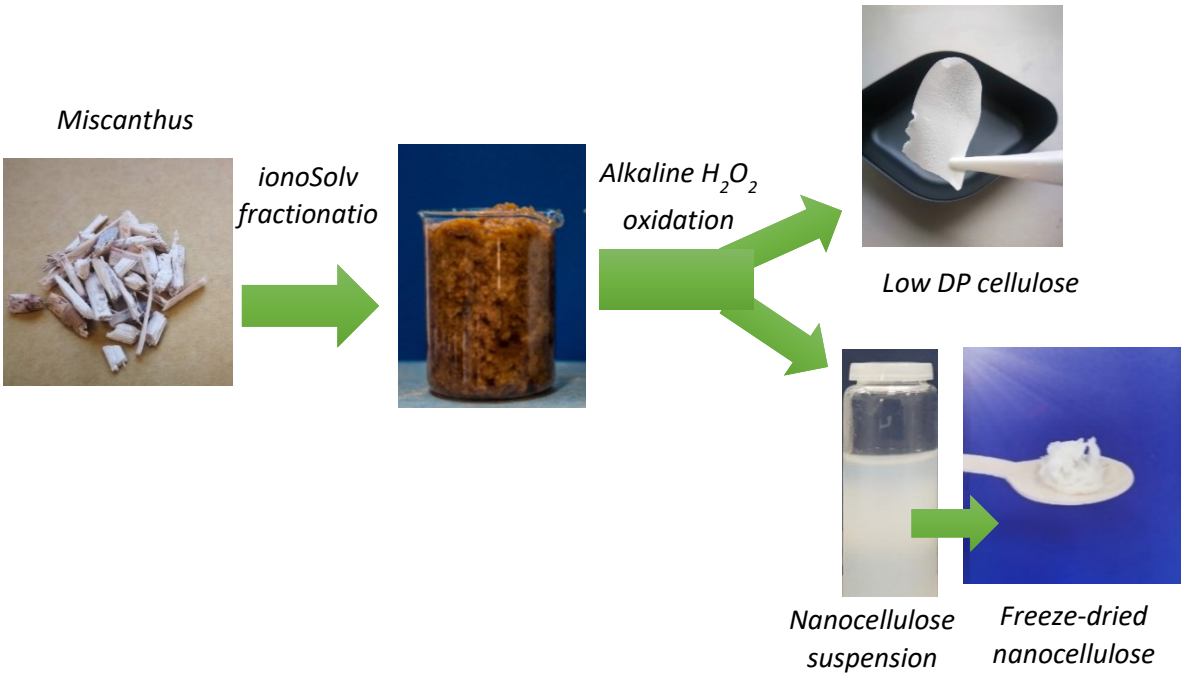

Figure 6.1: ionoSolv + alkaline H_2O_2 oxidation process two-step process to produce anionic charged carboxylic-CNCs and low DP cellulose substrate residue after oxidation

6.2 Materials and Methods

Materials: *Miscanthus x giganteus* was acquired from Silwood Park campus, Imperial College London. Starting materials for ionic liquid synthesis and alkaline H_2O_2 oxidation method were purchased from Sigma Aldrich and, unless stated otherwise, used as received. The synthesis procedure of *N,N,N*-dimethyl-butylammonium hydrogen sulfate [DMBA][HSO_4] was described in details in Section 2.2.3.

6.2.1 Biomass fractionation

Pretreatment was conducted according to the standard operating procedure from our laboratory.[24] Determination of oven dried weight of biomass and cellulose pulps (air-dried and wet conditions) were conducted according to the NREL protocol "Determination of Total Solids in Biomass and Total Dissolved Solids in Liquid Process Samples".[25] The water content of the prepared IL solutions was determined using Karl Fisher volumetric Titrator (Mettler-Toledo). The IL solution was then mixed with 2 g of biomass (on an oven-dried weight basis) in a pressure tube, corresponding to a biomass to solvent ratio of 1:5 g g^{-1}. The pretreatment was conducted at oven temperature of 120

°C and 170 °C for 6 hours and 45 minutes, respectively. Detailed procedure can be found in Section 2.2.4.

6.2.2 Alkaline H_2O_2 oxidative preparation of CNCs

Air dry *Miscanthus* pulp (5 g) was added to 250 mL in a three-neck round-bottom flask and mixed with 10 wt% NaOH solution (25 mL) for 15 minutes at 80 °C using a heating plate as monitored by a thermometer inside the flask. After 15 minutes of stirring, 30 wt% H_2O_2 solution (25 mL) was added carefully dropwise using a volumetric funnel and the reaction proceeded for 45 minutes. The drop-wise addition of H_2O_2 needs to be carefully monitored at all times during the reaction course. The round-bottom flask was covered with aluminium foil and the reaction mixture was constantly stirred at 100 rpm. After the process was completed, the final volume of the suspension was adjusted to 200 mL with cold deionized water to terminate the reaction. The resulting product mixture contained the cellulose residue solids and the CNCs particles in suspension which was centrifuged at 4000 rpm for 30 mins. The first supernatant fluid was discarded to remove NaOH/H_2O_2 reaction mixture. The cellulose residue solids were repeatedly washed with DI water and centrifuged at 4000 rpm for 30 minutes until the pH reached 8 (samples named as BM120 and BM170). The successive decanted washings containing the CNC particles were collected and dialyzed against deionized water. A small fraction of the CNC dialyzed suspension was freeze-dried for analysis. The reminder CNC suspension was stored in fridge at 4 °C.

6.2.3 Chemical compositional analysis

Compositional analysis was carried out according to the published procedure 'Determination of Structural Carbohydrates and Lignin in Biomass' by the NREL.[26] The detailed procedure can be found in the ESI. Compositional analysis determines the following structural components: i) carbohydrates content, namely glucose, xylose, arabinose and mannose, ii) acid insoluble lignin, iii) acid soluble lignin, iv) acid insoluble ash. A Prominence HPLC system (Shimadzu) with RI detector was used to quantify the sugars, employing an Aminex HPX- 87P column operated at 85 °C with purified water at a flow. Detailed procedure can be found in Chapter 2.

6.2.4 Gel permeation chromatography (GPC) analysis

The cellulose ionoSolv pulps and cellulose residues after H_2O_2 oxidation were analysed for their molar weight distribution at the Department of Forest Products Technology at

Aalto University, Finland. Prior to the analysis, the samples were ground to particles smaller than 60 mesh size and delignified with sodium chlorite aqueous solution. The delignified samples were pre-activated by a water/acetone/*N*,*N*-dimethylacetamide (DMAc) solvent exchange sequence. The samples were then dissolved at 90 g/L in a lithium chloride (LiCl)/DMAc mixture at room temperature. The solutions were diluted to 9 g/L LiCl/DMAc and filtered through a 0.2 mm syringe filter and analyzed with a Dionex Ultimate 3000 system with refractive index (RI) detection (Shodex RI-101). This analysis was conduced by Dr. Eero Kontturi in Aalto University. Average degree of polymerization ($DP_{average}$) was calculated by dividing the average molecular weight (M_w) by the molecular weight of the anhydrous glucose unit (162 g/mol).

6.2.5 X-ray diffraction (XRD) and crystallinity analysis

XRD patterns were collected with Xpert pro PANalytical (Malvern Panalytical, Spectris UK) X-ray operated at 40 kV and 40 mA with a CuKa radiation source at room temperature. The scattering angle range was 5°−45° 2θ at a scanning speed of 70s per step and a 2θ step interval of 0.02°. The crystallinity index (CrI) was calculated following Segal method using the Equation:

$$CrI = \frac{(I_{002} - \mathrm{I}_{am})}{I_{002}} \text{ x100} \qquad (7.1)$$

Where, I_{002} is the intensity of the peak at position 2θ = 22.5°, assigned to the crystalline portion of cellulose, and I_{am} is the intensity of the peak at position of 2θ = 18°, which assigned as the amorphous portion of cellulose.

6.2.6 Fourier Transform Infrared (FT-IR) Spectroscopy

Samples were characterized with an FT-IR spectrometer using Perkin-Elmer with a diamond ATR single reflection crystal. Initial background spectra were taken and subtracted from the sample measurement. Solid samples were placed directly on the ATR crystal, and maximum pressure was applied by lowering the tip of the pressure clamp using a rachet-type clutch mechanism. All of the spectra of measured samples were averaged from 32 scans from 550 to 4000 cm^{-1} with a resolution of 2 cm^{-1}.

6.2.7 Zeta Potential (ZP) analysis

Zeta potential values were determined using the Brookhaven ZetaPals (BrookHaven Instruments, Nova instruments, USA). The measurements were conducted in triplicates

for each sample, with 10 runs per sample and 15 cycles per run and the average value is reported. All measurements are conducted in DI water at pH of 6.5

6.2.10 Morphological studies of CNCs

Scanning electron microscopy (SEM) images were taken by Dr. Ecaterina Ware, Materials Department using SEM, JOEL 6010A microscope. Samples were coated with a thin layer of gold and images were captured up with 10 kV accelerated voltage. The Atomic Force Microscopy (AFM) was conducted by Dr. Eero Kontturi in Aalto University. AFM metal disc was glued by freshly cleaved mica and coated with APTES using the vapor-phase method 0.01 wt% TOCNF was spin-coated on the surface-modi- fied metal disc to obtain separate single nanofibers.

6.2.8 UV-vis spectroscopy

The optical transmittance of CNCs suspensions (0.1 wt%) were measured using Shimadzu UV-1800 UV spectrophotometer. A background spectrum was first acquired from the empty sample holder. The spectra were acquired from 200 to 900 nm with a data interval of 1 nm.

6.2.9 Thermogravimetric (TG) analysis

Thermogravimetric analysis on freeze-dried CNC samples was performed using TA Instruments Q500 TG analyzer. Samples (about 5 mg) were heated in a pure nitrogen atmosphere (flow rate 60 mL/min) from 25 °C to 600 °C at a rate of 10 °C/min.

6.3 Results and Discussions

6.3.1 Cellulose Characterization

6.3.1.1 Chemical compositional analysis

The effect of *Miscanthus* fractionation by [DMBA][HSO_4]:H_2O = 80:20 wt% mixture ([DMBA][HSO_4]$_{80\%}$) was quantified by analysing the structural compositions of the feedstock and cellulose pulps.

Fractionation experiments were conducted using [DMBA][HSO_4]$_{80\%}$ at two conditions: 170 °C for 45 minutes (high severity) and 120 °C for 6 hours (low severity). Cellulose pulp samples were labelled according to the fractionation conditions as **M120** and **M170,** such that *Miscanthus* pulp treated at 120 °C for 6 hours is indicated as **M120**. Letter **B** is used to indicate the treated alkaline H_2O_2 cellulose residue **BM120** and

BM170. Commercial grade dissolving pulp and market pulps were also analysed for their structural compositions and they were compared to the quality of the cellulose pulps. Dissolving pulp is a high-grade cellulose pulp with cellulose content >90% typically used for textile and regenerated cellulose applications whereas market pulp is a lower-grade cellulose pulp used for paper applications.[27] Table 6.1 presents the numerical values of the glucan, hemicellulose, Klason lignin and ash contents for the untreated *Miscanthus* , ionoSolv treated cellulose pulps and the alkaline H_2O_2 cellulose residues. Figure 6.2 shows the structural compositions of the untreated *Miscanthus* as well as the cellulose pulps obtained from the fractionation using 80 wt% [DMBA][HSO_4]. It was interesting to note that the lower severity conditions resulted in higher delignification with 81% delignification achieved for the M120 pulp compared to only 44.5% delignification for the M170 pulp.

Table 6.1: Structural composition of untreated Miscanthus, ionoSolv cellulose pulps, ionoSolv + alkaline H_2O_2 oxidized cellulose residues, dissolving pulp and market pulp. ionoSolv fractionation experiments were conducted at 120 °C for 6 hours (M120) or 170 °C for 45 minutes (M170) using 80 wt% [DMBA][HSO_4] and 20 wt% solids loading. Alkaline H_2O_2 oxidation were conducted using 10 wt% NaOH and 30 wt% H_2O_2 using at 80 °C 10 wt% solids loading

Sample	Glucan	Hemicellulose	Klason Lignin	Ash	Extractives
Miscanthus untreated	48.2	21.9	27.3	1.1	1.5
M170	66.6	0	31.6	1.8	-
M120	84.4	5.1	9.2	1.3	-
BM170	93.2	0	5.1	1.7	-
BM120	93.3	1.3	4.8	0.6	-
Dissolving pulp	92.8	0.4	5.3	1.5	-
Market pulp	85.0	7.2	6.7	1.1	-

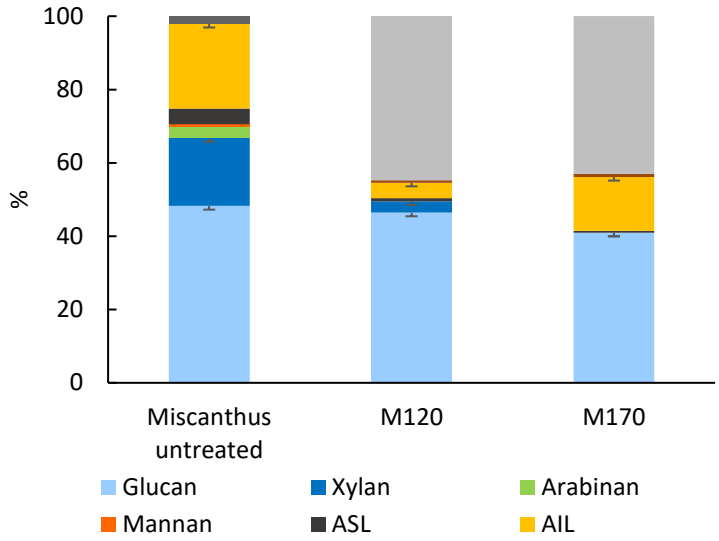

Figure 6.2: Composition of untreated Miscanthus and Miscanthus cellulose pulps at 120 °C for 6 hours (M120) and for 170 °C for 45 minutes (M170). The cellulose pulp composition values are normalized using the gravimetrical pulp yield. Fractionation experiments were conducted using [DMBA][HSO_4] mixed with 20 wt% H_2O at 20 wt% solids loading

The higher lignin content of 31.6% in M170 compared to the 9.2% lignin content in M120 is likely related to the rapid delignification and subsequent pseudo lignin formation kinetics in [DMBA][HSO_4] at 170 °C compared to 120 °C as shown in a previous ionoSolv study.[28] The fast and higher likelihood of pseudo lignin deposition on cellulose pulp surface at high severity fractionation conditions increased the overall Kalson lignin content in cellulose pulp where it exceeds the lignin content in the untreated biomass (Table 6.1).[29] Figure 6.3 shows the impact of the fractionation conditions on the cellulose pulp brightness, with cellulose pulps treated at low severity (M120) showing lighter colours compared to M170.

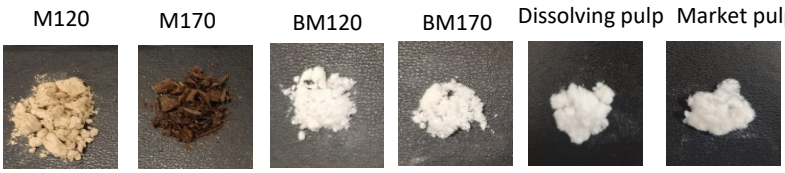

Figure 6.3: Cellulose pulps treated using ionoSolv fractionation and ionoSolv + alkaline H_2O_2 oxidation treatment, dissolving and market pulps.

On the other hand, removal of hemicellulose was more effective at higher severity conditions with quantitative removal achieved for M170 while a lower hemicellulose removal of 87% was obtained for M120. Effective removal of hemicellulose is one of the key features of ionoSolv process due to the acidic nature of the protic IL [DMBA][HSO_4], promoting the depolymerization and hydrolysis of hemicellulose into monomeric sugars (e.g. xylose, mannose), oligomers and their dehydration products (furfural, 5-HMF).[30] Producing hemicellulose-lean cellulose pulps is of a key significance in cellulose pulp processing, particularly to produce dissolving pulp, regenerated cellulose products and cellulose derivatives since the hemicellulose interferes in the regeneration process of cellulose due to its chemical similarities.[31] Currently, wood-derived dissolving pulps are produced by the acid sulphite or the pre-hydrolysis kraft processes. Effective removal of hemicellulose in both processes is insufficient and therefore subsequent hot and/or cold caustic soda extractions steps are integrated to achieve required extraction.[27] However, the effective hemicellulose removal at high severity pretreatment was compromised by the higher degradation of glucan with M170 losing 15.1% of glucan relative to the initial glucan content. Lower severity fractionation preserved the glucan cellulose more intact with glucan losses of 3.8% only for M120.

Figure 6.4-a presents the structural carbohydrate, lignin and ash composition of the cellulose residue BM120 and BM170 after the alkaline H_2O_2 oxidation. The alkaline H_2O_2 oxidation of ionoSolv cellulose pulps resulted in significant improvement in the cellulose residue purity by further removing hemicellulose and residual lignin. BM120 had the lowest amount of residual lignin of 4.8% with a cellulose content of 93% and hemicellulose content of 1.3%. The glucan composition of BM170 was very similar to BM120 with slightly higher lignin content of 5.1% and no hemicellulose content. We compared the lignin extraction achieved during the alkaline H_2O_2 oxidation between the ionoSolv pulps obtained at different fractionation severity conditions (Figure 6.4b). It was noticeable that lignin extraction from M120 cellulose pulp was significantly lower (48%) compared to lignin extraction from M170 cellulose pulps (84%) although M170 had a higher initial Kalson lignin content (31.6%) compared to M120 (9.2%), which is attributed to pseudo lignin formation as explained earlier.

This gave us a new insight that although high severity ionoSolv fractionation conditions promotes deposition of pseudo lignin on the cellulose pulps, this pseudo lignin is easier to extract during the alkaline H_2O_2 oxidation as it not covalently bound to the cellulose as native lignin.[29]

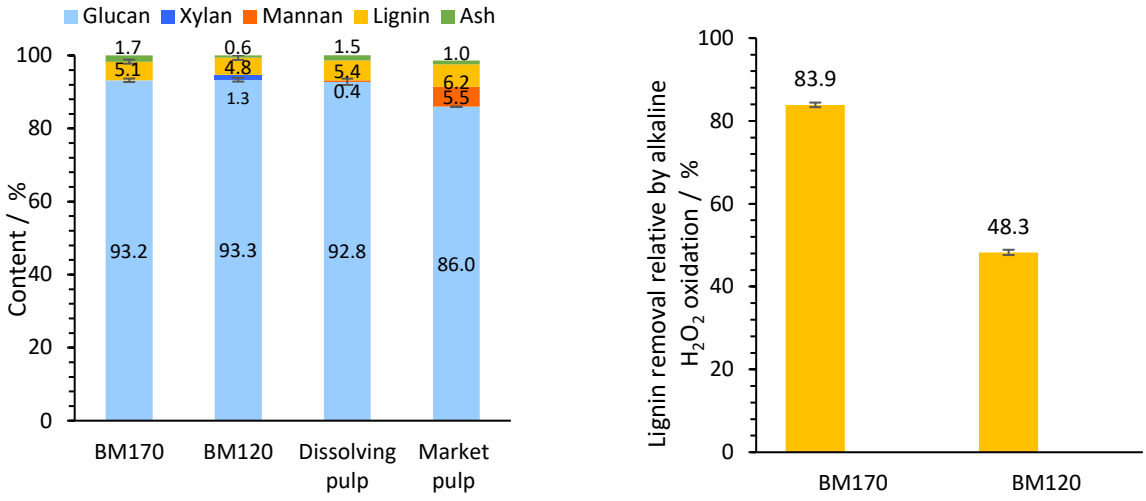

Figure 6.4: (a) Structural composition of commercial grade dissolving pulp, market pulp and the alkaline H_2O_2 cellulose residues BM170 and BM120. (b) Lignin extraction by alkaline H_2O_2 oxidation relative to lignin content in ionoSolv cellulose pulps M170 and M120. Alkaline H_2O_2 oxidation was conducted at 80 °C using 10 wt% NaOH and 30 wt% H_2O_2 using 10 wt% solids loading.

Figure 6.5 shows SEM image of the M170 cellulose pulp where pseudo lignin deposition can be seen as spherical droplets on the surface of the fibers. Spherical lignin droplets are typically reported to describe pseudo lignin formed during high severity dilute acid pretreatment as a result of lignin migration from the cell wall to the bulk liquid followed by its re-deposition on the cellulose surface.[29]

The structural composition of the alkaline H_2O_2 cellulose residues BM120 and BM170 showed higher purity of glucan (>90%) compared to commercial market pulp quality and a comparable glucan and lignin composition to dissolving pulp. **This highlights that effectiveness of the alkaline H_2O_2 in removing residual lignin to low levels similar to commercial bleaching processes**. It should be noted that the obtained commercial dissolving and market pulps were bleached using Elemental Chlorine Free (EFC) process, where chlorine dioxide and H_2O_2 are used as bleaching agents. Prior to the bleaching, oxygen delignification was also conducted to reduce lignin levels, and subsequently reduce bleaching chemicals requirement. The use of H_2O_2 for cellulose

bleaching is typically accomplished under a sequence of oxygen-alkaline-H_2O_2 bleaching stages, which improves the delignification (lignin content <5%). [27]

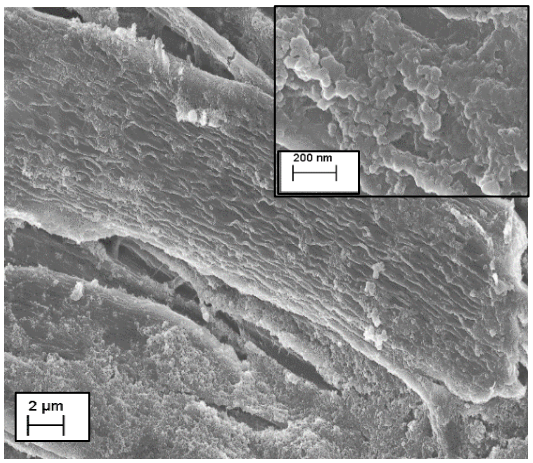

Figure 6.5: SEM image of M170 ionoSolv treated pulp showing the pseudo lignin droplets deposition on the cellulose fibers

6.3.1.2 Molecular weight distribution of cellulose pulps

Figure 6.6 presents the degree of polymerization (DP) distribution of cellulose in ionoSolv pulps and in the cellulose residues from the alkaline H_2O_2 oxidation using gel permeation chromatography (GPC). The weight average molecular weight (M_w) and the weight average DP ($DP_{average} = M_w/162$) are also presented in Figure 6.7.

Conducting the GPC analysis on the initial feedstock was not possible due to the high amount of initial lignin present that prevented the sample from solubilization as part of the sample preparation procedure. During the ionoSolv fractionation process, the biomass feedstock is subject to highly acidic conditions.[32] It is well known that when cellulose is subjected to an acid, the glucosidic linkages in the cellulose fibers are broken and the DP decreases.[32] For ionoSolv treated pulps, *Miscanthus* treated at high severity condition (M170) had a substantially lower M_w of 93 kDa mol^{-1} ($DP_{average}$ = 574) compared to M120 with M_w of 214 kDa mol^{-1} ($DP_{average}$ = 1318). The DP distribution showed that 20% of the cellulose chains in M120 had DP >2000 compared to only 3.8 % for M170. **This indicates that low severity conditions keep the high DP cellulose chains more intact with only minimal degradation and hydrolysis of amorphous cellulose in the IL media as shown earlier**. On the other hand, the high severity

conditions promoted faster and more severe depolymerization and hydrolysis of both the amorphous portion of the cellulose as well as the crystalline regions, resulting in lower M_w and DP_{ave}.

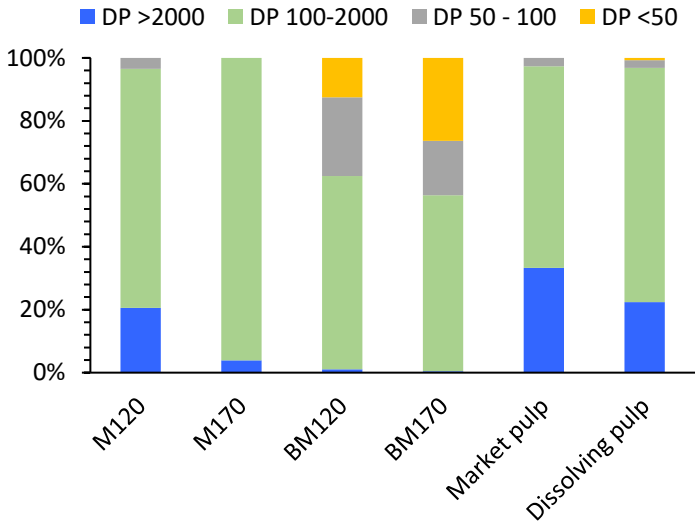

Figure 6.6: DP distribution of ionoSolv treated pulps, alkaline H_2O_2 cellulose residues, dissolving pulp and market pulp. Fractionation experiments were conducted using [DMBA][HSO4] mixed with 20 wt% H_2O at 20 wt% solid loading. Alkaline H_2O_2 oxidation was conducted at 80 °C using 10 wt% NaOH and 30 wt% H_2O_2 using 10 wt% solids loading.

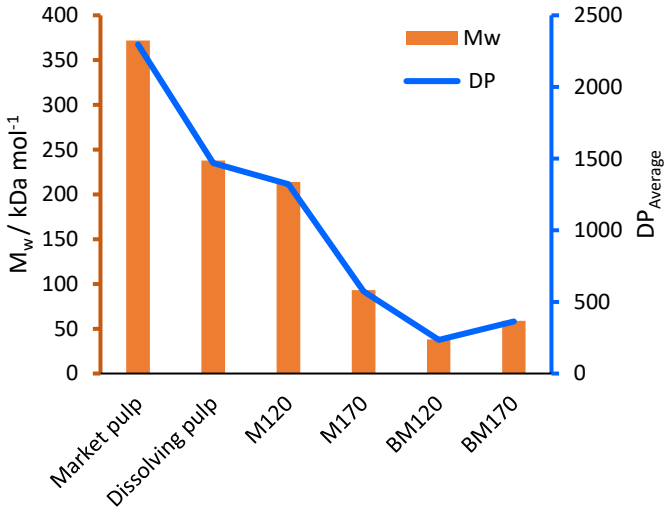

Figure 6.7: Molecular weight and average degree of polymerization of ionoSolv treated pulps and alkaline H_2O_2 cellulose residues. Fractionation experiments were conducted using [DMBA][HSO_4] mixed with 20 wt% H_2O at 20 wt% solids loading. Alkaline H_2O_2 oxidation was conducted at 80 °C using 10 wt% NaOH and 30 wt% H_2O_2 using 10 wt% solids loading.

It is important to note that the DP distribution of the M120 ionoSolv cellulose pulp ($DP_{average}$ = 1321) was very close to the DP distribution of the dissolving pulp ($DP_{average}$ = 1469), whereas the DP distribution of market pulp showed higher proportion of >2000 DP cellulose chains, and therefore a higher $DP_{average}$ of 2296. On the other hand, the DP distribution of M170 had a much lower proportion of high DP cellulose chains compared to market pulp, dissolving pulp and M120 with $DP_{average}$ =574. Both the market pulp and dissolving pulp are bleached pulps that have been subjected to multiple purification and bleaching steps after primary extraction with kraft or sulfite pulping. **This show that depending on the fractionation conditions, the unbleached cellulose-rich pulps produced by the ionoSolv process can have relatively similar or lower M_w and $DP_{average}$ than the bleached wood pulps reported here and in other studies.** For example, Palme *et al.* measured the average M_w of two dissolving pulps; i) Scandinavian softwood from a Sulfite process was reported to be 283 kDa (DP = 761) and, ii) eucalyptus pulp produced by a pre-hydrolysis kraft process was reported to be 182 KDa (DP =1095). **This can be highlighted as a key feature of the ionoSolv process. While this feature might be a disadvantage for conventional cellulose pulp applications (e.g. textiles and paper), it can be an advantage for CNCs-based applications where the use of bleached cellulose substrate (low DP, high cellulose content) or the use of the low DP microcrystalline cellulose (MCC) has proven essential for effective CNC extraction.**

The alkaline H_2O_2 oxidation caused significant depolymerization of the cellulose chains as the M_w of BM120 and BM170 dropped to 38 kDa mol^{-1} and 59 kDa mol^{-1} with a $DP_{average}$ of 234 and 364, respectively. In fact, the low DP cellulose chains or crystallites (DP < 50 and 50 < DP < 100) accounted for approximately 45% of the overall cellulose DP of the cellulose residues. Cellulose depolymerization routes in this method could be due to the cleavage of (1 → 4) -β-glycoside bonds by hydroxyl and/or other radical species formed as side reactions during the alkaline H_2O_2 oxidation. **The similar DP of BM120 and BM170 shows that the severity of cellulose depolymerization during the oxidative alkaline H_2O_2 process is independent of the of the DP of the starting material (DP for M120 = 1321 vs. DP for M170 = 574).**[33] The NaOH alkaline medium

may have also facilitated the swelling of the cellulose fibers, which improved their accessibility and depolymerization.

In addition, the low DP values for cellulose residues are similar to the so-called level-off degree of polymerization (LODP) found in higher plant cellulose after acid hydrolysis.[34] The LODP value is typically used to describe the rapid reduction in DP of cellulose during acid hydrolysis due to the dissolution of the amorphous regions of cellulose until the DP reaches a constant LODP value as the attack on crystalline regions is much slower. The LODP values are typically are in the range of 140 to 200 for bleached wood pulp and 300 for ramie fiber.[35] Oxidation processes also have a similar significant reduction in cellulose DP where wood cellulose DP reduced from 1270 to 300 – 500 after TEMPO-mediated oxidation.[33] The near-LODP sized cellulose residues will be ideal as cellulose substrates for further processing to CNCs or CNFs. Ji *et al.* have recently investigated applying acid hydrolysis using citric acid to bleached bagasse pulp where the remaining low DP cellulose residue after the hydrolysis was mechanically fibrillated to produce CNFs.[17]

6.3.1.3 Crystallinity X-ray diffraction

The crystalline structure of the cellulose was characterized using X-ray diffraction and the patterns are presented in Figure 6.8. Table 6.2 presents the crystallinity index (CrI) values. The crystallinity index values were calculated as the ratio of the maximum intensity at 2θ around 22.6° to the minimum intensity of the amorphous region between the (200) and (110) peaks at around 18.5. The crystalline structure of ionoSolv treated pulp (M120 and M170) remained unchanged from native cellulose I in the untreated biomass with main diffraction angles around 22.5°, 14.5°, and 16.5° (appears as broad signal around 15°) which corresponds to the primary lattice plane (200) and the overlapped (110) and ($\underline{110}$) crystallographic planes peaks, respectively. M170 cellulose pulp also showed an additional peak at 21° corresponding to (012) plane in cellulose I polymorph. The CrI values of M120 and M170 were 68.7% and 60.3%, respectively which corresponds to crystallinity enhancement of 25 and 15% relative to the untreated *Miscanthus* (51.8%). The increase in crystallinity in the cellulose pulp is related to the removal of the amorphous lignin and branched hemicellulose polymers from the lignocellulose matrix.[36]

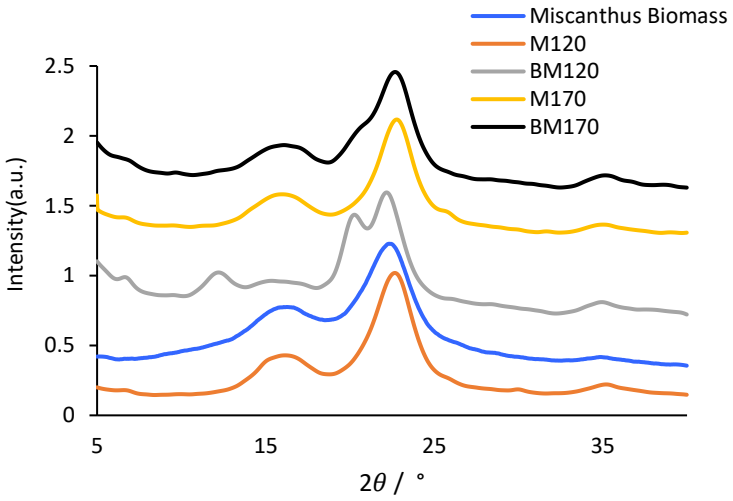

Figure 6.8: XRD patterns for untreated Miscanthus, ionoSolv cellulose pulps and cellulose residue from the alkaline H_2O_2 oxidation.

The slightly higher crystallinity of M120 compared to M170 indicates that the high severity fractionation conditions in the acidic [DMBA][HSO_4] medium attacked some of the crystalline region in cellulose in addition to the amorphous region, which is also evidenced by the higher glucan degradation (Table 6.1).

The XRD diffraction pattern of BM120 alkaline H_2O_2 cellulose treated pulp have the characteristic of cellulose II as observed by the appearance of cellulose II diffraction angles at 22°, 20°, and 12°corresponding to (020), (110), and (1$\underline{1}$0) lattice planes, respectively. The result aligns with the observations of M120 cellulose dissolution and mercerization during the experiment, causing the cellulose polymorphs to rearrange from cellulose I to cellulose II. On the other hand, the XRD pattern of BM170 remained unchanged showing the characteristic cellulose I polymorph diffraction angles. **The fact that BM120 and BM170 showed different cellulose polymorphs highlights the different cellulose substrate reactivity level (M120 and M170) during the alkaline H_2O_2 oxidative treatment.** As M170 had lower initial cellulose content compared to M120, the cellulose fibers of M120 had larger and longer exposure to the alkaline H_2O_2 medium, which made it more prone to fiber swelling and subsequent mercerization. The CrI of cellulose residues BM120 and BM170 decreased by 12 and 10%, respectively compared to their precursors (Table 6.2). **The slight decrease in crystallinity indicates that the alkaline H_2O_2 oxidative treatment did not only solubilize the amorphous regions of the cellulose but it also depolymerizes some of crystalline high DP cellulose surface, leading to a less crystalline cellulose residue.**

Table 6.2: Crystallinity index of ionoSolv treated cellulose pulps and alkaline hydrogen peroxide cellulose residues.

Sample	CrI (%)
Miscanthus untreated	51.86
M120	68.75
M170	65.18
BM120	60.32
BM170	58.68

6.3.2 CNC Characterization

6.3.2.1 Chemical structure and crystallinity

The nanocellulose suspensions (as well as their freeze-dried form) obtained by the alkaline H_2O_2 oxidation of M120 and M170 were labelled as **NBM120** and **NBM170**, respectively (Figure A26). Figure 6.9 shows the XRD patterns for NBM120 and NBM170 obtained by H_2O_2 oxidation. The diffraction patterns show key characteristics of both cellulose I and cellulose II polymorphs. A sharp peak at 2θ = 22.5° corresponding (200) lattice plane and a broader peak at 15° and 16.5° for the (110) and (1$\underline{10}$) planes found in cellulose I as well as two diffraction peaks at 12° and 20° corresponding to the (1$\underline{10}$) (020) planes in cellulose II polymorphs. This indicates that some of the CNCs produced in suspension during the alkaline H_2O_2 were transformed from native cellulose I to cellulose II. A similar mixture of cellulose I and cellulose II CNC suspensions was obtained using concentrated sulfuric acid (>64%) and prolonged hydrolysis times (>50 minutes) using MCC as a substrate.[37] The phenomena was attributed to the fact that concentrated mineral acids can have similar mercerization effects as strong aqueous alkali solutions. **The result supports that the transformation of cellulose polymorph was promoted by the fiber swelling in the alkaline NaOH solution.**

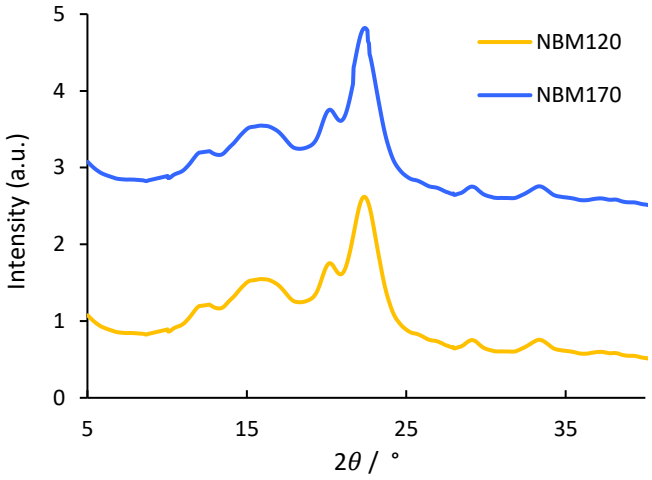

Figure 6.9: XRD diffraction pattern for freeze-dried CNCs samples NBM170 and NBM120 produced by the alkaline H_2O_2 oxidation.

The CrI of the NBM170 and NBM120 were determined as 55.2% and 51.5%, respectively. It is interesting to note that both samples showed a lower crystallinity compared to the solid cellulose residue BM170 and BM120 (Table 6.3). The lower crystallinity of CNCs relative to the cellulose substrate have also been reported when using other oxidation methods such as catalyst-assisted H_2O_2 oxidation and periodate oxidation.[20,38] It is well known that the amorphous regions of cellulose are more accessible for dissolution, leaving the crystalline cellulose I behind. **The exposure of cellulose I in NaOH solution caused destruction and rearrangement of the intramolecular and intermolecular hydrogen bonds network during the mercerization process, formatting cellulose II**.[39,38] Gong *et al.* investigated the morphology and crystallinity of CNCs extracted from different cellulose sources, their conclusion indicated that transformation in cellulose polymorph from cellulose I to cellulose II leads to reduction in crystallinity.[40] Lower crystallinity of CNCs relative to the starting cellulose was also reported using other CNC extraction methods. Zhang *et al.* reported crystallinity reduction of 20% of cellulose II CNCs extracted from cellulose I substrate using mercerization in NaOH/thiorua.[41] Wang *et al.* reported similar lower CrI of the CNCs relative to the starting substrate cellulose when extracted by acid hydrolysis using a mixture of H_2SO_4/HCl.[42] The relatively low crystallinity of the obtained CNCs can be improved by carefully optimizing the alkaline H_2O_2 oxidation conditions (temperature, time, NaOH and H_2O_2 concentration), which will be conducted in a future study. It should be noted that while high crystallinity of CNCs is important in several intended

applications e.g. to improve barrier properties of composite, crystallinity is not critical for other CNCs composite applications where the nanocellulose is mixed with other highly crystalline structures e.g. graphene oxide.[43]

The obtained suspensions were highly stable as no precipitate was observed for over 6 months. This indicates that the nanoparticles generated were small and negatively charged, preventing their agglomeration to larger particles over a long period of time. To assess the colloidal stability of the suspensions, the surface charge of the CNC suspensions was examined using zeta potential (ZP) measurements (Table 6.3). Both NBM120 and NBM170 samples showed similar negative ZP of -32 and -31 mV, respectively which is within the common values of CNC obtained by acid hydrolysis and TEMPO oxidation methods (-20 to -40 mV) and slightly higher than the reported ZP values of ~-20 mV using catalyst-assisted H_2O_2 and APS oxidization methods.[38,44] **The ZP values indicate that there is a relatively strong repulsive electrostatic force among the CNCs in suspension due to the presence of the negatively charged groups on the surface.** High dispersibility of CNCs is critical for applications requiring composite preparation in solvent/polymer matrices.

To gain further insights on the structure and functionality of the CNCs were recorded and compared to the spectrums of the cellulose residues BM120 and BM170 and the untreated *Miscanthus* (Figure 6.10). Both NBM120 and NBM170 showed new high intensity peak at 1593 cm^{-1} which corresponds to C=O stretching and medium intensity peaks at 1313 cm^{-1} to 1364 cm^{-1} which corresponds to characteristic C-O stretching in carboxylate moieties.[45,46] **The analysis confirms that NBM120 and NBM170 contain carboxylated nanocellulose particles.** The mechanism of cellulose oxidation by H_2O_2 has been reported to be similar to TEMPO-mediated oxidation where carboxyl groups are introduced in the *C*6 position.[38,47] The mechanism of introducing the carboxyl group on to the nanocellulose surface could have been through a metal-assisted catalysis originating from the metal-rich ash content in the cellulose pulp (ash content of M120 and M170 is 1.3% and 1.8%, respectively – Table 6.1). It is well-known that the presence of trace metals (e.g. Fe^{+2}, Cu^{+2}) drives the formation of hydroxyl radicals in H_2O_2 oxidation reactions. Equations 6.1-6.3 shows the possible radical formation pathway in the presence of a catalytic amount of trace metal M^{+2} proposed by Carvalho do Lago *et al.*[48]

$$M^{+2} + H_2O_2 \rightarrow M^{+1} + \cdot O_2^- + 2H^+ \quad (6.1)$$

$$M^{+1} + H_2O_2 \rightarrow M^{+2} + \cdot OH + OH^- \quad (6.2)$$

$$M^{+1} + H_2O_2 \rightarrow M^{+2} + \cdot OH + OH^- \quad (6.3)$$

The radicals formed react with the primary hydroxyl group at C6 position during the oxidation, introducing aldehyde and carboxyl groups, according to the possible pathway (Equation 6.4-6.5)[38]

$$RCH_2OH + \cdot OH \rightarrow R \cdot CHOH + H_2O \quad (6.4)$$

$$R \cdot CHOH + H_2O_2 \rightarrow RCHO + \cdot OH + H_2O_2 \quad (6.5)$$

$$RCHO + 2 \cdot OH \rightarrow RCOOH + H_2O \quad (6.6)$$

The carboxyl band at 1593 cm^{-1} did not appear in the cellulose residue BM120 and BM170, however the medium intensity peak at 1313 cm^{-1} to 1364 cm^{-1} corresponding to characteristic C-O stretching of carboxylate was present. **This indicates that even the cellulose residues BM120 and BM170 were also potentially oxidized to presumably lower level compared to the CNCs.** This is probably because the size of the CNCs is smaller which provides larger contact surface area to undergo oxidation compared to the insoluble cellulose residue.[49] In addition, the appearance of the absorption band at FT-IR spectrum at 1593 cm^{-1} indicates that the carboxyl group is present on the CNC surface in its carboxylate form and not in carboxylic acid form where the absorption band typically appears at 1730 cm^{-1}. This is expected since the oxidation is conducted at alkaline conditions.

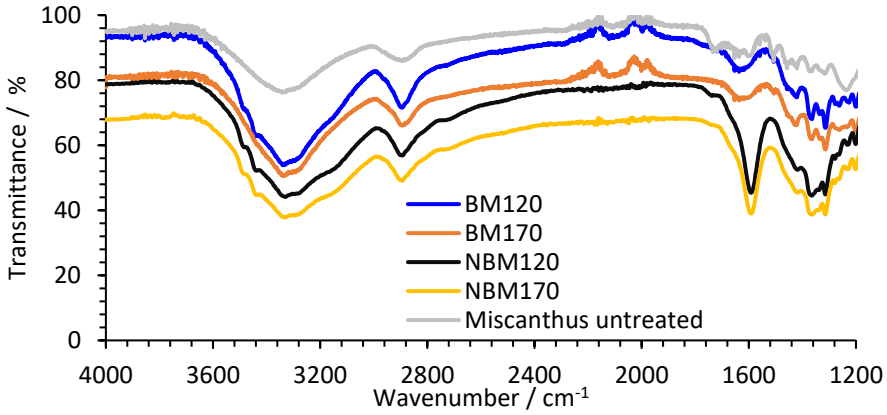

Figure 6.10: FT-IR spectra of untreated Miscanthus and CNCs samples NBM170 and NBM120 produced by the alkaline H_2O_2.

6.3.2.2 Morphology and dimension

The morphology of the obtained CNCs in the cellulose suspension was observed using SEM (Figure 6.11 a,b). The nanoparticles were aggregated in both suspensions, forming large group of bundles of smaller particles which were clearly visualized. Some of these bundles could have been formed *in-situ* during sample drying as part of the sample preparation, especially since no additional dispersing agents were used.[50] A similar alignment of nanorods bundles was observed by Koshani *et al.* for copper assisted H_2O_2 oxidation for CNC isolation from softwood pulp.[38] It is interesting to observe the topographical morphology differences at higher magnification between the two samples where the nanocellulose bundles of NBM120 look more like rod-like whereas NBM170 nanocellulose look more quasispherical (Figure 6.11, c,d). Well-dispersed CNCs could be seen clearly from the AFM images (Figure 6.11-e,f). Both NBM120 and NBM170 showed a needle-like CNC, and the CNC was fairly individualized, which supports that the crystallites aggregate observed by SEM was mostly induced by the *in-situ* drying during sample preparation. Unfortauntely, due to time constraint as well as COVID-19 lockdown, TEM analysis wasn't conducted and therefore accurate estimation of the CNC dimensions couldn't be obtained. The measurement is still planned to be conducted as part of preperation for manuscript for publication.

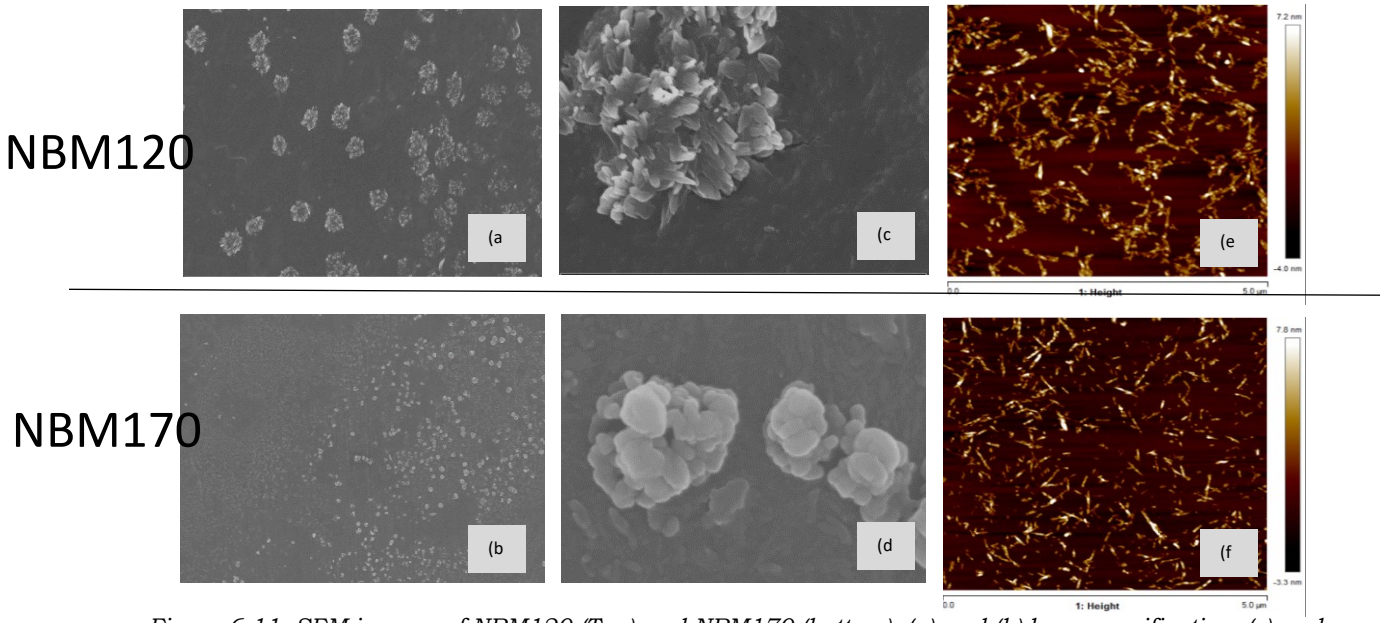

Figure 6.11: SEM images of NBM120 (Top) and NBM170 (bottom). (a) and (b) low magnification, (c) and (d) high magnification. (e) and (f) AFM height image for NM120 (top) and NMB170 (bottom)

6.3.2.3 Thermal stability and UV transmittance

Thermal stability of CNCs is an important property for several potential applications such as composites for electronic devices and fire retardants. Figure 6.12-a shows the TG curves for the obtained CNCs. The weight loss before 150 °C was attributed to water evaporation. NBM120 showed slightly higher thermal stability with T_0 of 230 °C compared to 210 °C for NBM170. These temperatures are within the T_0 range typically obtained for TEMPO-oxidized CNC/CNFs. The lower thermal stability of CNCs compared to the substrate cellulose pulps (typically T_0 >250 °C) is related to the significant reduction of DP and more importantly to the introduction of the carboxyl groups on their surface which are thermally unstable and naturally hydrophilic.[51,52] The char contents of NBM120 and NBM170 after thermal decomposition were 32% and 38%, respectively. **The high char content highlights the significant influence of surface functionalization on the thermal stability of the obtained CNCs and it is within the range of char content obtained from other oxidized CNCs.** Lichtenstein and Lavoine studied the thermal degradation mechanism of TEMPO-oxidized CNFs and their study showed that the surface chemistry of the oxidized CNFs had a significant impact on the lower thermal stability compared to non-oxidized CNFs.[52] The ash content of the

TEMPO-oxidized CNFs were 10 to 20% higher compared to the non-oxidized CNFs which is attributed to the extensive change in surface chemistry. While many CNCs applications are based on their use in reinforced composites, there has been growing interest on the use of CNCs as self-standing films or aerogels and foams. Freeze drying the CNC suspensions produced ultra-light white foam (Figure 6.12-b) which were characterized by SEM to show an amorphous architecture with mushroom-like morphology (Figure 6.12-c). **On the other hand, casting the CNC suspensions on petri dish at ambient temperature formed a nanofilm.** Because of the dense packing of the CNCs, the nanofilm was highly transparent (Figure 6.12-d). Figure 6.12-e presents the optical transparency of 0.1 wt% CNCs aqueous suspensions. The optical transparency of NBM120 and NBM170 at 600 nm were 83% and 89%, respectively, similar to those of previous reports. The transmittance of the CNC solution in the UV-vis spectrum is a result of both light absorption and scattering, which can be affected by the chemical structure and the size of the CNCs particles. As the particles in NBM120 suspension was larger compared to the particles in NBM170, it is expected that the amount of light scattered also to be higher which results in the observed decreased of optical transmittance.

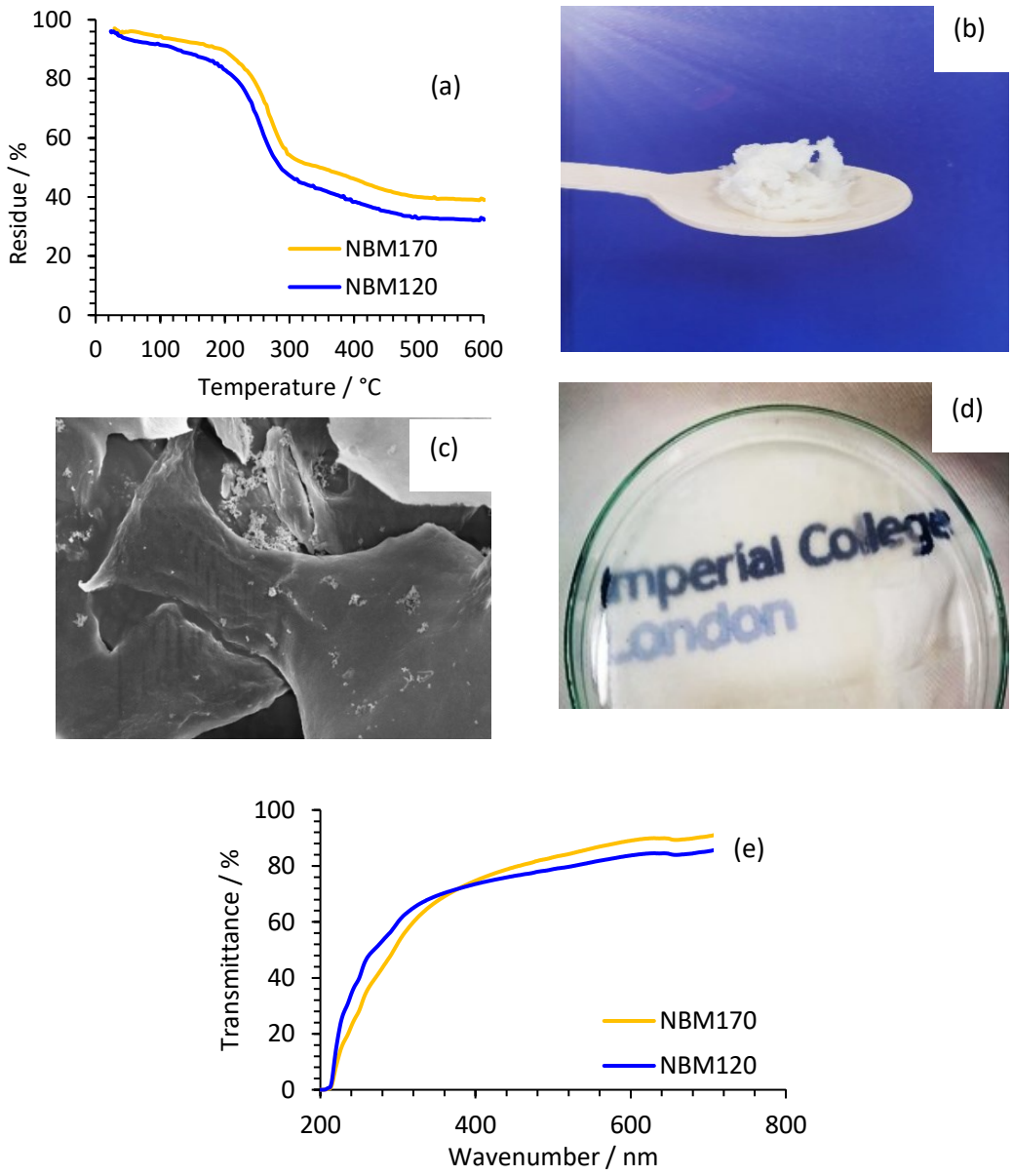

Figure 6.12: (a) TG curves for freeze-dried CNCs (b) freeze-dried CNCs suspension (c) SEM of freeze dried CNCs (d) nanofilm formation on petri-dish (e) UV-vis spectrum for CNCs suspensions.

6.4 Conclusion

The study demonstrates a simple one-step alkaline H_2O_2 oxidation procedure to produce carboxylated nanocellulose using unbleached cellulose substrates produced by ionoSolv fractionation process. We showed that pretreatment severity had a significant impact on the cellulose composition and purity and consequently, in its reactivity with the oxidation process reagents. The more delignified pulp M120 was mercerized during the alkaline oxidation treatment as evidenced by the change in the cellulose polymorph from cellulose I to cellulose II. The results also showed that ionoSolv cellulose substrates have relatively low Mw and DP compared to commercially bleached pulp. The followed alkaline oxidation procedure also resulted in significant reduction in the cellulose M_w and DP producing a near-LODP cellulose reside that can be further processed to CNFs or CNCs using few processing steps. Analysis of the cellulose-rich suspensions showed the generation of negatively charged, electrostatically stable, needle-like CNCs. The crystallinity of the CNCs were lower compared to their precursors, which indicates the high level of degradation of crystalline regions in cellulose. Further control over the oxidation reagents and pretreatment conditions could potentially improve the generated CNCs crystallinity. The produced CNCs showed the attachment of carboxyl functional groups which explains the stability of the suspension. The carboxylation of the CNCs surface caused a slight decrease in their thermal stability which is a known effect when using oxidation methods to produce CNCs.

References

(1) Hon, D. N. S. Cellulose: A Random Walk along Its Historical Path. Cellulose 1994, 1 (1), 1–25. https://doi.org/10.1007/BF00818796.

(2) Brandt, A.; Gräsvik, J.; Hallett, J. P.; Welton, T. Deconstruction of Lignocellulosic Biomass with Ionic Liquids. Green Chem. 2013, 15 (3), 550–583. https://doi.org/10.1039/c2gc36364j.

(3) Chen, C.; Duan, C.; Li, J.; Liu, Y.; Ma, X. Cellulose (Dissolving Pulp) Manufacturing Processes: A Mini Review. Bioresources 2016, 11 (2), 5553–5564.

(4) Ignatyev, I. Cellulose Valorization in Ionic Liquids; 2011.

(5) Nechyporchuk, O.; Belgacem, M. N.; Bras, J. Production of Cellulose Nanofibrils: A Review of Recent Advances. Industrial Crops and Products. Elsevier B.V. December 25, 2016, pp 2–25. https://doi.org/10.1016/j.indcrop.2016.02.016.

(6) Eichhorn, S. J.; Dufresne, A.; Aranguren, M.; Marcovich, N. E.; Capadona, J. R.; Rowan, S. J.; Weder, C.; Thielemans, W.; Roman, M.; Renneckar, S.; Gindl, W.; Veigel, S.; Keckes, J.; Yano, H.; Abe, K.; Nogi, M.; Nakagaito, A. N.; Mangalam, A.; Simonsen, J.; Benight, A. S.; Bismarck, A.; Berglund, L. A.; Peijs, T. Review: Current International Research into Cellulose Nanofibers and Nanocomposites. J. Mater. Sci. 2010, 45 (1), 1–33. https://doi.org/10.1007/s10853-009-3874-0.

(7) Klemm, D.; Kramer, F.; Moritz, S.; Lindström, T.; Ankerfors, M.; Gray, D.; Dorris, A. Nanocellulosses: A New Family of Nature-Based Materials. Angewandte Chemie - International Edition. June 6, 2011, pp 5438–5466. https://doi.org/10.1002/anie.201001273.

(8) Foster, E. J.; Moon, R. J.; Agarwal, U. P.; Bortner, M. J.; Bras, J.; Camarero-Espinosa, S.; Chan, K. J.; Clift, M. J. D.; Cranston, E. D.; Eichhorn, S. J.; Fox, D. M.; Hamad, W. Y.; Heux, L.; Jean, B.; Korey, M.; Nieh, W.; Ong, K. J.; Reid, M. S.; Renneckar, S.; Roberts, R.; Shatkin, J. A.; Simonsen, J.; Stinson-Bagby, K.; Wanasekara, N.; Youngblood, J. Current Characterization Methods for Cellulose Nanomaterials. Chem. Soc. Rev. 2018, 47 (8), 2609–2679. https://doi.org/10.1039/c6cs00895j.

(9) Yang, H.; Tejado, A.; Alam, N.; Antal, M.; Van De Ven, T. G. M. Films Prepared from Electrosterically Stabilized Nanocrystalline Cellulose. Langmuir 2012, 28 (20), 7834–7842. https://doi.org/10.1021/la2049663.

(10) Hoeng, F.; Denneulin, A.; Bras, J. Use of Nanocellulose in Printed Electronics: A Review. Nanoscale 2016, 8 (27), 13131–13154. https://doi.org/10.1039/c6nr03054h.

(11) Sharma, A.; Thakur, M.; Bhattacharya, M.; Mandal, T.; Goswami, S. Commercial Application of Cellulose Nano-Composites – A Review. Biotechnology Reports. Elsevier B.V. March 1, 2019, p e00316. https://doi.org/10.1016/j.btre.2019.e00316.

(12) Ludwicka, K.; Jedrzejczak-Krzepkowska, M.; Kubiak, K.; Kolodziejczyk, M.; Pankiewicz, T.; Bielecki, S. Medical and Cosmetic Applications of Bacterial NanoCellulose. In Bacterial Nanocellulose: From Biotechnology to Bio-Economy;

Elsevier Inc., 2016; pp 145–165. https://doi.org/10.1016/B978-0-444-63458-0.00009-3.

(13) Chen, W.; Yu, H.; Lee, S. Y.; Wei, T.; Li, J.; Fan, Z. Nanocellulose: A Promising Nanomaterial for Advanced Electrochemical Energy Storage. Chemical Society Reviews. Royal Society of Chemistry April 21, 2018, pp 2837–2872. https://doi.org/10.1039/c7cs00790f.

(14) Li, M. C.; Wu, Q.; Song, K.; Qing, Y.; Wu, Y. Cellulose Nanoparticles as Modifiers for Rheology and Fluid Loss in Bentonite Water-Based Fluids. ACS Appl. Mater. Interfaces 2015, 7 (8), 5009–5016. https://doi.org/10.1021/acsami.5b00498.

(15) Chen, L.; Zhu, J. Y.; Baez, C.; Kitin, P.; Elder, T. Highly Thermal-Stable and Functional Cellulose Nanocrystals and Nanofibrils Produced Using Fully Recyclable Organic Acids. Green Chem. 2016, 18 (13), 3835–3843. https://doi.org/10.1039/c6gc00687f.

(16) Isogai, T.; Saito, T.; Isogai, A. Wood Cellulose Nanofibrils Prepared by TEMPO Electro-Mediated Oxidation. Cellulose 2011, 18 (2), 421–431. https://doi.org/10.1007/s10570-010-9484-9.

(17) Ji, H.; Xiang, Z.; Qi, H.; Han, T.; Pranovich, A.; Song, T. Strategy towards One-Step Preparation of Carboxylic Cellulose Nanocrystals and Nanofibrils with High Yield, Carboxylation and Highly Stable Dispersibility Using Innocuous Citric Acid. Green Chem. 2019, 21 (8), 1956–1964. https://doi.org/10.1039/c8gc03493a.

(18) Isbell, H. S.; Frush, H. L. Mechanisms for Hydroperoxide Degradation of Disaccharides and Related Compounds. Carbohydr. Res. 1987, 161 (2), 181–193. https://doi.org/10.1016/S0008-6215(00)90076-4.

(19) Peng, C.; Liu, C.; Xie, Z. Preparation of a Fluorescent Silver Nanoprism-Dye Complex for Detection of Hydrogen Peroxide in Milk. Anal. Methods 2015, 7 (23), 9749–9752. https://doi.org/10.1039/c5ay01261a.

(20) Koshani, R.; Van De Ven, T. G. M.; Madadlou, A. Characterization of Carboxylated Cellulose Nanocrytals Isolated through Catalyst-Assisted H2O2 Oxidation in a One-Step Procedure. J. Agric. Food Chem. 2018, 66 (29), 7692–7700. https://doi.org/10.1021/acs.jafc.8b00080.

(21) Li, Y.; Liu, Y.; Chen, W.; Wang, Q.; Liu, Y.; Li, J.; Yu, H. Facile Extraction of Cellulose Nanocrystals from Wood Using Ethanol and Peroxide Solvothermal Pretreatment Followed by Ultrasonic Nanofibrillation. Green Chem. 2016, 18 (4), 1010–1018. https://doi.org/10.1039/c5gc02576a.

(22) Budtova, T.; Navard, P. Cellulose in NaOH–Water Based Solvents: A Review. Cellulose. Springer Netherlands February 1, 2016, pp 5–55. https://doi.org/10.1007/s10570-015-0779-8.

(23) Pönni, R.; Pääkkönen, T.; Nuopponen, M.; Pere, J.; Vuorinen, T. Alkali Treatment of Birch Kraft Pulp to Enhance Its TEMPO Catalyzed Oxidation with Hypochlorite. Cellulose 2014, 21 (4), 2859–2869. https://doi.org/10.1007/s10570-014-0278-3.

(24) Gschwend, F. J. V.; Brandt, A.; Chambon, C. L.; Tu, W. C.; Weigand, L.; Hallett, J. P. Pretreatment of Lignocellulosic Biomass with Low-Cost Lonic Liquids. J. Vis. Exp. 2016, 2016 (114). https://doi.org/10.3791/54246.

(25) Sluiter, A.; Hames, B.; Hyman, D.; Payne, R.; Scarlata, C.; Sluiter, J.; Templeton, D.; Wolfe, J. Determination of Total Solids in Biomass and Total Dissolved Solids in Liquid Process Samples; 2008

(26) Sluiter, a.; Hames, B.; Ruiz, R.; Scarlata, C.; Sluiter, J.; Templeton, D.; Crocker, D. Determination of Structural Carbohydrates and Lignin in Biomass; 2012.

(27) Liu, Y.; Shi, L.; Cheng, D.; He, Z. Dissolving Pulp Market and Technologies: Chinese Prospective - a Mini-Review. BioResources 2016, 11 (3), 7902–7916. https://doi.org/10.15376/biores.11.3.Liu.

(28) Gschwend, F. J. V.; Brandt-Talbot, A. Rapid Pretreatment of Miscanthus Using the Low-Cost Ionic Liquid Triethylammonium Hydrogen Sulfate at Elevated Temperatures. Green Chem. 2016, 20 (15), 3486–3498. https://doi.org/10.1039/c8gc00837j.

(29) Shinde, S. D.; Meng, X.; Kumar, R.; Ragauskas, A. J. Recent Advances in Understanding the Pseudo-Lignin Formation in a Lignocellulosic Biorefinery. Green Chem. 2018, 20 (10), 2192–2205. https://doi.org/10.1039/c8gc00353j.

(30) Brandt-Talbot, A.; Gschwend, F. J. V.; Fennell, P. S.; Lammens, T. M.; Tan, B.; Weale, J.; Hallett, J. P. An Economically Viable Ionic Liquid for the Fractionation of Lignocellulosic Biomass. Green Chem. 2017, 19 (13), 3078–3102. https://doi.org/10.1039/C7GC00705A.

(31) Froschauer, C.; Hummel, M.; Iakovlev, M.; Roselli, A.; Schottenberger, H.; Sixta, H. Separation of Hemicellulose and Cellulose from Wood Pulp by Means of Ionic Liquid/Cosolvent Systems. Biomacromolecules 2013, 14 (6), 1741–1750. https://doi.org/10.1021/bm400106h.

(32) Gregorio, G. F. De; Weber, C. C.; Gräsvik, J.; Welton, T. Mechanistic Insights into Lignin Depolymerisation in Acidic Ionic Liquids. Green Chem. 2016. https://doi.org/10.1039/c6gc01295g.

(33) Shinoda, R.; Saito, T.; Okita, Y.; Isogai, A. Relationship between Length and Degree of Polymerization of TEMPO-Oxidized Cellulose Nanofibrils. Biomacromolecules 2012, 13 (3), 842–849. https://doi.org/10.1021/bm2017542.

(34) Sirviö, J. A. Fabrication of Regenerated Cellulose Nanoparticles by Mechanical Disintegration of Cellulose after Dissolution and Regeneration from a Deep Eutectic Solvent. J. Mater. Chem. A 2019, 7 (2), 755–763. https://doi.org/10.1039/c8ta09959f.

(35) Habibi, Y.; Lucia, L. A.; Rojas, O. J. Cellulose Nanocrystals: Chemistry, Self-Assembly, and Applications. Chem. Rev. 2010, 110 (6), 3479–3500. https://doi.org/10.1021/cr900339w.

(36) Tu, W. C.; Weigand, L.; Hummel, M.; Sixta, H.; Brandt-Talbot, A.; Hallett, J. P. Characterisation of Cellulose Pulps Isolated from Miscanthus Using a Low-Cost Acidic Ionic Liquid. Cellulose 2020, 1–17. https://doi.org/10.1007/s10570-020-03073-1.

(37) Sèbe, G.; Ham-Pichavant, F.; Ibarboure, E.; Koffi, A. L. C.; Tingaut, P. Supramolecular Structure Characterization of Cellulose II Nanowhiskers Produced by Acid Hydrolysis of Cellulose i Substrates. Biomacromolecules 2012, 13 (2), 570–578. https://doi.org/10.1021/bm201777j.

(38) Koshani, R.; Van De Ven, T. G. M.; Madadlou, A. Characterization of Carboxylated Cellulose Nanocrytals Isolated through Catalyst-Assisted H2O2 Oxidation in a One-Step Procedure. J. Agric. Food Chem. 2018, 66 (29), 7692–7700. https://doi.org/10.1021/acs.jafc.8b00080.

(39) Chen, D.; van de Ven, T. G. M. Morphological Changes of Sterically Stabilized Nanocrystalline Cellulose after Periodate Oxidation. Cellulose 2016, 23 (2), 1051–1059. https://doi.org/10.1007/s10570-016-0862-9.

(40) Gong, J.; Li, J.; Xu, J.; Xiang, Z.; Mo, L. Research on Cellulose Nanocrystals Produced from Cellulose Sources with Various Polymorphs. RSC Adv. 2017, 7 (53), 33486–33493. https://doi.org/10.1039/c7ra06222b.

(41) Zhang, S.; Zhang, F.; Jin, L.; Liu, B.; Mao, Y.; Liu, Y.; Huang, J. Preparation of Spherical Nanocellulose from Waste Paper by Aqueous NaOH/Thiourea. Cellulose 2019, 26 (8), 5177–5185. https://doi.org/10.1007/s10570-019-02434-9.

(42) Neng, W.; Enyong, D.; Rongshi, C. Preparation and Liquid Crystalline Properties of Spherical Cellulose Nanocrystals. Langmuir 2008, 24 (1), 5–8. https://doi.org/10.1021/la702923w.

(43) Lou, H.; Zhu, D.; Yuan, L.; Lin, H.; Lin, X.; Qiu, X. Fabrication and Properties of Low Crystallinity Nanofibrillar Cellulose and a Nanofibrillar Cellulose-Graphene Oxide Composite. RSC Adv. 2015, 5 (83), 67568–67573. https://doi.org/10.1039/c5ra13181b.

(44) Abraham, E.; Deepa, B.; Pothan, L. A.; Jacob, M.; Thomas, S.; Cvelbar, U.; Anandjiwala, R. Extraction of Nanocellulose Fibrils from Lignocellulosic Fibers : A Novel Approach. Carbohydr. Polym. 2011, 86 (4), 1468–1475. https://doi.org/10.1016/j.carbpol.2011.06.034.

(45) Zhu, C.; Soldatov, A.; Mathew, A. P. Advanced Microscopy and Spectroscopy Reveal the Adsorption and Clustering of Cu(II) onto TEMPO-Oxidized Cellulose Nanofibers †. Nanoscale 2017, 9. https://doi.org/10.1039/c7nr01566f.

(46) Chen, M.; Ma, Q.; Zhu, J. Y.; Martin Alonso, D.; Runge, T. GVL Pulping Facilitates Nanocellulose Production from Woody Biomass. Green Chem. 2019, 21 (19), 5316–5325. https://doi.org/10.1039/c9gc01490j.

(47) Zhang, S. D.; Zhang, Y. R.; Wang, X. L.; Wang, Y. Z. High Carbonyl Content Oxidized Starch Prepared by Hydrogen Peroxide and Its Thermoplastic Application. Starch/Staerke 2009, 61 (11), 646–655. https://doi.org/10.1002/star.200900130.

(48) Fukaya, Y.; Iizuka, Y.; Sekikawa, K.; Ohno, H. Bio Ionic Liquids: Room Temperature Ionic Liquids Composed Wholly of Biomaterials. Green Chem. 2007, 9 (11), 1155. https://doi.org/10.1039/b706571j.

(49) Ji, H.; Xiang, Z.; Qi, H.; Han, T.; Pranovich, A.; Song, T. Strategy towards One-Step Preparation of Carboxylic Cellulose Nanocrystals and Nanofibrils with High Yield,

Carboxylation and Highly Stable Dispersibility Using Innocuous Citric Acid. Green Chem. 2019, 21 (8), 1956–1964. https://doi.org/10.1039/c8gc03493a.

(50) Stinson-Bagby, K. L.; Roberts, R.; Foster, E. J. Effective Cellulose Nanocrystal Imaging Using Transmission Electron Microscopy. Carbohydr. Polym. 2018, 186, 429–438. https://doi.org/10.1016/j.carbpol.2018.01.054.

(51) Chen, M.; Ma, Q.; Zhu, J. Y.; Martin Alonso, D.; Runge, T. GVL Pulping Facilitates Nanocellulose Production from Woody Biomass. Green Chem. 2019, 21 (19), 5316–5325. https://doi.org/10.1039/c9gc01490j.

(52) Lichtenstein, K.; Lavoine, N. Toward a Deeper Understanding of the Thermal Degradation Mechanism of Nanocellulose. Polym. Degrad. Stab. 2017, 146, 53–60. https://doi.org/10.1016/j.polymdegradstab.2017.09.018.

Chapter 7 : Dye Recycle - A Holistic Circular Approach for Textile Industry

S7.1 Introduction

The fashion industry was worth £32 billion to the UK economy in 2017. The growth rate of the industry is overtaking high growth sectors such as technology and communication. However, the growth of the industry is equivalent to the growth of the environmental issue its creating: textile waste and remarkable carbon footprint (1.2 billion tonnes of CO_2 equivalent per year - more than international flights and maritime shipping combined).[1] According to Ellen MacArthur Foundation, $500 billion of value is lost every year due to clothing underutilisation and the lack of recycling.[2] The UK WRAP report estimates that £140 million worth of clothing goes to landfill every year.[3] Large contributor to this number is the unprecedented growth of fast fashion retailers and online stores who provide hundreds to thousands of new designs every week, encouraging over-consumption and generating excessive waste.[4]

This level of production and consumption is against a key UN Sustainable Development Goal (goal no. 12): responsible consumption and production and climate action. Today, fashion industry is under tremendous pressure to provide more sustainable and more transparent solutions across the entire supply chain. Pushing retailers toward using recycled materials, particularly recycled polyester (rPET) and recycled nylon, became key trends among sustainable brands. In 2018, Textile Exchange, non-profit organization, challenged 50 textile and retail companies to increase their rPET use by 25% by 2020. The use of rPET provides key environmental saving, where it was estimated that manufacturing of rPET requires 59% less energy compared to virgin PET (32% less CO_2 emissions). However, it is key to know two key points when considering rPET. First, the sources of rPET is currently plastic bottles which are recycled mechanically to produce rPET, once the rPET is made into fibers , it can't be recycled again using mechanical recycling method. Chemical recycling which involves the depolymerization of the polymer into its monomer is more expensive and energy consuming and only demonstrated at pilot scale. Therefore, all the fabrics made of rPET will not be able to be reused again to produce another fabric, until fiber-to-fiber technologies become fully realized at commercial scale. Second, rPET is usually still

mixed with virgin polyester to improve its properties, especially the mechanical strength that is lost during the mechanical recycling process.[5]

Large amount of post-consumer textile waste in the UK ends up at charity shops, which are currently considered the key textile waste infrastructure. The price for post-consumer textile waste range between £180/tonne to £410/tonne.[6] On the other hand, an estimated 300,000 tons per year of textile waste in the UK still end-up in municipal waste streams where 80% of it is incinerated and 20% is landfilled.[6] The amount of pre-consumer textile waste is even higher with 800,000 tons per year of clothing waste was generated in the UK (2016) just during the design and production of the fabrics.[3,6] Tighter regulations and higher taxes are expected to be taken in the future for textile suppliers and brands to minimize the amount of pre-consumer textile waste generated.

Despite the growing efforts to reduce textile waste and the use of more sustainable materials, the fashion and textile industry production rate is projected to continue to increase in the near term. The high demand drives high demand and growth for the downstream industry including the $7 billion textile dyes market.[7] The recent environmental and safety regulations in the dyeing industry in China have caused a surge in the dyestuff prices, particularly disperse dyes – class of dyes used to dye synthetic fibers , mainly polyester. The regulations came after the horrific explosion in March 2018 at the Jiangsu Tianjiayi Chemical factory in China, one of the largest disperse dye producers in the world (150 ktonns per year) causing the death for 78 people. The explosion caused the prices of some disperse dyes to increase from £20/kg to £55/kg.[7] The prices of reactive dyes have also experienced similar skyrocketing increase in price due to the stricter environmental regulations and shut down of many factories in China which caused the price of some reactive dyes and their intermediates to increase from £4/kg to £9/kg. [7] In 2018, BASF made statement that the prices of dyes and pigments to their customers will increase by 15% due to the increase in the prices of raw materials and stricter regulations. The increase in dyes prices directly pushed up production costs of printing and dyeing enterprises.[8]

Demand for more eco-friendly dyes and dyeing methods started to gain attention only recently. Archroma, industrial chemical dyes giant, have launched recently an eco-friendly dye formulation, called EarthColors that is derived from biomass waste.[8] The

colours provided are limited to shades of brown as the biomass waste used is mostly nutshells. In addition, more sustainable dye formulations are becoming more popular using Bluesign certification system. Bluesign is a swiss company that provides certification for textile companies and dyeing manufacturers via what they refer to as Bluesign approved chemicals, which increases the safety of the chemicals along the supply chain. The firm offers full certification, which means that a dyehouse has been completely converted to meet Bluesign's specifications. Obtaining the full certification was communicated to be expensive, and therefore some dyeing houses who are under pressure by some "sustainable brands" choose an alternative route where they do not get full certification but certify certain number of dyes through Bluesign. The dyeing house still needs to learn how to use those new certified dyes.[9] However, currently, the certified dyes account for small fraction of the total number of synthetic dyes used in the dyeing houses as large sustainable fashion brands only make small fraction of the dye house total business.[9] The use of supercritical fluids, particularly sCO_2 have studied extensively in literature due to their high dye dissolving power and unform dyeing performance.[10–13] Several new dyeing methods were also developed at lab-scale during the past two decades, these include the use of organic solvents such as glycerol and ethanol[14,15] as well as aprotic ionic liquids[16–18] as the dyeing medium.

As discussed in Chapter 1 section 1.10.4, dye removal technologies from textile substrates did not receive huge attention compared to dyeing technologies simply because there was no obvious need for these technologies. The recent increasing trend and demand of mechanical and chemical fiber recycling technologies, the presence of dyes in the fibers have been identified as a source of contamination. The recent need to remove dyes from textile waste sparked the interest to explore dye removal technologies as described by few recent patents.[19,20] The common aspect of these patents is the use of organic solvents such as xylene, acetone and ethylene glycol as the solvent of choice to remove disperse dye from polyester-based textiles. In addition, none of the patents described the state of the extracted dyes or any potential use. The Hong Kong Research Institute of Textiles and Apparel (HKRITA) has recently developed a hydrothermal technology to remove dyes from textile waste followed by capturing the extracted dye in activated carbon adsorption column – and therefore showing no intended use for the extracted dye.[21]

Towards the end of this PhD research work, an dye-recycle process concept was developed. The process contributes to solve two key environmental challenges faced by the PET recycling sector and the textile industry: i) decoloured PET that meets PET recycling specifications and, ii) sustainable circular dyeing using textile waste as feedstock for dyes. The integrated process uses low-cost protic IL to selectively extract dyes from textile fibers, particularly synthetic fibers, and then the same extraction solvent medium is used as a dye bath to dye new piece of garment. Therefore, the technology provides an innovative concept of "recycled synthetic dyes". To the best of our knowledge, there is no existing technology that provides this type of solution which opens the possibility to reduce the consumption of virgin synthetic dyes via recycling the existing dyes and therefore provides carbon, water and chemical saving throughout the entire manufacturing and transportation of virgin synthetic dyes. The process provides a unique dyeing and a fiber decontaminations service that none of the existing technologies provide.

Figure 7.1 shows the vision of where the proposed dye recycle process fit in the supply chain of the textile industry. The two product streams are i) de-coloured polyester textile waste sent for PET recycling facilities, and ii) coloured polyester fabric sent for textile suppliers. The input stream of the process can be either post-consumer textile waste or pre-consumer textile waste from the textile suppliers/brands.

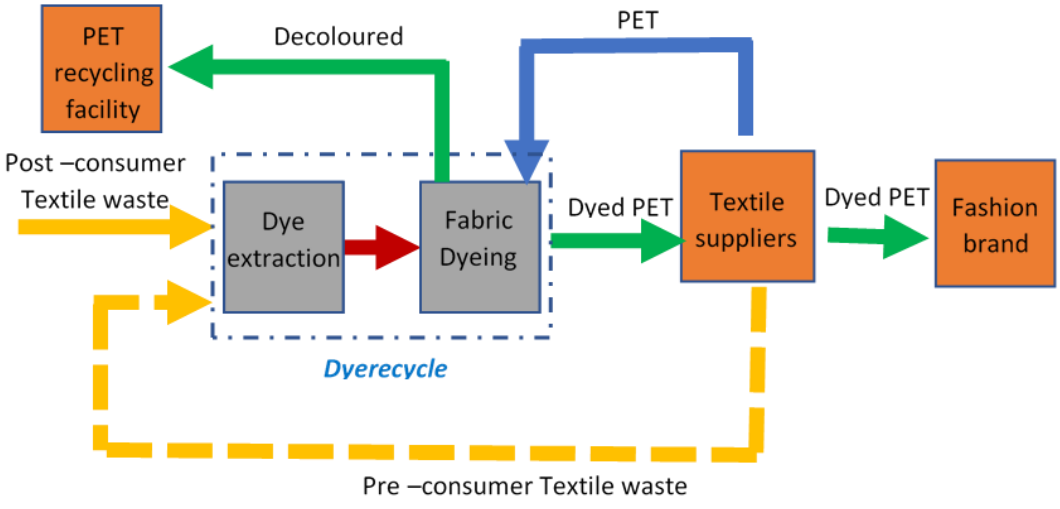

Figure 7.1: Proposed dye recycle process using ionic liquids to extract dyes from textile waste and subsequently used the extracted dyes to dye new fibers

7.2 Materials & Methods

Materials: The post-consumer textile materials (cotton and polyester) were purchased from Red Cross Charity shop in Chelsea, London. The orange polycotton fabric was purchased from UK Fabrics and the white polyester used for dyeing experiment was purchased from H&M (white T-shirt, 100% polyester). The chemical reagents used for [DMBA][HSO_4] synthesis was purchased from Sigma Aldrich. Synthesis of the ionic liquid was described in detail in Chapter 2 section 2.2.3.

7.2.1 Dye extraction procedure

Post-consumer polyester pieces were cut into small squares and rectangles and pre-weighted and inserted in the pressure tube. The IL solution of pre-determined concentration was added into the pressure tube and the mixture is vortexed thoroughly to ensure that the entire fabric content was wetted and in contact with the IL medium. The pressure tubes were then placed in the pre-heated oven to perform the dye extraction process for a defined time. When the time of the experiment elapsed, the pressure tubes were taken out and left to cool down in the fume hood by convection. After, the pressure tubes were opened and with the help of spatula, the polyester piece was pushed down to squeeze all the IL out of it and the IL was decanted in 15-mL falcon tube. It is very important to conduct these steps in fume hood as sometimes there was an unpleasant strong odour after the treatment. The de-coloured polyester was then placed in a 50-mL falcon tubes and washed thoroughly x4 with de-ionized water and then left to air-dry. For time effect experiments, the temperature of the extraction was fixed to 150 °C using 80 wt% [DMBA][HSO_4] and solid loading of 1:10 g g^{-1}. For IL concentration effect, the conditions were set to 150 °C for 30 minutes and a solid loading of 1:5 g g^{-1}. For temperature effect, the experiments were conducted at 120 °C, 150 °C and 170 °C for 30 minutes at 1 : 5 g g^{-1} solid loading. For the solid loading effect, the experiments were conducted at 150 °C for 45 minutes using 80 wt% [DMBA][HSO_4] solution using 7% solid loading (0.7 g farbic in 10 g IL solution) and 21% solid loading (2.1 g fabric in 10 g IL solution). For multiple extraction experiment, the conditions were sat to 150 °C for 45 minutes with solid loading of 1:10 g g^{-1} . When cotton fabric is used instead of polyester, the same steps are followed, and the experiments were conducted at 150 °C for 30 minutes using 1:10 g g^{-1} solid loading. The disintegrated cotton powder is separated from the IL solution by careful decanting and the powder is washed

thoroughly with DI water, separated by centrifugation at (3500 rpm) for 1 hour and then freeze-dried.

7.2.2 PET dyeing in IL bath

Pre-weighted white polyester fabric was placed inside the pressure tube and the IL solution of pre-determined concentration that contains the extracted dye was added. The content of the pressure tube was mixed using vortex to ensure maximum contact between the fibers and the IL + dye solution. The dyeing experiments were then performed by pre-heating the pressure tube at 70 °C for 30 minutes, followed by heating the dye bath to 150 °C for additional 30 minutes. The solid loading used in the dyeing experiments were 1:10 g g^{-1} and 1:5 g g^{-1}. After the time elapsed, the pressure tubes were placed in the fume hood to cool down. Once cooled, the pressure tubes were opened at the exhaust dye bath was separated from the newly dyed polyester fabric. The dyed fabric was transferred into 50-mL falcon tube where it was washed thoroughly with de-ionized water and then left to air-dry.

7.2.3 UV-vis spectroscopy

Colour strength of the fabric samples and absorbance of IL solutions were analysed by using a Shimadzu UV-1800 UV spectrophotometer. A background spectrum was first acquired from the empty sample holder. The spectra were acquired from 200 to 900 nm with a data interval of 1 nm. The K/S value represents the colour depth/intensity in a material, the higher the value, the higher the intensity and vice versa. The K/S value is calculated based on the following Equation:

$$\frac{K}{S} = \frac{(1-R_{min})^2}{2R_{min}} \qquad (7.1)$$

Where, K is the absorbance, S is the scattering and R_{min} is the lowest reflectance value (highest absorbance) at characteristic wavelength λ of every colour, in the case of red dyed polyester λ = 517 nm. For characterization of IL+ dye solutions, the dilutions of the IL + dye solutions were done using ethanol as a solvent due to the insolubility of disperse dyes in water.

7.2.4 Scanning electron microscopy (SEM)

Scanning electron microscopy images were taken by Dr. Ecaterina Ware, Materials Department using SEM, JOEL 6010A microscope. Samples were coated with a thin layer of gold and images were captured up with 10 kV accelerated voltage.

7.3 Results & Discussion

7.3.1 Dye extraction from textile waste

The extraction of disperse dyes from polyester textiles using low cost *N,N,N*-dimethylbutylammonium hydrogen sulfate [DMBA][HSO_4] was investigated. The choice of the solvent was based on a preliminary screening conducted where few ionic liquids, including the PILs [H_1Cim]Cl, [H_1Cim][HSO_4] and [MBHA][HSO_4] and the APIL [C_2C_1im][OAc] were screened to extract the dye from a polycotton fabric (Figure A27). Following, the effect of several key process parameters was investigated, namely residence time of dye extraction, temperature of extraction, solid loading, IL concentration and exposed surface area. The following sections discuss the results obtained.

Time effect

The first parameter that was studied was the extraction time to investigate its effect on the dye extraction using IL mixed with 20 wt% water. The temperature for the extraction was fixed to be 150 °C as a preliminary test showed good extraction at this temperature. The extraction time is believed to play an important role in the process as it impacts a) decolourization efficiency of the textile by allowing enough contact time to swell the fiber and remove the embedded disperse dye, and b) the stability and extent of decomposition of the extracted dye in the IL. **As the process as an extraction-dyeing process, the aim is to obtain satisfactory dye removal while maintaining minimum dye decomposition in the IL.** Figure 7.2 presents the UV-vis reflectance of decoloured fabrics at different times at 150 °C at a solid loading (i.e. g fabric to g of IL solution) of 1 : 10 g g^{-1}. The original fabric is a real post-consumer red 100% polyester obtained from a charity shop. From the UV vis spectrums, K/S values were calculated to measure the colour reduction % relative to the original fabric as presented in Table 7.1.

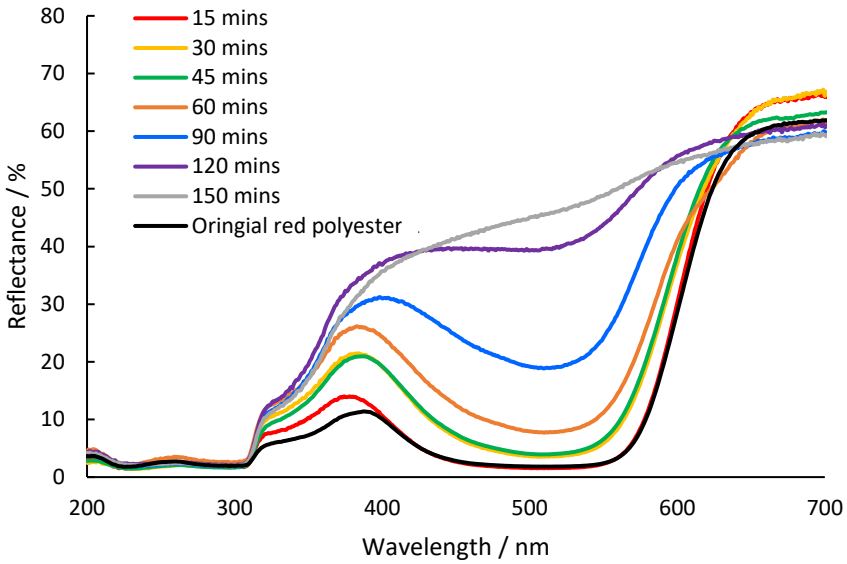

Figure 7.2: UV-vis spectrum of polyester extracted fabrics at different times using IL at 150 ℃ and 1:10 g g^{-1} loading

The dye extraction started after 30 minutes of treatment time as no colour reduction happened in the first 15 minutes. Colour reduction of 51% was achieved in 30 minutes with further reduction to 66% in 45 minutes and 79% in 60 minutes. At 90 minutes of treatment time, the colour reduction reached to 96% and further increasing treatment time resulted in 98% reduction and the fabric looked almost white as seen in Figure 7.3.

Table 7.1: K/S values of dye extracted polyester fabric at 150 ℃ at different time intervals

Time (mins)	K/S	%Colour reduction
15	26.02	1.0%
30	12.90	50.9%
45	8.80	66.4%
60	5.44	79.3%
90	1.08	95.9%
120	0.46	98.3%
150	0.32	98.8%
Original red polyester	26.29	

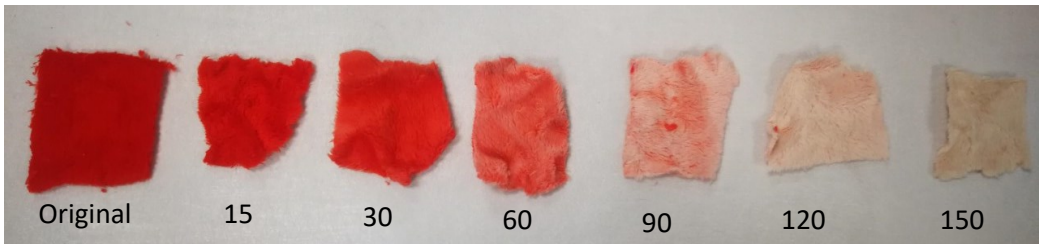

Figure 7.3: original picture of dye extracted polyester at different times using IL at 150 °C

As mentioned earlier, the aim of the process is to maintain a balance between the dye extraction efficiency and the stability and state of the dye such that it can be re-used in a dyeing bath. Therefore, it was important monitor the state and concentration of the dye in the IL. Figure 7.4-a shows the UV spectrums for the IL solutions and an image of the solutions. Figure 7.4-b shows the original photo of the IL + dye extracted solutions at different extraction times. **The dye absorbance was the highest at 30 minutes, and it started to decrease at longer times indicating that the dye started to decompose.** At 90 minutes time, the dye started showing a fader colour of red and longer extraction time led to complete decomposition of the dye. **Therefore, we highlight that at this temperature, the dye extraction should not exceed 45 minutes to avoid dye degradation**. It is important to note that quantification of the dye concentration in the IL is still undergoing. The challenge in this task is that dye concentration is much smaller compared to the IL concentration which makes determining its structure using mass spectroscopy not possible. In addition, a calibration curve can not be made to determine the extension coefficient as the initial concentration of the dye in the IL is not known and the structure of the dye is not known, which makes it very challenging to quantify the concentration – especially with vast number of commercial dyes available. Future study should investigate on methods to isolate the dye from the IL medium via for example sublimation since disperse dyes typically have high vapor pressures.[22] However, in this part, the key point was to determine the K/S value which determine the extraction efficiency and from the absorbance values we can qualitatively evaluate the dye concentration/decomposition as it is directly proportional to the measured absorbance.

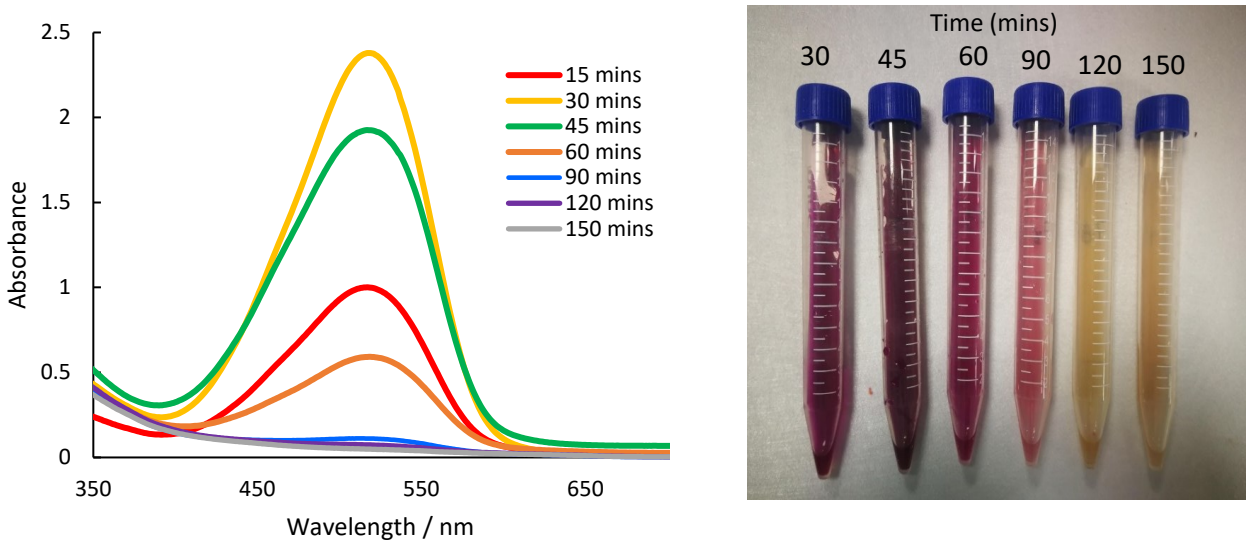

Figure 7.4: (a) UV-vis spectrums of IL solutions after dye extraction at different temperatures. (b) Original picture of the IL + dye solutions

Ionic Liquid concentration effect

Another key parameter in this process is the IL concentration and its impact on the dye extraction efficiency. Figure 7.5 shows the UV vis spectrums of the IL + dye solutions after extraction experiment at 150 °C for 30 minutes and solid loading of 1 : 5 g g^{-1}. It is can be clearly seen that the IL concentration plays a key role in determining the extraction efficiency with absorbance dropping by 50% when increasing the water concentration mixed with IL from 20 wt% to 30 wt%. The absorbance, and therefore the dye concertation, drops significantly to almost zero when reducing the IL wt% to 50 wt% and 20 wt%. **The findings show that high concentration of IL is essentially important to swell the fibers and achieve high dye extraction from PET fibers.**

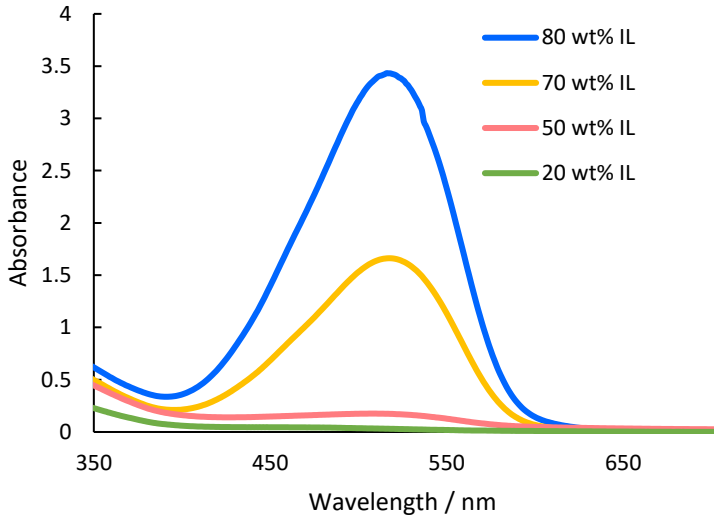

Figure 7.5: UV-vis spectrums of dye extractions using different IL concentrations at 150 °C and 30 minutes

Temperature effect

The impact of temperature on the extraction is shown in Figure 7.5-a below. The experiments were conducted using 80 wt% IL for 30 minutes at 1 : 5 g g^{-1} solid loading. There is a clear absorbance optimum at 150 °C, operating the process at lower temperature of 120 °C didn't extract as much dye and operating the process at 170 °C caused the dye to decompse, indicated by the fade red colour of the IL solution. The absorbance of the dye reduced significantly from 3.4 to 0.8 upon increasing the temperature from 170 °C to 150 °C, corresponding to 76% reduction in absorbance, and therbay dye concentration. Figure 7.6-b shows the refletance of the extracted fabrics vs. the original fabric. **Both fabrics extracted at 150 and 170 °C showed the same level of colour reduction (K/S = 12.75) , wheras the fabirc extract at 120 °C showed the same reflectance of the untreated orignal material (K/S = 26.29), indicating that there is no signifcant colour reduction achieved.** It is important to note that operating the process at high temperature can impact the PET morphology and crystallinity, particularly the amorphous part of the polymer.[13] To have a comprehensive understanding about the extraction efficiency as a function of temperature, different time points at each temperature should be conducted such that the combined time-temperature effect is studied. However, this is not a crucial point at this point of the study and **therefore the optimum operating parameters for extraction taken as 150 °C, 30 minutes and 80 wt% IL which was used for the following experiments.**

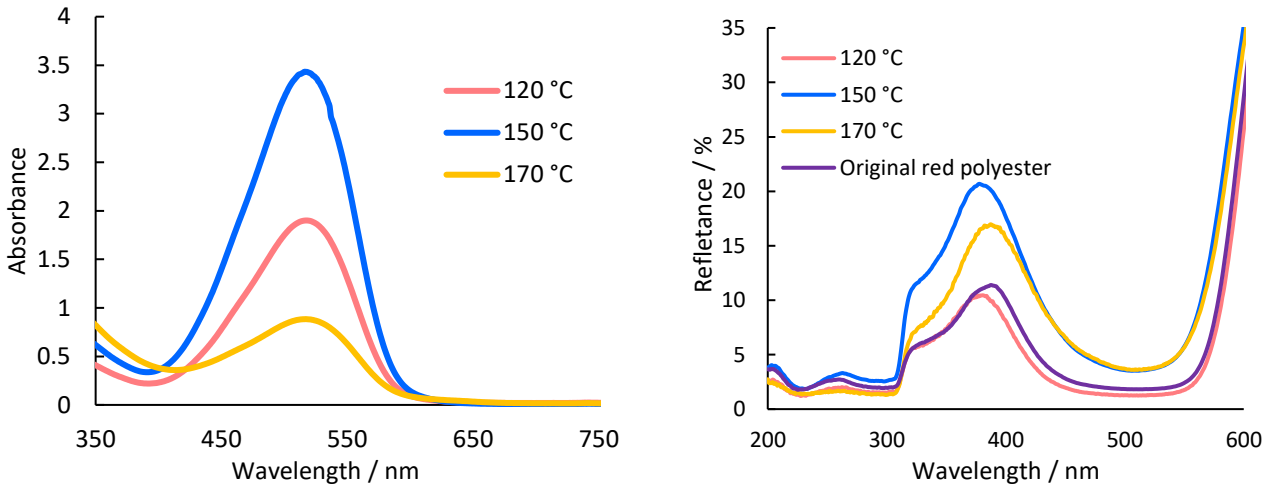

Figure 7.6: (a) UV vis spectrum of IL + dye solutions extracted at different temperatures. (b) UV-vis spectrum for polyester extracted fabric at different temperatures for 30 minutes using 1:5 g g^{-1} solid loading

Fabric loading and surface area effect

Solid loading is one of the key economic parameters in the process, particularly if the process is conducted in a batch operation. To study the solid loading effect, the experiments were conducted at 150 °C for 45 minutes using 80 wt% [DMBA][HSO_4] solution. Figure 7.7 shows the impact of the solid loading on the dye extraction efficiency as a function of the solid loading, defined as the g of fabric solid per g of IL solution. **Increasing the solid loading from 7% to 21% decreased the extraction efficiency of the dye very slightly where the colour reduction decreased from 79% to 71%, respectively (Table 7.2). The finding highlights the high efficiency of the IL to extract dye at more-industrially- relevant solid loadings.**

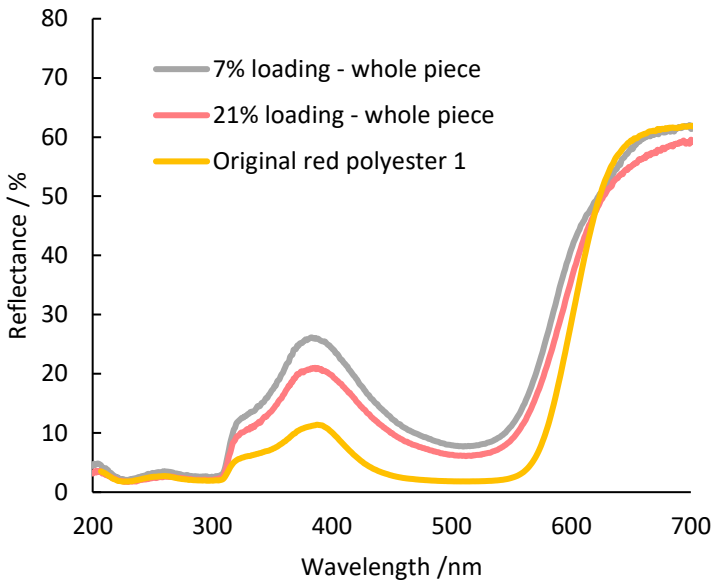

Figure 7.7: (a) UV vis spectrum of IL + dye solutions extracted at different temperatures. (b) UV-vis spectrum for polyester extracted fabric at different temperatures for 30 minutes using 1:5 g g^{-1} solid loading

Operating the process at higher solid loading is very important from an economic prespertive as it corresponds to less g of IL used per g of fabric input. The solid loading in batch dyeing operations are highly variable ranging between 1:5 g g^{-1} to 1:40 g g^{-1}. The more recent dyeing machines typically operate between 1:5 g g^{-1} to 1:10 g g^{-1}. Therefore, taken into consideration that our dye extraction set-up is not optimized for this specific application and there is no stirring applied, the obtained results are highly promising with potentially better and higher extractions can be achieved using an improved set-up and introducing stirring/agitation in the process to enhance and accelerate the dye diffusion.

We also investigated the impact of the physical size of the polyester on the extraction efficiency of the dye as higher exposed surface area of the yarn should improve the extraction efficiency compared to using a woven piece of fabric, keeping the solid loading constant of 1 : 5 g g^{-1} and extraction conditions of 150 °C and 30 minutes. Figure 7.8 shows the difference in the extraction efficiency when treating a whole piece woven polyester material (4x4 cm^2) vs. when cutting the material into thin pieces like threads (d = 0.5 cm). The colour reduction improves signfricantly when using the polyester threads vs. the whole woven piece of fabric from 77% to 98% (Table 7.2).

This shows the exceptional extraction ability of the ILs that high extraction can be achieved by increasing the surface area of exposure, while at the same time maintaing the stability of the dye in the IL for later use as a dye bath.

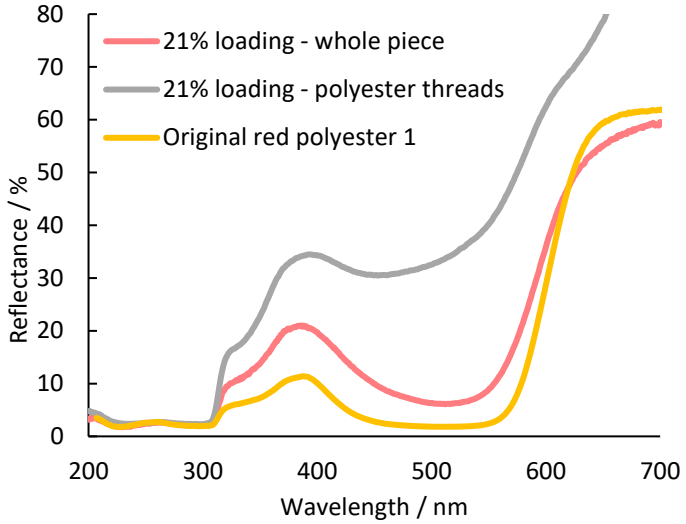

Figure 7.8: UV vis spectrums for dye extracted fabrics as a whole piece (4x4 cm^2) vs. threads of shredded polyester (d= 0.5 cm) at 150 °C and 45 minutes

Table 7.2: K/S values of dye extracted polyester pieces at different loadings and different shapes. Extraction conducted using red 100% polyester at 150 °C and 45 minutes

Description	K/S	% Colour reduction
7% loading - whole piece	7.82	79.3%
21% loading - whole piece	6.15	72.8%
21% loading - polyester threads	0.534	98.0%
Original red polyester	26.30	-

Multiple extraction

We expanded the investigation to use other polyester coloured fabric and polyester-based material such as polycotton. The extractions were conducted at 150 °C for 45 minutes with solid loading of 1 : 10 g g^{-1}. Three extractions were performed on the same piece of fabric by removing the IL+dye solution after every extraction, and then introducing a new IL solution to extract more dye from the same piece. The extractions were done using three PET-based fabrics: red coloured post-consumer 100% polyester

– which was the main fabric used in the previous experiments, pink coloured post-consumer 100% polyester, and an orange colour pre-consumer polycotton with 65% polyester and 35% cotton. The 100% red and pink polyester fabrics were real post-consumer textiles obtained from a charity shop (pink T-shirt and red blanket). The polycotton fabric was a pre-consumer textile purchased from https://ukfabricsonline.com/.

It is important to note that at the timeline of the project, this experiment was done very early on before optimizing the different extraction parameters. Therefore, the extractions do not necessarily represent the best extractions that can be obtained. In particular, the size of the fabrics used were relatively large dimensions of 5x5 cm^2 for 100% red PET, 7x6 cm^2 100% pink PET and 6.5 x 6.5cm^2 for the orange polycotton fabric. As shown previously, the exposed surface area seems to have a significant impact on the extraction efficiency, and therefore higher extractions can be achieved by conducting the experiments with smaller pieces of fabrics. Shredding the fabrics into small pieces can be easily achieved in an industrial scale and heavy-duty textile waste shredders are becoming very popular in the textile industry to achieve volume reduction for textile waste. Table 7.3 shows the K/S values of untreated fabrics and dye extracted fabrics as well as the colour reduction percentages relative to the original fabric. It should be noted that the reported percentages of colour reduction are all based on the original fabric, and not the previous extraction cycle. The K/S value, representing the colour strength of the fabric, varied across the original untreated materials, from very high deeply coloured red polyester blanket with K/S of 26.1, to the pink polyester T-shirt with K/S of 1.9.

The first extraction for all the three fabrics showed approximately 45-55% reduction in colour relative to untreated original fabric material. The 2nd extraction of the same piece of fabric showed considerable extraction for the red and pink polyesters, with increase in colour reduction by 35% relative to the 1st extraction cycle. Dye extraction from the orange polycotton still increased but to a lesser extent, showing only 14% further colour reduction from the 1st extraction cycle.

Table 7.3: K/S values of untreated fabrics and dye extracted fabrics as well as the colour reduction percentages relative to the original fabric. Subsequent extraction experiments were conducted at 150 °C and 45 minutes at 1:10 g g^{-1} solid loading

	Red polyester		**Pink polyester**		**Orange polycotton**	
Extraction #	K/S	Colour reduction%	K/S	Colour reduction%	K/S	Colour reduction%
0	26.1	-	1.9	-	7.2	-
1	11.4	56.3%	1.0	49.4%	4.0	45.1%
2	7.6	70.9%	0.7	65.9%	3.4	52.2%
3	4.5	82.8%	0.6	68.5%	3.0	57.8%

The 3rd extraction cycle showed a considerable dye extraction for the red polyester, reducing the colour by 41% relative to the 2nd extraction. The 3rd extraction of the pink polyester did not show the same significant improvement as the red polyester with only 8% colour reduction relative to the previous cycle. This could be due to the high initial colour strength of the red polyester (K/S 26.1) compared to the pink polyester (1.94), which indicates that the **red polyester contains higher dye concentration compared to the pink polyester fabric, therefore the driving force of dye extraction is greater for the red polyester case.**

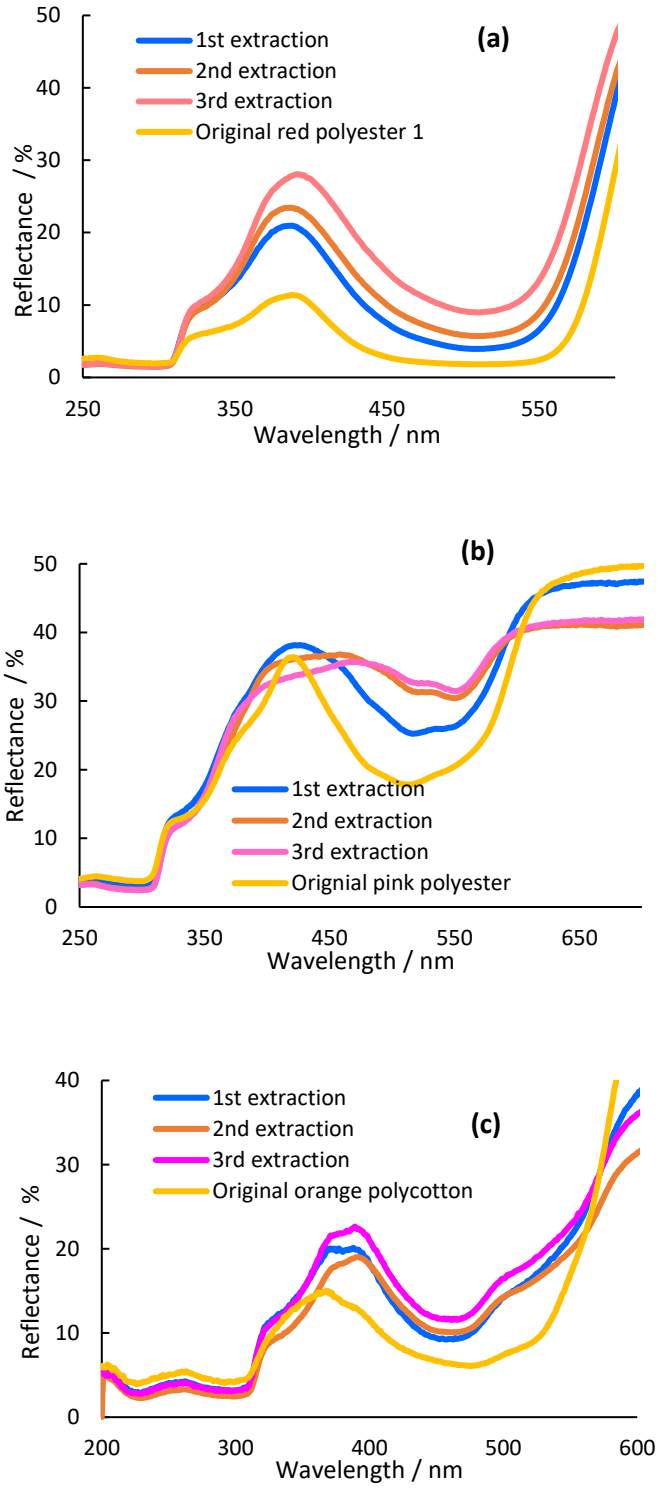

Figure 7.9: UV vis spectrums for dye extracted fabric 3 extraction cycles at 150 °C and 45 minutes using 1 : 10 g g^{-1} solid loading (a) 100% red post-consumer fabric (b) 100% pink post-consumer fabric (c) pre-consumer polycotton 65% polyester and 35% cotton.

Figure 7.10-a shows the original three fabrics before extraction and the extracted fabrics that were processed through 1, 2 and 3 extractions sequentially. It can be visually seen that for the pink polyester case, the fabric extracted two times and the fabric extracted three times showed almost no change in colour, whereas the red polyester shows more visual change in colour. The 3rd extraction of the orange polycotton showed colour reduction of 11% compared to 2nd extraction. Overall, the highest dye extractions were achieved from the red dye polyester, followed by the pink polyester and lastly the orange polycotton. **We believe that the relatively low extractions achieved for the orange polycotton compared to the polyesters could be related to the fact that this fabric was a purchased pre-consumer fabric, whereas the other two polyester were real post-consumers**. The multiple washing cycles of these fabrics during their "consumer-life" swell the fibers over time, which can make the dye extraction more efficient. At this point this is only a hypothesis, and future experiments should be done to confirm this. As mentioned earlier, it is very important to extract the dye considerably from the fabric, but at the same time to have a healthy-looking dye bath where the dye is not decomposed such that the IL can be reused for dyeing as shown in Figure 7.10-b. Figure 7.11 shows the absorbance of the IL+dye solutions obtained. The first extraction always showed the highest absorbance as the dye extraction driving force (*i.e.* dye concentration gradient) is the highest initially.

Figure 7.10: (a) Original photograph of original fabrics and the dye extracted fabrics from extraction1 to 3 (b) ionic liquid + dye solutions after the dye extraction experiments

The dye concentration in IL used in the 2nd extraction cycle decreased by approximately 54%, 74% and 50% for the red, pink and orange dyes, respectively compared to the dye

concentration in the 1st extraction cycle. In the third extraction, the IL was able to extract relatively the same amount of dye as the absorbance level between the IL used in the 2nd extraction and the IL used in 3rd extraction was the same. For the pink and the orange dye, the dye concentration in the IL used in 3rd extraction decreased which can be attributed to the lower concentration gradient and lower driving force for extraction as these fabrics have lower dye content compared to the red dye.

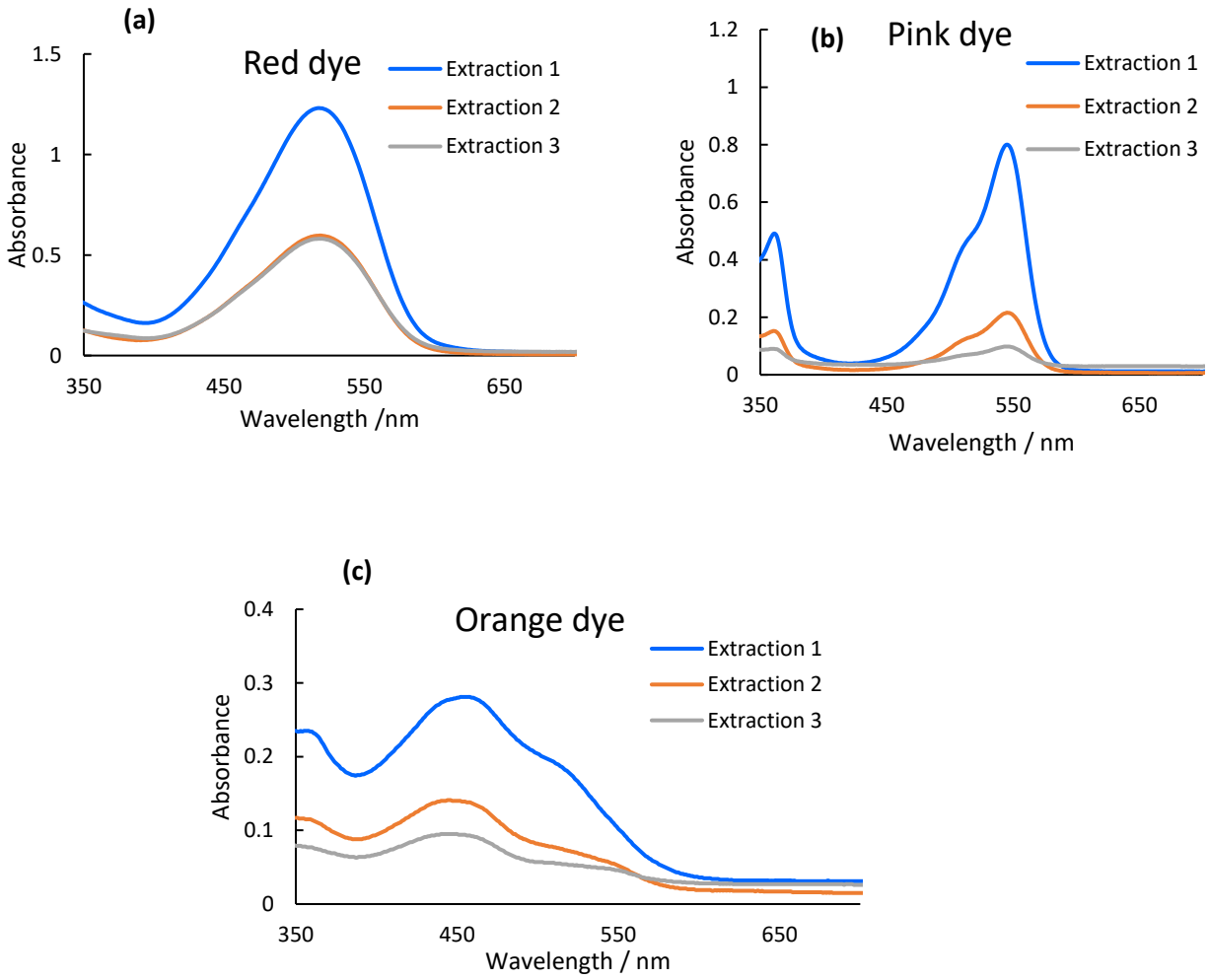

Figure 7.11: Absorbance of IL + dye solutions at extraction cycle 1 to 3 (a) red dye from 100% red polyester, (b) pink dye from 100% pink polyester and (c) orange dye from polycotton (65% polyester, 35% cotton)

We also investigated the applicability of IL extraction not only with PET and PET-based fabrics, but also with acrylic fabric as the same class of dyes (disperse dyes) are used to colour both materials. Figure 7.12-a shows the UV-vis spectra for the before and after

dye extraction of brown coloured post-consumer acrylic fabric and Figure 7.12-b shows the original photograph of the acrylic fabric before and after dye extraction. **The extraction achieved was very high with colour reduction of 92% (Table 7.4) at 150 °C for 30 minutes and solid loading of 1:10 g g^{-1}. The results highlight the high potential of the process to be applied for synthetic fabrics such as nylon as well**. Future work should investigate the tolerance of the other types of synthetic PET fabrics mixed with other polymers such as spandex, which is often used in sport clothes.

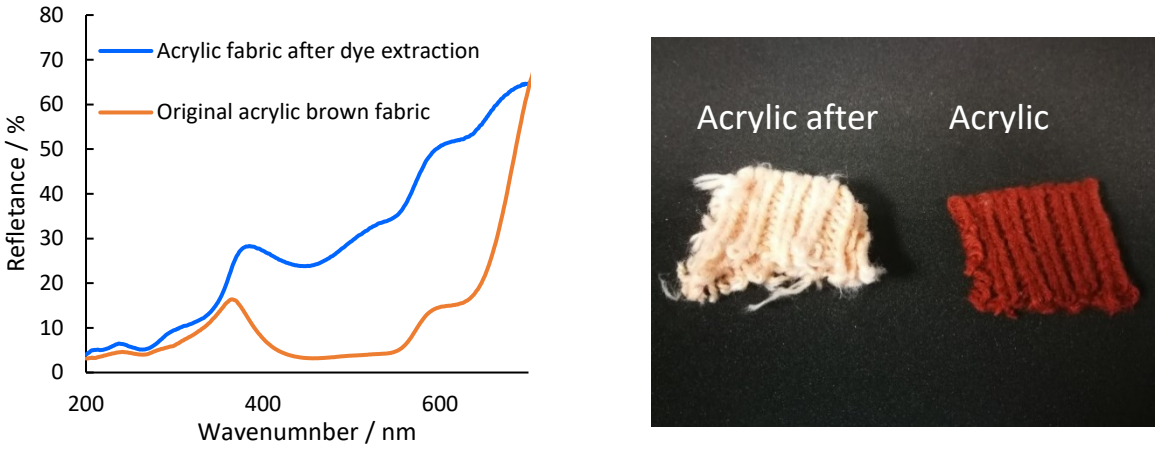

Figure 7.12 (a) UV-vis spectrum for orignal acrylic fabric and dye extracted acrylic fabric (b) original photograph of acrylic fabric before and after extraction. Dye extraction was conducted at 150° C for 30 minutes at 1:10 g g^{-1} solid loading

Table 7.4: K/S value of acrylic fabric before and after dye extraction

	Acrylic fabric before dye extraction	Acrylic fabric after dye extraction
K/S	12.32	0.95
Colour reduction %	-	92.27%

7.3.2 Dyeing with dye-rich IL bath

One of the key parameters to optimize for in this part of the process is the IL concentration. It is evident thusi far that disperse dyes have high solubility in the IL, however these dyes are essentially insoluble in water.

Therefore, it is expected that the reducing the IL concentration by adding water will achieve more efficient dyeing as we reduce the dye solubility in the medium and shift the equilibrium towards dyeing and not extraction. Therefore, as the two processes require essentially two thermodynamic states (high IL concentration for extraction, low IL concentration for dyeing), it was important to investigate the impact of IL concentration on the dyeing process efficiency.
Diluting the IL with water has its own disadvantages as this would: (a) dilute the dye concentration in the dye bath and, (b) require removing the added water by energy intensive evaporation process to recycle the IL for the extraction process. Therefore, investigating the dyeing efficiency as function of IL concentration is very important since the dye extraction results showed that the IL concentration seems to have an extremely important role in dye solubility and extraction.

To do so, we used ILs + extracted dye solutions as a dyeing bath to colour new PET-based materials. The dyeing process took place using the following conditions: pre-heating the extracted IL+dye solution at 70 °C for 30 minutes, followed by heating the dye bath to 150 °C for additional 30 minutes. The solid loading used in the dyeing experiments are 1:10 g g^{-1}. We used the extracted red dye from the 100% polyester and the extracted dye from the 100% pink polyester and re-used those two as dyeing solutions to dye 100% PET white polyester. The white polyester T-shirt was purchased from H&M and cut into smaller rectangular pieces of approximately 6x7 cm^2.
We investigated four IL concentrations: 80 wt% (*i.e.* use of IL + dye solution as is with no dilution), 60 wt% IL, 40 wt% IL and 20 wt% IL. The diluted IL+ dye solutions were prepared by diluting the 80 wt% IL + dye solution with water. This process essentially reduces the dye concentration in the dye bath medium by factor of 1.03, 2 and 4 for 60, 40 and 20 wt% IL, respectively (Table 7.5). Therefore, it is important to keep in mind that the dye concentration is <u>not constant</u> in this comparison.

Figure 7.13 shows the UV-vis spectrums for the dyed fabrics using the IL + extracted pink dye as well as the spectrum of the original pink polyester fabric where the dye was extracted, and Figure 7.13 shows the corresponding calculated K/S ratio. Figure 7.13-b shows the original photo of the white polyester fabric used before performing any dyeing and the pink dyed fabric using 80, 60,40 and 20 wt% IL solution. As expected,

dyeing using the IL + dye solution as it is after the extraction process (i.e. 80 wt% IL) resulted in the lowest K/S of 1.6. **Reducing the IL content in the dye bath from 80 wt% to 60 wt% increased the K/S ratio to 3.7 (dye concentration dilution factor of 1.33), which is 55% higher compared to the dyeing at 20 wt% water**. Increasing the water concentration further by using 40 wt% IL slightly decreased the K/S ratio compared to the fabric dyed at 60 wt%. However, the K/S was still higher compared the dyed fabric using 80 wt% IL with no dilution. Further increasing the water concentration resulted in decreasing the K/S value, becoming relatively close to the K/S value of the fabric dyed with 80 wt% IL. It is important to note that even though the K/S values of the dyed fabric decreases after 60 wt% IL, **the dyeing efficiency is still very high considering the fact the dye concentration in the bath is diluted by a factor of 2 and 4 in the 40 wt% IL and 20 wt% IL dye bath, respectively.**

Table 7.5: Dye dilution factor in the IL + dye bath solutions prepared for dyeing experiments

IL concentration in the dye bath	Dye dilution factor in the dye bath
80%	-
60%	1.33
40%	2
20%	4

However, it is very interesting to note that the K/S value of the dyed fabric using 60, 40 and 20 wt% IL were higher than the K/S value of the original pink polyester fabric. **This indicates that the IL dyeing can achieve very good colour strength that is comparable to the already established colour strength using aqueous dyeing processes potentially without the need of using many auxiliary chemicals (e.g. dispersing agents).**

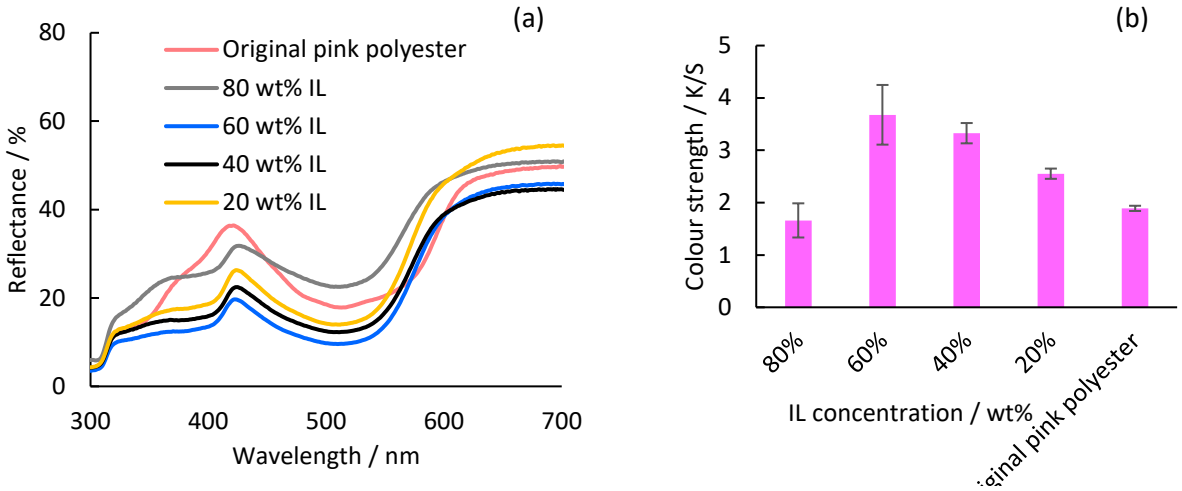

Figure 7.13: UV-vis spectrums (left) and calculated K/S values (right) of pink dyed fabrics using different IL concentrations and original pink polyester

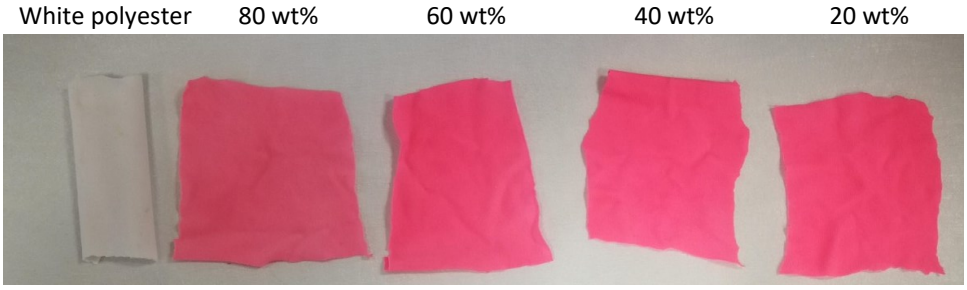

Figure 7.14: original photograph of white polyester before dyeing and dyed pink polyester using ILs dye bath at different IL concentrations

The dyeing experiments were also performed using the red dye IL solution extracted from the 100% red polyester. Figure 7.15 5shows the UV-vis spectrums of the dyed fabrics at 80, 60,40,20 wt% ILs and the corresponding K/S ratio. Figure 7.16 shows the original photo of the white polyester before dyeing and the red dyed polyester using the IL at different water concentrations. A similar trend of the K/S values was found in the pink dyed fabrics. Dyeing with 80 wt% IL solution produced a fabric with K/S colour strength of 2.2, while further diluting the solution improved the colour strength to 3.6. Additional dilution to the IL solutions by factor of 2 and 4 lower the colour strength to 2.7 and 2.5, respectively. It is important to note that the K/S ratio of the newly coloured fabric was significantly lower compared to the K/S ratio of the original polyester material (*i.e.* K/S = 26). We believe that the reason

behind this huge variation is related to the nature/state of the fabric itself. The original red polyester fabric was a fibrous blanket, and therefore the colour strength represents the cumulative colour strength of each fiber – giving this high colour intensity. On the other hand, the fabric that was used in this dyeing experiment was a regular woven fabric (T-shirt), therefore the overall colour intensity/strength was lower. Comparing the colour strength of the newly dyed fabric with the previous pink pre-consumer T-shirt (original pink), we can see that the IL-dyed fabric is of similar intensity to commercially dyed fabric using aqueous-based processes. The outcomes of this section highlight that: i) IL-based dyeing can provide similar colour intensity of aqueous-based dyeing, and ii) no substantial dilution is needed for the IL-dye rich solution for the subsequent dyeing step. **According to the outcomes herein, diluting the IL to 60 wt% provides the optimal colour strength, therefore, we anticipate that the process dehydration energy needed to re-concentrate the IL back to 80 wt% will not be exceptionally large.**

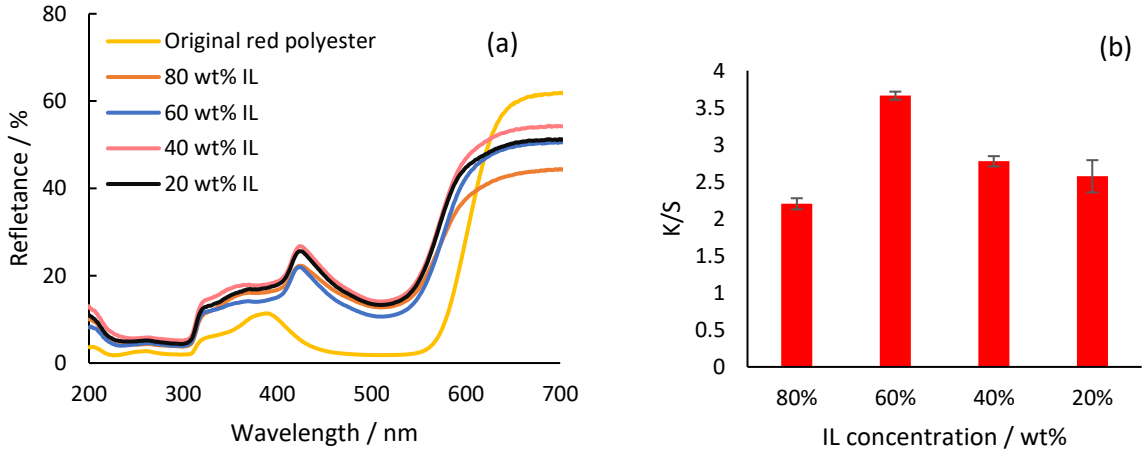

Figure 7.15:UV-vis spectrums (left) and calculated K/S values (right) of pink dyed fabrics using different IL concentrations and original red polyester

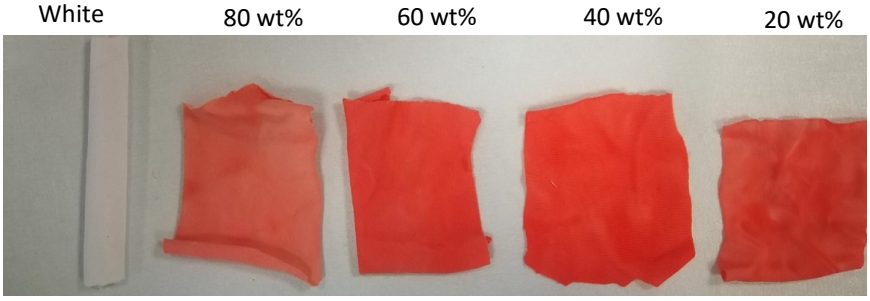

Figure 7.16: Original photograph of white polyester before dyeing and dyed red polyester using ILs dye bath at different IL concentrations

By the end of the project, the extraction-dyeing process was conducted on few other polyester-based textile waste materials. Figure 7.17 shows the dyed woven fabric and fibers using extracted blue, green, red, pink, orange and yellow dyes. **This highlights the robustness of the IL dye recycle process and its applicability to extract and dye different colours of synthetic dyes.**

Figure 7.17: Polyester fibers and fabrics dyed with recycled synthetic dye using [DMBA][HSO_4] dye extraction-dyeing process

It was important to investigate the impact of dyeing on the polyester fabric mechanical properties and structural integrity. Unfortunately, due to time limitations, the mechanical and chemical properties of the PET fiber in terms of tensile strength as well as degree of polymerization were not investigated. It is essential to investigate these properties of both the newly dyed polyester fibers as well as the decoloured PET in a future study. Ideally, the process parameters should be optimized not only to obtain the required decolourization and colorization, but also to maintain the structural integrity of the PET. In this study, the SEM images for the newly dyed PET fibers as well as the decoloured PET were obtained. Figure 7.18 shows SEM images of white polyester substrate used in the dyeing experiment, polyester dyed with 15 wt% [DMBA][HSO_4] solution and polyester dyed with 50 wt% [DMBA][HSO_4] solution, with each fiber image taken at two magnifications. The dye-rich [DMBA][HSO_4] solutions were obtained from

the red polyester dye extraction. **The images provide a good preliminary indication that the PET structure remained unchanged as no structural damages can be observed, however a verification by other methods is needed to draw a solid conclusion.**

It should be noted that IL-assisted dyeing for polyester fabric received little attention. Opwis *et al.* have investigated the use of commonly used aprotic ionic liquids for polyester dyeing using ionic liquids that are comprised of 1-ethyl-3-methyl-imidazolium cation and various anions.[17] The evidence of effective dyeing was presented in the paper as original photographs and unfortunately no quantification in terms of K/S ratio was made to allow the comparison with the process developed herein. Similarly, Bianchini *et al.* screened several protic and aprotic ILs for polyester, cotton and wool dyeing, however no quantification of colour strength in terms of K/S ratio was provided.[25] Andrade *et al.* investigated the use a wide range of acetate, lactate and formate-based PILs as dyeing mediums and they reported K/S ratios, however the study used cotton as substrates. The reported K/S ratio were very low, with a maximum of 0.07, which indicates that virtually no dyeing was done. The study claimed that the dyeing process was efficient and comparable to aqueous-base dyeing. These claims were criticized by Andreaus *et al.* who published comments on the manuscript.[26] The comments questioned and challenged the results obtained by Andrade *et al.* given the very low K/S values which means that fabrics were practically uncoloured. The lack of literature studies as well as the lack of quantitative results in the few existing studies make the comparison with other dyeing processes using IL mediums to be challenging.

Comparing the dyeing results we obtained herein with dyeing using sCO_2, it is clear that there is high potential in dyeing using [DMBA][HSO_4]. Long *et al.* presented the pilot-plant results of polyester dyeing using sCO_2 and disperse Red 74 at 20 MPa, duration of 60 minutes and fluid flow rate of 30 L min^{-1}.[27] The K/S ratio for the dyed polyester fabrics were 6 and 11 produced at 120 °C and 130 °C, respectively. Considering that these pilot-plant results were obtained after years of lab-scale optimization (reactor configuration, fluid flow rate, dyeing method), the results obtained herein are promising, especially that they are with recycled dyes and static dyeing (K/S ratios of 2 to 3.6). Another study that investigated dyeing polyester using sCO_2 reported K/S ratios of 11 to 15 using 25 MPa, 120 °C and duration of 60 to 80 minutes.[28] The colour strengths

obtained are higher than the colour strengths obtained in this study. However, there is a huge room for optimization in the current set-up and dyeing procedure that was used in this dye recycling study. In addition, both the dye extraction and subsequent dyeing steps were conducted at near atmospheric pressure. This provides a key advantage over sCO_2 dyeing that is conducted at very high pressures.

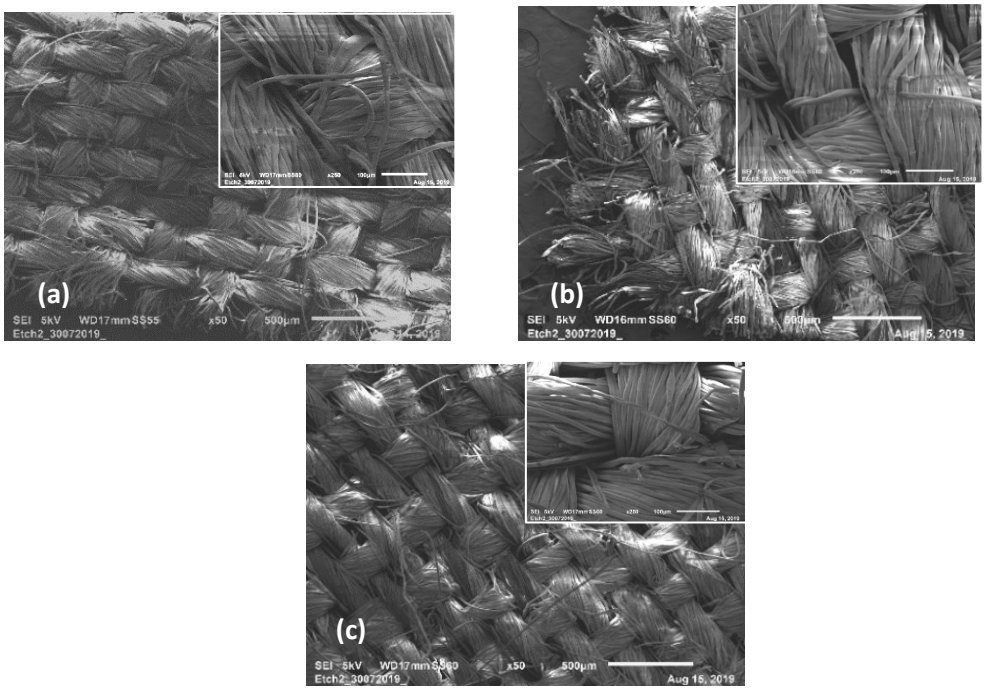

Figure 7.18: SEM images for a) white polyester fiber used for dyeing experiments, b) polyester dyed with extracted red dye in 15 wt% [DMBA][HSO_4] , c) polyester dyed with extracted red dye in 50 wt% [DMBA][HSO_4] (red dye)

Figure 7.19 shows another set of SEM image obtained from another set of PET dye extraction and subsequent PET dyeing. Figure 7.19-a shows the original post-consumer red polyester used in the previous dye extraction sections before the dyeing extraction takes place while Figure 7.19-b shows the same piece after the dye was extracted. **The image shows that no significant changes to the fibers before and after dye extractions, where the fibers remained their random orientation.** Figure 7.18-c shows a piece of the white polyester used for the dyeing experiments and Figure 7.18-d shows the same piece of fiber after it was dyed with an extracted pink dye using 80 wt%

IL solution as shown in the previous section. Similarly, no changes were observed in the PET fibers as the yarns kept their woven orientation and structure. These SEM images show good indication that the PET fiber before and after dye extraction as well as before and after dyeing remain intact during the two processes. However, as mentioned before, an in-depth investigation regarding the changes in the molecular weight and degree of polymerization of the PET as well as its tensile strength need to be conducted to identify and quantify these changes.

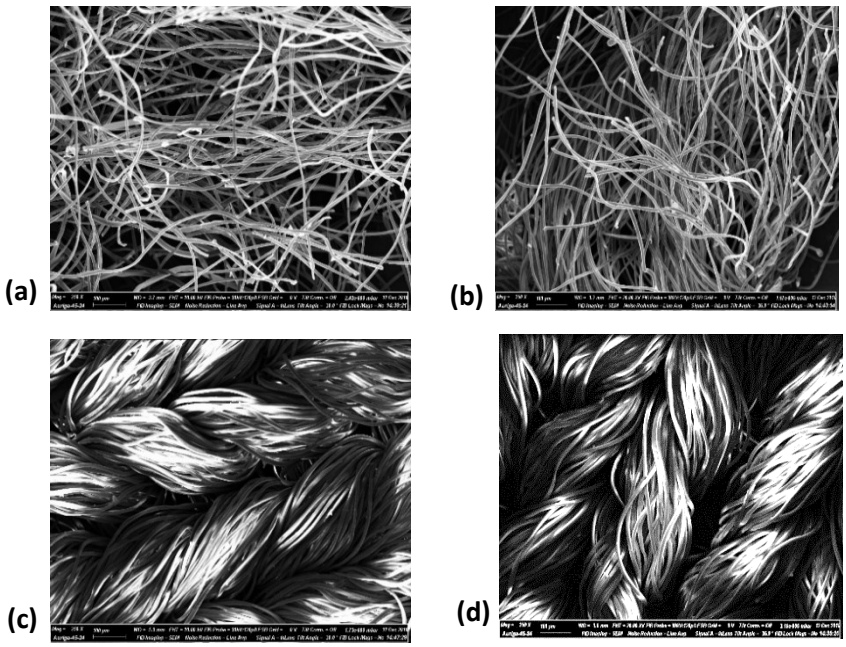

Figure 7.19: SEM images of a) original red post-consumer polyester, b) de-coloured polyester after dye extraction using 80 wt% [DMBA][HSO4], c) white polyester used for dyeing experiments, d) newly dyed polyester with pink dye using 80 wt% [DMBA][HSO$_4$] as a dye bath

7.3.3 From cotton to pigments

Cotton is the largest used natural fiber and the oldest fiber used for textile applications with its first use as textile fiber dating back to 6000 B.C. Several classes of dyes are used to dye and colour cotton, namely reactive dyes, vat dyes, direct dyes and sulfur dyes. Each class of these dyes have its unique characteristics and properties that satisfy the end application.[23] Denim fabric is one of the most commonly used cotton-based fabric and it is particularly distinguished with its blue colour thanks to the unique indigo dye. The indigo dye belongs to the vat dyes, a class of dyes that are insoluble in

water and requires highly controlled conditions for the dyeing to take place. In the case of indigo dye, the dyeing is conducted by controlling the reduction-oxidation state of the dye.[24] Under reduced anaerobic condition, indigo dye is soluble in water and therefore the dye can impregnate the open spaces within the fibers effectively. At the end of the dyeing process, the fibers are brought back to atmospheric conditions where the dye molecules return to their oxidized state and water insoluble form while they are trapped within the fiber.

It was of an interest to see how the protic IL would interact with the cotton and how would it particularly interact with the typically challenging indigo dye. Therefore, the same principle of "dye extraction" process was applied in here, but this time with using denim textile waste. The first set of experiment was conducted on discarded denim using 80 wt% [DMBA][HSO_4] at 150 °C for 30 minutes at solid loading of 10 wt%. At the end of the experiment the [DMBA][HSO_4] solution was decanted in a falcon tube, and the highly disintegrated denim piece was carefully transferred to another falcon tube. The decanted ionic liquid was turbid with dark blue appearing colour. A small sample of the IL was filtered using a syringe filter to confirm whether the indigo dye is soluble in the IL. After filtration, the ionic liquid solution was pale yellow, indicating that indigo dye was not dissolved in the IL and that the colour was from the very fine cotton particles in the IL solution. Water was added to the falcon tube containing the denim piece to wash off the residual IL. Upon water addition, the denim piece started to further disintegrate into a fine powder. The washing containing the powder was combined with the IL (that also contains fine powder) and the diluted IL was separated from the powder by centrifugation. The washing and centrifugation of the powder continued until no further powder precipitated and the remaining residual piece was in the form of light blue threads. Figure 7.20 shows real photos and SEM images of a) the denim piece before treatment, b) the threads remaining after the treatment and air-drying and, c) the freeze-dried powder after the treatment. It was very interesting to see how the denim piece fractionated into thread and powder particles. The degradation of cotton by the [DMBA][HSO_4] was in fact expected due to the high acidity of the IL and its tendency to hydrolyse cellulosic substrate.

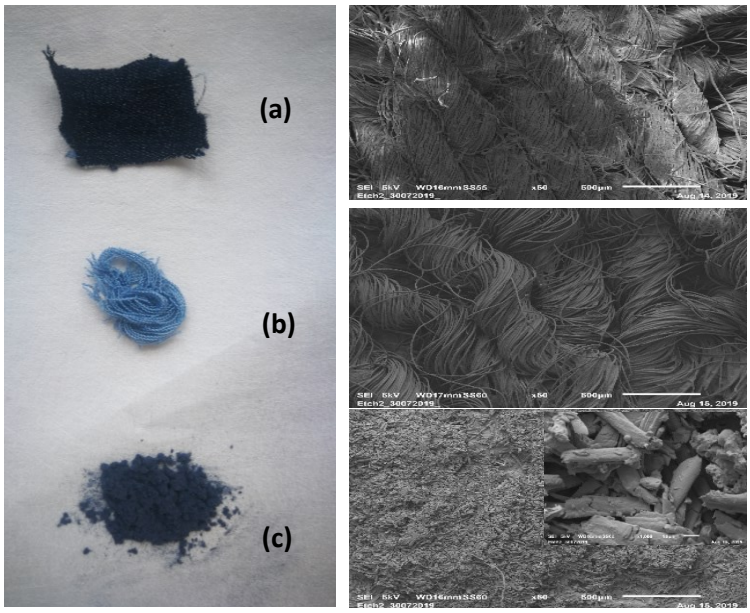

Figure 7.20: Original images and SEM images of a) 100% denim cotton piece, b) remaining cotton threads after treatment, c) cotton powder after treatment

The cotton powder obtained could be potentially used as a new type of pigment. The key difference between dyes and pigments is their particle size, with dyes having a much smaller particle size compared to pigments. This makes dyes more effective in penetrating the substrate material, on the other hand pigments are typically applied for surface applications. In addition, several classes of dyes are water-soluble, whereas pigments are always insoluble and remain in suspension.[29] Another major difference between the two colorants is that dyes are organic compounds whereas pigments are typically inorganic and often contains a heavy metal in their structure, namely chromium, cadmium, cobalt, lead, titanium and iron. The famous American yellow school bus is painted using chromium-based pigment (chrome yellow).[30] Figure 7.21-a shows the cotton powder pigmentation effect once it is mixed with small amount of almond oil. When the powder is mixed with a solvent that can dissolve the indigo dye such as dimethyl sulfoxide (DMSO), a rich-blue solution is obtained (Figure 7.21—b). Once DMSO is evaporated, a very small amount of the indigo dye is obtained. This can provide a potential route to recover indigo dye from denim waste.

Another interesting observation during the exploration of this process was related to the indigo dye solubility in the IL depending on the gas environment. As indicated previously, upon filtering the IL, the IL turned to a pale-yellow colour then to a brownish

shade after few hours. Since indigo dyeing takes place by controlling the oxidation-reduction state of the dye, we conducted an experiment where the IL after the treatment was carefully decanted to a falcon tube under N_2 atmosphere. In this case, the IL was blue in colour, which indicates that the indigo dye was soluble whereas when the IL was left in contact with air, the colour of the solution turned pale-yellow (Figure 7.20-c). The solubility of indigo dye in IL is interesting as the dye in insoluble in many common solvents such as alcohols. The samples were capped and taken immediately for UV-vis analysis to minimize air exposure. Figure 7.22 shows the UV-vis spectrums and indigo absorbance peak (λ = 662, ε = 20,000 M^{-1} cm^{-1}). The DMSO solvent mixed with the cellulose powder had high absorbance with corresponding calculated concentration of 76 ppm. The IL with indigo at N_2 atmosphere had only 7 ppm whereas IL at atmospheric pressure showed no absorbance, which aligns with the visual observations. Leaving the IL that was initially kept under N_2 atmosphere exposed to air have turned the solution to pale-yellow in few hours.

Figure 7.21: a) pigmentation effect of the generated cotton powder, b) cotton powder in DMSO solvent and, c) pale-yellow IL solution after treatment exposed to air and blue coloured IL that was kept under N_2 after the treatment

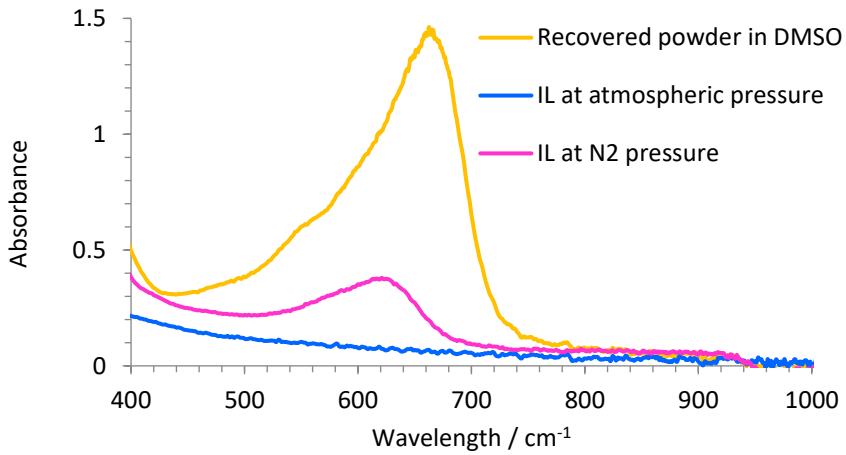

Figure 7.22: UV-vis absorbance for IL solutions obtained at different gas environment and the DMSO solvent mixed with the recovered cotton powder

The same treatment was applied for other cotton waste that is not denim to see whether the same effect will be obtained. It was observed that using other cotton fibers, the entire cotton piece after treatment with 80 wt% [DMBA][HSO_4] at 150 °C for 30 minutes becomes highly disintegrated, turning entirely to a powder (Figure 7.23). The transformation of fibers into dyestuff pigments is a novel process, and currently only one textile chemical company (Officina+39) is preparing scale up the production of dyestuff pigment powders made from used textile waste. Therefore, the exploration of this cotton to pigment route is very interesting and promising. In-depth testing, characterization and analysis are needed to verify the applicability and properties of these generated pigments and if any additives are needed to improve their pigmentation performance.

Figure 7.23: Cotton pieces before being treated with 80 wt% [DMBA][HSO_4] (bottom) dyestuff pigments made of cotton after treatment with 80 wt% [DMBA][HSO_4] (top)

7.4 Conclusions

The chapter presented a newly developed process to recycle synthetic dyes from synthetic fibers using low-cost protic IL as a solvent for dye extraction and solvent-assisted dyeing. The process uses textile waste as a new feedstock for synthetic dyes which are extracted and re-used to colour new synthetic fibers. We investigated the role of key operating variables on the dye extraction efficiency, namely time, temperature, IL concentration, fabric loading and surface area. We showed that to achieve optimal extraction without causing severe decomposition for the extracted dye, the time of extraction should not exceed 45 minutes at 150 °C. We also showed that temperatures higher than 150 °C result in higher thermal decomposition of the extracted dye. The results also indicate that IL plays a major role as an extracting agent as the dye extraction efficiency decrease significantly when the IL concentration decreases. The second part of the process uses the dye-rich IL solvent to dye newly introduced white fibers. With the prior knowledge of the importance of energy-efficient IL recycling and dehydration, we investigated the dyeing efficiency using different IL concentration to determine the dilution factor needed. The results showed that slight dilution of the IL from 80 wt% to 60 wt% improve the dyeing efficiency by 55% whereas further dilution of the medium reduces the dyeing efficiency. We further explored the potential use of the process on natural fibers such as cotton and denim material. This approach can transform the entire cellulosic-based fabric into a pigment-rich material which can be used as a more sustainable alternative to the current heavy-metals based pigments.

References

(1) House of Commons Environmnetal Audit Committee. Fixing Fashion: Clothing Consumption and Sustainability: Government Respnse to the Committee's Sixteenth Report; 2019.

(2) Foushee, Susan Nolen, Remy, Nathalie, Schmidt, J. Creating Value in Fashion: How to Make the Dream Come True | McKinsey Company; 2015.

(3) WRAP. Valuing Our Clothes: The Cost of UK Fashion; UK, 2017.

(4) Ellen MacArthur Foundation. A New Textiles Economy: Redesigning Fashion's Future; 2017.

(5) Rui, W. The Prices of Reactive Dyes and Intermediates Skyrocketed in China , and the Reproduction for Those Manufacuters May Be Very Difficult in June ,2018 | LinkedIn. 2018.

(6) Girn, D. T.; Livingstone, D. C.; Limited, A. B.; Calliafas, P.; Ltd, P. E. Fiber to Fiber Recycling : An Economic & Financial Sustainability Assessment; 2019.

(7) R Ananthashankar, A. G. Production, Characterization and Treatment of Textile Effluents: A Critical Review. J. Chem. Eng. Process Technol. 2013, 05 (01). https://doi.org/10.4172/2157-7048.1000182.

(8) Gentile, L. BASF increases prices for pigments, dyes and preparations worldwide https://www.basf.com/global/en/media/news-releases/2018/01/p-18-113.html (accessed May 1, 2020).

(9) CERNANSKY, R. Fashion Has a Waste Problem. These Companies Want to Fix It. Vogue Business. 2020.

(10) Fernandez Cid, M. V.; Van Spronsen, J.; Van Der Kraan, M.; Veugelers, W. J. T.; Woerlee, G. F.; Witkamp, G. J. Excellent Dye Fixation on Cotton Dyed in Supercritical Carbon Dioxide Using Fluorotriazine Reactive Dyes. Green Chem. 2005, 7 (8), 609–616. https://doi.org/10.1039/b503801d.

(11) Hou, A.; Chen, B.; Dai, J.; Zhang, K. Using Supercritical Carbon Dioxide as Solvent to Replace Water in Polyethylene Terephthalate (PET) Fabric Dyeing Procedures. J. Clean. Prod. 2010, 18 (10–11), 1009–1014. https://doi.org/10.1016/j.jclepro.2010.03.001.

(12) Gao, D.; Yang, D. F.; Cui, H. S.; Huang, T. T.; Lin, J. X. Supercritical Carbon Dioxide Dyeing for PET and Cotton Fabric with Synthesized Dyes by a Modified

Apparatus. ACS Sustain. Chem. Eng. 2015, 3 (4), 668–674. https://doi.org/10.1021/sc500844d.
(13) Banchero, M. Supercritical Fluid Dyeing of Synthetic and Natural Textiles - a Review. Color. Technol. 2013, 129 (1), 2–17. https://doi.org/10.1111/cote.12005.
(14) Ferrero, F.; Periolatto, M. Glycerol in Comparison with Ethanol in Alcohol-Assisted Dyeing. J. Clean. Prod. 2012, 33, 127–131. https://doi.org/10.1016/j.jclepro.2012.04.018.
(15) Ferrero, F.; Periolatto, M.; Rovero, G.; Giansetti, M. Alcohol-Assisted Dyeing Processes: A Chemical Substitution Study. J. Clean. Prod. 2011, 19 (12), 1377–1384. https://doi.org/10.1016/j.jclepro.2011.04.008.
(16) Bianchini, R.; Cevasco, G.; Chiappe, C.; Pomelli, C. S.; Rodríguez Douton, M. J. Ionic Liquids Can Significantly Improve Textile Dyeing: An Innovative Application Assuring Economic and Environmental Benefits. ACS Sustain. Chem. Eng. 2015, 3 (9), 2303–2308. https://doi.org/10.1021/acssuschemeng.5b00578.
(17) Opwis, K.; Benken, R.; Knittel, D.; Gutmann, J. S. Dyeing of PET Fibers in Ionic Liquids. Int. J. New. Tech. Res. 2017, 11, 101–108.
(18) Andrade, R.; Torres, D.; Ribeiro, F. R.; Chiari-Andréo, B. G.; Oshiro Junior, J. A.; Iglesias, M. Sustainable Cotton Dyeing in Nonaqueous Medium Applying Protic Ionic Liquids. ACS Sustain. Chem. Eng. 2017, 5 (10), 8756–8765. https://doi.org/10.1021/acssuschemeng.7b01555.
(19) Walker, A. Recycling Process, 2017.
(20) Pang-Chin, L. I. U.; Cheng, H.; Cheng-Ting, W. Method for Decolorization of a Dyed Polyester Fiber, 2015.
(21) Keh, E. New Paradigm for R&D and Business Model of Textile Circularity. In An Introduction to Circular Economy; Springer; pp 325–347.
(22) Bradley, R. S.; Bird, C. L.; Jones, F. The Vapour Pressures and Heats of Sublimation of Some Disperse Dyes. Trans. Faraday Soc. 1960, 56 (0), 23–28. https://doi.org/10.1039/tf9605600023.
(23) Haslinger, S.; Wang, Y.; Rissanen, M.; Lossa, M. B.; Tanttu, M.; Ilen, E.; Määttänen, M.; Harlin, A.; Hummel, M.; Sixta, H. Recycling of Vat and Reactive Dyed Textile Waste to New Colored Man-Made Cellulose Fibers. Green Chem. 2019, 21 (20), 5598–5610. https://doi.org/10.1039/c9gc02776a.

(24) Wambuguh, D.; Chianelli, R. R. Indigo Dye Waste Recovery from Blue Denim Textile Effluent: A by-Product Synergy Approach. New J. Chem. 2008, 32 (12), 2189–2194. https://doi.org/10.1039/b806213g.

(25) Bianchini, R.; Cevasco, G.; Chiappe, C.; Pomelli, C. S.; Rodríguez Douton, M. J. Ionic Liquids Can Significantly Improve Textile Dyeing: An Innovative Application Assuring Economic and Environmental Benefits. ACS Sustain. Chem. Eng. 2015, 3 (9), 2303–2308. https://doi.org/10.1021/acssuschemeng.5b00578

(26) Andreaus, J., & Sidou, L. F. Comment on "Sustainable Cotton Dyeing in Nonaqueous Medium Applying Protic Ionic Liquids". 2019, ACS Sustain. Chem. Eng. 7(9), 7999-8000. https://doi.org/10.1021/acssuschemeng.9b01112

(27) Long, J. J., Xu, H. M., Cui, C. L., Wei, X. C., Chen, F., & Cheng, A. K. A novel plant for fabric rope dyeing in supercritical carbon dioxide and its cleaner production. J. Clean. Prod. 2014, 65, 574-582. https://doi.org/10.1016/j.jclepro.2013.08.008

(28) Bai, T., Kobayashi, K., Tamura, K., Jun, Y., & Zheng, L. Supercritical CO2 dyeing for nylon, acrylic, polyester, and casein buttons and their optimum dyeing conditions by design of experiments. J. CO2 Util. 2019, 33, 253-261. https://doi.org/10.1016/j.jcou.2019.05.013

(29) Reife, A., & Freeman, H. S. (Eds.). 1996. Environmental chemistry of dyes and pigments. John Wiley & Sons.

(30) Lunk, H. J. Discovery, properties and applications of chromium and its compounds. ChemTexts. 2015, 1(1), 1-17. https://doi.org/10.1007/s40828-015-0007-z

Chapter 8 : Conclusions & Future Work

8.1 Research Work Conclusions

Since Prof. Ken Seddon's realization of ILs great potential in chemical industry in the early 1980s, research related to ILs grew almost exponentially. What helped the popularization of ILs as new chemical solvents was also the Green Chemistry movement in the late 1980s. Clean Air Legislations related to the emissions of organic solvents of high vapor pressure inspired Prof. Ken to popularize ILs as alternative new category of solvents. Today, chemists and engineers are experimenting with ILs to discover new reaction chemistries and new processes to replace the hundreds of years old organic solvents.

The research work in this thesis tackled the development of sustainable chemical processes to decontaminate and valorize waste streams using low-cost protic ILs. For the most of it, the work focused on the development of **ionoSolv biomass fractionation** process using key process development strategies. **i) explore new feedstock** through investigating the applicability of new feedstocks that offer economic and ecological advantages (Chapter 2 and 3), **ii) explore process conditions** by developing an in-depth evaluation on the impact of water use, process conditions and severity on biomass fractionation to alter, predict and optimize the process outcomes (Chapter 4 and 5), and **iii) explore new product** through exploring new promising products that can be obtained from the ionoSolv process other than the struggling market of 2nd generation biofuel (Chapter 6). Chapter 7 in this thesis capitalizes on the unique properties of protic ILs that are by paving the development of a **new dye recycling process.** The process was developed a result of an exploratory curiosity experiment to study the impact protic ILs have on polyester textiles, which have not been investigated in literature up to date.

In Chapter 2, a novel processing strategy of utilizing heavy metal contaminated post-consumer waste wood as a viable feedstock for 2nd generation biorefinery was investigated. A comprehensive characterization of waste wood as a feedstock and its fractionation behavior in IL systems was explored in-depth using series of analytical techniques. It was confirmed that despite the subtler changes in delignification behavior between the different IL mediums, glucose release from the cellulose substrate is largely governed by the structures of the remaining/re-deposited lignin on the cellulose surface.

The protic IL [H_1Cim]Cl was demonstrated to be the ideal IL to process post-consumer waste wood, releasing >90% glucose from the cellulose pulp, due to its relatively high delignification ability and lower tendency to form condensed lignin structures. In addition to its excellent biomass delignification ability, [H_1Cim]Cl was shown to be the ideal IL to decontaminate waste wood given the high heavy metals chelating power of the cation and the anion constituents. The process was demonstrated to be highly effective at intensified biomass loading and viable for both heavy metal contaminated waste wood fines and chips. The recovery of heavy metals from the IL liquor was also demonstrated successfully using electrodeposition. The study presents an original contribution to the current knowledge as it sets the first valorization and decontamination example of post-consumer waste wood to biopolymers and fermentable sugar using a circular IL-based process.

In Chapter 3, the novel strategy of using heavily contaminated waste biomass as a feedstock for IL-based biorefinery was expanded to include the hazardous creosote waste wood. Currently, there are no established valorization routes for creosote treated wood by the end of its service life other than the very limited and unpopular heat recovery application for such a heavily contaminated waste. The characterization of the real reclaimed creosote wood from railway sleepers showed the high level of PAH contamination. In terms of biomass fractionation, it was shown that the use of the low-cost PIL [DMBA][HSO_4] as a pretreatment medium achieves 60% delignification and 70% glucose release from subsequent enzymatic hydrolysis of the cellulose pulp. It was demonstrated that [DMBA][HSO_4] simultaneously extracts the embedded PAH-creosote compounds during the pretreatment, producing PAH-free cellulose pulps. Through tracing the PAH compounds in the process streams, it was discovered that the extracted PAH compounds co-precipitate with lignin, thereby creating a self-cleaning route for the IL liquor. Although the presence of PAH in lignin stream elevates the hazard level of lignin, the process can be perceived as a waste minimization and valorization strategy. The outcomes of the study provide for the first time a unique waste minimization and valorization strategy for creosote-treated waste wood, producing fermentable sugar for 2^{nd} generation biorefinery using negative-cost feedstock.

In Chapter 4, the process development was shifted to focus on process conditions and parameters, specifically by focusing on water-use in the process and its key effect on

the fractionation outcomes and process energy. The outcomes of the study revealed that the impact of water as a co-solvent on the fractionation power of [DMBA][HSO_4] is feedstock dependent. The fractionation of softwood feedstock showed the highest dependence on water concentration in the medium, with high biomass delignification only achieved at low water concentration. On the other hand, *Miscanthus* and post-consumer waste wood showed very little variation in their fractionation behavior with varying water concentration in the pretreatment medium. The outcomes of the analysis show that the IL use in the process can be potentially reduced using certain feedstocks, thereby increasing process flexibility, and lowering IL associated cost. The role of water as anti-solvent for lignin precipitation was also evaluated through one-pass pretreatment experiment and recycling experiments. The use of 1 water equivalent relative to the classical 3 equivalents proved to be as effective without compensating the fractionation outcomes while offering 65% savings in process dehydration energy. The study highlighted the importance of evaluating process conditions and water use using variety of promising lignocellulosic feedstocks.

The investigation of process conditions and its impact on lignocellulose fractionation using [DMBA][HSO_4] was further expanded in Chapter 5. The current literature studies lack for a suitable definition of a pretreatment severity factor that is applicable for IL-based pretreatment processes. The study evaluated the use of a modified pretreatment severity factor to better reflect and predict the pretreatment severity conditions and outcomes using protic acidic ILs by incorporating the Hammett acidity function. The outcomes of the analysis highlighted that modified pretreatment severity factor can better predict the fractionation performance of [DMBA][HSO_4] particularly in terms of hemicellulose extraction and delignification. The modified severity factor can be used as a viable tool to predict the process performance; however, it was cannot fully explain the fate and the conversion of hemicellulose components in the process given the complex reaction chemistry between hemicellulose dehydration products and solubilized lignin fragments.

Exploring the development of new products other than fermentable sugar for 2nd generation biorefinery is essential particularly as the outputs of ionoSolv process are two platform biopolymers: cellulose and lignin. Chapter 6 focused on the facile extraction of functionalized nanocellulose via applying an oxidative alkaline-H_2O_2

method on unbleached cellulose substrates obtained from ionoSolv process. The originality of this study stems from: i) the use of unbleached cellulose substrates which is uncommon in literature given the limited prospected success, and ii) the use of alkaline-H_2O_2 oxidation which is also a less commonly used method relative to traditional nanocellulose extraction methods (*i.e.* acid hydrolysis and TEMPO-mediated oxidation). The new process paradigm produced two streams: a) a low molecular weight near LODP cellulose residues that can be further processed to produce CNF or CNC and, b) a functionalized nanocellulose with carboxyl groups. The characterization of the ionoSolv cellulose substrates, cellulose residues after oxidation and extracted nanocellulose revealed the key impacts the ionoSolv processing conditions have on the properties on the three streams. The loss in crystallinity of cellulose residues as well as the nanocellulose obtained suggested that the severity of oxidation conditions needs to be altered to obtain highly crystalline nanocellulose. The study demonstrated for the first time the facile extraction of nanocellulose using unbleached ionoSolv cellulose pulps using a newly developed oxidation method.

In Chapter 7, a new field was explored where protic ILs can offer new processing advantages. A dye recycling process where synthetic dyes from polyester-based textile waste can be extracted and reused was developed using [DMBA][HSO_4]. The concept of dye recycling from textile waste is novel and the process provides an untapped opportunity to recycle synthetic dyes and eliminate virgin dye use in dyeing processes. The study demonstrated that by optimizing the process conditions, dyes from polyester can be selectively extracting into the IL, leaving the polyester highly intact. The dye-rich IL solution can be further used to dye new polyester fabric and the IL can be recycled to extract a new batch. The outcomes of the process were demonstrated and analyzed using real post-consumer polyester fabric with wide range of colors. Although the process at very early-stage of development, it shows high potential given the fact that it provides a circular dyeing method using recycled synthetic dyes as well as a light colored (or white) fabric that can be favorably upcycled. The interaction of protic IL with cellulosic-based textiles such as cotton and viscose resulted in the degradation of the entire material, forming a color-rich and pigment like powder. The potential use of the pigment to color objects or textiles is yet to be explored.

The research presented in this PhD provides evidence of the immense potential of low-cost protic ILs have in the fields of biomass processing, waste valorization, decontamination, minimization, and recycling via providing provide novel processing strategies. These newly explored and popularized solvents will continue to attract researchers' attention as a replacement to conventional organic solvents given their ease of synthesis, low cost, low volatility, and high dissolving power.

The robustness of ionoSolv process and its real potential to provide a new sustainable fractionation strategy for lignocellulose biomass is currently being translated from lab-scale to pilot-scale by Lixea Ltd – Imperial College London spinout company. The pilot-scale will mark a significant milestone not only for ionoSolv process, but for the entire ILs field given the very limited use of ILs at industrial scale at the present time. The work conduced in this step contribute towards the commercialization of ionoSolv process to produce sustainable bio-derived products and fuels from contaminated and virgin feedstocks. In addition, translating the dye recycling research to into a commercial process is currently being evaluated through developing business models, approaching potential interested parties and market research. There remains, however, further future work and remaining knowledge gaps that need to be addressed in the journey of developing ionoSolv and dye recycle processes from lab-scale to commercial-scale. The following section highlights the identified current gaps for future research.

8.2 Remaining Gaps and Proposed Future Work

The use of ILs in chemical industry might soon be a reality. The key word is: low-cost. The chemical industry is used to working with cheap, inexpensive solvents that are produced as by-products from chemical processing. For example, acetone is a byproduct of phenol production, toluene is a byproduct of gasoline production). Therefore, the use of ILs at large-scale will have to pass the tough exam of cost and economics. According to Abouelela et. al, solving the cost driver (i.e. IL cost) was the game-changing milestone in the development of ionoSolv biomass fractionation process.[1] The commercial development of the process is now continuing and pursuing pilot-scale testing. This would not have been possible if the IL used requires +20 synthesis steps. The use of these low-cost, easy to synthesize protic ionic liquids became popular in the recent few years, with more researchers recognizing their great potential.[2,3] Further development related to ionoSolv process needs to be conducted at a pilot-scale to evaluate key

processing steps: separation of solids (cellulose and lignin, specifically) as well as IL dehydration step. The separation of cellulose should be more straightforward to develop as commercial units used in Kraft and Sulfite pulping can be used. However, there can be still operational challenges due to the unknown rheological properties of the produced slurries. Therefore, it is important to establish and quantify these properties during the evaluation of filtration and separation units. Lignin filtration and separation can be more challenging than cellulose due to its smaller particle size. In-depth evaluation and testing with industrially relevant filtration unit are therefore important the effectiveness of separation. More importantly, the washing of cellulose and lignin in-situ during the filtration process or in a separate subsequent process needs to be also evaluated. Having an effective and economically viable washing is very important as it directly impacts the IL recycling rate, water use in the process, as well as the wastewater treatment capacity. Therefore, it is highly important to evaluate the washing of cellulose and lignin and quantify the residual IL vs. water requirement. The IL dehydration step also needs to be investigated and demonstrated at a pilot-scale as it could be indeed a process-limiting step. In addition, most of the pretreatment experiments conducted in our laboratory are based on the use of finely grounded biomass which does not represent the real size of biomass used in industrial scale. Further development should consider large biomass chips in different reactor configuration.

Another important area that is key for process development is the reactor design. Throughout this research work, the fractionation reaction was done in small unstirred pressure tubes placed in an oven. Developing a reactor design that integrates heat, mass and momentum transport will be an essential step to scale-up the process. In addition, although fermentable C6 sugar was the main product in 5 Chapters in this thesis, actual fermentation experiments were not conducted to demonstrate the bioethanol production step. Although other researchers in the group have conducted few experiments to demonstrate the fermentation step, there is still a need to evaluate the impact of hemicellulose and lignin degradation products as well as residual IL on the microbial activity during the fermentation step.

The use of post-consumer waste wood as a feedstock in ionoSolv process presents a key economic opportunity as described previously. Throughout the study, we consistently obtained low delignification, which can be an interesting phenomenon to explore from a

chemistry point-of-view. Further work should be conducted to examine the lignin structure of post-consumer wood to evaluate its cross-linking and condensation relative to regular virgin wood. This could be done by subjecting a lignin sample extracted from a virgin biomass and subjecting to UV-light to accelerate the process, and then characterize the lignin over certain period to examine its structure.

Although post-consumer waste wood creates an excellent valorization and decontamination strategy, the addition of electrodeposition step in the process might increase the process complexity and therefore slow the process development. Therefore, an in-depth evaluation on the entire economics of the process including electrodeposition unit should be conducted. If the objective is to expedite commercial development, considering other waste biomass that are not heavily or chemically contaminated might be an easier route. The use creosote wood makes a special case as it is highly contaminated, yet the process did not require the addition of a processing unit (except for WID boiler rather than regular boiler). Investigating other lignocellulosic-rich waste feedstocks that are specific for certain regions can also provide a valuable economic advantage such as almond and walnut shell waste in the US or empty fruit brunches in Malaysia and Indonesia. Exploring the interaction of these newly used protic low-cost ILs with other waste streams such as food waste or fishery waste can also provide new insights or develop new processes.

More importantly, an in-depth characterization study of the cellulose pulps needs to be conducted. The development of ionoSolv process so far was entirely focused on the production of 2nd generation bioethanol, and therefore the enzymatic digestibility of the cellulose pulps was taken as the key success indicator. However, it is important to explore the ionoSolv process as a new "pulping" technology, and which require the characterization of the cellulose-pulps according to the standards of the pulp and paper industry. The characterization can provide new insights on potential end-uses and markets that are more established compared to the 2nd generation bioethanol market, which is struggling to pick-off. In addition, as we saw in this thesis, exploring new products such as nanocellulose-based materials can also provide key advantages, particularly as the ionoSolv cellulose pulps show relatively low M_w. More comprehensive studies should be conducted investigating the different effects of temperature and reagent concentrations (NaOH and H_2O_2) on the functionality and morphology of

nanocellulose. In addition, improving the nanocellulose extraction needs to be investigated by incorporating an ultrasonication step on the cellulose residue. alternatively produce nanocellulose fibers by mechanically homogenizing the cellulose residues. Alternative interesting route to produce nanocellulose is to try to conduct acid hydrolysis using [DMBA][HSO_4] instead of conventional mineral acid.

As mentioned earlier, the use of low-cost PILs that was popularized by Prof. Jason Hallett group started to gain the attention of other research groups around the world. This recent popularization will encourage more processes to develop around the use of these low-cost PILs as solvents. In here, the example of dye recycle process was demonstrated, highlighting how these newly explored solvents can be used to create new processes. There are many different aspects that still needs to be investigated and explored in the dye recycle process such as fiber quality, status, finishing and composition and different colors and dye formulations. Isolating the dyes from the IL liquor potentially using a strong anti-solvent or sublimation is also an important route that needs to be investigated. More importantly, more in-depth characterization of the newly dyed fibers needs to be conducted to confirm that the quality of the fibers is not being compromised during the dyeing process. Our initial results do not show any damage, yet further confirmation is needed. Measuring the dye fastness properties (washing, rubbing, sunlight) is essential in determining the dyeing technology quality, and therefore more investigation is needed in this area. Similarly, more comprehensive analysis needs to be conducted for the de-colored polyester to confirm that the mechanical integrity of the fiber remains intact. The use of the PILs to produce pigments from denim waste and cotton waste was also briefly explored in this study. This route of processing is indeed worth exploring as it provides a simpler processing advantages compared to the integrated extraction-dyeing process. The interaction of PILs with protein-based fibers such as wool remains unexplored and a future study that combines the use of cotton (plant-based), polyester (synthetic-based) and wool (protein based) will provide key insights and, potentially, different processing routes as it is likely that the PIL will interact differently with these fibers. Evaluating the technoeconomic standing of the process is also highly important to assess the key bottleneck challenges in the process.

Finally, I hope that the work done in this thesis will inspire young new PhD students to develop new chemical processes using low-cost PILs. I also hope that this research work will contribute to building more sustainable and circular-based processes for the future generations.

References

(1) Abouelela, A. R.; Gschwend, F. V; Malaret, F.; Hallett, J. P. Commercial Aspects of Biomass Deconstruction with Ionic Liquids. In Commercial Applications of Ionic Liquids; Shiflett, M. B., Ed.; Springer International Publishing: Cham, 2020; pp 87–127. https://doi.org/10.1007/978-3-030-35245-5_5.

(2) Dastyar, W.; Zhao, M.; Yuan, W.; Li, H.; Ting, Z. J.; Ghaedi, H.; Yuan, H.; Li, X.; Wang, W. Effective Pretreatment of Heavy Metal-Contaminated Biomass Using a Low-Cost Ionic Liquid (Triethylammonium Hydrogen Sulfate): Optimization by Response Surface Methodology-Box Behnken Design. ACS Sustain. Chem. Eng. 2019, 7 (13), 11571–11581. https://doi.org/10.1021/acssuschemeng.9b01457.

(3) Penín, L.; Lange, H.; Santos, V.; Crestini, C.; Parajó, J. C. Characterization of Eucalyptus Nitens Lignins Obtained by Biorefinery Methods Based on Ionic Liquids. Molecules 2020, 25 (2). https://doi.org/10.3390/molecules25020425.

Appendix

Chapter 2

<Sample Information>

Sample Name	: 2 mg/mL standard		
Sample ID	: 2mg/mL standard		
Data Filename	: 2 mg$mL standard_25092018_1639_004.lcd		
Method Filename	: Mixed sugar standard method with calibration 9.6.14.lcm		
Batch Filename	: BATCH TABLE Aida_031017.lcb		
Vial #	: 1-3	Sample Type	: Standard
Injection Volume	: 10 uL	Level	: 2
Date Acquired	: 25/09/2018 21:07:16	Acquired by	: System Administrator
Date Processed	: 25/09/2018 21:27:16	Processed by	: System Administrator

<Chromatogram>

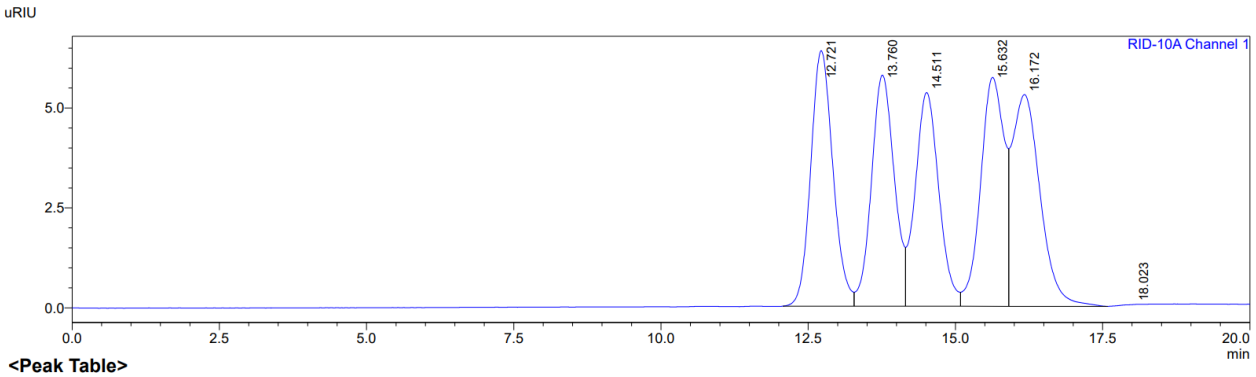

<Peak Table>

RID-10A Channel 1

Peak#	Name	Ret. Time	Area	Height	Conc.	Unit
1	Glucose	12.721	168325	6393	1.166	mg/mL
2	Xylose	13.760	156823	5785	1.165	mg/mL
3	Galactose	14.511	150309	5347	1.167	mg/mL
4		15.632	160797	5728	0.000	
5	Arabinose	16.172	174573	5298	1.162	mg/mL
6	Mannose	18.023	0	0	0.000	mg/mL
Total			810827	28551		

Figure A1: HPLC chromatogram example for 2 mg/L sugar mix standard. Shimadzu HPLC with an AMINEX HPX-97P column (Bio rad, 300 x 7.8 mm) with purified water as mobile phase (0.6 mL/min). The column temperature was 85°C and acquisition was run for 20 min

^{1}H and ^{13}C NMR spectra for ILs

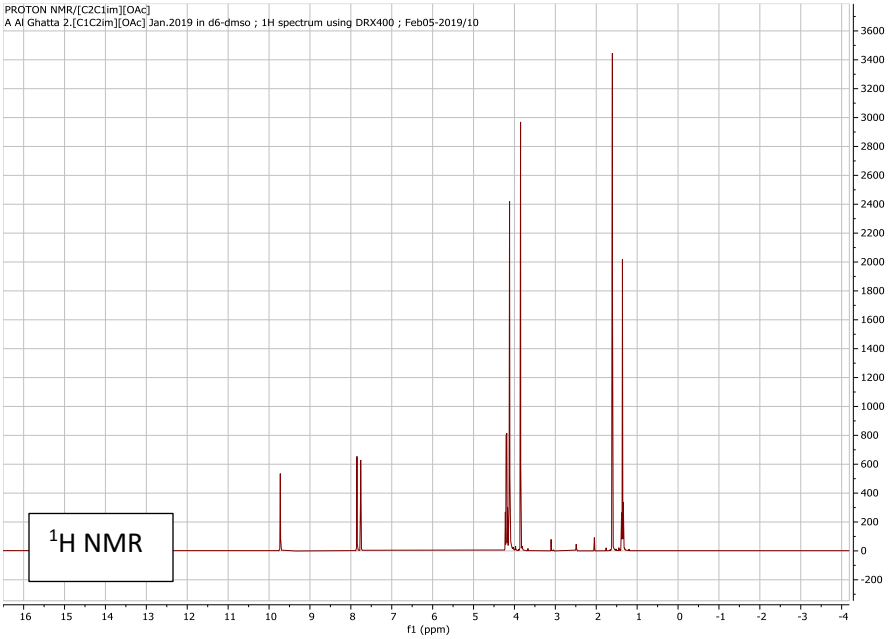

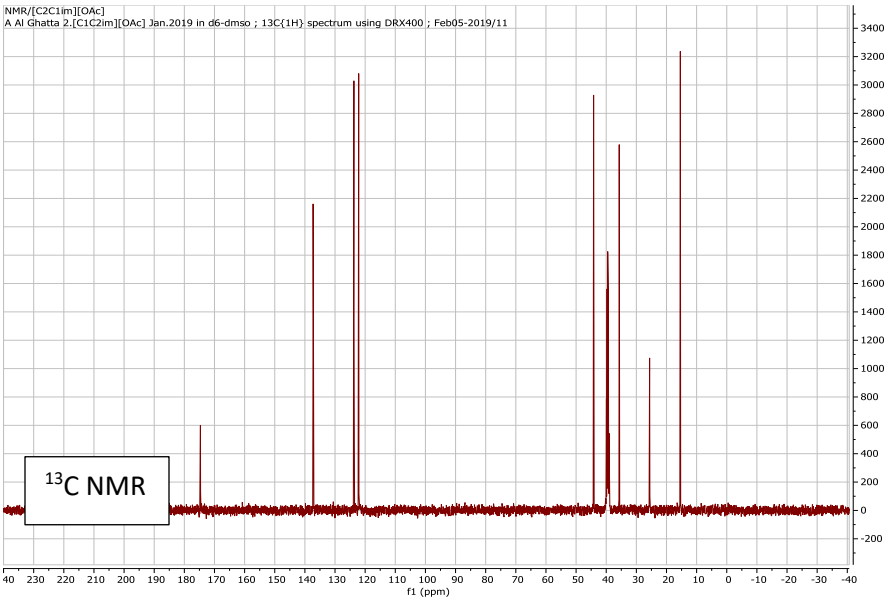

Figure A2: 1-ethyl-3-methylimidazolium acetate [C_2C_1im][OAc]

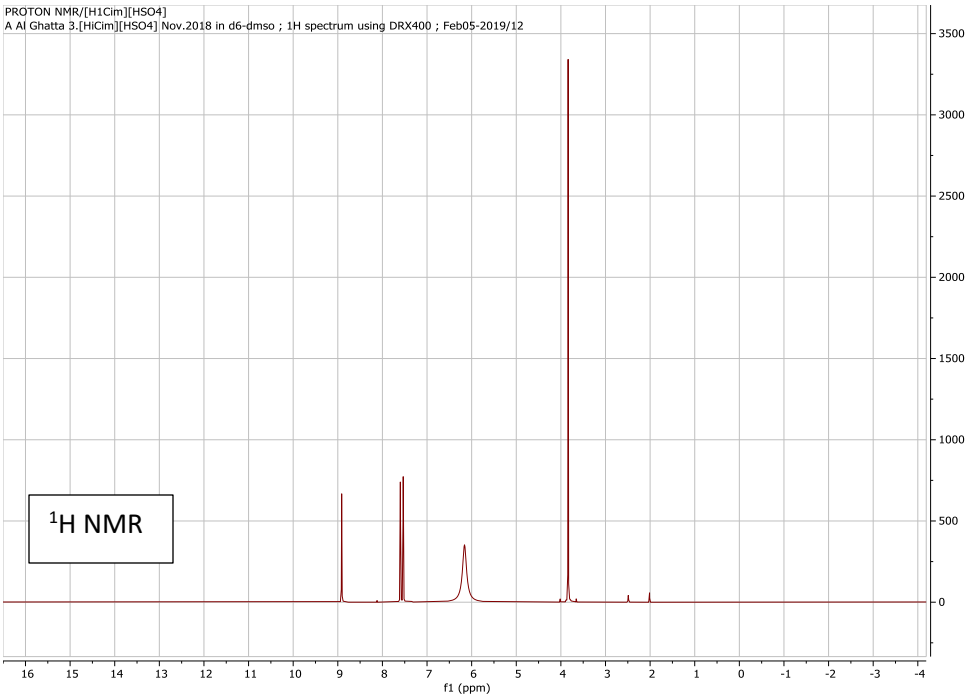

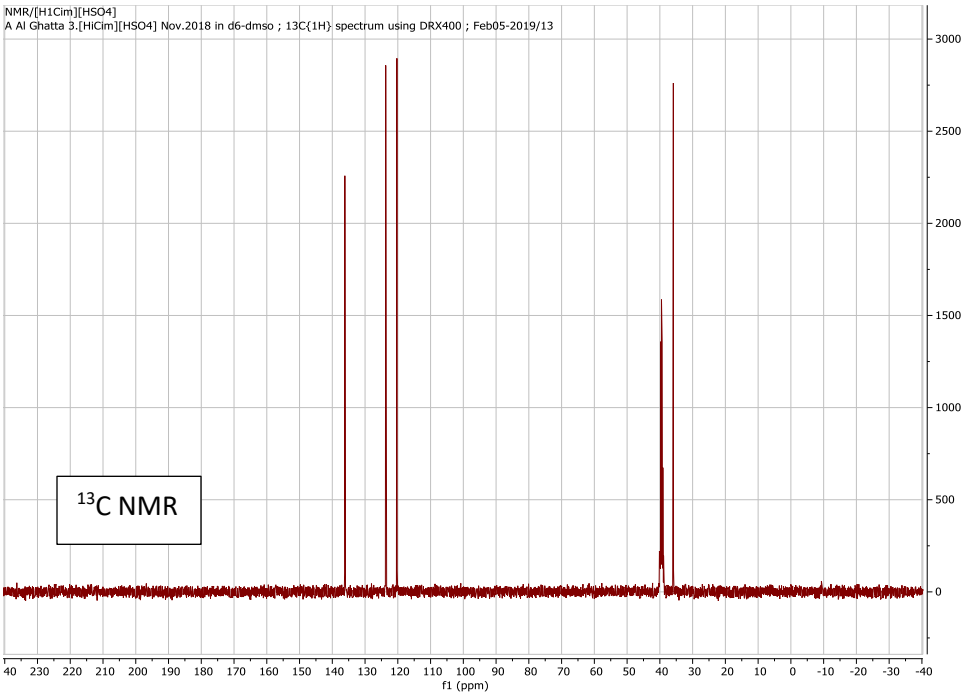

Figure A3: 1-methylimidazolium hydrogen sulfate [H_1Cim][HSO_4]

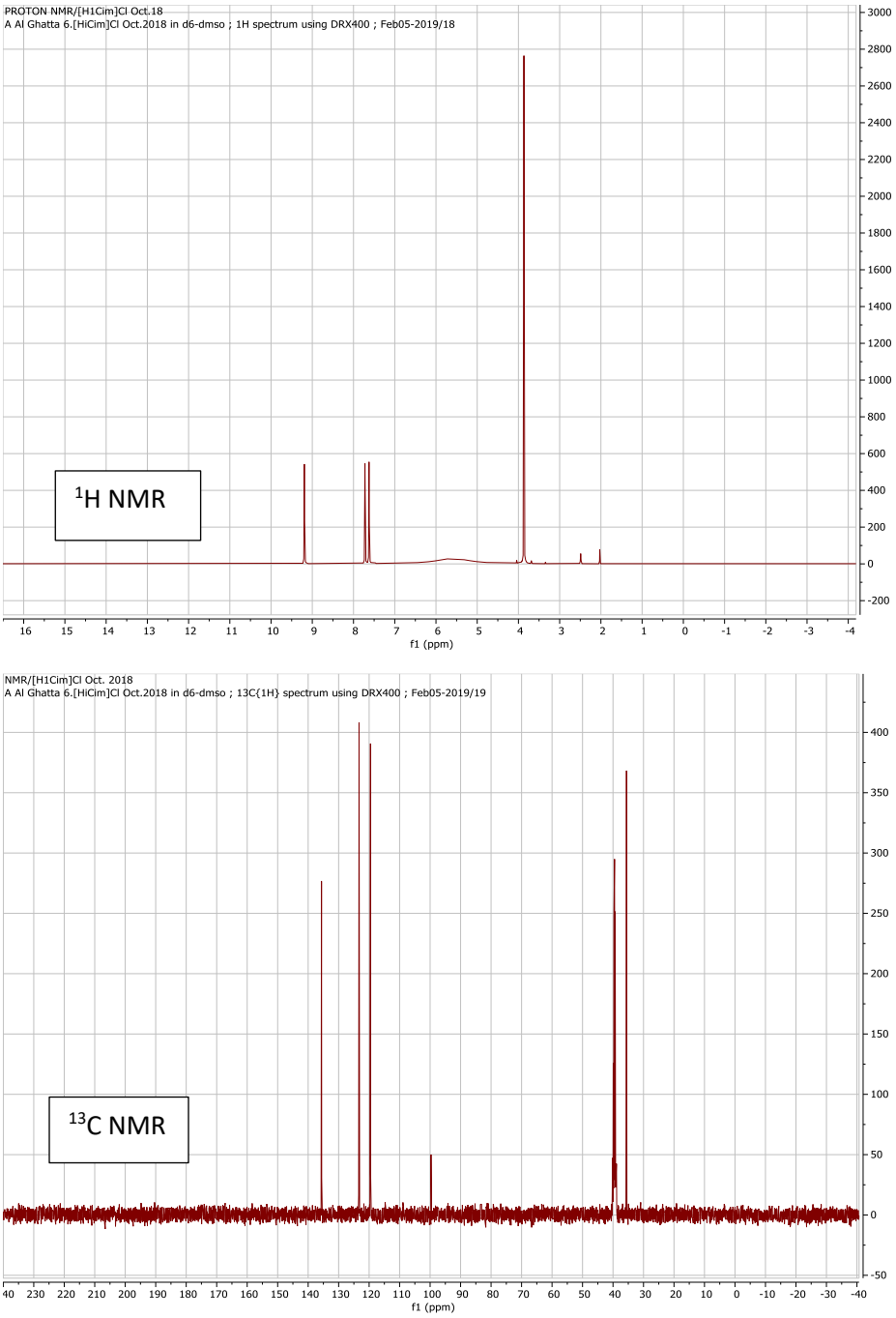

Figure A4: 1-methylimidazolium chloride [H_1Cim]Cl

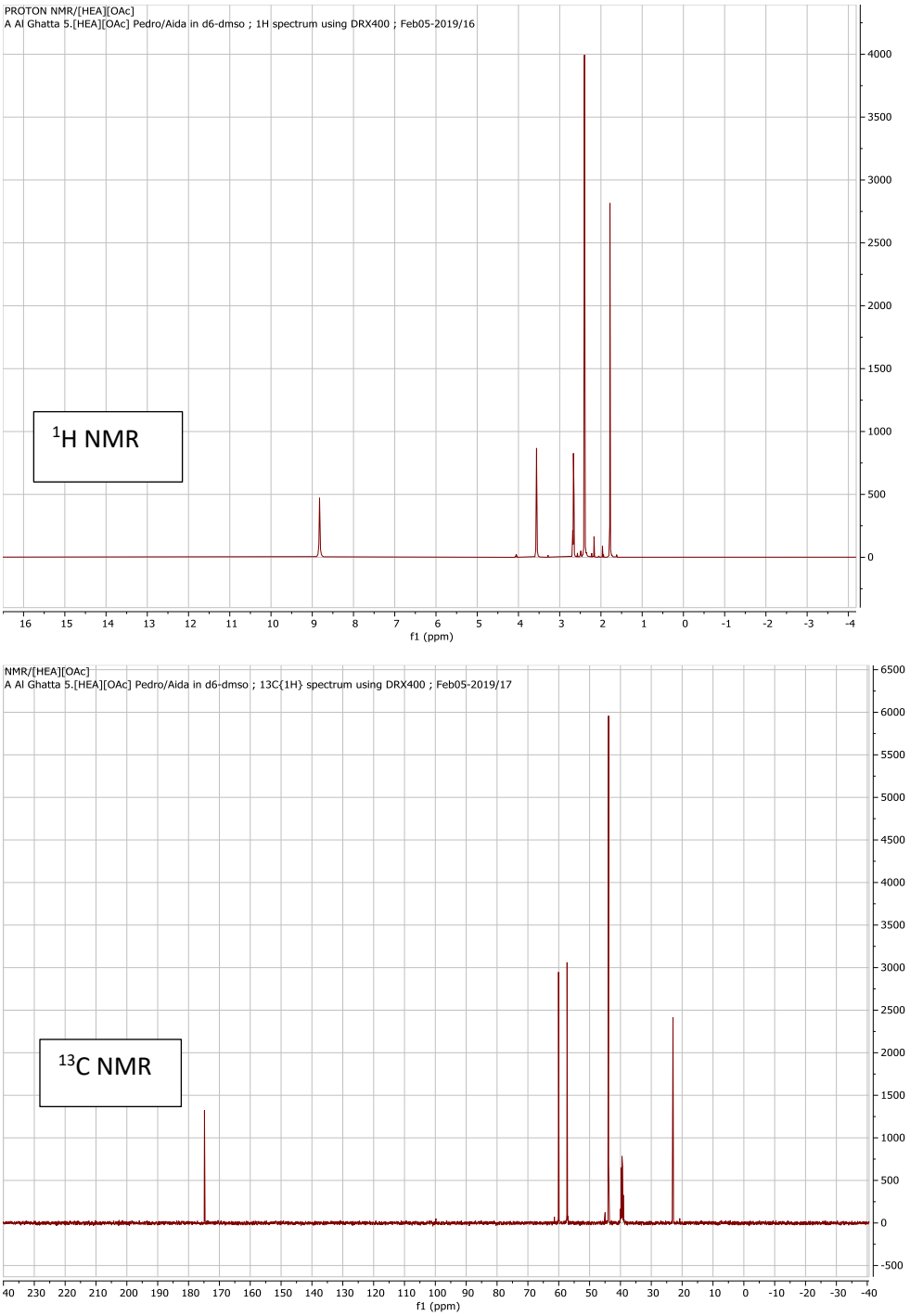

Figure A5: 2-hydroxyethylammonium acetate [2-HEA][OAc]

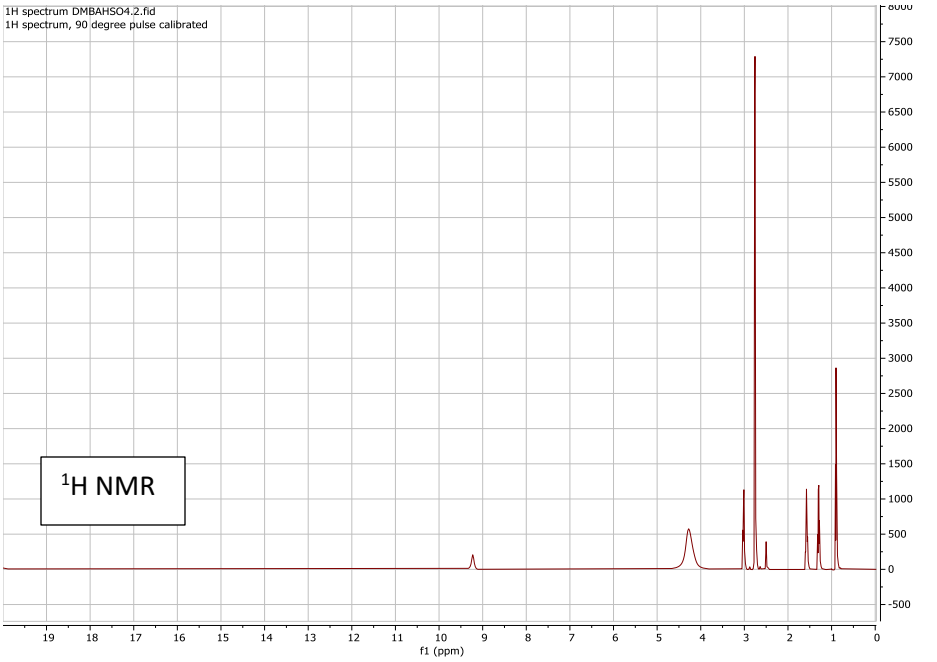

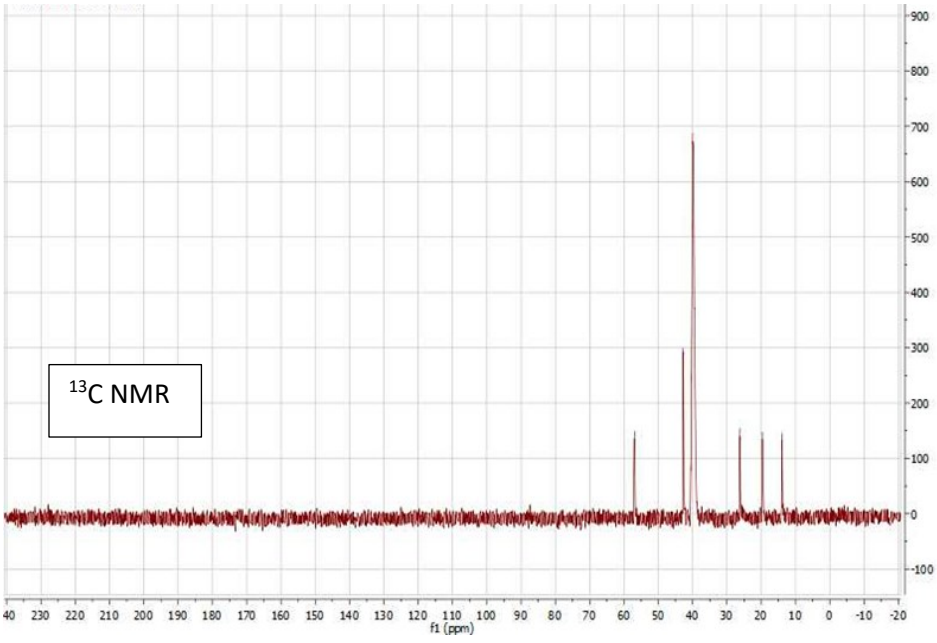

Figure A6: N,N,N dimethylbutylammonium hydrogen sulfate [DMBA][HSO_4]

Lignin HSQC NMR – IL comparison

2D HSQC NMR spectroscopy of lignins Method description Obtaining fully quantitative data is hindered by the rather long relaxation time of the 13C nucleus, making these experiments extremely time-consuming. Instead, semi-quantitative data were obtained using shortened experiments by comparing the peak volume of a certain correlation with respect to another correlation that is considered constant over a range of experiments. The volume of the G2 signal on the guaiacyl (G) sub-unit can be used as such a reference in the case of softwood lignin, which consists predominantly of G units and condensation in the 2-position is highly unlikely. In the experiments presented in this thesis, the abundance of different sub-units and linkages in lignin are reported by using volume integration with reference to the G2 + G2,cond integral, obtained using a pulse sequence that gives only semi-quantitative information. Full spectra are presented below.

Table A1: Signal assignment showing center of integrated area for HSQC NMR spectra of lignins

Bond/structure	δH/pp	δC/ppm
β-β'	4.6	84.82
β-O-4'	4.8	71.01
β-1'	5.01	79.99
β-5'	5.48	87.15
G2cond	6.76	112.09
G2	7.01	109.8
G5	6.69	115.16
G6	6.73	119.75

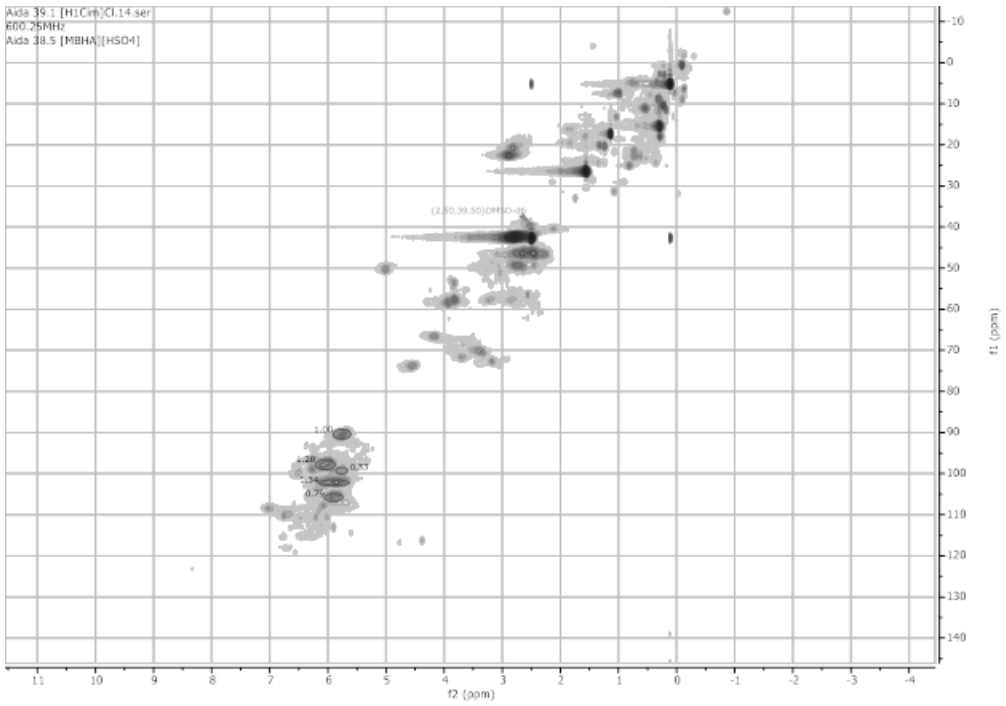

Figure A7: HSQC spectra for lignin from [H1Cim]Cl fractionation

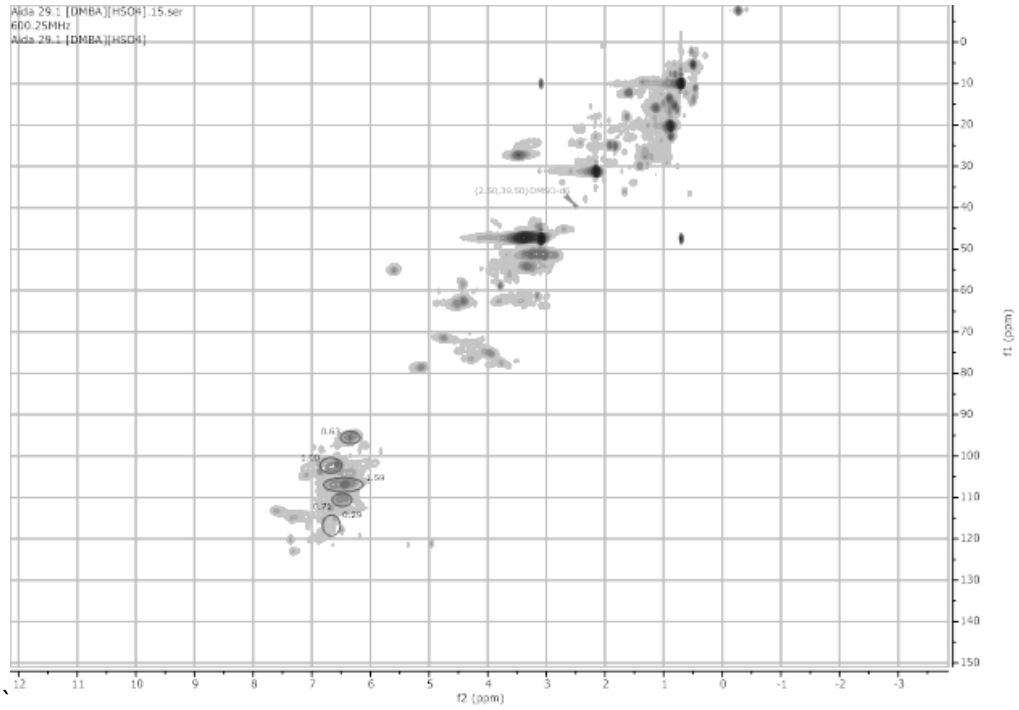

Figure A8: HSQC spectra for lignin from [DMBA][HSO4] fractionation

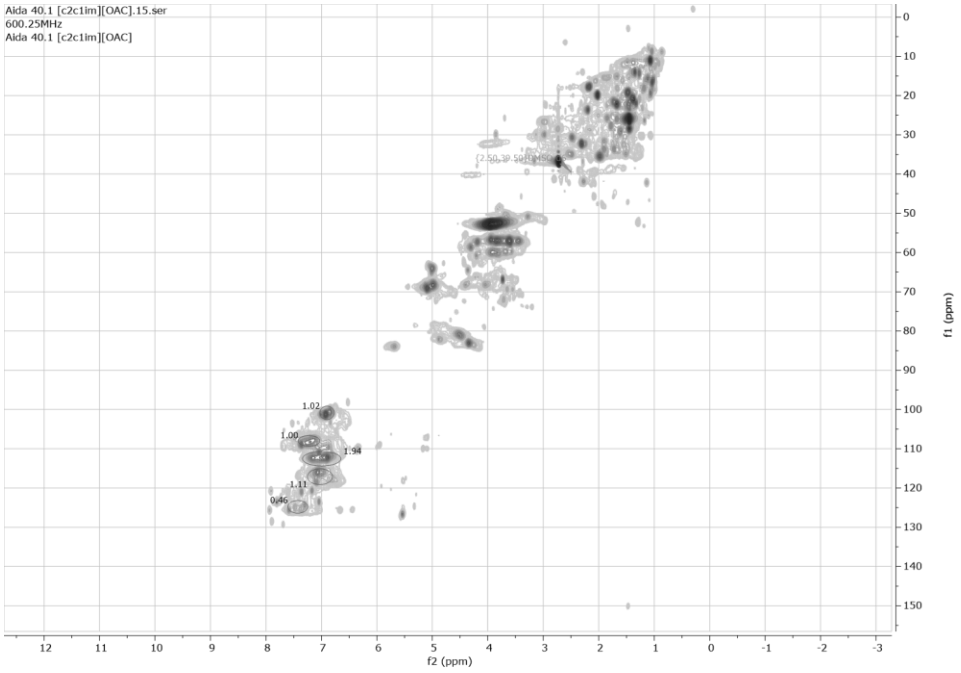

Figure A9: HSQC spectra for lignin from [C_2C_1im][OAc] fractionation

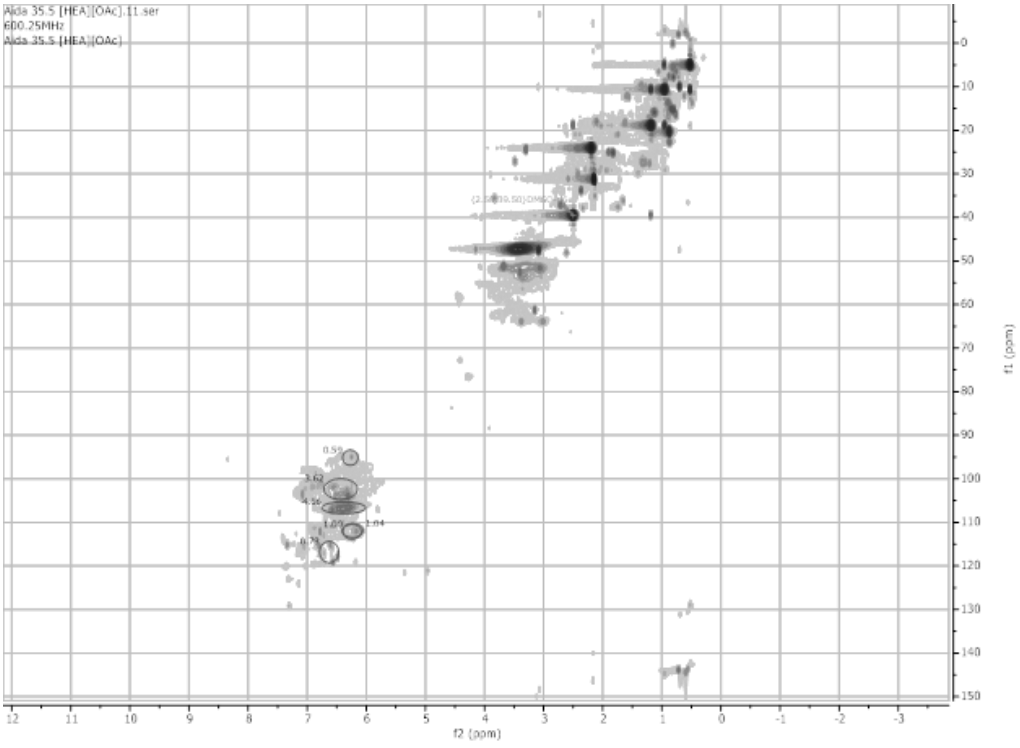

Figure A10: HSQC spectra for lignin from [2-HEA][OAc] fractionation

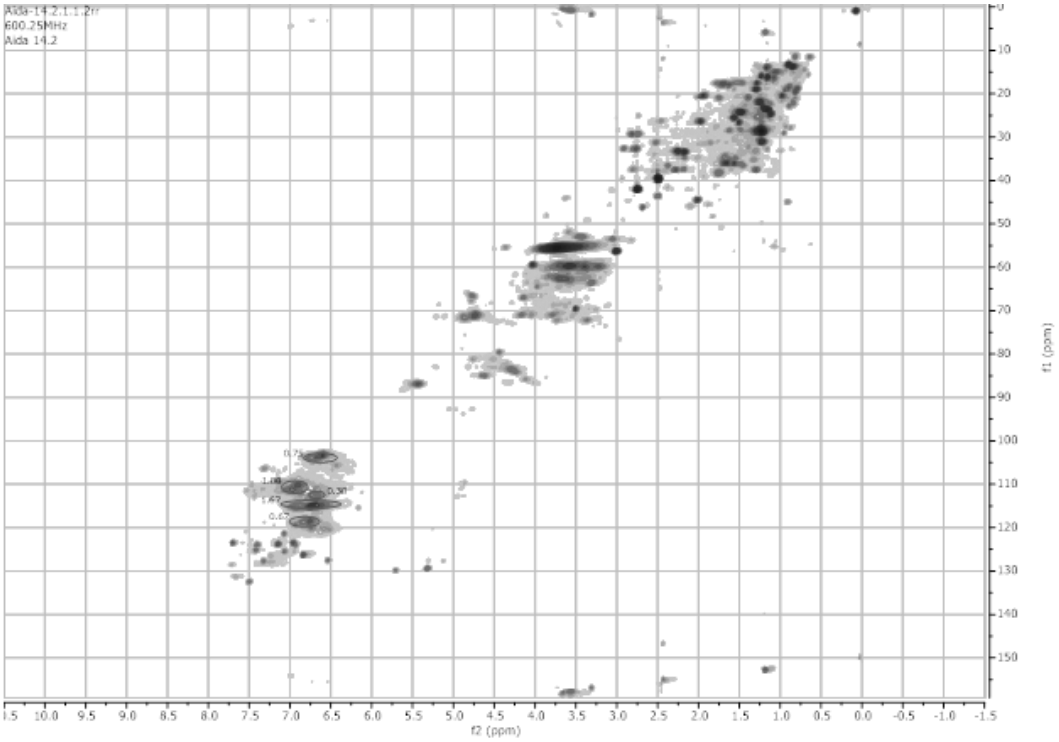

Figure A11: HSQC spectra for lignin from [H1Cim][HSO4] fractionation

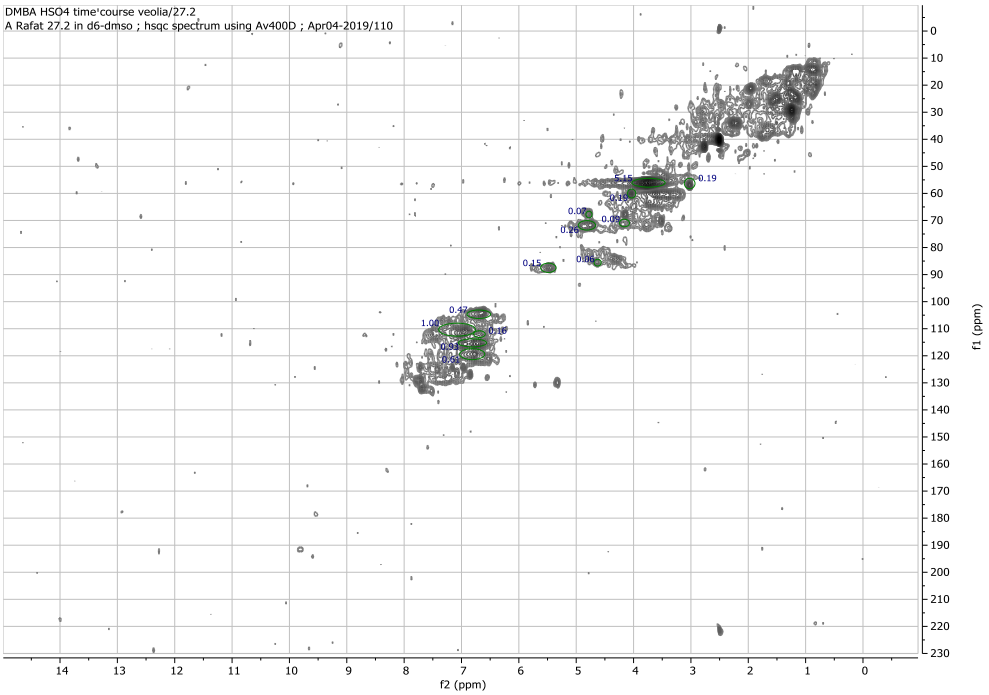

Figure A12: Lignin HSQC spectra from [DMBA][HSO_4] fractionation for 30 minutes

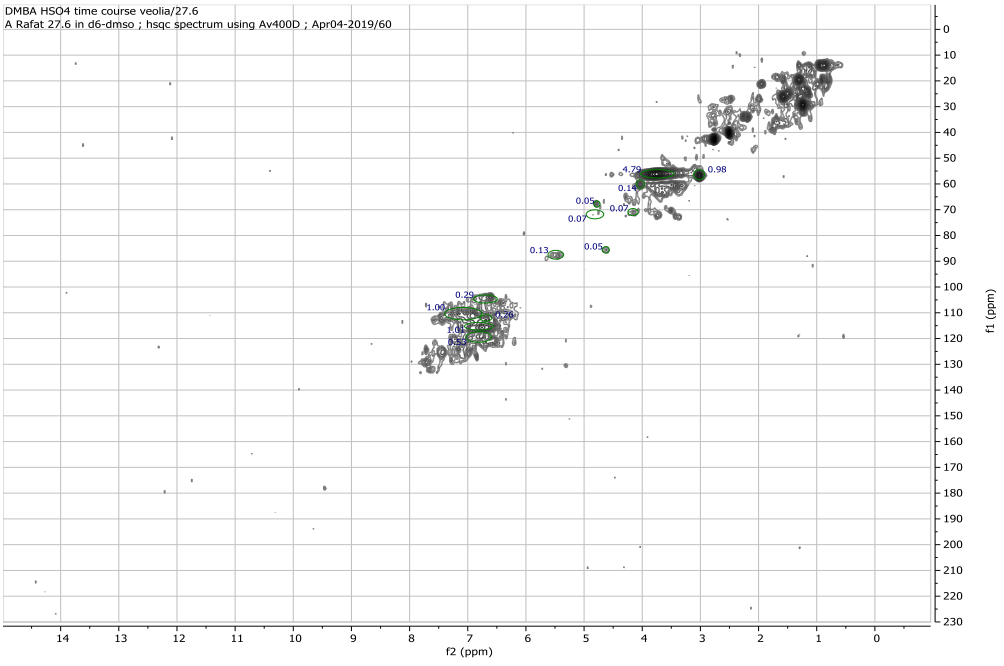

Figure A13: Lignin HSQC NMR spectra from [DMBA][HSO_4] fractionation for 45 minutes

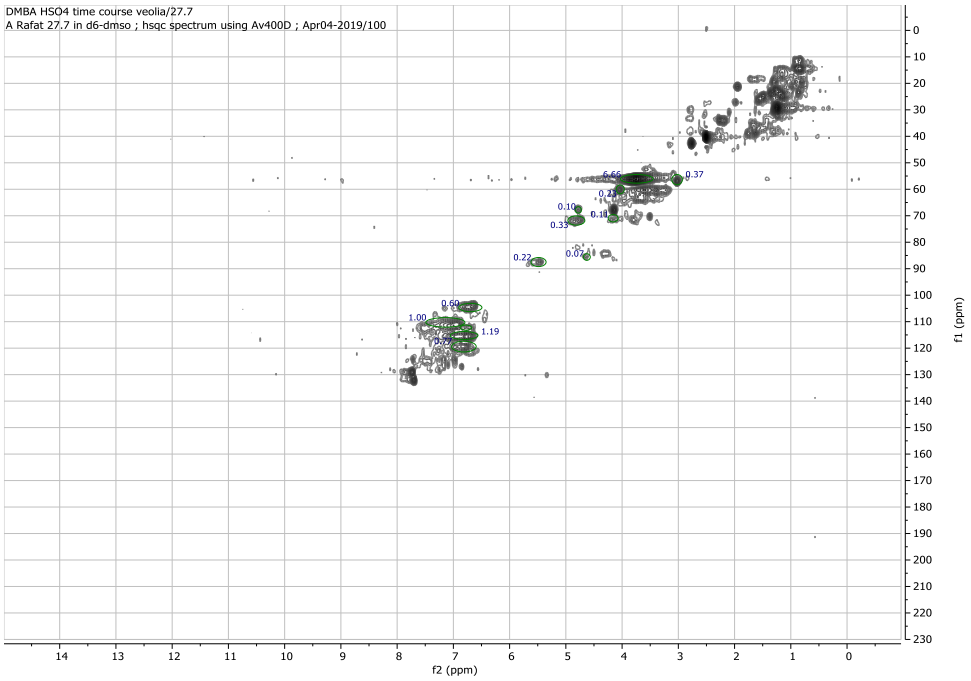

Figure A14: Lignin HSQC NMR spectra from [DMBA][HSO_4] fractionation for 75 minutes

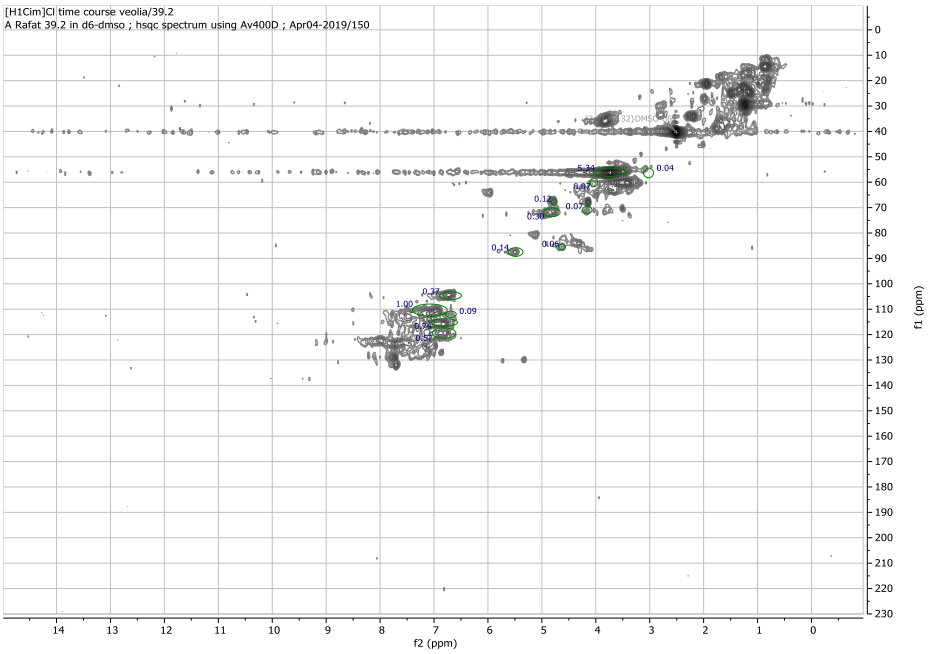

Figure A15: Lignin HSQC NMR spectra from [H_1Cim]Cl fractionation for 30 minutes

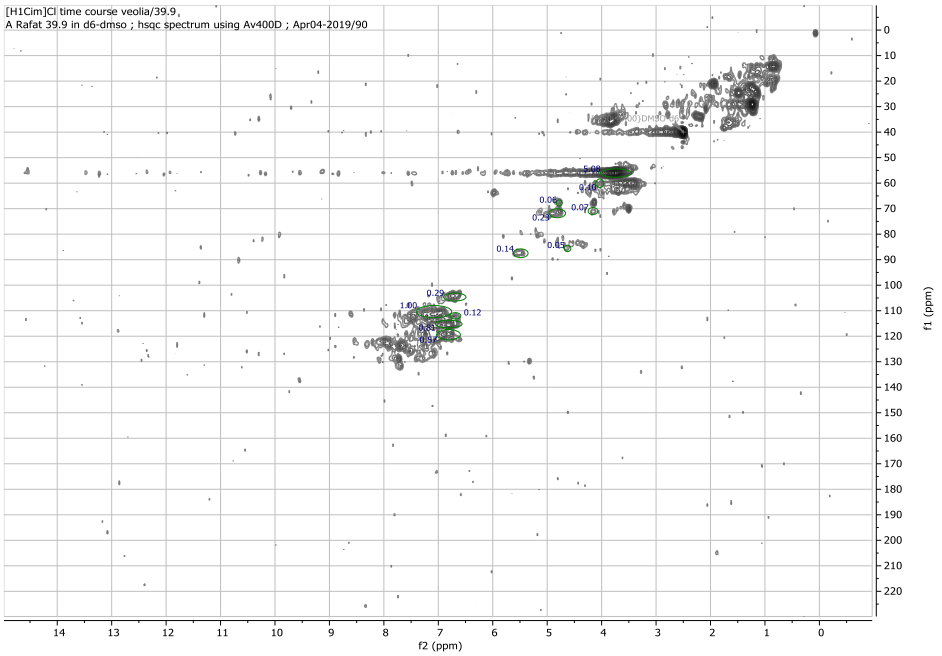

Figure A16: Lignin HSQC NMR spectra from [H1Cim]Cl fractionation for 45 minutes

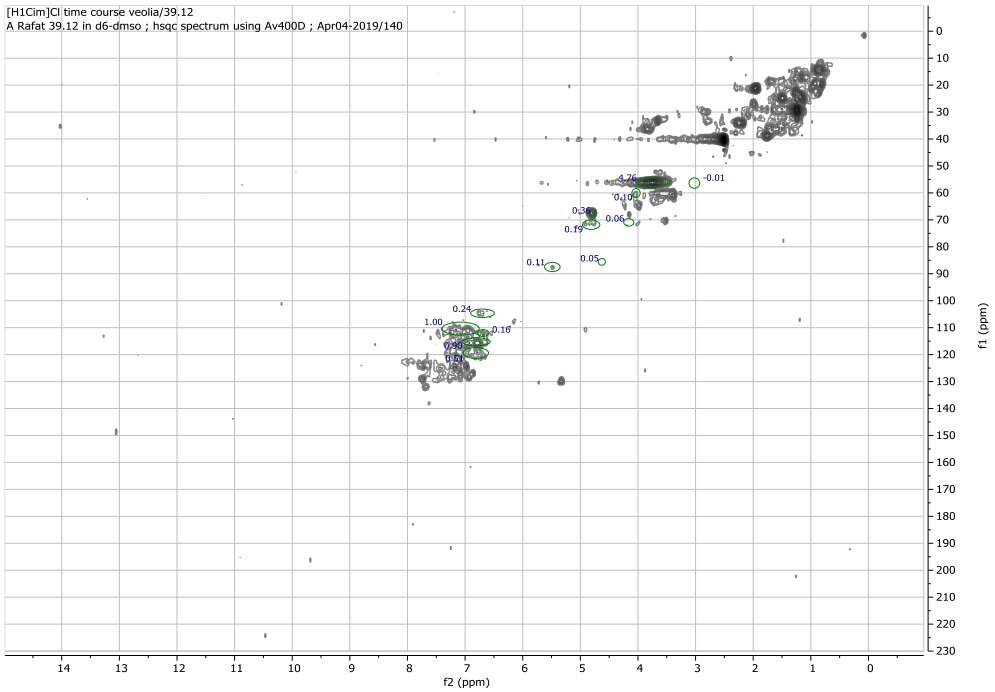

Figure A17: Lignin HSQC NMR spectra from [H1Cim]Cl fractionation for 75 minutes

Table A2: X-ray fluorescence (XRF) data of direct ash of untreated virgin pine wood and waste wood fines

	Untreated virgin pine wood	Waste wood fines	Unit
Ti	1.86	18.74	%
Si	0.90	13.61	%
S	3.86	8.41	%
Fe	1.64	7.99	%
Mg	7.17	0.65	%
P	2.20	0.71	%
K	21.23	4.54	%
Ca	48.06	35.17	%
Mn	12.45	0.58	%
Eu	0.62	0.09	%
Ni	-	427.1	ppm
Sr	-	332.5	ppm
Zr	-	192.8	ppm
As	-	570.7	ppm
Pb	-	0.93	%
Cl	-	2.03	%
Cr	-	0.33	%
Cu	-	0.17	%
Al	-	3.51	%
Na	-	1.33	%
Zn	-	0.93	%
Ba	-	0.11	%

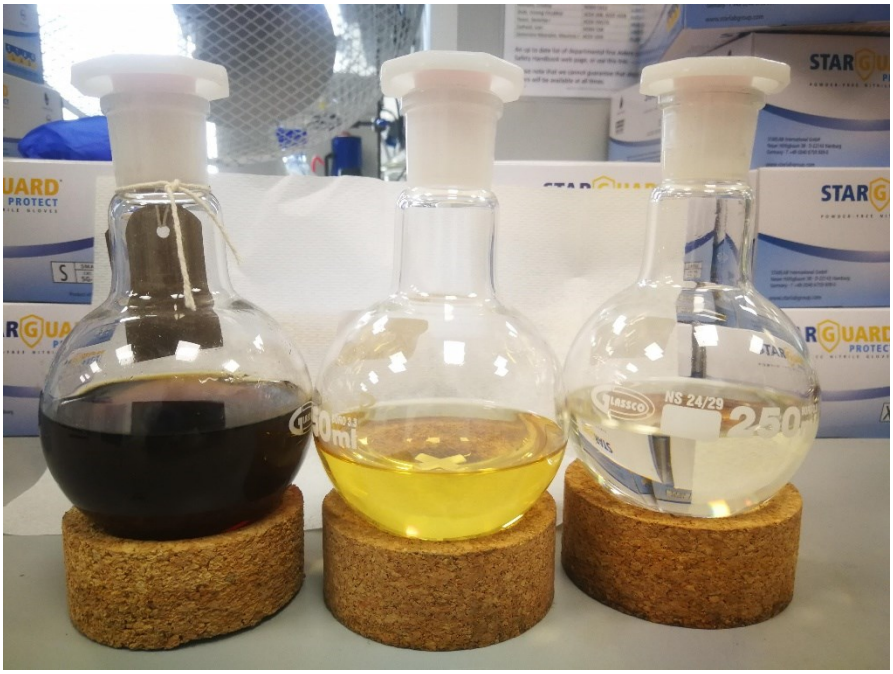

Figure A18: Toluene extract from Soxhlet extraction. Left to right: creosote wood dark, creosote wood mixed and pine wood

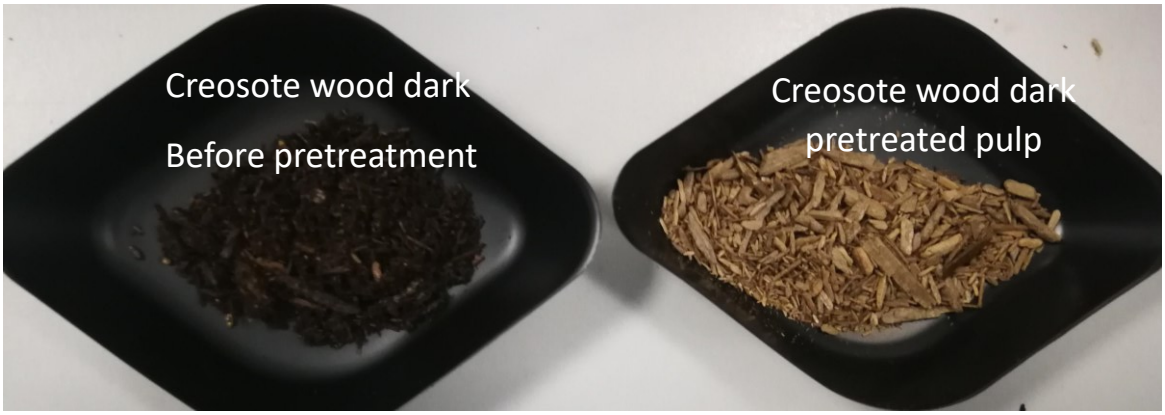

Figure A19: Creosote wood dark before pretreatment and creosote dark pulp after pretreatment using [DMBA][HSO4] at 170 °C and 45 minutes

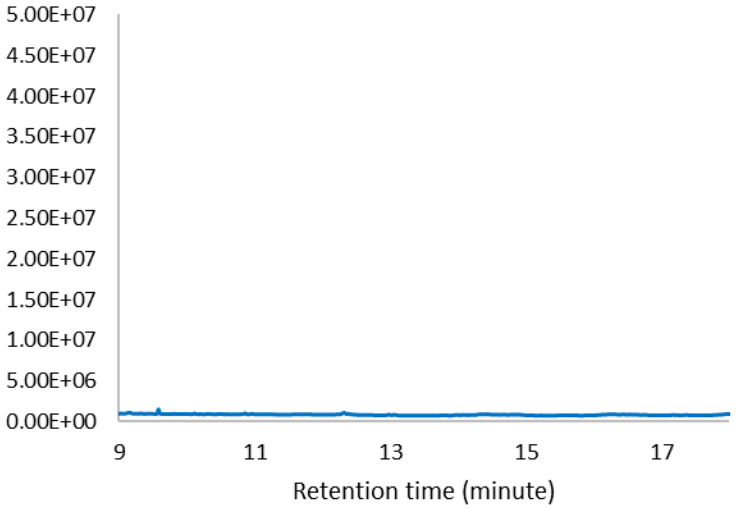

Figure A20: GC-FID chromatogram of toluene extract of pine wood

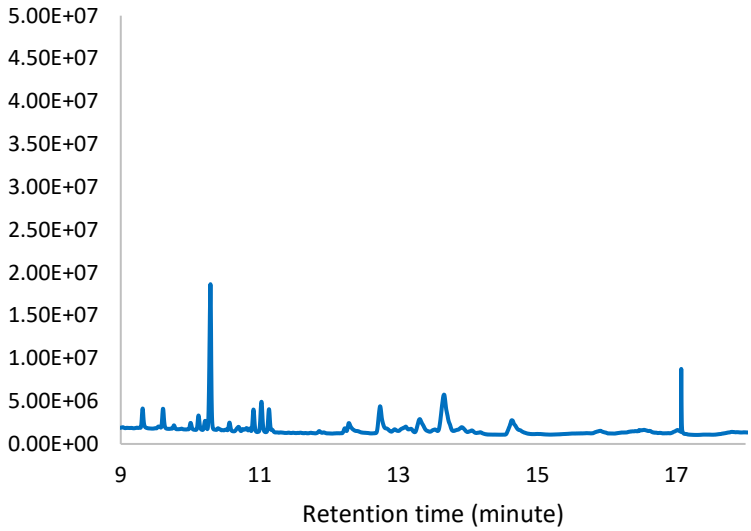

Figure A21: GC-FID chromatogram of toluene extract of pine wood lignin

Table A2: Normalized composition of cellulose pulps recovered in each cycle using 3 and 1 water equivalent to precipitate lignin

Cycle / water equivalent	Glucan	Xylan	Manan	AIL	ASL	Ash	Extractives
1st cycle, 3 equivalent	33.33	0.38	1.48	11.21	0.50	0.07	0.00
1st cycle, 1 equivalent	33.31	0.38	1.46	11.02	0.50	0.07	0.00
2nd cycle, 3 equivalent	37.42	1.11	2.36	13.89	0.63	0.29	0.00
2nd cycle, 1 equivalent	36.46	1.08	2.30	14.10	0.64	0.38	0.00
3rd cycle, 3 equivalent	34.86	0.92	2.70	12.71	0.62	0.00	0.00
3rd cycle, 1 equivalent	33.80	0.88	2.34	13.59	0.60	0.00	0.00
4th cycle, 3 equivalent	37.04	1.04	2.29	15.76	0.65	0.35	0.00
4th cycle, 1 equivalent	35.80	0.96	2.13	16.08	0.64	0.33	0.00
5th cycle, 3 equivalent	36.94	0.99	3.15	16.80	0.72	0.00	0.00
5th cycle, 1 equivalent	41.23	1.00	3.22	18.73	0.74	0.00	0.00
6th cycle, 3 equivalent	39.24	0.99	2.51	16.22	0.75	0.32	0.00
6th cycle, 1 equivalent	39.16	1.02	2.93	17.08	0.75	0.44	0.00

Figure A22: Cellulose pulp from pretreatment with [DMBA][HSO_4] mixed with different water concentrations. (Left) softwood pine pulps and (Right) Miscanthus cellulose pulps

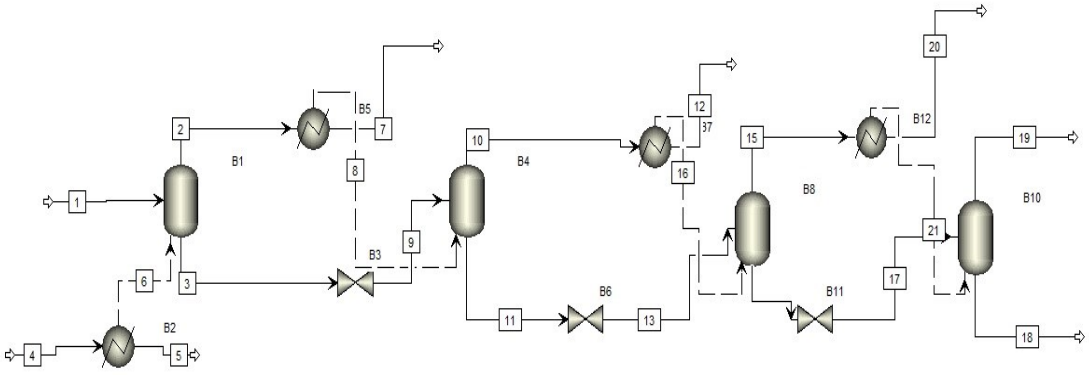

Figure A23: Multi-effect evaporator for IL dehydration and re-concentration. Stream 1 is diluted IL after lignin precipitation. Stream 18 is the re-concentrated IL (80 wt%). Stream 6 is the steam energy input in the 1st evaporator. Stream 7,12, 19 and 20 are the total water removed. Stream 9, 13, 17 are the cascaded IL/H_2O streams at lower pressure to the next effect for further water removal.

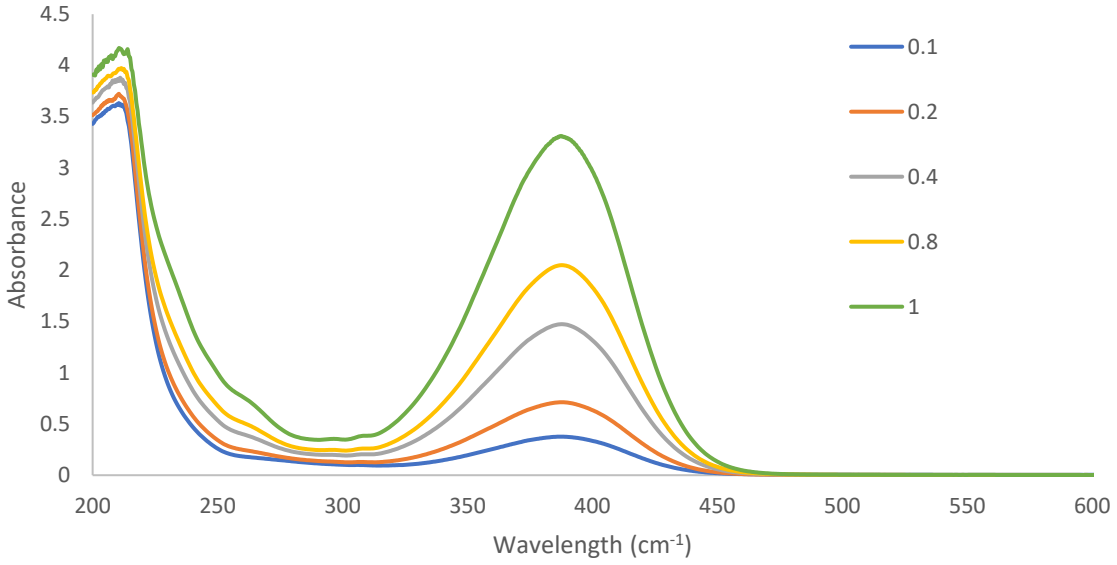

Figure A24: Hammett acidity measurements using UV-vis. 4-nitroaniline between 0.1mM to 1mM were prepared in anhydrous DCM.

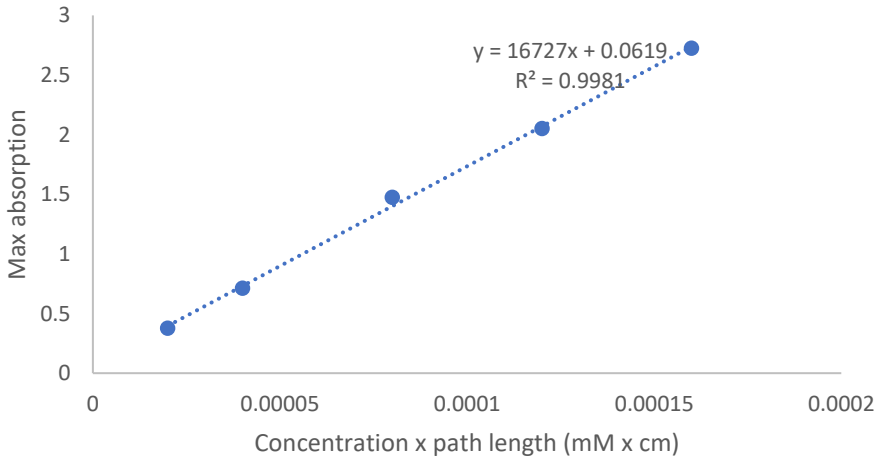

Figure A25: UV-Vis spectra of these solutions were measured and using the Beer-Lambert law (Eq. 5.5), the extinction coefficient of the 4-nitroaniline $\boldsymbol{\varepsilon}_0$ was calculated using the maximum absorbance at 350 nm.

Table A4 shows the statistical significance of the model term coefficients determined by the student's *t*-test and *p*-test. The analysis shows that all the quadratic model terms are statistically significant ($p < 0.01$) and therefore no term can be eliminated from the model. The second order polynomial model fit to the experimental data predict the response using the following Equation:

$$\textit{Delignification Response} = \mathbf{74.50} + \mathbf{2.87} \times ((T - 170) / 10) + \mathbf{6.51} \times ((t - 30) / 10) + \mathbf{6.81} \times ((C - 80) / 10) \mathbf{-10.33} \times ((T - 170) \times (t - 30))/10 \mathbf{- 5.58} \times ((T - 170) \times (C - 80))/ 10 \mathbf{- 5.53} \times ((t - 30) \times (C - 80))/ 10 \mathbf{- 3.68} \times (T - 170)^2 / 10 \mathbf{- 9.149} (t - 30)^2/ 10 \mathbf{- 13.08} \times (C - 80)^2/ 10$$

Where T, t and C represent the temperature (° C), time (minutes) and IL concentration (wt%), respectively. The model Equation can be used to make predictions for softwood delignification response using [DMBA][HSO_4] in the experimental domain explored. This highlights the importance of carefully balancing these variables to optimize the delignification during the [HSO_4]-based protic IL pretreatment.

Table A3: Model fit coefficients and the statistical significance of the model terms

Term	Coefficient	Std Error	t value	Prob>|t|
Intercept	74.50	0.73	101.44	<.0001
T	2.87	0.45	6.39	<.0001
t	6.51	0.45	14.48	<.0001
C	6.81	0.45	15.14	<.0001
T×t	-10.34	0.64	-16.25	<.0001
T×C	-5.59	0.64	-8.78	<.0001
t×C	-5.53	0.64	-8.70	<.0001
T^2	-3.68	0.66	-5.57	<.0001
t^2	-9.15	0.66	-13.82	<.0001
C^2	-13.08	0.66	-19.77	<.0001

Chapter 6

Figure A26: nanocellulose suspension after alkaline oxidation using H_2O_2 (left) suspensions right after the oxidation rection and (right) gel-like material upon filtering the suspension

Chapter 7

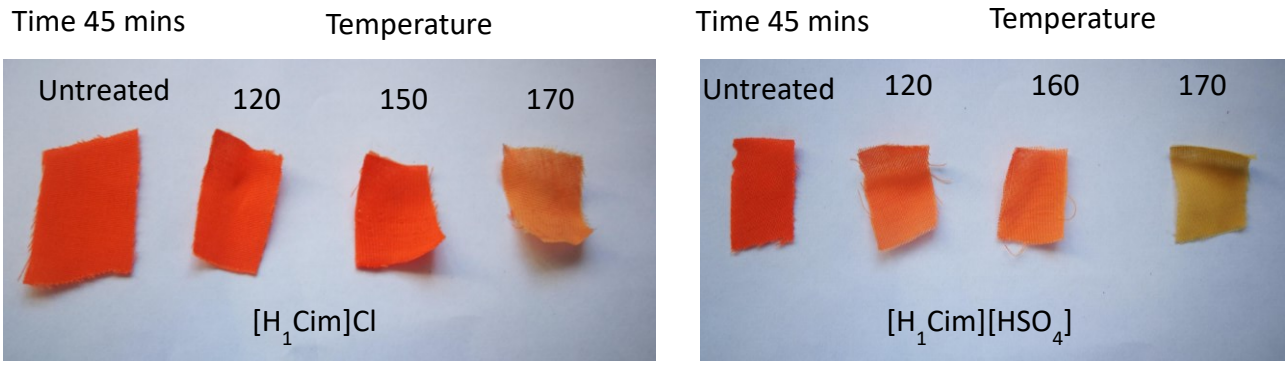

Figure A27: [H1Cim]Cl used for dye extraction at different temperatures (left) [H1Cim][HSO4] used for dye extraction at different temperatures (right)